Durham University

Durham E-Theses

The Synthesis and Photophysics of Cyclometalated Iridium Complexes and Photochromic Materials

ROBERT MATTHEW EDKINS

How to cite:

EDKINS, ROBERT MATTHEW (2013) The Synthesis and Photophysics of Cyclometalated Iridium Complexes and Photochromic Materials. Doctoral thesis, Durham University.

Use policy

The full-text may be used and/or reproduced, and given to third parties in any format or medium, without prior permission or charge, for personal research or study, educational, or not-for-profit purposes provided that:

- a full bibliographic reference is made to the original source
- a https://etheses.durham.ac.uk/id/eprint/7300/ is made to the metadata record in Durham E-Theses
- the full-text is not changed in any way

The full-text must not be sold in any format or medium without the formal permission of the copyright holders.

Please consult the full Durham E-Theses policy for further details.

Academic Support Office, The Palatine Centre, Durham University, Stockton Road, Durham, DH1 3LE
e-mail: e-theses.admin@durham.ac.uk Tel: +44 0191 334 6107
https://etheses.durham.ac.uk

The Synthesis and Photophysics of Cyclometalated Iridium Complexes and Photochromic Materials

Robert Matthew Edkins

Department of Chemistry

Durham University

Declaration

The work described in this thesis was carried out in the Department of Chemistry at Durham University between October 2009 and December 2012. This thesis is the work of the author except where acknowledged by reference and has not been submitted for any other degree.

Statement of copyright

The copyright of this thesis rests with the author. No quotation from it should be published without the author's prior written consent and information derived from it should be acknowledged.

‘Nature doesn’t ask you about it; she’s not concerned with your wishes or with whether you like her laws or not. You must take her as she is, and consequently all her results as well.’

Fyodor Dostoyevsky in Notes from Underground

Abstract

This thesis concerns two main themes: cyclometalated iridium complexes and organic photochromic materials. The presentation of the work has been split into two parts regarding these distinct topics, each having an introduction, discussion of results and suggestions for future work, followed by a combined experimental section.

Chapter 1 provides a general introduction to the photophysical concepts relevant to the whole thesis. Following this is an overview of cyclometalated iridium complexes, their synthesis, photophysical properties and applications. At the end of this chapter, palladium-catalysed cross-coupling reactions are reviewed due to their importance in preparing many of the materials described.

In Chapter 2, the results from the work conducted on cyclometalated iridium complexes are discussed. Tris-heteroleptic cyclometalated iridium complexes of the form [IrLL′(acac)] are first described. The synthesis of several examples of this class of complex and their photophysical properties are summarised, supported by theoretical calculations. A detailed study of the isomeric iridium complexes having 1- and 2-(2′-pyridyl)pyrene ligands is then presented, including a discussion of their syntheses, photophysics and electrochemistry as well as an evaluation of some TD-DFT methods for the accurate calculation of optical transitions. Subsequently, the time-gated two-photon spectroscopy of Ir-Eu and Ir-Tb dyads is demonstrated. Concluding this chapter is a discussion of the synthesis of a tris-heteroleptic iridium complex bearing a terminal acetylene substituent that is a divergent intermediate to further complexes having π-extended ligands. A photophysical and theoretical investigation of some derivatives synthesised by direct Sonogashira coupling of this intermediate is presented.

Chapter 3 introduces photochromism and provides an overview of some of the more common classes of molecules that exhibit this phenomenon. More specific detail is then given about the triphenylimidazolyl radical (TPIR) and dihydropyrene (DHP) systems that feature in Chapter 4.

Chapter 4 details the findings from the work conducted on the aforementioned TPIR and DHP photochromic materials. This includes the identification of a peroxide fatigue product of TPIRs and the isolation of a normally unstable dimerisation mode of a TPIR derivative by application of the photocrystallisation method. Attempts to synthesise DHP derivatives, and the associated challenges, are then described.

Finally, Chapter 5 contains the combined experimental detail and synthetic procedures for the work described in the previous chapters.

Acknowledgements

Firstly, many thanks go to Prof. Andy Beeby for all the advice and support throughout my time in his group – I have been around quite a while!

The inhabitants of CG2, 7 and 11, *viz*. Dr. Ben Coombs, Andy Duckworth, Vale Manici, Dr. Kate Nicholson, Dr. Robek Pal (honorary member), Geri Rosser and Dr. Adam Swinburne, are thanked for making it a great place to work. Thanks also to the former MChem students.

Alisdair Wriglesworth in particular is thanked for working with me on the development of the synthesis of tris-heteroleptic complexes (Section 2.1). Dr. Michael Peach is thanked for many helpful discussions about DFT and for running the TDA calculations on the pyridylpyrene compounds described in Section 2.2. Prof. Mike Ward and Dr. Daniel Sykes of the University of Sheffield are acknowledged for collaboration and supplying the complexes used for the two-photon absorption spectroscopy of iridium-lanthanide dyads (Section 2.3). For use of electrochemical equipment, Prof. Paul Low is acknowledged. Prof. Todd Marder is thanked for regular use of GC-MS and Dr. Andy Crawford for his help in the synthesis of 2-bromopyrene (Section 2.2). Drs. Kathi Fucke and Mike Probert are kindly acknowledged for all their hard work in determining single crystal X-ray structures for the iridium / DHP sections and the TPIR section, respectively (Dr. Craig Robertson is acknowledged for some initial data collection in the latter case). I am grateful also to the MS, NMR, EA and DSC service staff for running my samples and to the glass blowers for fixing the seemingly unfixable.

Durham University is thanked for a Durham Doctoral Fellowship that has funded my studies.

I wouldn't have got here without the support of my family and so many thanks go to them: Mum, Nan and Gran. Finally, thank you to Kathi for being there for me and making the last three and a half years so enjoyable!

Robert M. Edkins
April 2013

Contents

List of figures

Chapter 1

Chapter 2

Chapter 3

Chapter 4

List of schemes

Chapter 1

Chapter 2

Chapter 3

Chapter 4

List of tables

Chapter 1

Chapter 2

Abbreviations

A	Acceptor
A	Ancillary ligand
acacH	Acetylacetone (2,4-pentanedione)
Acc.	Accurate
Ar	Generic aromatic group
ASAP	Atmospheric pressure solids analysis probe
ATR	Attenuated total reflection
BPEB	Bis(phenylethynyl)benzene
B3LYP	Becke's three parameter exchange and Lee-Yang-Parr's correlation functional
bpy	2,2′-Bipyridine
btpH	2-(2′-Benzothienyl)pyridine
Bu	Butyl
CAM	Coulomb-attenuating method
Calcd.	Calculated
CCD	Charge-coupled device
CIE	Commission Internationale de l'Eclairage
COD	Cycloocta-1,5-diene
COE	*cis*-Cyclooctene
COSY	Correlation spectroscopy
Cp	Cyclopentadiene
Cp^*	Pentamethylcyclopentadiene
CSD	Cambridge structural database
CV	Cyclic voltammetry
D	Donor
d	Doublet (NMR)
dd	Doublet of doublet (NMR)
DFT	Density functional theory
DMF	*N*,*N*-Dimethylformamide
DSC	Differential scanning calorimetry
DSSC	Dye-sensitised solar cell
dtbpy	4,4′-Di-*tert*-butyl-2,2′-bipyridine
ECP	Effective core potential
E^nT	Energy transfer
EPR	Electron paramagnetic resonance
eq.	Equivalents
ESA	Excited state absorption
ESI	Electrospray ionisation
Et	Ethyl
ETL	Electron transport layer
F_2ppyH	2-(2′,4′-Difluorophenyl)pyridine
fac	Facial
Fc	Ferrocene

Fc*	Decamethylferrocene
fppyH	2-(4′-Formylphenyl)pyridine
FT	Fourier-transform
FWHM	Full width at half maximum
GC	Gas chromatography
HABI	Hexaarylbiimadazole
hfacH	1,1,1,5,5,5-Hexafluoropentane-2,4-dione
HMBC	Heteronuclear multiple bond correlation
HOMO	Highest occupied molecular orbital
HOMO-*N*	N^{th} orbital lower in energy than the HOMO
HOSO	Highest occupied spin orbital
HPLC	High-performance liquid chromatography
HSQC	Heteronuclear single quantum coherence
HTL	Hole transport layer
i-	*Iso-*
IC	Internal conversion
I^{ra}LCT	Intraligand charge transfer
I^{er}LCT	Interligand charge transfer
IR	Infrared
IRF	Instrument response function
ISC	Intersystem crossing
ISC′	Back intersystem crossing
ITO	Indium tin oxide
L	Generic cyclometalating ligand
LANL2DZ	Los Alamos National Laboratories 2nd double zeta
LC	Ligand centred
LCD	Liquid-crystal display
LEC	Light-emitting electrochemical cell
Ln	Generic lanthanide
LUMO	Lowest unoccupied molecular orbital
LUMO+*N*	N^{th} orbital higher in energy than the LUMO
LUSO	Lowest unoccupied spin orbital
M	Generic metal
m	Multiplet (NMR)
MALDI-TOF	Matrix assisted laser desorption/ionisation time-of-flight
Me	Methyl
mer	Meridional
MLCT	Metal to ligand charge transfer
M.p.	Melting point
n-	*Normal-*
ND	Neutral density
NIR	Near infrared
NLO	Non-linear optics
NMR	Nuclear magnetic resonance

NOESY	Nuclear Overhauser effect spectroscopy
OLED	Organic light emitting diode
OPA	One-photon absorption
OTf$^-$	Triflate (trifluoromethanesulfonate, $CF_3SO_3^-$)
PCM	Polarisable continuum model
PDT	Photodynamic therapy
peppyH	2-Phenyl-4-(phenylethynyl)pyridine
PES	Potential energy surface
Ph	Phenyl
PHA	Pulse height analyser
PMT	Photomultiplier tube
pin	Pinacolato, $(OCMe_2CMe_2O)^{2-}$
piqH	1-phenylisoquinoline
PLQY	Photoluminescence quantum yield
PMT	Photomultiplier tube
ppyH	2-Phenylpyridine
Pr	Propyl
pybpH	4-(2′-Pyridyl)benzophenone
1-pypyrH	1-Pyridylpyrene
2-pypyrH	2-Pyridylpyrene
q	Quartet (NMR)
R	Generic organic group or substituent
R	Reference
$\boldsymbol{R_f}$	Retention factor
r.t.	Room temperature
s	Singlet (NMR)
S	Sample
SCF	Self-consistent field
SC-XRD	Single crystal X-ray diffraction
SOC	Spin-orbit coupling
SOMO	Singly occupied molecular orbital
t	Triplet (NMR)
***t*-** or ***tert*-**	*Tertiary*-
TBA	Tetra-*n*-butylammonium
TCMPC	Time-correlated muti-photon counting
TCSPC	Time-correlated single photon counting
td	Triplet of doublets (NMR)
TDA	Tamm-Dancoff Approximation
TD-DFT	Time-dependent density functional theory
THF	Tetrahydrofuran
TLC	Thin layer chromatography
TFA$^-$	Trifluoroacetate
TIPS	Triisopropylsilyl
TMS	Trimethylsilyl

TMSA	Trimethylsilylacetylene
TPA	Two-photon absorption
TPIR	2,4,5-Triphenylimidazolyl radical
UAKS	United atom Kohn-Sham
UV	Ultraviolet
ver.	version
VR	Vibrational relaxation
X	Generic halide or triflate substituent
ΔSCF	Difference between two self-consistent field energies

Non-SI units, Quantities and Symbols

A	Absorbance
a_0	Atomic unit or bohr, 1 a_0 = 5.29 x 10^{-11} m
Å	Ångström, 1 Å = 10^{-10} m
a.u.	Arbitrary units
C	Coulomb, 1 C = 1 A s
c	Concentration, mol dm^{-3}
c	Speed of light, 3.00 x 10^{8} m s^{-1}
e	Electron charge, 1.60 x 10^{-19} C
eV	Electron volt, 1 eV = 1.60 x 10^{-19} J
f	Oscillator strength
$F(\lambda)$	Integrated photoluminescence spectrum, counts
GM	Göppert-Mayer unit, 1 GM = 10^{-50} cm^4 s $photon^{-1}$
h	Hour, 1 h = 3600 s
h	Planck Constant, 6.63 x 10^{-34} J s
Hz	Hertz, 1 Hz = 1 s^{-1}
I	Intensity, a.u.
J	*J*-coupling constant, Hz
K_A	Equilibrium constant
k_{nr}	Non-radiative rate constant, s^{-1}
k_r	Radiative rate constant, s^{-1}
l	Path length, cm
$\mathbf{L}_i$	Orbital angular momentum operator
$\mathbf{M}^+$	Molecular ion
M	Molar concentration, 1 M = 1 mol dm^{-3}
m_e	Electron rest mass, 9.11 x 10^{-31} kg
min	Minute, 1 min = 60 s
mol%	Percentage by amount
m/z	Mass to charge ratio
n	Refractive index
ppm	Parts per million
r	Distance, m
S	Total spin quantum number
S_0	Ground state of a closed shell molecule

$\mathbf{S}_i$	Spin angular momentum operator
$\mathbf{S}_n$	n^{th} Singlet (excited) state
$\mathbf{T}_n$	n^{th} Triplet (excited) state
V	Volt, 1 V = J C^{-1}
v*/*v	Ratio by volume
vol%	Percentage by volume
wt%	Percentage by weight
Z	Atomic number
Δ	Heat
Δ*E*	Difference in energy, eV or cm^{-1}
δ	Chemical shift, ppm
ε	Extinction coefficient, dm^3 mol^{-1} cm^{-1}
ξ_{SOC}	Spin orbit coupling constant
η	Hapticity of a ligand
κ	Used to indicate coordinating atom
λ	Wavelength, nm
λ_{em}	Emission wavelength, nm
λ_{ex}	Excitation wavelength, nm
λ_{max}	Emission maximum, nm
μ	Used to denote a bridging ligand
μW	Microwave irradiation
μ	Dipole moment, D
ν	Frequency, s^{-1}
ν	Scan rate, mV s^{-1}
π	Pi symmetry (*e.g.* π-bonding and π-conjugation)
σ	Sigma symmetry (*e.g.* σ-bonding)
σ_2	Two-photon cross-section, GM
τ	Excited state lifetime, s
τ_0	Pure radiative lifetime, s
Φ	Quantum yield of photoluminescence
Φ_Δ	Quantum yield of singlet oxygen formation
Φ_T	Quantum yield of triplet formation
χ^2	Chi-squared (statistical tool)
ω_{STAB}	Eigenvalues of stability calculations

Publications

Researcher ID: F-5451-2011 (www.researcherid.com/rid/F-5451-2011)

8. *Photocrystallization of the 2C-2'C dimer of a triphenylimidazolyl radical*
   R. M. Edkins, M. R. Probert, C. M. Robertson, J. A. K. Howard and A. Beeby, *Submitted*

7. *Syntheses, structures and comparison of the photophysical properties of cyclometalated iridium complexes containing the isomeric 1- and 2-(2'-pyridyl)pyrene ligands*
   R. M. Edkins, K. Fucke, A. G. Crawford, T. B. Marder and A. Beeby, *Accepted May 2013, Inorg. Chem.*

6. *The formation of peroxide degradation products of photochromic triphenylimidazolyl radical-dimer systems*
   R. M. Edkins, M. R. Probert, K. Fucke, C. M. Robertson, J. A. K. Howard and A. Beeby, *Phys. Chem. Chem. Phys.*, 2013, **15**, 7848

5. *Combined two-photon excitation and d→f energy-transfer in Ir/lanthanide dyads with time-gated selection from a two-component emission spectrum*
   R. M. Edkins, D. Sykes, A. Beeby and M. D. Ward, *Chem. Commun.*, 2012, **48**, 9977

4. *Photophysical property trends for a homologous series of bis-ethynyl-substituted benzochalcogendiazoles*
   B. A. Coombs, B. D. Lindner, R. M. Edkins, F. Rominger, A. Beeby and U. H. F. Bunz, *New J. Chem.*, 2012, **36**, 550

3. *Phosphorescent mer and fac cyclometalated iridium(III) complexes of phenylpyrido[4,3-b]indole derivatives: an unusual thermally-induced defluorination reaction of a homoleptic complex*
   Y. Zheng, A. S. Batsanov, R. M. Edkins, A. Beeby and M. R. Bryce, *Inorg. Chem.*, 2012, **51**, 290

2. *Two-photon spectroscopy of cyclometalated iridium complexes*
   R. M. Edkins, S. Bettington, A. Goeta and A. Beeby, *Dalton Trans.*, 2011, **40**, 12765

1. *The synthesis and photophysics of tris-heteroleptic cyclometalated iridium complexes*
   R. M. Edkins, A. Wriglesworth, K. Fucke, S. L. Bettington and A. Beeby, *Dalton Trans.*, 2011, **40**, 9672-9678; inside front cover: *Dalton Trans.*, 2011, **40**, 9622

Talks

4. *Two-photon spectroscopy of cyclometalated iridium complexes*

   31/07/2012 1st Northern Chemistry Postgraduate Research Conference, Newcastle (U.K.)

3. *Two-photon spectroscopy of cyclometalated iridium complexes*

   16/07/2012 XXIV IUPAC Symposium on Photochemistry, Coimbra (Portugal)

2. *Tris-heteroleptic iridium complexes: synthesis, photophysics and donor-acceptor compounds*

   13/06/2012 Durham Graduate Symposium 2012, Durham (U.K.)

1. *Designer cyclometalated iridium complexes and the fate of imidazolyl photochromic dimers*

   04/05/2012 **Invited** Julius-Maximilians-Universität Würzburg, Institut für Anorganische Chemie, Würzburg (Germany)

Posters

4. *The synthesis and photophysics of tris-heteroleptic cyclometalated iridium complexes*

   R. M. Edkins, A. Wriglesworth, K. Fucke, S. L. Bettington and A. Beeby

   Dalton Division Joint Interest Groups Meeting, 2012 (Warwick, U.K.)

3. *The synthesis and photophysics of tris-heteroleptic cyclometalated iridium complexes*

   R. M. Edkins, A. Wriglesworth, K. Fucke, S. L. Bettington and A. Beeby

   Durham Graduate Symposium, 2011 (Durham, U.K.)

2. *Phosphorescent iridium complexes with 1- and 2-(2'-pyridyl)pyrene ligands*

   R. M. Edkins and A. Beeby

   1st Dalton Division "Electronic Structural Methods in Inorganic Chemistry" Summer School, 2010 (Edinburgh, U.K.)

1. *Imidazolyl association: modulating dimerisation via UV irradiation*

   C. M. Robertson, R. M. Edkins, A. Beeby and J. A. K. Howard

   29th Annual Spring Meeting of the British Crystallographic Association, 2010, (Keele, U.K.)

Chapter 1

Cyclometalated Iridium Complexes: Introduction

1. Introduction

The photophysical properties of transition metal complexes, especially those of the platinum group metals (PGM: Ru, Os, Rh, Ir, Pd and Pt), has become a subject of intense contemporary research.[1-4] In particular, octahedral cyclometalated complexes of low spin d^6 Ir(III) have received considerable attention due to their large photoluminescence quantum yields (PLQY, Φ),[5-7] facile colour tuning by ligand modification[8-12] and relatively short phosphorescence lifetimes (typically τ = 1-5 μs). The favourable photophysical properties of these complexes are augmented by their relatively high solution and device photo-, electro- and thermal stability.[13] The interest in these materials has been spurred by their commercialisation as fundamental components of organic light emitting devices (OLEDs).[14, 15] OLEDs promise to provide a low cost and low energy, but high performance, alternative to the current benchmark of liquid crystalline (LCD) displays. With their wide viewing angles, well defined, intense colours and slim, flexible design, OLEDs are an attractive display technology. In addition to their manifold benefits for the end-user, the ability to construct OLEDs by solution-based processing is particularly advantageous for device manufacturers.[16]

Ir complexes have also been investigated for use as photosensitisers in dye-sensitised solar cells (DSSC)[17] and as photocatalysts for water-splitting[18] and CO_2 reduction.[19] DSSCs[20, 21] and photocatalytic water-splitting,[22, 23] in general terms, are possible environmentally benign alternatives for sustainable, low-carbon electricity and fuel (hydrogen) production, respectively. For these applications, light-harvesting components that share some similarities with the materials designed for OLEDs are required. The luminescence of these compounds has also been utilised in biological imaging[24, 25] and various sensing applications, typically by designing complexes whose emissive properties are changed in some parameter upon non-covalent binding of an analyte or following chemical reaction with the substrate of interest.[26] Sensing of oxygen is also possible based upon the quenching of the long lived triplet emission,[27-29] a property that has been exploited for detecting hypoxia associated with cancer cells.[30] For all of these additional applications, charged complexes are often used to increase water solubility, which can be enhanced further by the introduction of polar groups.[31] These varied applications demonstrate the breadth of continued interest in the photophysical properties of cyclometalated iridium complexes. Whilst substantial

efforts have been made in the study of the properties and applications of these compounds, the extent of the possibilities has yet to be reached and much is still to be understood at the fundamental level.

Before these materials and their applications are described in any greater detail, the basic concepts of molecular photophysics are outlined to provide the necessary background to explain the processes discussed. Towards the end of this chapter, Pd-catalysed cross-coupling reactions are reviewed due to their central role in constructing the ligands reported herein. It is the intention with this chapter to cover the topics of relevance in the broadest possible way; thus, an approach where concepts are more central to the discussion than particular examples has been taken. The necessity for this style is partly borne out of the large body of literature on the subject of cyclometalated iridium complexes that has amassed over recent years, which cannot be hoped to be covered comprehensively in these few short pages.

1.1. Molecular photophysics

In the absence of an energetic perturbation, a molecule will reside in its lowest energy electronic state, which is also referred to as its ground state. In this state, the molecular orbitals (MOs) are occupied according to the *aufbau* principle, with the lowest energy orbitals being filled before those lying higher on the energy ladder. The Pauli Exclusion Principle ensures that a maximum of two electrons with opposite spin *z*-projection ($m_s = \pm ½$) occupy any one orbital and Hund's 1st Rule produces the configuration of highest spin multiplicity ($2\mathbf{S}+1$, where $\mathbf{S} = \Sigma m_s$) in the case of a degenerate highest occupied molecular orbital (HOMO).

The aforementioned Hund's 1st Rule and the Pauli Exclusion Principle are consequences of the more fundamental Pauli Principle. The Pauli Principle, when applied to electrons in a molecule, states that the total wavefunction, whose absolute square defines the electron probability density, must be mathematically antisymmetric with respect to exchange of the labels of any two of the electrons. This esoteric sounding statement has several important implications for this work; thus, it is instructive to consider it in further detail. The total wavefunction can be written as the normalised product of a spin and a spatial wavefunction, each of which may themselves be symmetric or anti-symmetric.[32] If a two electron system is considered, which is exact for a He atom, and is used here as an approximation for a pair of electrons in any

molecule, the symmetric, (**1**), and antisymmetric, (**2**), spatial wavefunctions can be written:

$$\frac{1}{\sqrt{2}}[\psi_a(r_1)\psi_b(r_2) + \psi_b(r_1)\psi_a(r_2)] \quad (\mathbf{1})$$

$$\frac{1}{\sqrt{2}}[\psi_a(r_1)\psi_b(r_2) - \psi_b(r_1)\psi_a(r_2)] \quad (\mathbf{2})$$

where $\psi_{a,b}$ are the wavefunctions for MOs *a* and *b*, and $r_{1,2}$ are the coordinates of the electrons labelled 1 and 2. To ensure an antisymmetric total wavefunction, the symmetric spatial function (**1**) is associated with the one possible antisymmetric spin function (**3**), the product of which describes a singlet state. There are three possible symmetric spin functions, (**4**), paired with the antisymmetric spatial function (**2**) to generate a triplet state. These can be expressed as:

$$\frac{1}{\sqrt{2}}(\alpha\beta - \beta\alpha) \quad (\mathbf{3})$$

$$\alpha\alpha$$

$$\frac{1}{\sqrt{2}}(\alpha\beta + \beta\alpha) \quad (\mathbf{4})$$

$$\beta\beta$$

where α and β represent the two possible values of m_s for a spin ½ electron (often referred to as up and down). If the two electrons are in the same orbital ($\psi_a = \psi_b$), equation (**2**), the spatial part of the triplet state, is equal to zero and there is zero probability of finding two electrons of the same spin in the same orbital. Thus, for two electrons to exist in the same orbital they must also have opposite spin: this is the Pauli Exclusion Principle. This results in even electron molecules with a non-degenerate HOMO having a singlet ground state, a situation describing the majority of organic molecules. The second observation is that when $\psi_a \neq \psi_b$, such as can occur when a

molecule has a degenerate HOMO or when a molecule is in an excited state, as $r_1 \rightarrow r_2$ (*i.e.* the two electrons become close in space), the spatial function (**2**) tends to zero, so that two electrons in a triplet state tend to avoid each other. This node in the wavefunction is known as a Fermi Hole and the two electrons are said to be correlated because their trajectories are not independent. This serves to reduce both the Coulombic repulsion and magnetic dipole-dipole interactions between the two electrons, lowering the overall total energy of the triplet state. Conversely, in a singlet state, the spatial wavefunction (**1**) tends to a maximum as $r_1 \rightarrow r_2$; consequently, the wavefunction exhibits a Fermi Heap and the Coulomb repulsion is greater than would be expected if the electrons were not correlated. The result of this effect is that the energy of the triplet state is always lower than that of the corresponding singlet state.[33] In the ground state, this leads to Hund's 1st Rule. The energy difference between the singlet and the triplet excited state of a molecule is determined by the spatial overlap of the orbitals involved and, hence, to what extent electron correlation influences the energy of those states.

A molecule can be excited from its ground state to an excited state when an incident photon of electromagnetic radiation is energetically matched to a suitable energy spacing of the molecule according to the Planck relation:

$$\Delta E = h\nu = \frac{hc}{\lambda} \qquad (5)$$

where ΔE is the energy spacing of concern in the molecule, h is Planck's constant and ν is the frequency of the incident light. The absorption process may occur only if certain conditions, or selection rules, allow it, namely that there is no change of spin between the states ($\Delta \mathbf{S} = 0$, spin selection rule), that there is a change in orbital momentum ($\Delta \mathbf{L} = \pm 1$, orbital selection rule) and that there is a change in parity for centrosymmetric molecules (Laporte selection rule). The spin and orbital selection rules are consequences of the need to conserve total angular momentum.

The absorption of photons in the ultraviolet (UV) and visible spectral regions by polyatomic molecules and the fates of these excited species under such irradiation are the most pertinent photophysical phenomena to this study. The ground and excited states, and the processes leading to transitions between them, can be summarised in a Jablonski diagram, an example of which is shown in Figure 1.1.

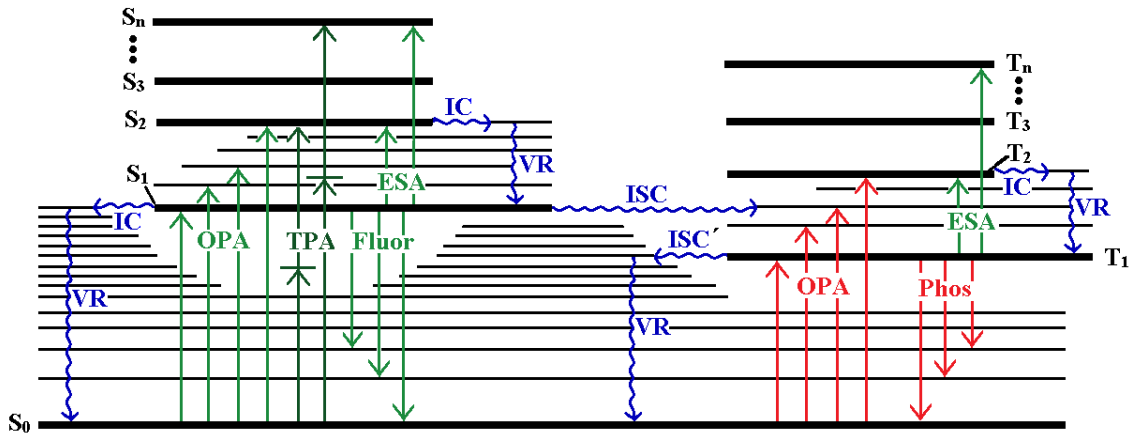

Figure 1.1. A simplified Jablonski diagram. Radiative and non-radiative transitions are represented by straight and wavy arrows, respectively. Radiative processes that are formally spin allowed and spin forbidden are shown as green and red arrows, respectively. S_n = n^{th} singlet state (S_0 ground state); T_n = n^{th} triplet state; OPA = one-photon absorption; TPA = two-photon absorption; ESA = excited state absorption; IC = internal conversion; ISC = intersystem crossing; ISC′ = back intersystem crossing; VR = vibrational relaxation; Fluor = fluorescence; Phos = phosphorescence.

The electronic redistribution between the frontier orbitals as a result of excitation can sometimes be viewed simply as a transition of a single electron between the HOMO and the lowest unoccupied molecular orbital (LUMO) of the ground state. However, oftentimes, a multi-component description of the transition using the HOMO-*N* and LUMO+*N* orbitals is required. An important characteristic of the excited state is its spin multiplicity. In an electronically excited state, the two highest energy electrons are in different orbitals and can exist as either a spin antiparallel **S** = 0 singlet state (n^{th} singlet state S_n, $n \geq 1$), or spin parallel **S** = 1 triplet state (n^{th} triplet state T_n, $n \geq 1$). Hund's 1^{st} Rule, as derived and applied to the ground state above, serves equally well for excited states and implies that the lowest triplet excited state will lie below that of the lowest singlet excited state. The energy difference between these two will be influenced by the spatial overlap of the two orbitals and thus will determine the magnitude of energy reduction through electron correlation in the triplet state.

During the absorption process, which occurs on the femtosecond or quicker timescale, the nuclei are considered to remain essentially stationary. Thus, initially, the excited state maintains the geometry of the ground state (a vertical transition) before energetic redistribution occurs to generate the relaxed geometry. The initially formed

state is called the Franck-Condon state and the same idea can be applied equally well to the emission process. The requirement to form the Franck-Condon state can be relaxed by vibronic coupling, which can lend some intensity to otherwise symmetry-forbidden transitions. Non-radiative vibrational relaxation (VR) of an excited state is very rapid ($k_{VR} = 10^{12} – 10^{14}$ s^{-1}) and so, typically, a ground vibrational level is populated before further processes occur. If a higher electronic excited state is formed during the absorption, isoelectronic internal conversion (IC) between states of the same multiplicity can take place. IC also provides a non-radiative pathway for deactivation of an excited state to the ground state of the same multiplicity and occurs at a rate of *ca.* $k_{IC} = 10^{10} – 10^{14}$ s^{-1}. Intersystem crossing (ISC) between an excited state of one multiplicity and another state of a different multiplicity (for example, $S_1 \rightarrow T_1$) is a formally forbidden process and, therefore, for light atom molecules in particular, tends to be significantly slower than either radiative or non-radiative decay of an excited state of the same multiplicity as the ground state. The reverse process of back intersystem crossing (ISC′) to the ground state is also viable, usually enhanced by the same factors as ISC (*vide infra*). It is possible for ISC to populate a higher state before undergoing IC to the lowest state of that multiplicity. The crossing point of two surfaces involved in IC or ISC can be affected by external factors such as solvent polarity, leading to more complicated dynamics. This non-radiative decay can occur by vibrational coupling of two states or *via* a conical intersection and the excess energy following VR is redistributed to the solvent and surroundings. Molecules in excited states may also undergo chemical reactions, although these varied and multifaceted photochemical processes will not be discussed here.[34]

The intensity of a one-photon absorption process is quantified by its oscillator strength, *f*, which is related to the experimentally measured molar extinction coefficient, ε, of a bulk sample. The extent to which a transition is allowed is ultimately allied to the transition dipole moment of the transition, calculated for all the electrons and nuclei, which incorporates spin, symmetry and orbital overlap components.

Radiative decay of an excited state is termed luminescence and is sub-divided based on its origin. Photoluminescence describes radiative decay from a light induced excitation, of the type described above, which is important to this work. Other methods of excitation that can lead to emission include, but are not limited to, electroluminescence (electrical excitation), triboluminescence (mechanical excitation)

and bio/chemiluminescence (biochemical or chemical reaction leading to a product in an excited state capable of emission). Luminescence can also be sub-divided based on its spin change, $\Delta\mathbf{S}$, during the transition. Fluorescence is an allowed process according to the spin selection rule, occurring between states of the same multiplicity, $\Delta\mathbf{S} = 0$. Typically, the rate constant for fluorescent radiative decay is $k_r = 10^7 - 10^{12}$ s^{-1}, while phosphorescence is a formally forbidden transition between states of different multiplicity, $\Delta\mathbf{S} \neq 0$, with $k_r = 10^{-2} - 10^6$ s^{-1}. Due to the spin allowed nature of fluorescence, the observed lifetime of the excited state is relatively short, typically less than 10 ns for an organic molecule, although there are exceptions, usually when the transition is not allowed by symmetry.

The spin-forbidden nature of phosphorescence makes the triplet excited state lifetimes of ground state S_0 organic molecules long lived and such states are often only weakly emissive. However the spin selection rule can be relaxed in the presence of a heavy atom that can induce spin-orbit coupling (SOC). The SOC Hamiltonian is given by:

$$\hat{H}_{SOC} = \sum_i \frac{Ze^2}{2m_e^2c^2}\left\langle \frac{1}{r^3} \right\rangle \hat{\boldsymbol{L}}_i \hat{\boldsymbol{S}}_i \qquad (6)$$

where Z is the atomic number, e is the charge on an electron, m_e is the rest mass of an electron, c is the speed of light, r is the distance between the atom of interest and the chromophore, $\hat{L}_i$ is the orbital angular momentum operator and $\hat{S}_i$ is the spin angular momentum operator. The $<1/r^3>$ term, evaluated for a p-orbital of an atom, is dependent on Z^3 and, thus, $\hat{H}_{SOC}$ is often said to depend on Z^4. This strong dependence of the SOC magnitude on the atomic number results in this phenomenon being manifested predominantly for heavy atoms. In cases where SOC is efficient, the spin-selection rule must be recast as a requirement for conservation of total angular momentum. The consequence of the molecule of interest containing an atom that promotes SOC is that phosphorescence becomes allowed to an extent related to the magnitude of the SOC for that excited state. Absorption and intersystem crossing to states of different multiplicity can also become more allowed. Heavy atom SOC can be either an internal effect, such as when the molecule under study contains a heavy atom, for instance a 3rd row transition metal (SOC constants: $\zeta_{Ir} = 3909$ cm^{-1}, $\zeta_{Pt} = 4481$ cm^{-1}, $\zeta_{Au} = 5104$ cm^{-1}),[35] or

an external effect, when either the solvent contains a heavy atom, for example ethyl iodide (ζ_I = 5069 cm^{-1})[35] or dimethylmercury (ζ_{Hg} = 4270 cm^{-1}),[35] or the measurement is conducted under an atmosphere of a heavy gas such as xenon, (ζ_{Xe} = 6080 cm^{-1}).[35] It is the former process that is of particular interest here. The heavy atom effect occurs because electrons close to these highly charged nuclei are accelerated in their electric field to high speeds, often to where relativistic effects must be considered. These fast moving charged particles have a large magnetic field associated with them, which can couple the magnetic moment of the electron, due to its spin, with its orbital motion. The degree of SOC will, therefore, depend on the orbital angular momentum of the electron, thus it is also dependent on the type of orbital it occupies, *e.g.* an *s*-orbital has zero orbital angular momentum and so experiences zero SOC, while an electron in a *p*-orbital can contribute to the SOC. Further, it is also oxidation state dependent, which is of particular importance to transition metal phosphorescent materials. The distance between the heavy atom and the chromophore is crucial in determining the size of the SOC effect. It is worth noting that SOC is also induced when there is a large change in orbital angular momentum for example, the $\pi^* \leftarrow n$ transitions of aromatic ketones, which leads to phosphorescence emission from, for example, benzophenone.[36] Related to this is El Sayed's Rule, which states that ISC will be efficient between states for which there is a change in excited state type, for instance, ISC between the $\pi^* \leftarrow \pi$ singlet state and the triplet $\pi^* \leftarrow n$ state in benzophenone occurs extremely rapidly and has a quantum yield of unity, Φ_{ISC} = 1.0.

Oxygen is a ground state triplet molecule and can quench the emission of long lived excited states. This is of particular relevance to triplet emitters, although it can be important in long lived fluorescent molecules as well. Whilst this quenching is sometimes considered a nuisance while making spectroscopic measurements, necessitating the rigorous degassing of samples expected to have long lived excited states, the photogeneration of highly reactive and cytotoxic singlet oxygen ($^1O_2$) through such quenching has garnered significant interest for use in photodynamic therapy. In this clinical technique, $^1O_2$ is produced locally within a particular cell type or region of the body upon excitation of a photosensitiser to induce selective cell death.[37]

The concept of the quantum yield is central to molecular photophysics as it quantifies the number of molecules undergoing a particular transition or process as a ratio to the number of photons absorbed. For example, the photoluminescence quantum

yield is the ratio of the number of photons emitted to the number absorbed. Kasha's Rule[38] states that emission occurs from the lowest vibrational level of the lowest excited state, although, like most rules, this has exceptions, such as the emission from the S_2 state of azulene.[39] The justification for Kasha's Rule is that sequential IC between S_n and S_1 *via* any intermediate states is a considerably faster process than emission from these higher energy levels. This is due to the often small energy gap between high lying excited states that results in good overlap with the overtone vibrational modes of a lower energy state and allows efficient IC. For a fluorescent molecule, the S_1 to S_0 energy gap is usually much larger and, thus, emission can compete with IC to the ground state. In azulene, however, the energy gap between S_2 and S_1 is approximately the same as between S_1 and S_0 and, therefore, emission from S_2 becomes competitive with IC to S_1; in addition, there is facile IC from S_1 to S_0, depleting S_1 and emphasising the emission from S_2. The corollary to Kasha's Rule is the Kasha-Vavilov Rule that states that the PLQY is independent of the excitation wavelength. Adherence to the Kasha-Vavilov Rule can be verified for a particular compound by observing a good match between its absorption and excitation spectra.[40]

1.2. Cyclometalated iridium complexes

A cyclometalated ligand can be defined as a multidentate, chelated ligand with one or more metal–carbon covalent bonds as part of a metallacycle.[41] Typically, this is a formally anionic ligand where bonding occurs through a metal–carbon and a metal–heteroatom (predominantly nitrogen) σ-bond. The archetypal cyclometalating ligand is 2-phenylpyridine (ppyH), which is shown in Figure 1.2 as part of the neutral tris-cyclometalated complex [Ir(ppy)$_3$], first isolated in 1984 as a reaction by-product.[42] This complex can be produced either as the facial (*fac*) or the meridional (*mer*) isomer, both having a slightly distorted octahedral geometry.

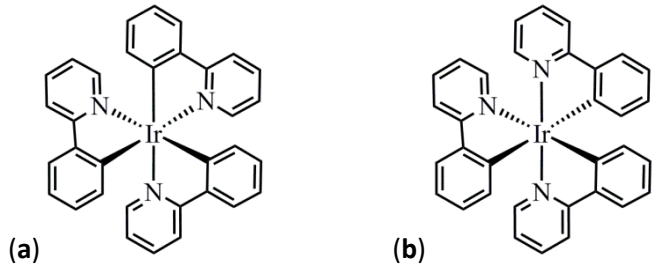

Figure 1.2. The compound tris(2-phenylpyridine-κ*N*,C$^{2'}$)iridium(III) ([Ir(ppy)$_3$]) as its (**a**) *fac* and (**b**) *mer* geometrical isomers. Both forms also exist as pairs of stereoisomers (Δ and Λ forms); however, most often these complexes are studied as racemic mixtures.

The distinction between the two geometrical isomers is important because, in general, the *fac* isomer has the more attractive photophysical properties, such as higher PLQYs (up to ten times as large) and longer lifetimes.[43] In addition, the *mer*-isomer can be considered as metastable as it can be photochemically transformed to the *fac*-isomer during device use or sample measurement, leading to a mixture of two compounds. As these isomers have very different photophysical properties, this is clearly not a desirable trait. There are, however, examples of some efficient *mer* complexes, and so these should not be excluded from study completely.[44] Each of these geometrical isomers also exists as a pair of stereoisomers (Δ and Λ), but these are rarely resolved, except as a proof of principle.[45, 46] The resolved complexes emit circularly polarised emission, with tris-cyclometalated complexes having relatively large emission dissymmetry ratios.[45] Using chiral 2-(2′-phenolate)oxazoline ancillary ligands, diastereomeric monometallic complexes have been resolved recently.[47]

The tris-cyclometalated complex [Ir(ppy)$_3$] can be synthesised by several approaches, with the most common methods summarised in Scheme 1.1. Conceptually, the simplest of these is the reaction of [Ir(acac)$_3$],[48] where acac$^-$ is deprotonated acetylacetone (acacH), with a suitable cyclometalating ligand, heated at high temperature (200 °C, step **a**). This offers a route to the *fac* isomer of [Ir(ppy)$_3$] and can be applied to other derivatives of 2-phenylpyridine,[49] although the highly forcing conditions make it incompatible with ligands having thermally sensitive functional groups. The sequential incorporation of cyclometalating ligands ensures the synthesis of the pure *fac* isomer. The strong *trans*-effect of the cyclometalated phenyl ring induces labilisation of the coordinated oxygen atom of the acac$^-$ ligand located *trans* to it and subsequent coordination of the pyridine of a second ppyH-type ligand exclusively at the

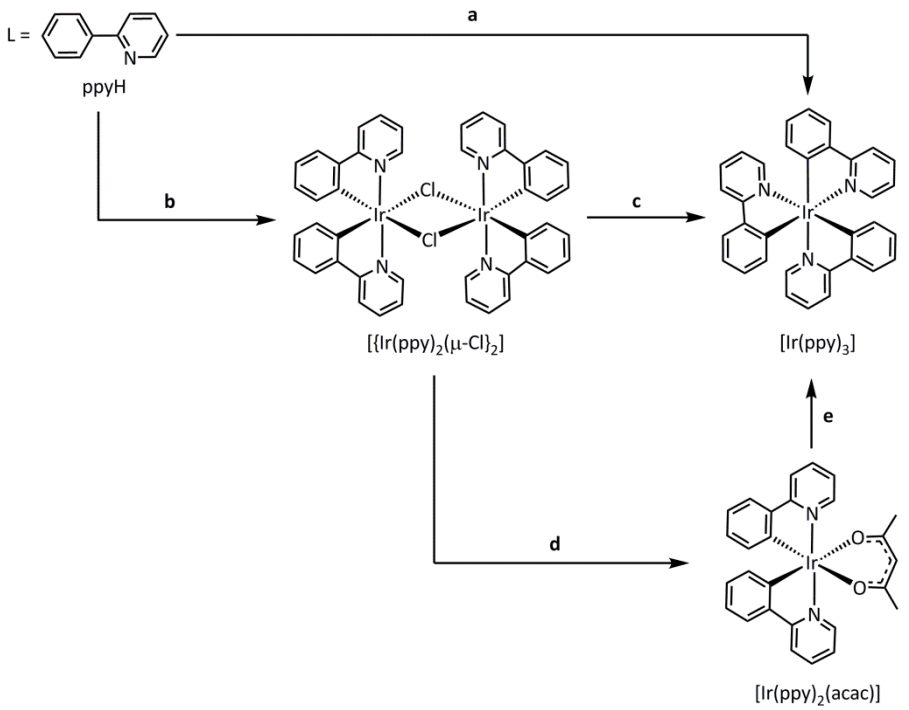

Scheme 1.1. Literature methods for the synthesis of [{Ir(ppy)$_2$(μ-Cl}$_2$], [Ir(ppy)$_2$(acac)] and [Ir(ppy)$_3$]. (**a**) [Ir(acac)$_3$], 3 eq. L, glycerol, 200 °C. (**b**) $IrCl_3 \cdot 3H_2O$, 2 eq. L, 1:1 2-ethoxyethanol:H_2O, 110 °C. (**c**) AgTFA, 2 eq. L or L′, 2-ethoxyethanol, 170 °C (*fac*) or 130 °C (*mer*). (**d**) 2 eq. acacH, K_2CO_3, 2-ethoxyethanol, 60 °C. (**e**) 1 eq. L or L′, 2-ethoxyethanol, 170 °C (*fac*) or 130 °C (*mer*).

newly generated free coordination site, leading to purely *trans* C to N arrangements. A disadvantage of this method though is the relatively high cost of commercial [Ir(acac)$_3$] or the need to synthesise it from $IrCl_3 \cdot 3H_2O$.

Probably the most widely used route proceeds *via* a bis(μ-chloro)-bridged diiridium dimer, first reported by Nonoyama *et al*.[50] and later developed by Sprouse and co-workers.[42] In this reaction, $IrCl_3 \cdot 3H_2O$ is heated to reflux with two equivalents of the cyclometalating ligand in aqueous 2-ethoxyethanol (step **b**). A silver(I) salt, typically silver trifluoroacetate (TFA^-) or triflate (OTf^-),[51] is then used as a chloride abstractor in the reaction of the dimer and a third cyclometalating ligand (step **c**). Careful control of the temperature allows the synthesis of either the kinetically preferred *mer* product (< 150 °C) or the thermodynamically more stable *fac* isomer (> 150 °C).[52] Higher temperatures are often required to generate the *fac* isomers of fluorinated ppy^- derivatives and in some cases only the *mer* isomers can be produced thermally.[53, 54] It is also possible to convert the *mer* isomer to the *fac* isomer by thermal or photochemical

methods,[55] although it is preferable to synthesise the *fac* isomer directly.[56] The thermal isomerisation process has been suggested to proceed *via* formation of an alkoxide complex intermediate and is, thus, a bimolecular process, requiring participation of the solvent.[52] The photochemical conversion is believed to be a unimolecular process in which one of the coordinating pyridine rings (in the case of ppyH-type ligands) is dissociated from the *mer*-complex to give a five coordinate trigonal bipyramidal excited state geometry that, upon relaxation to the ground state, statistically recombines to either of the two isomers.[55] Once the lower energy *fac*-isomer has been formed, the thermodynamic minimum has been reached and this isomer accumulates as the product of the photoisomerisation. Experimentally, the two isomers can be differentiated by NMR. In the case of the *fac* isomer, all of the ligands are magnetically equivalent, thus a single set of resonances is observed, whereas for the *mer* isomer, the ligands are not in the same environment and consequently have their own distinct signals in the spectrum. An example of the photochemical conversion of a *fac* isomer to a *mer* isomer of a functionalised phenyl-*γ*-carboline ligand is illustrated in Figure 1.3.[54]

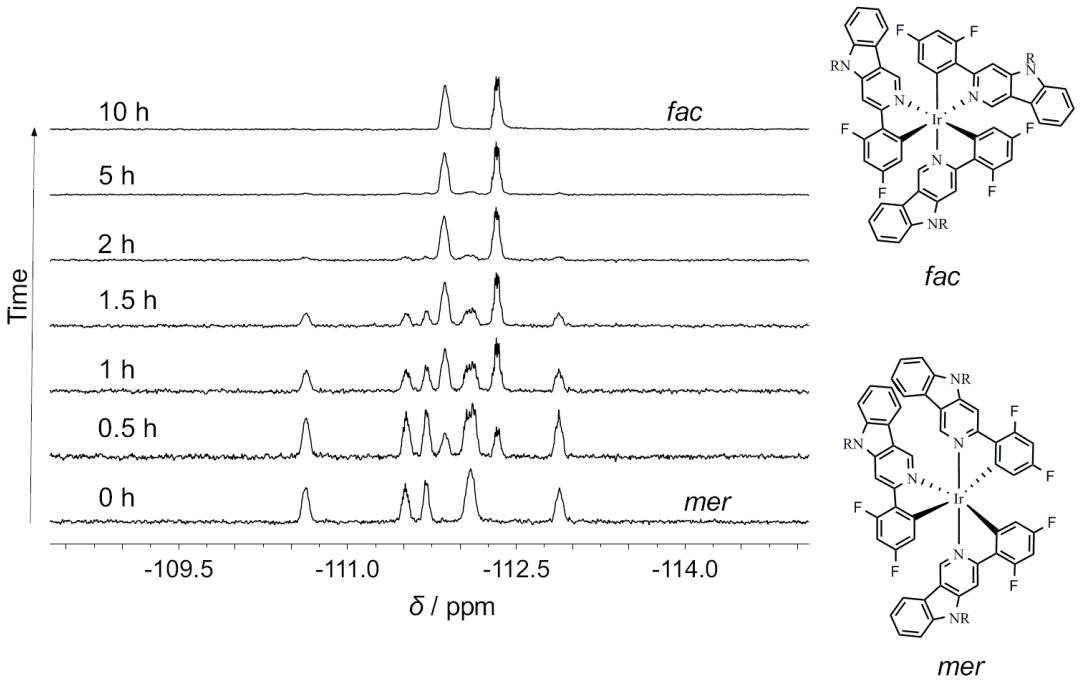

Figure 1.3. 376 MHz ^{19}F NMR spectroscopic monitoring of the quantitative photochemical conversion between the *mer* and *fac* isomers of a tris-cyclometalated homoleptic iridium complex with *N*-alkylated 2-(4′,6′-difluorophenyl)-*γ*-carboline ligands (shown right) in degassed CD_2Cl_2. The sample was irradiated by two LEDs at 365 nm (~100 mW each) positioned 2 cm from the sample for a total period of 10 h with intermittent agitation. R = 2-ethylhexyl.[54]

The route *via* the synthesis of the dimer affords an opportunity to synthesise a heteroleptic complex, which is a complex containing two or more different ligands and contrasts the homoleptic complexes of the form [IrL_3] discussed previously. This is achieved by simply heating the dimer with a different L in the second stage of the synthesis (Scheme 1.1 step **c**).[57] If the dimer is instead treated with a non-cyclometalating ligand, such as acacH in the presence of base, a different type of heteroleptic complex can be produced (step **d**). These complexes have the general form [IrL_2A], where the ligand A is termed ancillary due to its lower importance in determining the electronic, and subsequently photophysical, properties of the complex. The ancillary ligands can, however, be used to tune the energy of the metal orbitals through the spectrochemical series. Bis-cyclometalated complexes of this type are also highly efficient emitters and are simpler to produce in generally higher yield than the tris-cyclometalated analogues.[58] Other examples of ancillary ligands that may be employed are picolinate (pic^-), 2,2′-bipyridine (bpy) derivatives (to give cationic complexes)[59, 60] and pyridine, DMSO, CO or PR_3 in combination with Cl^- or CN^-.[58] It is also possible to generate anionic complexes with two CN^- ancillary ligands.[61] Complexes based on a single ppy^- and four monodentate ancillary ligands have been reported that also show similar photophysical properties to their bis- and tris-cyclometalated analogues. Thus, cyclometalated iridium complexes represent a well explored part of chemical space.

Complexes of the form [IrL_2(acac)] can also be converted to tris-cyclometalated complexes, providing a third route,[43] which may be more desirable in some cases; however, it is often lower yielding and can result in scrambling of ligands to give a complex mixture of products (Scheme 1.1 step **e**).[46]

Figure 1.4 shows the general approach taken in this work, in which the bis(μ-chloro)-bridged diiridium dimer is produced from potentially cyclometalating ligands and a third ligand, here acacH, is used to form the final complex using steps **b** and **c** of Scheme 1.1. Of particular note is the *trans* configuration of the pyridine rings and mutually *cis* arrangement of the phenyl rings in both the dimer and the final bis-heteroleptic complex. This is a result of the strong *trans* effect of the *σ*-bonded phenyl rings that results in a *trans* bridging chloride ligand. Under the mild conditions employed for the installation of the ancillary $acac^-$ ligand, this geometry is maintained

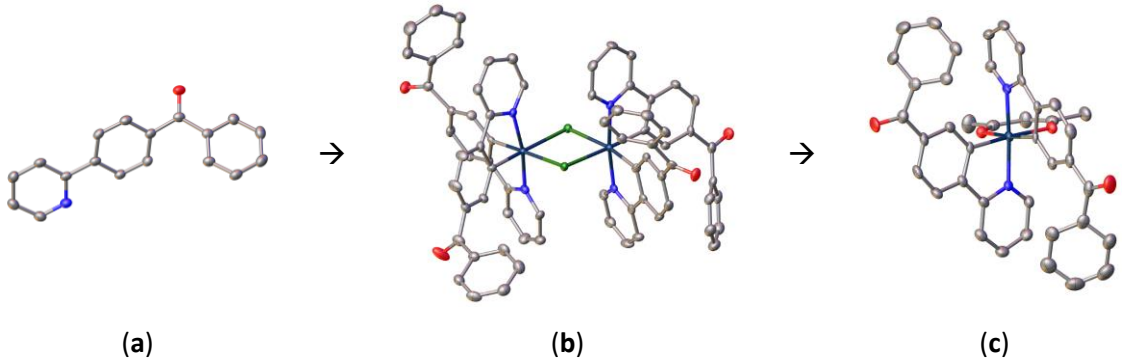

Figure 1.4. General approach in which (**a**) a cyclometalating ligand, here 4-(2′-pyridyl)benzophenone, is reacted under Nonoyama conditions[50] to give (**b**) the μ-dichloro-bridged dimer. Reaction with acetylacetone and base gives (**c**) the bis-heteroleptic complex under mild conditions with retention of the *trans* N–N arrangement.[8] Images are molecular structures obtained by single-crystal X-ray diffraction (SC-XRD). Atomic displacement parameters are shown at 50% probability. Hydrogen atoms, a second symmetry independent molecule of the ligand, three acetone solvent molecules from the dimer and a disordered $CDCl_3$ solvent molecule from the bis-heteroleptic complex are omitted for clarity.[62]

in the monomeric complex. Only in rare cases, where the ligands are bulky, do the dimers not contain this arrangement of ligands. An example of an anomaly is found upon the inclusion of benzylsulfonyl groups at the 4-position of the phenyl ring of a ppy-type ligand where the dimer adopts a geometry having one pair of *cis* and one pair of *trans* carbon and nitrogen atoms.[63] It has also been shown that sublimation of certain bis-cyclometalated complexes with pic^- ancillary ligands can result in a rearrangement leading to a *cis* pyridine configuration of the ppy^- ligands. Thus, the pyridine ring of one of the ppy^- ligands is *trans* to the pyridine ring of the pic^- ligand and the other is *trans* to the phenyl ring of the second ppy^- ligand.[64]

The key to understanding cyclometalated iridium compounds, from a photophysical point of view, is knowledge of their electronic distribution in the ground and excited states. While spectroscopic studies allow a certain degree of experimental determination of these distributions, theoretical studies are becoming increasingly recognised as an important complementary and supporting approach to this problem. Undoubtedly, density functional theory (DFT) calculations have taken a central role in this regard due to their relatively good agreement with experimental data at a reasonable

computational cost; indeed, it is rare to find a paper in the field nowadays that does not call upon theoretical calculations to gain a deeper insight into some experimental result. Early DFT calculations performed by Hay[65] on [Ir(ppy)$_2$(bza)], where bzaH is 1-benzylbuta-1,3-dione, revealed that the HOMO resides predominantly on the phenyl ring and the metal, while the LUMO is almost completely based upon the pyridine moiety, and comparable distributions for [Ir(ppy)$_2$(acac)] are depicted in Figure 1.5.[i] This has been further corroborated by similar calculations on many other complexes.[66] Population of the T_1 state is facilitated by the large SOC of iridium by direct absorption from the S_0 ground state and by highly efficient ISC from the S_1 excited state (quantum yield of ISC $\Phi_{ISC} \approx 1$) that occurs in less than 100 fs.[67, 68] As implied by the name, the triplet state is composed of three sublevels, which, in the case of [Ir(ppy)$_3$], are separated by only 83 cm^{-1}.[69] These three sublevels of [Ir(ppy)$_3$] have different photophysical properties, for example, their lifetimes span two orders of magnitude (τ = 750 ns, 11 μs and 145 μs). It is the average behaviour of the triplet state that is observed at room temperature, and even at 77 K, weighted for the Boltzmann distribution of the sublevels (τ = 1.6 μs); however, the individual sublevels can be important at extremely low temperatures or in the presence of strong magnetic fields.[7] In general, these more subtle effects are not of great consequence to this work and are not considered here further.

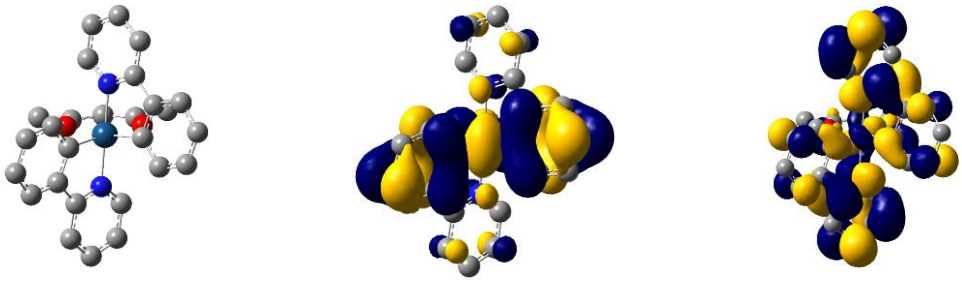

[Ir(ppy)$_2$(acac)] HOMO LUMO

Figure 1.5. DFT (B3LYP/6-31G(d)/LANL2DZ) calculated HOMO and LUMO of the compound [Ir(ppy)$_2$(acac)].

[i] Both here and elsewhere in this work, DFT calculated Kohn-Sham orbitals are used synonymously with molecular orbitals and their distributions and relative energies discussed qualitatively.

The T_1 states of cyclometalated Ir(III) complexes are often described as a metal-to-ligand charge-transfer (MLCT) state in which there is significant redistribution of electron density from the metal centre to the ligand.[69] However, the excited states of these complexes should be regarded as being much more mixed in character and instead be described by a linear combination of MLCT, ligand-centred (LC) $\pi^* \leftarrow \pi$ transitions and intraligand charge transfer (I^{ra}LCT) (**7**):[10]

$$\Psi = a\psi_{MLCT} + b\psi_{LC} + c\psi_{I^{ra}LCT} \quad (\mathbf{7})$$

where the weighting coefficients *a*, *b* and *c* are determined by the nature of the substituents on the complex and their effect on the ground state electronic distribution and excited state redistribution. This formulation is intended to be very flexible, allowing descriptions of the excited states that range from purely one transition type through to a mixture of all three types. In addition, the absorption spectra of cyclometalated iridium complexes are often assigned as being composed of individual LC and MLCT bands with the MLCT transitions placed at lower energy. This assignment does not always truly reflect the character of the transitions and may also belie the high density of potentially accessible excited states that can produce significantly overlapping bands. The designation of absorption bands as being of a particular type has often been based on theoretical and experimental studies of the parent complex [Ir(ppy)$_3$] and related compounds,[65] with the assumption that assignment by analogy will hold. Moreover, the singlet or triplet nature of these transitions may not be defined absolutely due to the large SOC induced by the iridium atom; notwithstanding this, bands will be referred to as formally singlet or triplet here for simplicity.

As a further complication, interligand charge transfer (I^{er}LCT) excited states are sometimes possible wherein excitation between two ligands occurs. I^{er}LCT is, however, usually of lower importance than the other three named contributions in the description of the initial excitation for neutral Ir complexes. Furthermore, metal centred (MC) $d(e_g^*) \leftarrow d(t_{2g})$ transitions have not been included in (**7**). These transitions are weak due to the Laporte selection rule that requires a change of parity in the transition, whilst *d-d* transitions retain *gerade* symmetry (note this rule is not completely applicable as the complexes are not truly centrosymmetric). In addition, as a third row transition metal, Ir has a large octahedral splitting parameter, enhanced further by the high field

2-phenylpyridine ligands that cause the MC transitions to be very high in energy. MC states can become important though for blue emitters where they may be thermally accessible from a lower lying MLCT/LC excited state and provide a non-radiative relaxation pathway. The use of high field ancillary ligands, such as *N*-heterocyclic carbenes, induces a rise in the energy of the MC state, diminishing its role in non-radiative deactivation.[70]

Time-dependent DFT (TD-DFT) calculations point to highly complicated multi-component excited states that involve not only the frontier HOMO and LUMO orbitals, but also HOMO-*N* and LUMO+*N* orbitals.[71] Experimentally, a greater contribution from a ^{3}MLCT state can be observed by a broad emission profile that exhibits a positive solvatochromic shift. A large ^{3}LC state participation meanwhile is evinced by long pure radiative lifetimes, a sharper emission profile having vibrational structure and an emission spectrum that is virtually insensitive to solvent polarity. The solvatochromic shift for a charge transfer state, such ^{3}MLCT or ^{3}I^{ra}LCT, is a result of a change (typically increase) in the dipole moment from the ground state to the excited state. Around this new dipole, the solvent sphere relaxes, lowering the energy; the energetic stabilisation from this effect is greatest for more polar solvents, bathochromically shifting the emission in the case of positive solvatochromism. The longer lifetime of the ^{3}LC state is due to both a smaller metal contribution to the state and a smaller orbital momentum change, resulting in less SOC, which makes the phosphorescence less allowed.[16]

Absorption,[72, 73] electroabsorption[74] and Raman studies[75] of d^6 [Ru(bpy)]$^{3+}$ show that the excited state resides on a single ligand. Further, transient absorption spectroscopic studies have shown that absorption initially results in charge delocalisation across all three ligands before relaxation occurs to leave the excited state located on a single ligand. It is conjectured here that a similar process occurs in Ir(III) complexes. In the case of a heteroleptic complex, the excited state populates the lowest energy ligand available and thus the emission wavelength is determined almost completely by the energy of this ligand. However, it is not completely resolved as to how this localisation is manifested when there are two or more degenerate ligands on a complex. Only a small geometric change causes localisation on a particular ligand and during the relatively long lifetime of these excited states, further thermally activated geometric variation would be expected, which might lead to a shift in the localisation

from one ligand to another in a dynamic process. This is somewhat reminiscent of a Jahn-Teller distortion where orbital degeneracy is lifted by geometric perturbation, *e.g.* by elongation of a bond in a particular direction.

It is worthwhile comparing the photophysical properties of cyclometalated iridium complexes with complexes containing terpyridine-type ligands, $[Ir(N\hat{}N\hat{}N)_2]^{3+}$. Not only does this result in charged species, which, from the point of view of application in OLED devices, is undesirable due to drift upon application of an electric potential, but it also influences the photophysics substantially. The electron density at the metal centre is lower in the absence of the strongly σ-donating, formally anionic phenyl component of the ppy^- ligand, which makes MLCT less favourable, resulting in almost completely ligand-based transitions. Consequently, the excited state lifetimes of this type of complex are generally much longer due to the small metal contribution and low SOC. Such long lifetime complexes are favourable for imaging and sensing applications due to the ease with which the emission can be time-gated to remove autofluorescence. When the N^N^N ligand is increased in conjugation, the lifetime also increases. There is a well developed chemistry of C^N^N, N^C^N, C^C^N and C^N^C[76, 77] type ligands with somewhat intermediate and specific photophysical properties, including a greater prevalence of I^{er}LCT.[78] One key structural difference between complexes with terdentate and bidentate ligands is that the former are achiral: a property that is particularly appealing for avoiding diastereoisomerism in the construction of multi-metallic assemblies with potentially long lived, charge-separated excited states for photovoltaic applications.[79] Cationic complexes have recently been gaining renewed interest for use in light-emitting electrochemical cells (LECs or sometimes LEECs),[80] which are an alternative to OLEDs with potentially simpler devices, requiring fewer layers and all-solution processing.[81] The major drawback of LECs is their long turn on times (seconds for the best devices, but more typically minutes to hours) as a result of the need for charge migration of the complex and its counterion to opposite electrodes before the device becomes efficient. This problem has yet to be fully resolved.[82]

The major impetus to study these compounds has been their utility as the light-emitting component of OLEDs, and so it is useful to briefly discuss their use in this regard. In a very basic three layer device, an emissive layer (molecular or polymeric) is sandwiched between a transparent anode, such as indium tin oxide (ITO),

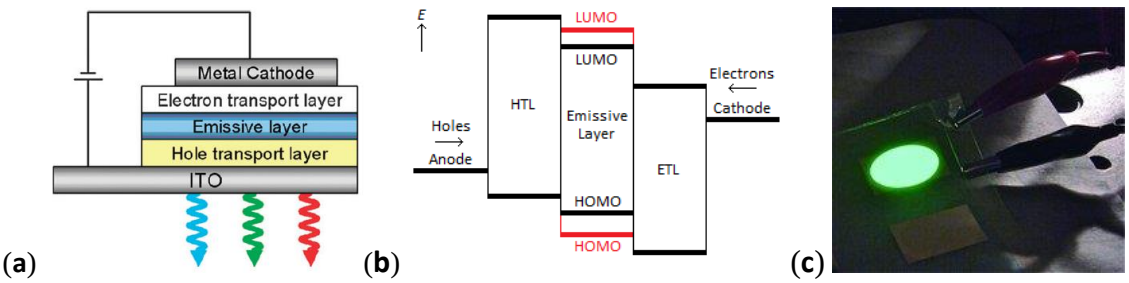

Figure 1.6. (**a**) A basic OLED structure. Reproduced from reference 83. (**b**) Energy levels of a basic device. The HOMO and LUMO levels in red refer to those of the host material. HTL and ETL refer to the hole and electron transporting layers, respectively. (**c**) An operating device. Reproduced from reference 84.

and a low work function metal cathode. Upon application of an external electrical bias, holes are injected at the anode and electrons at the cathode, and current flows between the electrodes (Figure 1.6). As the electrons and holes migrate through the device, they may form a bound pair known as an exciton. These are essentially electrically produced excited states and, therefore, may be either singlet or triplet in character, obeying the same spin statistics given by the spin wavefunctions in equations (**3**).[85] However, because the excitons are produced electrically, they are not subject to the spin selection rules that govern optical transitions; hence, a purely statistical 3:1 triplet:singlet ratio is expected to be formed (this ratio has been contended by Monkman and co-workers who concluded that a 44% yield of singlet states is produced[86]). When conductive organic polymers, *e.g.* poly(*p*-phenylene vinylene), or fluorescent molecules are used as the emissive components, only singlet excitons may radiatively combine because the spin selection rule does apply to the emission. By incorporating a phosphorescent heavy metal compound, such as a cyclometalated iridium complex, into the device, triplet excitons can also be harvested. The inclusion of compounds of this nature can theoretically increase the internal quantum efficiency from 25% (purely singlet exciton emission) to 100% (singlet and triplet emission). The complex $[Ir(ppy)_3]$ was the first of many cyclometalated iridium complexes to be utilised successfully in an OLED with an efficiency of 3.3% in a fairly optimised device.[14] This approach uses the Ir complex in a cascade Förster resonance energy transfer sequence: energy is transferred from the initially-formed high lying excited state of the organic matrix to a lower lying excited state of the complex that then emits. Although this was the original design, it was

argued that this was only appropriate for green to red emission and that it would be hard to produce good blue emitters due to the necessity of having an even higher energy host.[87] Alternatively, the complexes can be used as the sole emitting species so that excitons are formed upon them directly and can thus emit with both higher energy and efficiency, although even then it is crucial to have a high triplet energy host in order to avoid quenching of the luminescent complex.[88] To produce a truly practical device requires further modification of its structure, namely, a move to a multi-layer design to modulate the hole and electron migration.

The ease with which the emission energies of cyclometalated complexes can be tuned in a quasi-predictable manner makes them particularly attractive as triplet emitters for OLEDs. The approach to modulate the emission energy taken by many researchers has been to consider the emission of Ir complexes as being crudely described by a LUMO → HOMO transition (ground state orbital labels) and identify methods to tune the energies of these two orbitals independently. The relatively decoupled spatial extent of the HOMO and LUMO makes such an approach feasible: certain substitution patterns preferentially impact the energy of one orbital over the other. For instance, introducing electron withdrawing groups, often fluorine substituents, onto the phenyl moiety of a ppy^- derivative lowers the HOMO energy of the complex and consequently hypsochromically shifts the emission. By making the phenyl portion more electron-rich, a bathochromic shift can be achieved. Independently, the LUMO energy can be tuned by adjustment of the pyridyl portion of the ligand. In particular, extending its conjugation lowers the energy of the LUMO and, accordingly, the emission. Conversely, electron donating groups on the pyridyl moiety increase the orbital energy gap.[89] Thus, using simple design rules, it is possible to produce complexes of almost any desired emission colour. To illustrate this tuning effect, Figure 1.7 summarises some simple ligand modifications that lead to complexes whose emission maxima span the complete visible spectrum.

Although this has been a particularly productive line of enquiry, it is not the only means to affect colour tuning. Success has also been achieved with the introduction of various main group electron accepting moieties upon the phenyl portion of the ppy^- ligand, changing the spatial confinement of the LUMO from the pyridyl ring to this new group.[12] With this strategy, tuning is possible across a wide range of wavelength between 505 and 609 nm, corresponding to green through to red light.

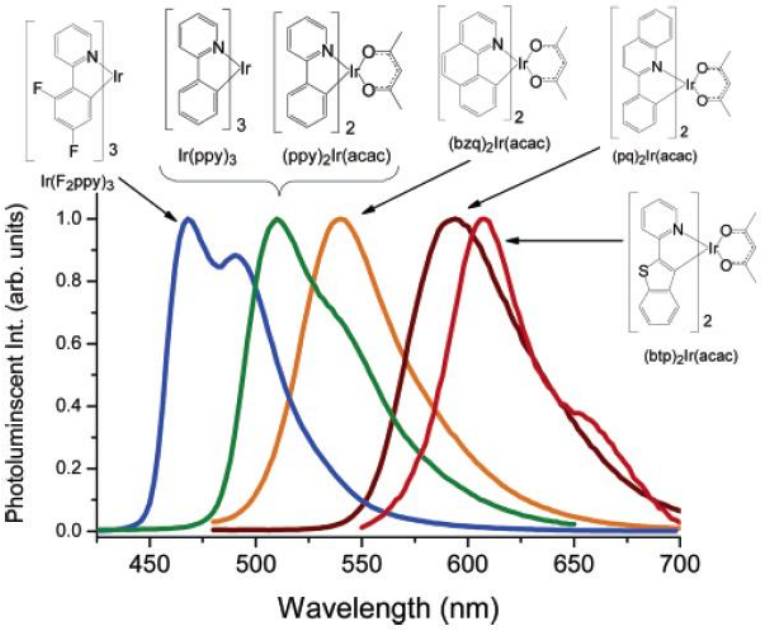

Figure 1.7. Tuning the emission of cyclometalated iridium complexes by ligand modification. Reproduced from reference 70.

Especially challenging is the synthesis of complexes with peak emission at the extremes of the visible range.[90] As already mentioned, blue emitting Ir complexes can suffer from coincidental ^{3}MC and ^{3}LC or ^{3}MLCT-type excited states that can lead to thermal population of the non-emissive ^{3}MC states. This can be overcome by the incorporation of strong field ligands that raise the energy of the pseudo e_g* orbital set. Exchange of the pyridyl moiety for a more electron rich heterocycle, such as 1,2,4-triazole,[91] can also be a viable approach to the synthesis of blue emitting complexes. Another approach is based on dendritic structures, in which a high energy iridium complex is hosted at the core, leading to reported PLQYs as high as 0.94.[92] As well as providing steric protection to the excited state of the Ir complex that leads to a reduction in k_{nr}, the dendron can act as a high energy host, allowing devices created from neat amorphous films of the complex to be produced. However, it is questionable as to whether such intricate and difficult to synthesise species are of any practical use for mass production when large quantities of the material may be required.

At the other end of the spectrum, production of highly emissive red phosphors is also problematic. Here the issue derives from the energy gap law that states, within a set of structurally related compounds, as the energy between the excited state and the ground state is decreased, the efficiency of non-radiative internal conversion or back

intersystem will increase. This is due to a greater Franck-Condon overlap between the vibrational levels of the two states. By comparing a series of related complexes it has been shown that this law holds for cyclometalated Ir(III) complexes.[93] It has been suggested that rigidification of the complex and strengthening of the cyclometalated Ir–C bond while avoiding ^{ra}LCT transitions should lead to higher PLQYs.[90] Low energy emission can also be achieved through modification of just one ligand,[94] as shown for [Ir(fppy)(ppy)$_2$], which has very similar photophysical properties to [Ir(fppy)$_3$].[57] This is certainly a factor in favour of tuning the red emission as 'expensive' novel ligands are used in smaller quantities.

The intermediate bis(μ-chloro)-bridged diiridium dimers tend to be only weakly emissive due to low lying, non-emissive ^{3}MC states that can be thermal populated (*e.g.* [{Ir(ppy)$_2$(μ-Cl)}$_2$] Φ = 0.005).[95] However, with suitable low energy cyclometalating ligands[59] or substitution of the chlorides with an isolobal pseudo-halide[96, 97] such as NCO^-, or by substitution with a pyrazolyl bridging ligand[98] the PLQY can be increased, although only green or red emitting dimers are likely. This opens a further avenue of study of these compounds for OLEDs due to their relative ease of synthesis (they require one step fewer). However, they exist as a mixture of diastereomers (Δ,Δ; *meso*-Δ,Λ; Λ,Λ), which is less attractive because of the potentially different physical and photophysical properties for the different isomers. Separation of these isomers also presents a significant challenge.[99]

It is worth comparing the properties of Ir(III) complexes with those of other late transition metal phosphors, a selection of which are summarised in Figure 1.8.[ii] The most obvious comparison to make is to the next lightest congener of iridium, rhodium. The complex [Rh(ppy)$_3$] (**A**) was prepared at the same time as [Ir(ppy)$_3$] and has a similar absorption spectrum, albeit without the low energy singlet-to-triplet bands. In contrast, it is only weakly emissive at room temperature, gaining intensity when cooled. The excited state of [Rh(ppy)$_3$] is similarly described by a mixture of ^{3}LC and ^{3}MLCT, the latter of which shortens the emission lifetime, relative to other Rh complexes, to 46 μs at 77 K (*cf.* [Ir(ppy)$_3$] 5 μs at 77 K).[51] The value of ζ_{Rh} = 1200 cm^{-1} is significantly lower than that of Ir and so SOC is considered less efficient in this system. It has also

[ii] References in this section are limited to some recent examples or reviews of each class and are not intended to be comprehensive.

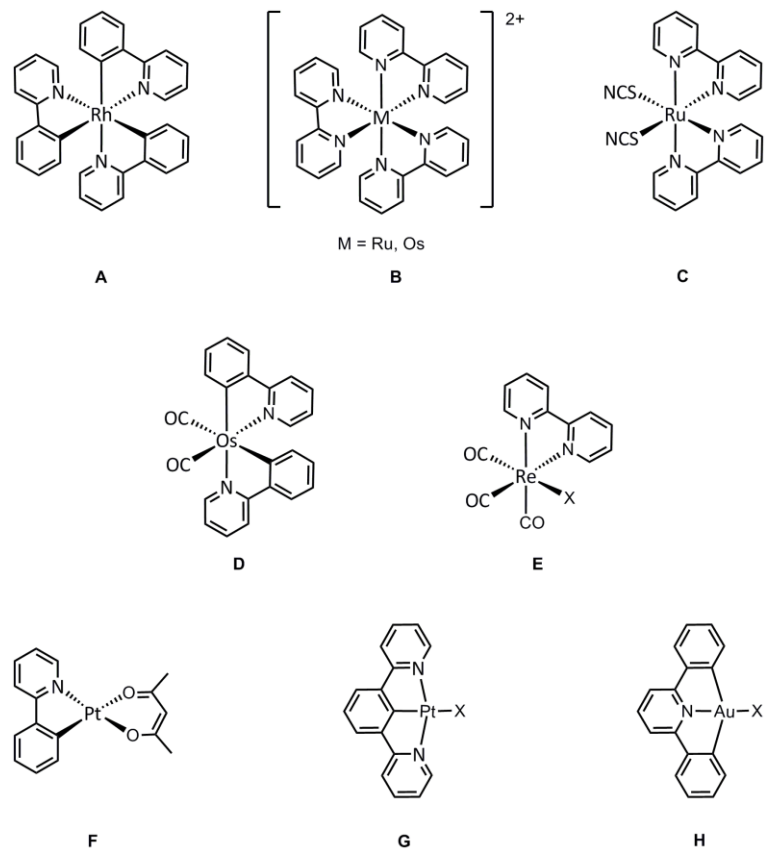

Figure 1.8. Structures of the more widely studied classes of luminescent d^6 and d^8 complexes reported in the literature. From the core motifs shown, many different complexes have been produced by derivatisation of the chelating aromatic ligand or by variation of X.

been reported that in related cyclopentadiene Rh complexes that the heavy atom effect is not seen at all, leading to the observation of pure fluorescence.[100]

Probably the most well studied systems, and some of the first to be studied in detail, are those based on Ru(II) with bpy derivatives as ligands (**B**), whose emission tends to be lower in energy than similar Ir(III) complexes and is almost purely ^{3}MLCT in nature.[101] Thus, although the SOC constant of Ru (ξ_{Ru} = 1042 cm^{-1}) is much lower than Ir, and similar to the often weakly emissive Rh, the inherent metal character of the transition makes phosphorescence fairly allowed and, subsequently, relatively short lived. The related neutral Ru(II) bis(bpy) complexes with thiocyanate ligands (**C**) and related compounds have been used extensively in the search for suitable photosensitisers for DSSCs.[102] Analogous bpy-ligated Os(II) complexes (ξ_{Os} = 3381 cm^{-1}) (**B**) have also been studied for their emissive properties; however, they suffer from a limited tuning range of the emission wavelength, with species emitting at

the red end of the visible spectrum being fairly simple to design, but higher energy examples being more challenging. The efficiency of the emission of these species is limited by the energy gap law at low energy. The use of the ligand ppy^- and its derivatives in combination with carbonyl ligand, leads to moderate hypsochromic shifts in the emission maxima (**D**).[103] The design of Os(II) complexes having emission maxima below 530 nm is still challenging.

Although not based on a PGM, complexes of d^6 Re(I) have elicited significant research interest as luminescent materials and, thus, are included here. In particular, $Re(CO)_3LX$ type systems (**E**) are well known, where L is typically a bpy derivative and X is a halogen[104] or alkynyl ligand[105] to give a neutral complex or where X is a neutral ligand, such as a substituted pyridine[106] or phosphine,[107] to give a charged complex. These compounds have been found to be both relatively stable and highly emissive (typically from a ^{3}MLCT state). These features make them suitable for use as imaging agents, photosensitisers and sensors.[108]

In addition to d^6 systems, square planar d^8 Pt(II) complexes have been investigated extensively, including those based on ppy^- (**F**)[109] and related terdentate ligands (**G**).[110, 111] They exhibit similar excited states to their Ir analogues, but often with longer excited state lifetimes. Such planar compounds can also form excimers that emit at a longer wavelength than the complex monomer. If a suitable mixture of monomer and excimer is formed, then white emission can be observed, and such systems are of interest for solid state lighting.[111] Isoelectronic Au(III) complexes having terdentate ligands (**H**), have gained some renewed interest lately for their emissive properties.[112] Strong field ligands are required to destabilise ^{3}MC transitions and a rigid structure is required to reduce k_{nr}, but once these two conditions are met, reasonable luminescence can be achieved from mixed $^3I^{ra}$LCT/^{3}MLCT excited states.

While there has been much development in the use of the PGM emissive components in the formation of OLEDs, there has also been a recent trend to utilise more Earth-abundant first row transition metals, such as Cu(I), which can also exhibit phosphorescence from certain complexes.[113] Taking this line of enquiry to the extreme and removing the requirement for a metal completely would be most beneficial. Adachi, one of the early developers of cyclometalated Ir complexes,[8] has advocated a new approach to harvest triplet excited states. It is proposed that a suitable organic fluorescent molecule with a small singlet-triplet energy gap should be able to convert

the usually wasteful triplet excitons to emissive singlet excitons through the mechanism of thermally activated delayed fluorescence (E-type fluorescence) and some success with this method has already been achieved.[114-116] This may well become a productive line of inquiry for the discovery of efficient and cheap materials for truly organic light emitting devices in the near future. However, for the moment at least, it is argued that the cyclometalated Ir complexes of King and co-workers[42] still reign as the most versatile phosphors for OLEDs.

1.3. Palladium-catalysed carbon-carbon cross-coupling reactions

During the course of this work, palladium-catalysed reactions have been used extensively for the synthesis of functionalised ligands. It is therefore instructive to review some of the salient features of this type of reaction and to describe the general synthetic strategy employed.

There exists a multitude of Pd-catalysed C–C bond forming reactions and the importance of this methodology was recognised in 2010 by the award of the Nobel Prize in Chemistry to R. Heck, E.-i. Negishi and A. Suzuki for the discovery of three eponymous variants. These reactions are fairly well understood in general terms, although full understanding of some of the specific details of their catalytic cycles remains elusive. Having elicited significant research effort in the past 35 years, their use is now ubiquitous, both in academia and in industry. The generic reaction (Figure 1.9) begins with the oxidative addition of an electrophilic R–X species to a Pd(0) species that is typically 14 electron. The identity of X is commonly either a halide (Cl, Br or I) or triflate (CF_3SO_3), and R can be any one from a wide variety of acyl, alkenyl, alkyl (although hard for systems with β-hydrogen atoms), alkynyl, allyl, aryl or heteroaryl groups, depending on the specific reaction being considered. Transmetalation of a second, nucleophilic coupling partner R′–M (where M is a metal (Mg, Zn, Sn or Cu), metalloid (B or Si) or, less commonly, a proton) to the oxidised, now Pd(II), catalyst then occurs with elimination of M–X. The group R′ has essentially the same scope as R, making these reactions very versatile and of wide ranging utility. Finally, reductive elimination of the cross-coupled product R–R′ regenerates the Pd(0) catalyst before a new cycle begins. The identity of the nucleophilic coupling partner essentially defines the reaction sub-class and some key examples are summarised in Table 1.1.

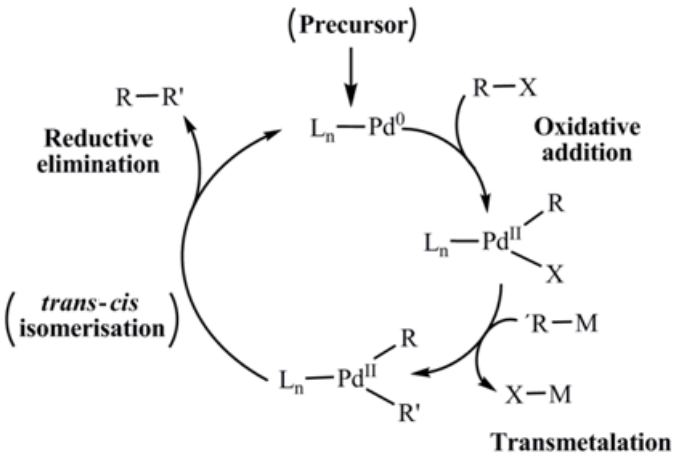

Figure 1.9. Catalytic cycle for a generic Pd-catalysed cross-coupling reaction.

Table 1.1. Key Pd-catalysed cross-coupling reactions, which have been classified by the identity of the nucleophilic coupling partner, R′-M. Those listed in bond typeface have been used during the course of this work.

R′–M	**Reaction name**
R′–MgBr	Kumada[117]
R′–SiR″$_3$ + F$^-$ or R′–SiR″$_2$OK	Hiyama[118]
R′(R″)–C=C–(R‴)H	Mizoroki-Heck[119, 120]
R′–ZnX	Negishi[121]
R′–C≡C–Cu (formed *in situ*)	**Sonogashira-Hagihira**[122]
R′–SnR″$_3$	**Stille**[123]
R′–B(OH)$_2$, R′–B(OR)$_2$ or R′–BF$_3$K	**Suzuki-Miyaura**[124]

In addition to illustrating the major steps of oxidative addition, transmetalation and reductive elimination in a generic Pd-catalysed cross-coupling reaction, Figure 1.9 also introduces the concept of using a catalyst precursor. The catalyst precursor may be of a different oxidation state to the resting state of the active catalyst and be converted *in situ* to the active form. Pd(II) pre-catalysts are normally favoured because they are more stable to air and moisture and are therefore easier to handle than Pd(0) alternatives. Additional steps in the catalytic cycle may be required, such as isomerisation from the *trans* configuration formed upon transmetalation to the *cis* arrangement, which is necessary for reductive elimination and which probably occurs *via* a ligand dissociation/association mechanism. The number of ligands coordinated to the metal centre, L_n, depends principally on the steric demand of the ligands. The ligands are

typically strong *σ*-donors, commonly phosphanes (trivial name: phosphines), with triphenylphosphane being the most common of all. When this ligand is used, two phosphanes are expected to be coordinated to the Pd, giving an active 14 electron species. Other classes of ligand such as *N*-heterocyclic carbenes,[125] have also been used to good effect with these more electron donating ligands enhancing the rate of oxidative addition. The number of ligands coordinated to the active catalyst is more than just a mere detail as it can influence both the steric and electronic properties of the catalyst and, therefore, its propensity to oxidatively add a particular substrate and reductively eliminate the product. For difficult cases, bulky and electron donating phosphane ligands, such as the *ortho*-biaryl phosphanes developed by Buchwald,[126] have been found to be particularly effective. The use of these ligands leads to monoligated, 12 electron species due to steric constraints,[127] and are partially stabilised by Pd···*π* interactions with the *ortho*-phenyl group.[128] These PdL compounds are even more coordinationally unsaturated and more nucleophilic than those formed using PPh_3. This also makes reductive elimination from the intermediate 14 electron [Pd(II)LRR′] species more favourable. These phosphanes have a weaker M–P bond than phosphanes of a smaller cone angle, increasing their lability. Advantageously, *trans-cis* isomerisation is obviously unnecessary in the monoligated case. Therefore, these are particular good catalysts for R–Cl electrophiles, sterically hindered R–X species and other challenging substrates.

The Sonogashira-Hagihara (herein Sonogashira) coupling of a terminal acetylene and arylhalide is the Pd-catalysed reaction that has been used predominantly in this work. Two excellent and extensive reviews of this reaction, its mechanism and its use in synthesis have been published by Chinchilla and Nájera.[129, 130] The general Pd-catalysed coupling mechanism of Figure 1.9 is expanded and explicitly illustrated for the case of the Sonogashira reaction in Figure 1.10. In an abridged form, the Sonogashira reaction proceeds *via* oxidative addition of a haloarene onto a ligated palladium species followed by transmetallation of a copper acetylide, formed *in situ*, and reductive elimination of the cross-coupled arylacetylene product. The formation of the copper acetylide cannot occur by simple deprotonation by the bases typically used, such as secondary and tertiary amines, for example triethylamine or Hünig's base (pK_as: phenylacetylene ≈ 29, NEt_3H^+ ≈ 11); therefore, it has been proposed that activation of

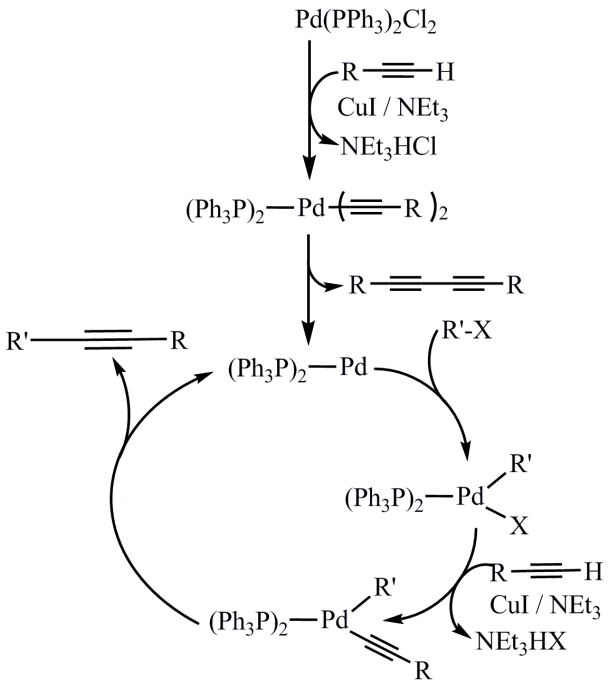

Figure 1.10. Catalytic cycle of the Sonogashira cross-coupling reaction.

the acetylene *via* η^2-coordination of copper iodide to the acetylene occurs first, weakening the C–H bond and facilitating formation of the copper acetylide.[131, 132]

The reaction can be conducted with a variety of different catalyst precursors and ligand combinations. The two catalysts predominantly used in this study are the common complexes $[PdCl_2(PPh_3)_2]$ (as its *cis* isomer) and $[Pd(PPh_3)_4]$, the first of which is an air-stable Pd(II) species capable of being reduced *in situ* by a stoichiometric homo-coupling of two terminal acetylenes.[133] In the presence of oxygen the generated Pd(0) species is re-oxidised to Pd(II), catalysing the undesired homo-coupling faster than the cross-coupling, necessitating the use of an inert atmosphere.[133] The latter is an air-sensitive Pd(0) catalyst that will not produce the diyne side product in the absence of oxygen, but is slightly more difficult to handle and store. The catalyst $[PdCl_2(PPh_3)_2]$ was selected when the cross-coupled product was of significantly different polarity to the homo-coupled product, allowing facile separation of the expected diyne side product from the desired cross-coupled product. It was also used when trimethylsilylacetylene was one of the coupling partners because the deprotected form of the homo-coupled product, butadiyne, is a gas and easily eliminated from the mixture in the next step of the synthesis. The nature of the haloarene is important in determining the rate of the reaction, with iodoarenes being easier to oxidatively add to Pd(0) than

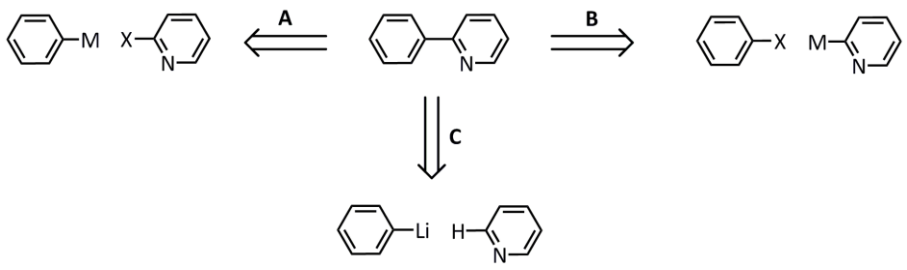

Scheme 1.2. Simplest disconnections of a 2-phenylpyridine ligand that were considered in this work, where X is a halide or pseudohalide and M is either a $B(OH)_2$ or SnR_3 group. Note that the phenyl, pyridyl or both portions of the ligand could be functionalised at various positions.

bromoarenes, while chloroarenes typically can only be used with bespoke electron donating ligands. Electron donating groups on the arene retard the rate of reaction by making the substrate more electron-rich and more difficult to oxidatively add to palladium; thus, iodinated arenes were preferred in such cases, where available.

In the synthesis of substituted phenylpyridine ligands, various disconnections were considered, which are summarised in Scheme 1.2. One potential disconnection is to an electrophilic 2-bromopyridine derivative and a nucleophilic phenylboronic acid or stannane that can be coupled *via* Suzuki-Miyaura or Stille reactions (**A**). A second approach is disconnection to 2-(tri-*n*-butylstannyl)pyridine or 2-pyridylboronic acid and an arylhalide (**B**). The final method considered was direct phenylation at the 2-position of a pyridine derivative with phenyllithium (**C**). When the desired ligand contained an otherwise unsubstituted pyridine ring, route **B** was typically employed using 2-(tri-*n*-butylstannyl)pyridine. Although organo-tin compounds are potentially toxic, this pyridine derivative is a stable and easily prepared species, which is in contrast to 2-pyridylboronic acid that is difficult to synthesise[134] and requires stabilisation as the less active boronate ester.[135] The Stille cross-coupling reaction of a stannane and an arylhalide or pseudohalide proceeds *via* the generic Pd cross-coupling mechanism depicted in Figure 1.9.[136] The reaction was conducted with the same catalysts as used for the Sonogashira reaction, *viz*. $[Pd(PPh_3)_4]$ or $[Pd(PPh_3)_2Cl_2]$. While the reaction does not require a co-catalyst, additives such as CuI or LiCl are often added in stoichiometric quantities as they are believed to activate the stannane and enhance the reaction yield.[136] Such activation of the stannane can be important in cases where there is limited difference in the rate of transmetalation of the R groups.[137] The Stille reaction can suffer from homocoupling, both of the stannane, but also more unusually of the electrophilic

partner due to scrambling between the Pd and Sn centres. Protodehalogenation and protodestannylation are other potential deleterious processes.[137] Despite several potential unwanted side reactions, the Stille coupling can be regarded as a fairly efficient and robust method and hence its use in this work. Route **B** was usually selected over route **A** because it is considered more divergent, using the stannane as a common intermediate to several derivatives.

Route **C**, direct phenylation with phenyllithium, was typically only selected when a 2-phenylpyridine derivative additionally substituted in the 4-position of the pyridine was the synthetic target. While this direct phenylation was not particularly high yielding, it circumvented the need to synthesis the more challenging 2,4-disubstituted pyridine derivatives required for use in the cross-coupling reactions of routes **A** and **B**. The regioselectivity of this reaction is also enhanced by having a substituent already at the 4-position of the pyridine.

1.4. Conclusion and outlook

The study of cyclometalated iridium complexes has received an enormous growth in attention over recent years and is rapidly becoming a mature field. Despite this, some fundamental aspects of their photophysics are not fully understood and they therefore deserve continued study. In this work, several ligands have been designed, synthesised and coordinated to iridium. The photophysics of these ligands and their complexes has been studied in detail, and aided by computational, structural and electrochemical studies, been placed in the context of related literature compounds. In addition, the tris-heteroleptic class of cyclometalated iridium complexes is introduced and the two-photon absorption spectroscopy of iridium-lanthanide dyads is described.

1.5. References

1. V. Balzani and S. Campagna (Eds), *Top. Curr. Chem. 280: Photochemistry and Photophysics of Coordination Compounds I*, Springer, Berlin and Heidelberg, Germany, 2007.
2. V. Balzani and S. Campagna (Eds), *Top. Curr. Chem. 281: Photochemistry and Photophysics of Coordination Compounds II*, Springer, Berlin and Heidelberg, Germany, 2007.
3. H. Le Bozec and V. Guerchais (Eds), *Top. Organomet. Chem. 28: Molecular Organometallic Materials for Optics*, Springer, Berlin and Heidelberg, Germany, 2010.
4. A. J. Lees (Ed.), *Top. Organomet. Chem. 29: Photophysics of Organometallics*, Springer, Berlin and Heidelberg, Germany, 2010.
5. A. Tsuboyama, H. Iwawaki, M. Furugori, T. Mukaide, J. Kamatani, S. Igawa, T. Moriyama, S. Miura, T. Takiguchi, S. Okada, M. Hoshino and K. Ueno, *J. Am. Chem. Soc.*, 2003, **125**, 12971.
6. C.-H. Yang, Y.-M. Cheng, Y. Chi, C.-J. Hsu, F.-C. Fang, K.-T. Wong, P.-T. Chou, C.-H. Chang, M.-H. Tsai and C.-C. Wu, *Angew. Chem. Int. Ed.*, 2007, **46**, 2418.
7. T. Hofbeck and H. Yersin, *Inorg. Chem.*, 2010, **49**, 9290.
8. S. Lamansky, P. Djurovich, D. Murphy, F. Abdel-Razzaq, H.-E. Lee, C. Adachi, P. E. Burrows, S. R. Forrest and M. E. Thompson, *J. Am. Chem. Soc.*, 2001, **123**, 4304.
9. L. Flamigni, A. Barbieri, C. Sabatini, B. Ventura and F. Barigelletti, *Top. Curr. Chem.*, 2007, **281**, 143.
10. M. S. Lowry and S. Bernhard, *Chem. Eur. J.*, 2006, **12**, 7970.
11. Y. You and S. Y. Park, *J. Am. Chem. Soc.*, 2005, **127**, 12438.
12. G. Zhou, C.-L. Ho, W.-Y. Wong, Q. Wang, D. Ma, L. Wang, Z. Lin, T. B. Marder and A. Beeby, *Adv. Funct. Mater.*, 2008, **18**, 499.
13. M. Tavasli, S. Bettington, M. R. Bryce, H. A. A. Attar, F. B. Dias, S. King and A. P. Monkman, *J. Mater. Chem.*, 2005, **15**, 4963.
14. M. A. Baldo, M. E. Thompson and S. R. Forrest, *Nature*, 2000, **403**, 750.

15. M. K. Nazeeruddin, R. Humphry-Baker, D. Berner, S. Rivier, L. Zuppiroli and M. Grätzel, *J. Am. Chem. Soc.*, 2003, **125**, 8790.
16. S. Kammer, I. Starke, A. Pietrucha, A. Kelling, W. Mickler, U. Schilde, C. Dosche, E. Kleinpeter and H.-J. Holdt, *Dalton Trans.*, 2012, **41**, 10219.
17. E. Baranoff, J.-H. Yum, I. Jung, R. Vulcano, M. Grätzel and M. K. Nazeeruddin, *Chem. Asian. J.*, 2010, **5**, 496.
18. Y.-J. Yuan, J.-Y. Zhang, Z.-T. Yu, J.-Y. Feng, W.-J. Luo, J.-H. Ye and Z.-G. Zou, *Inorg. Chem.*, 2012, **51**, 4123.
19. S. Sato, T. Morikawa, T. Kajino and O. Ishitani, *Angew. Chem. Int. Ed.*, 2013, **52**, 988.
20. B. O'Regan and M. Grätzel, *Nature*, 1991, **353**, 737.
21. M. Grätzel, *Acc. Chem. Res.*, 2009, **42**, 1788.
22. A. Harriman, G. Porter and M.-C. Richoux, *J. Chem. Soc., Faraday Trans. 2*, 1981, **77**, 833.
23. A. J. Bard and M. A. Fox, *Acc. Chem. Res.*, 1995, **28**, 141.
24. P. Steunenberg, A. Ruggi, N. S. van den Berg, T. Buckle, J. Kuil, F. W. B. van Leeuwen and A. H. Velders, *Inorg. Chem.*, 2012, **51**, 2105.
25. K. K. W. Lo and K. Y. Zhang, *RSC Adv.*, 2012, **2**, 12069.
26. Q. Zhao, F. Li and C. Huang, *Chem. Soc. Rev.*, 2010, **39**, 3007.
27. C. S. K. Mak, D. Pentlehner, M. Stich, O. S. Wolfbeis, W. K. Chan and H. Yersin, *Chem. Mater.*, 2009, **21**, 2173.
28. A. L. Medina-Castillo, J. F. Fernández-Sánchez, C. Klein, M. K. Nazeeruddin, A. Segura-Carretero, A. Fernández-Gutiérrez, M. Grätzel and U. E. Spichiger-Keller, *Analyst*, 2007, **132**, 929.
29. M. Marín-Suárez, B. F. E. Curchod, I. Tavernelli, U. Rothlisberger, R. Scopelliti, I. Jung, D. Di Censo, M. Grätzel, J. F. Fernández-Sánchez, A. Fernández-Gutiérrez, M. K. Nazeeruddin and E. Baranoff, *Chem. Mater.*, 2012, **24**, 2330.
30. S. Zhang, M. Hosaka, T. Yoshihara, K. Negishi, Y. Iida, S. Tobita and T. Takeuchi, *Cancer Res.*, 2010, **70**, 4490.
31. S. P.-Y. Li, H.-W. Liu, K. Y. Zhang and K. K.-W. Lo, *Chem. Eur. J.*, 2010, **16**, 8329.

32. P. W. Atkins and R. S. Friedman, *Molecular Quantum Mechanics*, Oxford University Press, United Kingdom, 3rd, 1997.
33. N. J. Turro, *J. Chem. Educ.*, 1969, **46**, 2.
34. N. J. Turro, V. Ramamurthy and J. Scaiano, *Modern Molecular Photochemistry of Organic Molecules*, University Science Books, Sausalito, CA, USA, 2010.
35. M. Montalti, A. Credi, L. Prodi and M. T. Gandolfi, *Handbook of Photochemistry, 3rd Edition*, CRC Press, Boca Raton, FL, USA, 2006, 619-623.
36. C. A. Parker and T. A. Joyce, *Chem. Commun.*, 1968, 749.
37. K. Plaetzer, B. Krammer, J. Berlanda, F. Berr and T. Kiesslich, *Lasers Med. Sci.*, 2009, **24**, 259.
38. M. Kasha, *Discuss. Faraday Soc.*, 1950, **9**, 14.
39. M. Beer and H. C. Longuet-Higgins, *J. Chem. Phys.*, 1955, **23**, 1390.
40. R. M. Williams and J. W. Verhoeven, *Spectrochim. Acta Part A*, 1994, **50**, 251.
41. M. Albrecht, *Chem. Rev.*, 2009, **110**, 576.
42. S. Sprouse, K. A. King, P. J. Spellane and R. J. Watts, *J. Am. Chem. Soc.*, 1984, **106**, 6647.
43. T. Karatsu, T. Nakamura, S. Yagai, A. Kitamura, K. Yamaguchi, Y. Matsushima, T. Iwata, Y. Hori and T. Hagiwara, *Chem. Lett.*, 2003, **32**, 886.
44. C.-H. Yang, K.-H. Fang, C.-H. Chen and I. W. Sun, *Chem. Commun.*, 2004, 2232.
45. F. J. Coughlin, M. S. Westrol, K. D. Oyler, N. Byrne, C. Kraml, E. Zysman-Colman, M. S. Lowry and S. Bernhard, *Inorg. Chem.*, 2008, **47**, 2039.
46. H. Sato, K. Tamura, M. Taniguchi and A. Yamagishi, *New J. Chem.*, 2010, **34**, 617.
47. E. Marchi, R. Sinisi, G. Bergamini, M. Tragni, M. Monari, M. Bandini and P. Ceroni, *Chem. Eur. J.*, 2012, **18**, 8765.
48. K. Dedeian, P. I. Djurovich, F. O. Garces, G. Carlson and R. J. Watts, *Inorg. Chem.*, 1991, **30**, 1685.
49. M. Tavasli, S. Bettington, I. F. Perepichka, A. S. Batsanov, M. R. Bryce, C. Rothe and A. P. Monkman, *Eur. J. Inorg. Chem.*, 2007, **2007**, 4808.

50. M. Nonoyama, *Bull. Chem. Soc. Jpn.*, 1974, **47**, 767.
51. M. G. Colombo, T. C. Brunold, T. Riedener, H. U. Güdel, M. Förtsch and H.-B. Bürgi, *Inorg. Chem.*, 1994, **33**, 545.
52. A. R. McDonald, M. Lutz, L. S. von Chrzanowski, G. P. M. van Klink, A. L. Spek and G. van Koten, *Inorg. Chem.*, 2008, **47**, 6681.
53. R. Ragni, E. A. Plummer, K. Brunner, J. W. Hofstraat, F. Babudri, G. M. Farinola, F. Naso and L. De Cola, *J. Mater. Chem.*, 2006, **16**, 1161.
54. Y. Zheng, A. S. Batsanov, R. M. Edkins, A. Beeby and M. R. Bryce, *Inorg. Chem.*, 2011, **51**, 290.
55. K. Tsuchiya, E. Ito, S. Yagai, A. Kitamura and T. Karatsu, *Eur. J. Inorg. Chem.*, 2009, 2104.
56. A. B. Tamayo, B. D. Alleyne, P. I. Djurovich, S. Lamansky, I. Tsyba, N. N. Ho, R. Bau and M. E. Thompson, *J. Am. Chem. Soc.*, 2003, **125**, 7377.
57. A. Beeby, S. Bettington, I. D. W. Samuel and Z. J. Wang, *J. Mater. Chem.*, 2003, **13**, 80.
58. S. Lamansky, P. Djurovich, D. Murphy, F. Abdel-Razzaq, R. Kwong, I. Tsyba, M. Bortz, B. Mui, R. Bau and M. E. Thompson, *Inorg. Chem.*, 2001, **40**, 1704.
59. K.-Y. Kim, R. T. Farley and K. S. Schanze, *J. Phys. Chem. B*, 2006, **110**, 17302.
60. J. I. Goldsmith, W. R. Hudson, M. S. Lowry, T. H. Anderson and S. Bernhard, *J. Am. Chem. Soc.*, 2005, **127**, 7502.
61. H.-F. Chen, C. Wu, M.-C. Kuo, M. E. Thompson and K.-T. Wong, *J. Mater. Chem.*, 2012, **22**, 9556.
62. R. M. Edkins, K. Fucke and A. Beeby, unpublished work.
63. R. Ragni, E. Orselli, G. S. Kottas, O. H. Omar, F. Babudri, A. Pedone, F. Naso, G. M. Farinola and L. De Cola, *Chem. Eur. J.*, 2009, **15**, 136.
64. E. Baranoff, S. p. Suàrez, P. Bugnon, C. Barolo, R. Buscaino, R. Scopelliti, L. Zuppiroli, M. Grätzel and M. K. Nazeeruddin, *Inorg. Chem.*, 2008, **47**, 6575.
65. P. J. Hay, *J. Phys. Chem. A*, 2002, **106**, 1634.
66. I. Avilov, P. Minoofar, J. Cornil and L. De Cola, *J. Am. Chem. Soc.*, 2007, **129**, 8247.

67. G. J. Hedley, A. Ruseckas and I. D. W. Samuel, *Chem. Phys. Lett.*, 2008, **450**, 292.
68. A. R. G. Smith, P. L. Burn and B. J. Powell, *ChemPhysChem*, 2011, **12**, 2429.
69. W. J. Finkenzeller and H. Yersin, *Chem. Phys. Lett.*, 2003, **377**, 299.
70. T. Sajoto, P. I. Djurovich, A. Tamayo, M. Yousufuddin, R. Bau, M. E. Thompson, R. J. Holmes and S. R. Forrest, *Inorg. Chem.*, 2005, **44**, 7992.
71. X. Li, B. Minaev, H. Agren and H. Tian, *Eur. J. Inorg. Chem.*, 2011, 2517.
72. H. Riesen, L. Wallace and E. Krausz, *Inorg. Chem.*, 1996, **35**, 6908.
73. J. S. Gold, S. J. Milder, J. W. Lewis and D. S. Kliger, *J. Am. Chem. Soc.*, 1985, **107**, 8285.
74. D. H. Oh, M. Sano and S. G. Boxer, *J. Am. Chem. Soc.*, 1991, **113**, 6880.
75. P. J. Carroll and L. E. Brus, *J. Am. Chem. Soc.*, 1987, **109**, 7613.
76. I. M. Dixon, J.-P. Collin, J.-P. Sauvage, L. Flamigni, S. Encinas and F. Barigelletti, *Chem. Soc. Rev.*, 2000, **29**, 385.
77. M. Polson, S. Fracasso, V. Bertolasi, M. Ravaglia and F. Scandola, *Inorg. Chem.*, 2004, **43**, 1950.
78. R. D. Costa, F. Monti, G. Accorsi, A. Barbieri, H. J. Bolink, E. Ortí and N. Armaroli, *Inorg. Chem.*, 2011, **50**, 7229.
79. V. L. Whittle and J. A. G. Williams, *Dalton Trans.*, 2009, **0**, 3929.
80. R. D. Costa, E. Ortí, H. J. Bolink, F. Monti, G. Accorsi and N. Armaroli, *Angew. Chem. Int. Ed.*, 2012, **51**, 8178.
81. C. Ulbricht, B. Beyer, C. Friebe, A. Winter and U. S. Schubert, *Adv. Mater.*, 2009, **21**, 4418.
82. E. Zysman-Colman, J. D. Slinker, J. B. Parker, G. G. Malliaras and S. Bernhard, *Chem. Mater.*, 2007, **20**, 388.
83. F. Huang, H. Wu and Y. Cao, *Chem. Soc. Rev.*, 2010, **39**, 2500.
84. C.-J. Chiang, A. Kimyonok, M. K. Etherington, G. C. Griffiths, V. Jankus, F. Turksoy and A. P. Monkman, *Adv. Funct. Mater.*, 2013, **23**, 739.
85. B. Minaev, V. Minaeva and H. Ågren, *J. Phys. Chem. A*, 2009, **113**, 726.
86. C. Rothe, S. M. King and A. P. Monkman, *Phys. Rev. Lett.*, 2006, **97**, 076602.
87. I. D. W. Samuel and A. Beeby, *Nature*, 2000, **403**, 710.

88. F. May, M. Al-Helwi, B. Baumeier, W. Kowalsky, E. Fuchs, C. Lennartz and D. Andrienko, *J. Am. Chem. Soc.*, 2012, **134**, 13818.

89. D. Di Censo, S. Fantacci, F. De Angelis, C. Klein, N. Evans, K. Kalyanasundaram, H. J. Bolink, M. Grätzel and M. K. Nazeeruddin, *Inorg. Chem.*, 2008, **47**, 980.

90. Y. You and S. Y. Park, *Dalton Trans.*, 2009, 1267.

91. J. M. Fernández-Hernández, J. I. Beltrán, V. Lemaur, M.-D. Gálvez-López, C.-H. Chien, F. Polo, E. Orselli, R. Fröhlich, J. Cornil and L. De Cola, *Inorg. Chem.*, 2013, **52**, 1812.

92. S.-C. Lo, R. E. Harding, C. P. Shipley, S. G. Stevenson, P. L. Burn and I. D. W. Samuel, *J. Am. Chem. Soc.*, 2009, **131**, 16681.

93. M. Xu, G. Wang, R. Zhou, Z. An, Q. Zhou and W. Li, *Inorg. Chim. Acta*, 2007, **360**, 3149.

94. J. C. Deaton, R. H. Young, J. R. Lenhard, M. Rajeswaran and S. Huo, *Inorg. Chem.*, 2010, **49**, 9151.

95. G. A. Carlson, P. I. Djurovich and R. J. Watts, *Inorg. Chem.*, 1993, **32**, 4483.

96. S. Bettington, M. Tavasli, M. R. Bryce, A. S. Batsanov, A. L. Thompson, H. A. Al-Attar, F. B. Dias and A. P. Monkman, *J. Mater. Chem.*, 2006, **16**, 1046.

97. A. M'Hamedi, A. S. Batsanov, M. A. Fox, M. R. Bryce, K. Abdullah, H. A. Al-Attar and A. P. Monkman, *J. Mater. Chem.*, 2012, **22**, 13529.

98. V. Chandrasekhar, B. Mahanti, P. Bandipalli and K. Bhanuprakash, *Inorg. Chem.*, 2012.

99. A. Auffrant, A. Barbieri, F. Barigelletti, J. Lacour, P. Mobian, J. P. Collin, J. P. Sauvage and B. Ventura, *Inorg. Chem.*, 2007, **46**, 6911.

100. A. Steffen, M. G. Tay, A. S. Batsanov, J. A. K. Howard, A. Beeby, K. Q. Vuong, X.-Z. Sun, M. W. George and T. B. Marder, *Angew. Chem.*, 2010, **122**, 2399.

101. L. De Cola, P. Belser, A. von Zelewsky and F. Vögtle, *Inorg. Chim. Acta*, 2007, **360**, 775.

102. J. F. Yin, M. Velayudham, D. Bhattacharya, H. C. Lin and K. L. Lu, *Coord. Chem. Rev.*, 2012, **256**, 3008.

103. K.-C. Hwang, J.-L. Chen, Y. Chi, C.-W. Lin, Y.-M. Cheng, G.-H. Lee, P.-T. Chou, S.-Y. Lin and C.-F. Shu, *Inorg. Chem.*, 2008, **47**, 3307.

104. A. Ito, Y. Kang, S. Saito, E. Sakuda and N. Kitamura, *Inorg. Chem.*, 2012, **51**, 7722.

105. S.-T. Lam, N. Zhu and V. W.-W. Yam, *Inorg. Chem.*, 2009, **48**, 9664.

106. M.-W. Louie, A. W.-T. Choi, H.-W. Liu, B. T.-N. Chan and K. K.-W. Lo, *Organometallics*, 2012, **31**, 5844.

107. T. M. McLean, J. L. Moody, M. R. Waterland and S. G. Telfer, *Inorg. Chem.*, 2011, **51**, 446.

108. A. Coleman, C. Brennan, J. G. Vos and M. T. Pryce, *Coord. Chem. Rev.*, 2008, **252**, 2585.

109. M. Spencer, A. Santoro, G. R. Freeman, A. Diez, P. R. Murray, J. Torroba, A. C. Whitwood, L. J. Yellowlees, J. A. G. Williams and D. W. Bruce, *Dalton Trans.*, 2012, **41**, 14244.

110. K. L. Garner, L. F. Parkes, J. D. Piper and J. A. G. Williams, *Inorg. Chem.*, 2009, **49**, 476.

111. L. Murphy, P. Brulatti, V. Fattori, M. Cocchi and J. A. G. Williams, *Chem. Commun.*, 2012, **48**, 5817.

112. C. Bronner and O. S. Wenger, *Dalton Trans.*, 2011, **40**, 12409.

113. V. A. Krylova, P. I. Djurovich, M. T. Whited and M. E. Thompson, *Chem. Commun.*, 2010, **46**, 6696.

114. H. Tanaka, K. Shizu, H. Miyazaki and C. Adachi, *Chem. Commun.*, 2012, **48**, 11392.

115. G. Méhes, H. Nomura, Q. Zhang, T. Nakagawa and C. Adachi, *Angew. Chem. Int. Ed.*, 2012, **51**, 11311.

116. Q. Zhang, J. Li, K. Shizu, S. Huang, S. Hirata, H. Miyazaki and C. Adachi, *J. Am. Chem. Soc.*, 2012, **134**, 14706.

117. K. Tamao, K. Sumitani and M. Kumada, *J. Am. Chem. Soc.*, 1972, **94**, 4374.

118. Y. Hatanaka and T. Hiyama, *J. Org. Chem.*, 1988, **53**, 918.

119. T. Mizoroki, K. Mori and A. Ozaki, *Bull. Chem. Soc. Jpn.*, 1971, **44**, 581.

120. R. F. Heck and J. P. Nolley, *J. Org. Chem.*, 1972, **37**, 2320.

121. A. O. King, N. Okukado and E.-i. Negishi, *J. Chem. Soc., Chem. Commun.*, 1977, 683.

122. K. Sonogashira, Y. Tohda and N. Hagihara, *Tetrahedron Lett.*, 1975, **16**, 4467.
123. D. Milstein and J. K. Stille, *J. Am. Chem. Soc.*, 1978, **100**, 3636.
124. N. Miyaura and A. Suzuki, *J. Chem. Soc., Chem. Commun.*, 1979, 866.
125. G. C. Fortman and S. P. Nolan, *Chem. Soc. Rev.*, 2011, **40**, 5151.
126. T. E. Barder, S. D. Walker, J. R. Martinelli and S. L. Buchwald, *J. Am. Chem. Soc.*, 2005, **127**, 4685.
127. J. P. Stambuli, M. Bühl and J. F. Hartwig, *J. Am. Chem. Soc.*, 2002, **124**, 9346.
128. D. S. Surry and S. L. Buchwald, *Angew. Chem. Int. Ed.*, 2008, **47**, 6338.
129. R. Chinchilla and C. Nájera, *Chem. Rev.*, 2007, **107**, 874.
130. R. Chinchilla and C. Nájera, *Chem. Soc. Rev.*, 2011, **40**, 5084.
131. P. Bertus, F. Fecourt, C. Bauder and P. Pale, *New J. Chem.*, 2004, **28**, 12.
132. F. Himo, T. Lovell, R. Hilgraf, V. V. Rostovtsev, L. Noodleman, K. B. Sharpless and V. V. Fokin, *J. Am. Chem. Soc.*, 2005, **127**, 210.
133. P. Nguyen, Y. A. Zheng, L. Agocs, G. Lesley and T. B. Marder, *Inorg. Chim. Acta*, 1994, **220**, 289.
134. A. A. Fuller, H. R. Hester, E. V. Salo and E. P. Stevens, *Tetrahedron Lett.*, 2003, **44**, 2935.
135. P. B. Hodgson and F. H. Salingue, *Tetrahedron Lett.*, 2004, **45**, 685.
136. P. Espinet and A. M. Echavarren, *Angew. Chem. Int. Ed.*, 2004, **43**, 4704.
137. G. P. McGlacken and I. J. S. Fairlamb, *Eur. J. Org. Chem.*, 2009, **2009**, 4011.

Chapter 2

Cyclometalated Iridium Complexes: Results and Discussion

2. Introduction

This chapter outlines the synthesis and photophysics of some cyclometalated iridium complexes. Tris-heteroleptic complexes are introduced as a means to generate multi-functional materials and are further used to probe the role of symmetry in determining excited state kinetics.[1] Next, the impact of exchanging the phenyl ring of the common 2-phenylpyridine ligand for two isomeric pyrenyl moieties is investigated, allowing a detailed comparison of their complexes. Two-photon excitation is demonstrated as a means of sensitising lanthanide luminescence in d-f hybrids constructed from a cyclometalated iridium sensitiser and a Eu or Tb complex, which is of potential interest for imaging applications.[2] Finally, tris-heteroleptic complexes are used to obtain unidirectional charge transfer from an iridium core to an organic accepting moiety.

2.1. The synthesis and photophysics of tris-heteroleptic cyclometalated iridium complexes

In this section, the synthesis and photophysical study of tris-heteroleptic complexes of the general formula [IrLL′(acac)], where L and L′ are two differently substituted 2-phenylpyridines and acacH is 2,4-pentanedione, is outlined, introducing a combinatorial approach that is demonstrated for several ligand combinations. The tris-heteroleptic complexes and the analogous bis-heteroleptic complexes of the form $[IrL_2(acac)]$ have been studied by a combination of absorption and photoluminescence spectroscopies, in conjunction with modelling by DFT and TD-DFT, to elucidate the nature and location of the excited state in the novel species.

Hitherto reported compounds can be divided into three main categories by ligand composition: $[IrL_3]$, $[IrL_2L']$ and $[IrL_2A]$, where L and L′ are different cyclometalating ligands and A is an ancillary ligand, such as a bidentate diketone, commonly 2,4-pentanedionate ($acac^-$), pic^- or a combination of two monodentate ligands such as Cl^- and PR_3.[3] Beeby *et al.* reported the synthesis of complexes of the type $[IrL_2L']$ by the reaction of ligand L′ with the diiridium μ-chloro-bridged dimer $[IrL_2Cl]_2$.[4] However, it has been found that this method can lead to some scrambling of the ligands under the forcing conditions employed for this reaction, resulting in the formation of complex mixtures containing all permutations of the two ligands. There has also been one report of the synthesis of systems of the type [IrLL′L″] as part of a

mixture for a white OLED, but the pure tris-heteroleptic species was not isolated.[5] Although heteroleptic complexes of the form [IrL_2A] have been known for more than a decade,[6] until the publication of the following work, there had been no report of the complete purification and photophysical study of a complex of the type [IrLL′A]. Felici *et al*. had attempted the synthesis of a charged, tris-heteroleptic complex with two cyclometalated 4-phenyl-1,2,3-triazole ligands, one of which was *N*-alkylated at the 1-position with a methyl group and the other with an adamantyl group, and a third, neutral ancillary ligand, 4-(2′-pyridyl)-1,2,3-triazole, also 1-*N*-substituted with an adamantyl group.[7] The use of an asymmetric ancillary ligand, however, led to a mixture of two possible structural isomers of the tris-heteroleptic complex, incorrectly described by the authors as diastereomers, which they were unable to separate, even by high-performance liquid chromatography (HPLC).

In this work, a facile synthetic protocol to access this previously unattainable group of complexes, along with a photophysical study backed up by molecular modelling, is described. It is known that the choice of the ancillary ligand, A, can influence the photophysical properties of the complex, hence in this study $acac^-$ was used consistently throughout. However, since the reaction of the diiridium μ-chloro-bridged dimer with the ancillary ligand is normally carried out under mild conditions, the same methodology could be applied to a number of other complexes.[8]

It is conceived that for use as imaging agents, one ligand could be utilised to control the photophysical properties, one to act as a site for functionalisation (*e.g.* with a targeting vector) and the third to tune physical properties, such as solubility in biological media. For OLED applications, it also has the potential to facilitate the synthesis of complexes with enhanced properties, for example solubility in a suitable organic solvent or the incorporation of anchoring groups. The asymmetry of the complexes may also be expected to lead to a change in physical properties, such as sublimation temperature, which may be advantageous for devices constructed in this way.

The approach is an adaption of the standard Nonoyama synthesis of cyclometalated iridium complexes,[3] based upon the formation of the mixed diiridium μ-chloro-bridged dimer, in which $IrCl_3 \cdot 3H_2O$ is refluxed in a mixture of water and 2-ethoxyethanol with two different cyclometalating ligands (Scheme 2.1). The crude product is subjected to flash chromatography to remove traces of tris-cyclometalated complexes that are formed as by-products in the reaction,[9] to furnish only the bridged

diiridium species. These are present as a complex mixture, containing at least seven combinations of ligands with L:L′ ratios of 4:0, 3:1, 2:2 (for which there are three structural isomers), 1:3 and 0:4, even without consideration of the formation of diastereomers. This mixture is reacted on in its crude form with acetylacetone in basic 2-ethoxyethanol or, more conveniently, a 1:1 mixture of acetone:ethanol, without further purification, yielding only three compounds, [IrL_2(acac)], [IrL'_2(acac)] and the coveted [IrLL′(acac)], which can be separated by column chromatography. For the photophysical studies presented here the products were required to a high degree of purity, and were isolated in yields of 7–11% based on the functionalised 2-phenylpyridine ligand. Although this method is low yielding, it is currently the only way to make this class of complex. The product mixture can be biased in favour of the desired compound by using an excess of one ligand over the other, but no further optimisation of the procedure was attempted. It was also possible to prepare the compounds using a one-pot method in which the cyclometalating ligands was heated with $IrCl_3 \cdot 3H_2O$ in aqueous 2-ethoxyethanol for four hours followed by the addition of acetylacetone and K_2CO_3. After a further 30 minutes of heating at reflux, the products could be isolated and separated using the same conditions as the two step procedure. Although this method is quicker, it is easier to obtain material of higher purity using the two-step procedure.

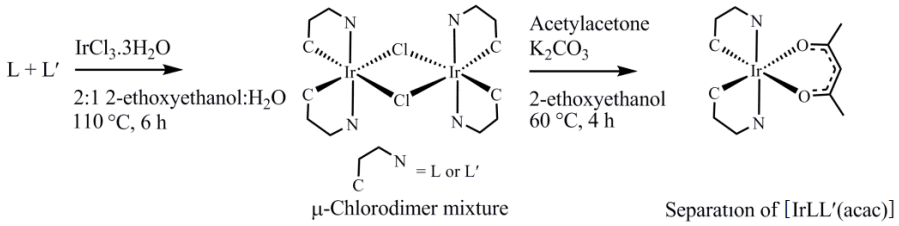

Scheme 2.1. Synthesis of cyclometalated iridium complexes of the form [IrLL′(acac)].

The chosen examples were selected as cases where separation might be anticipated to be challenging due to the similarity of the ligands, in order to prove the viability of the method. The target compounds contained a single ppy^- ligand, a substituted ppy^- derivative and an $acac^-$ ancillary ligand. The substituted ligands 2‑(4′‑phenylethynylphenyl)pyridine (2−(pep)pyH), 2−(4′−formylphenyl)pyridine (fppyH) and 2,4-diphenylpyridine (dppyH) were used to give the products shown in Figure 2.1.

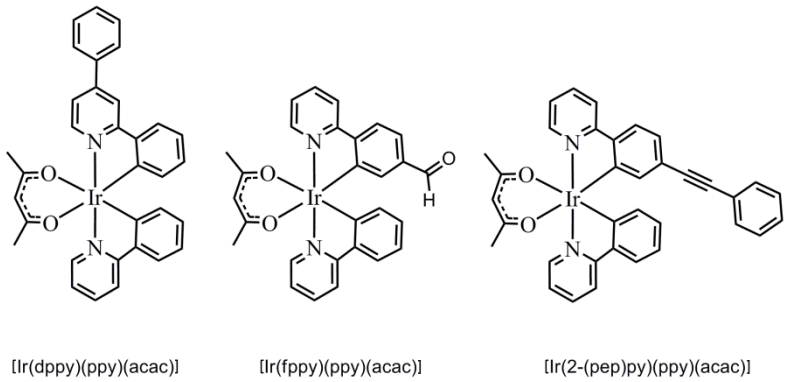

Figure 2.1. The novel tris-heteroleptic cyclometalated iridium complexes.

The compound dppyH has been reported previously, having been synthesised by various methods including the reaction of phenylmagnesium bromide and 4-phenylpyridine-*N*-oxide,[10] the $[PdCl_2(PPh_3)_2]$/CuI-catalysed cyclisation of phenylacetylene with an iodovinylimine[11] and the Suzuki-Miyaura coupling of 2,4-dibromopyridine with phenylboronic acid.[12] In this work, it was synthesised by a Suzuki-Miyaura coupling of 4-bromopyridine hydrochloride and phenylboronic acid using $[Pd(PPh_3)_4]$ catalyst and $NaOH_{(aq)}$ base (77% yield), followed by phenylation at the 2-position of the unactivated pyridine ring by reaction with phenyllithium in dry toluene. The work-up of this reaction was simply exposure to air and the addition of water, with no further oxidising agent required to affect re-aromatisation to the product (39% yield). The phenylethynyl derivative, 2-(pep)pyH, was prepared by the Suzuki-Miyaura coupling of 4-phenylethynylbenzeneboronic acid with 2-bromopyridine (76% yield).

The synthesis of the mixture of diiridium μ-chloro-bridged dimer intermediates, and subsequent complexes, was facile and proceeded under the usual conditions.[13] These complexes could be separated on an analytical and preparative scale by thin layer chromatography (TLC) and column chromatography, respectively. Excellent separation could be readily achieved under TLC conditions, and to illustrate this, Figure 2.2 shows a TLC plate illuminated under ultraviolet light, clearly showing the relatively large difference in the R_f values of the final products. The individual conditions used for the separation of compounds on a preparative scale are provided in the experimental section. Isolated complexes were characterised by ^1H, ^1H-^1H COSY and ^1H-^1H NOESY NMR experiments, through which every ^1H resonance could be unambiguously assigned (an example is shown in Figure 2.3). Accurate mass-spectrometry and high

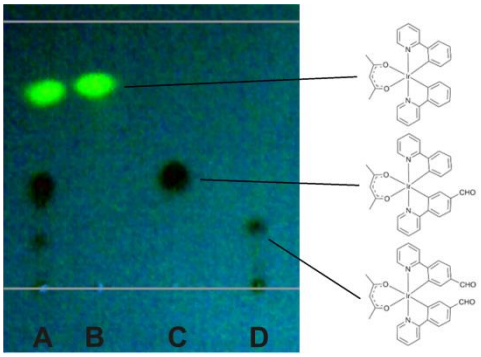

Figure 2.2. TLC plate (SiO_2; 5:1 CH_2Cl_2:MeCN; UV (365 nm) illumination) of (**A**) the crude mixture and (**B–D**) the separated fractions of [Ir(ppy)$_2$(acac)], [Ir(fppy)(ppy)(acac)] and [Ir(fppy)$_2$(acac)], respectively. The latter fraction includes additional material that remains at the baseline. The baseline and solvent front are highlighted.

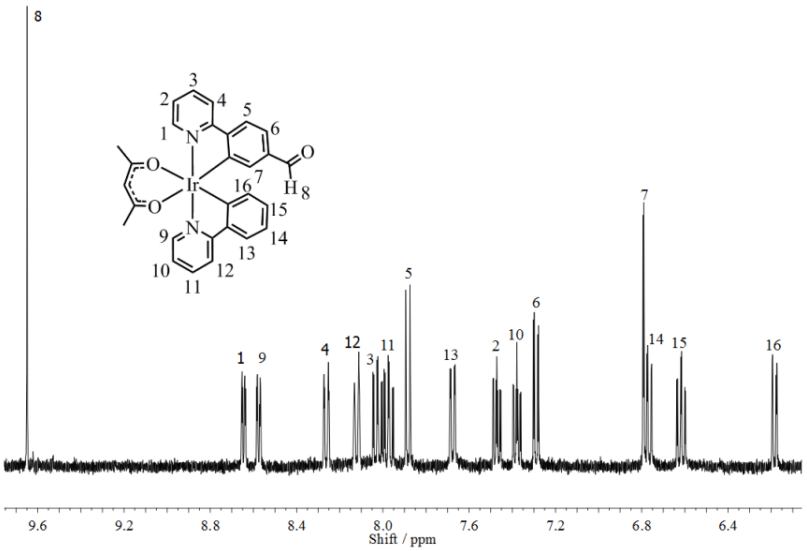

Figure 2.3. Low field (aromatic) region of the ^{1}H NMR spectrum (400 MHz; acetone-d_6) of [Ir(fppy)(ppy)(acac)] with all resonances assigned, aided by ^{1}H-^{1}H NOESY and ^{1}H-^{1}H COSY experiments. See inset for numbering system.

performance liquid chromatography (HPLC) were used to verify the composition and purity of the samples, respectively.

SC-XRD of [Ir(fppy)(ppy)(acac)] confirmed the identity of the complex and its tris-heteroleptic composition (Figure 2.4a). As is common with complexes of the form [IrL$_2$(acac)], the pyridine rings are mutually *trans* while the phenyl rings are in a mutually *cis* configuration due to the large *trans* influence of the formally anionic phenyl moieties. Complexes of the type [IrL$_2$(acac)] can usually be assigned as having

either *cis* or *trans* pyridines from the NMR spectrum due to the presence of equivalent protons on the cyclometalated ligands for the *trans* isomer and inequivalent protons for the *cis* isomer. However, in the case of the tris-heteroleptic complexes, the different identity of the two cyclometalated ligands meant that this could only be confirmed in a straightforward manner by the SC-XRD structure. The metal–ligand bond lengths (Ir–O (2.159(4) and 2.127(4) Å), Ir–N (2.040(5) and 2.033(5) Å) and Ir–C (1.996(6) and 1.988(6) Å)) are in the typical ranges for molecules of the type $[IrL_2(acac)]$. The difference in Ir–O bond lengths is small, but significant (0.03 Å), and arises due to the weaker *trans* influence of the aldehyde substituted phenyl ring compared to that of the unsubstituted phenyl ring of ppy^-. The molecule packs as a head-to-tail π-stacked dimer between the $fppy^-$ ligands, with an interplanar spacing of 3.4 Å, which is again typical in this regard (Figure 2.4b).[6]

Figure 2.5 shows the absorption and emission spectra of the novel tris-heteroleptic complexes, while Figure 2.6 shows a comparison of the emission spectra of the bis- and tris-heteroleptic complexes. Table 2.1 summarises the photophysical data for all of the complexes studied.

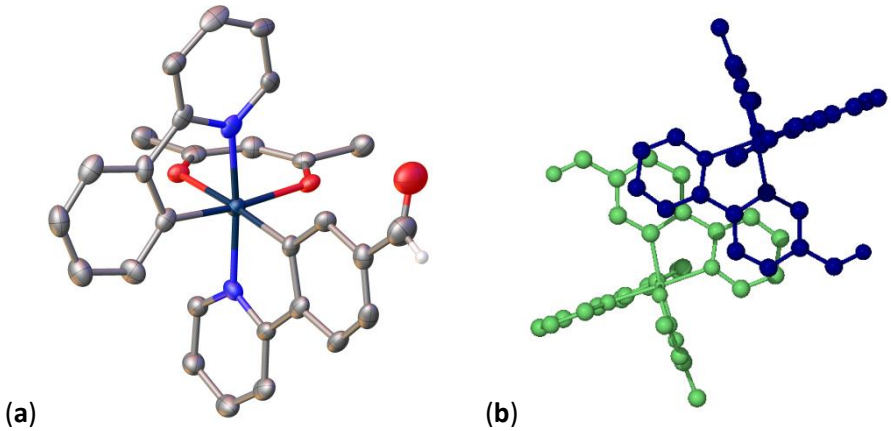

Figure 2.4. (**a**) Molecular structure of [Ir(ppy)(fppy)(acac)] as determined by SC-XRD. This is the first tris-heteroleptic cyclometalated iridium complex to be structurally characterised. Element (colour): iridium (dark green), carbon (grey), nitrogen (blue), oxygen (red) and hydrogen (white). Atomic displacement parameters are shown at 50% probability. Hydrogen atoms are omitted for clarity, with the exception of the formyl hydrogen. (**b**) Head-to-tail offset intermolecular π-stacking of the $fppy^-$ ligands of two molecules of [Ir(fppy)(ppy)(acac)] in the crystal structure.

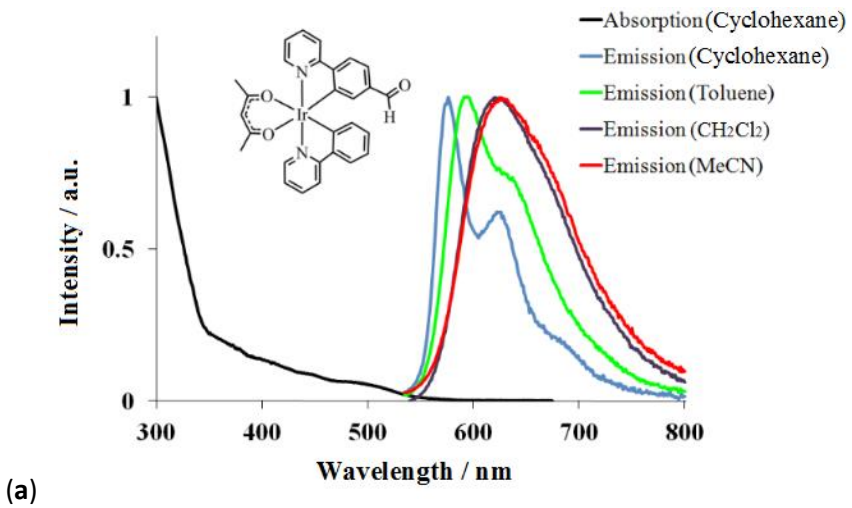

(**a**)

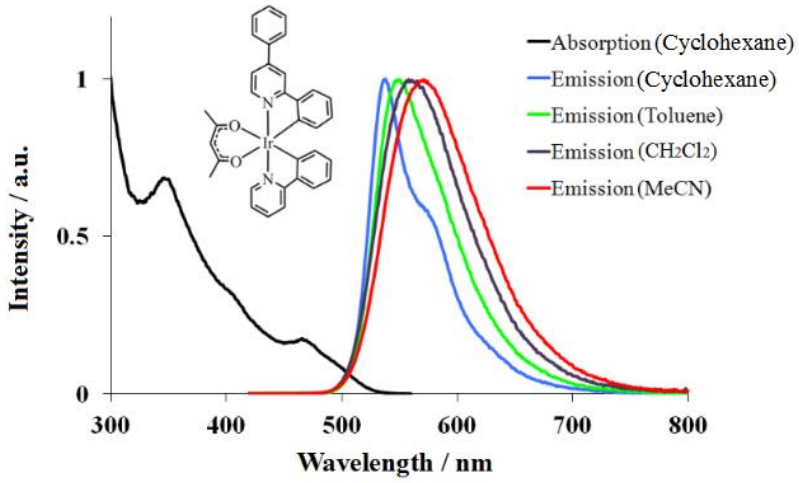

(**b**)

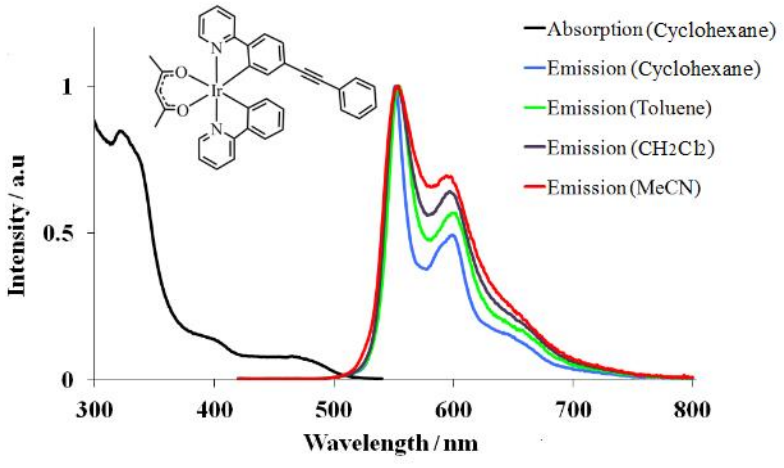

(**c**)

Figure 2.5. Normalised absorption and emission spectra of the tris-heteroleptic cyclometalated iridium complexes (**a**) [Ir(fppy)(ppy)(acac)], (**b**) [Ir(dppy)(ppy)(acac)] and (**c**) [Ir(2-(pep)ppy)(ppy)(acac)]. λ_{ex} = 525 nm (**a**) or 410 nm (**b** and **c**). All measurements were obtained in degassed solvent at 298 K.

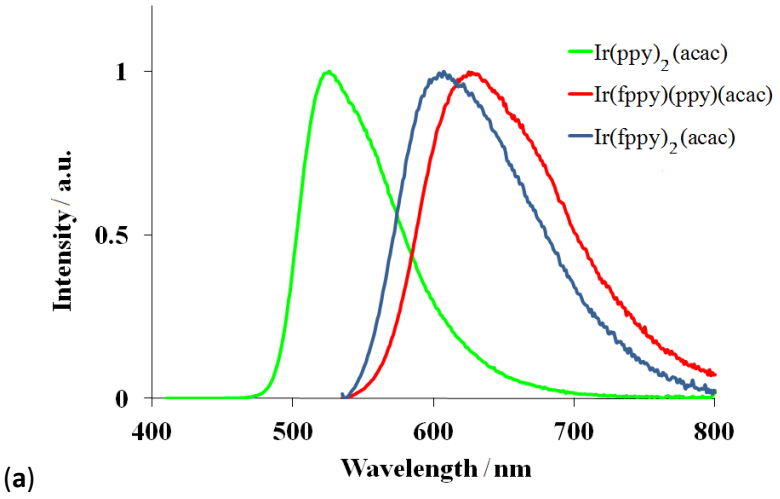

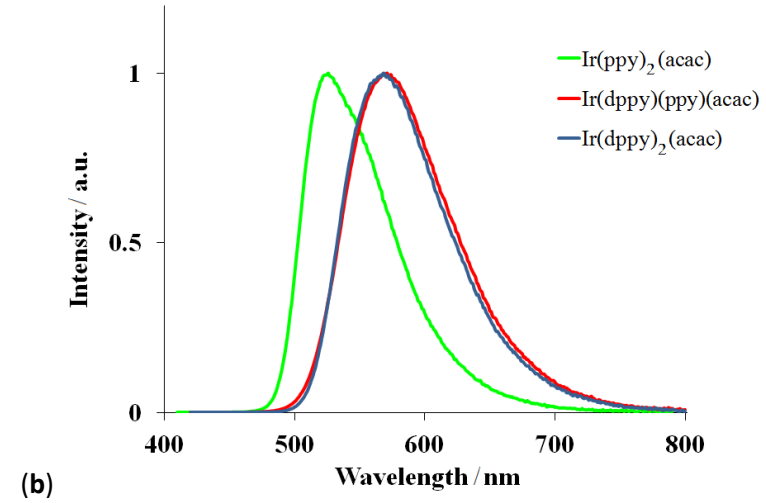

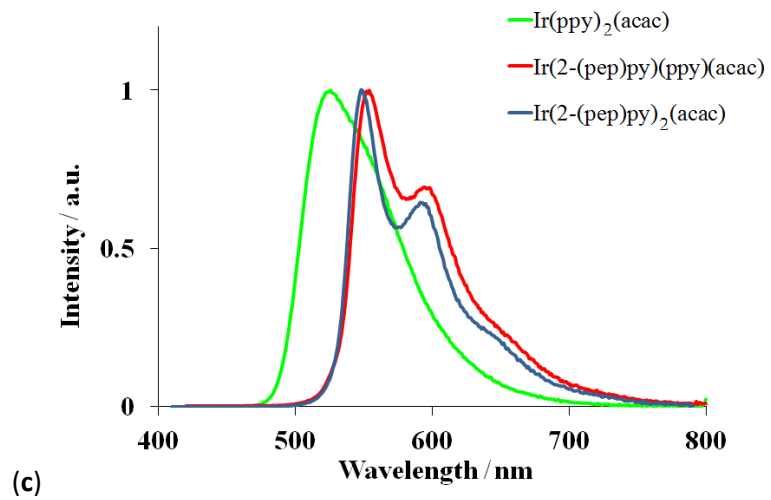

Figure 2.6. A comparison of the normalised emission spectra of the [IrLL′(acac)] complexes (**a**) [Ir(fppy)(ppy)(acac)], (**b**) [Ir(dppy)(ppy)(acac)] and (**c**) [Ir(2-(pep)ppy)(ppy)(acac)] and the related [IrL_2(acac)] complexes. λ_{ex} = 410 nm, except [Ir(fppy)(ppy)(acac)] for which λ_{ex} = 525 nm. All measurements were obtained in degassed MeCN solvent at 298 K.

Table 2.1. Spectroscopic data of bis- and tris-heteroleptic Ir(III) cyclometalated complexes measured in degassed solvents at 298 K.

Complex	λ_{abs} (ε) / nm ($\log(\varepsilon / M^{-1} cm^{-1})$[a]	λ_{em} / nm[b]				τ / µs[c]		Φ[bd]		τ_0 / µs[e]	
		Cyclohexane	Toluene	CH_2Cl_2	MeCN	Toluene	MeCN	Toluene	MeCN	Toluene	MeCN
$[Ir(ppy)_2(acac)]$[f]	262, 306, 344, 372, 415, 476	512	520	520	522	1.6	2.1	0.46	0.42	3.5	5.0
$[Ir(fppy)_2(acac)]$[fg]	286, 307, 365, 413, 508	564	585	600	603	1.8	0.9	0.04	0.12	45	7.5
$[Ir(dppy)_2(acac)]$[fg]	289, 354, 470, 501	539	550	560	565	1.0	1.2	0.33	0.42	3.3	2.9
$[Ir(2\text{-}(pep)py)_2(acac)]$[fg]	288, 351, 392, 471	549	550	550	548	2.6	2.9	0.22	0.23	12	13
[Ir(fppy)(ppy)(acac)]	292 (4.59), 356 (3.81), 404 (3.60), 443 (3.45), 492 (3.30)	574	590	620	623	1.3	0.3	0.02	0.11	65	2.7
[Ir(dppy)(ppy)(acac)]	288 (4.50), 350 (4.06), 380 (3.88), 409 (3.70), 468 (3.46), 495 (3.30)	535	545	556	567	1.1	1.5	0.48	0.63	2.3	2.3
[Ir(2-(pep)py)(ppy)(acac)]	330 (4.55), 386 (3.79), 456 (3.56), 490 (3.43)	551	553	553	552	2.4	2.9	0.23	0.32	10	9.1

[a] Measured in cyclohexane; [b] See Figures 2.5 and 2.6 for specific λ_{ex}; [c] Estimated error 5% of the value, λ_{ex} = 337 nm. λ_{em} equal to the emission maxima; [d] Estimated error 10% of the value; [e] Calculated using $\tau_0 = \tau.\Phi_T/\Phi$ and assuming $\Phi_T = 1$; [f] Extinction coefficient not measured; [g] Absorption spectrum measured in CH_2Cl_2 due to low solubility in cyclohexane.

In each example the emission spectra are red-shifted with respect to the parent [Ir(ppy)$_2$(acac)] and this is attributed to the increased conjugation of the substituted phenylpyridine ligands. The compounds show a marked difference in solvatochromism, observed phosphorescence lifetimes, Φ and pure-radiative lifetimes, τ_0. The emission from these complexes is an admixture of ^{3}MLCT and ^{3}LC transitions, with the dominant component depending on the precise nature of the ligands and the solvent conditions.

The phenylethynyl derivative, [Ir(2-(pep)py)(ppy)(acac)], exhibits a structured emission spectrum, which does not shift significantly upon moving from cyclohexane to acetonitrile. The structured emission, coupled with relatively long pure radiative lifetimes of 10.0 and 9.1 μs in toluene and acetonitrile, respectively, is indicative of a more ^{3}LC transition. A similar emission profile and long pure radiative lifetime are observed from the bis-heteroleptic derivative [Ir(2-(pep)py)$_2$(acac)]. These observations are evidence for the localisation of the excitation upon the ligand that gives rise to the lowest energy excited state, in this case the 2-(pep)py$^-$.

The tris-heteroleptic complex containing the dppy$^-$ ligand shows a small bathochromic shift upon moving to a more polar solvent environment. Furthermore, in a non-polar environment there is some evidence of vibrational fine structure that is lost in the more polar solvents. This complex has a comparatively short pure radiative lifetime of 2.3 μs and, on the basis of these observations, the emissive state is assigned as having mixed ^{3}LC and ^{3}MLCT character, with the former being more important in a non-polar medium, and the latter becoming more significant with increased solvent polarity.

High qua`1ntum yields are desirable for the application of these materials, in particular for OLEDs, sensing or imaging, with recent reviews dedicated to methods for increasing this parameter.[14] Interestingly, the mixed ligand systems described here have similar or higher quantum yields than the respective bis-heteroleptic complexes, [IrL$_2$(acac)], but retain a similar emission profile. The complex [Ir(dppy)(ppy)(acac)] has PLQYs of 0.48 (toluene) and 0.63 (MeCN), which are significantly enhanced compared to [Ir(dppy)$_2$(acac)], which has values of 0.33 (toluene) and 0.42 (MeCN). The radiative lifetimes, and hence k_r, of the complexes are comparable; hence, it is concluded that the increases in PLQYs are due to a decrease in non-radiative decay pathways. This may be due to the localisation of the excited state on a single ligand in the tris-heteroleptic complexes and hence a reduction in the number of vibrational states capable of non-radiative deactivation of the excited state compared to the higher symmetry bis-heteroleptic complex. There is the possibility that these mixed systems

offer an interesting method of enhancing the photoluminescence quantum yield, whilst leaving the emission spectrum essentially unchanged.

In order to understand the nature of the excited states further and the origins of the red-shift in terms of the modification of the HOMO and LUMO energies, DFT calculations were conducted to model the electronic structure of these complexes. The ground state geometries of the tris-heteroleptic complexes and their [IrL_2(acac)] analogues were calculated using DFT with the B3LYP functional and a mixed basis set and effective core potential of 6-31+G for light atoms and LANL2DZ for Ir, in a manner similar to that described by Hay[15] (see experimental, Chapter 5, for a discussion of the choice of method). For [Ir(fppy)(ppy)(acac)], calculated bond lengths for Ir–N, Ir–C and Ir–O bonds all agreed within ± 0.07 Å (3.2%) and with an average discrepancy of 1.5%, with the values derived from the experimentally determined X ray structure.

Table 2.1 (overleaf) summarises the spatial extent of the HOMO, LUMO and LUMO+1 orbitals for each of the complexes prepared. For all complexes, of both the form [IrL_2(acac)] and [IrLL′(acac)], the calculated HOMO is located primarily on the iridium atom and the coordinating phenyl rings. This is in agreement with previous work by Hay on related cyclometalated Ir(III) complexes.[15] In the case of the [IrL_2(acac)] complexes, the LUMO and the LUMO+1 are quasidegenerate and are equally distributed across both ligands (these molecules belong to the point group C_2 that precludes truly degenerate orbitals, a point often overlooked). However, for complexes of the form [IrLL′(acac)] this quasidegeneracy of the LUMO and LUMO+1 levels is lifted and the LUMO is located on the functionalised ppy^- ligand (*i.e.* $fppy^-$, $dppy^-$ or 2-(pep)py^-), while the LUMO+1 resides on the higher energy ppy^- ligand.

TD-DFT calculations were performed at the CAM B3LYP/6-31+G/LANL2DZ level in order to try to establish the nature of the excited triplet states of the materials. The CAM-B3LYP functional[16] was chosen due to its better description of states with charge-transfer character than the B3LYP functional used for optimisation calculations,[17] which is crucial for cyclometalated iridium compounds where MLCT is observed. Excitation energies and orbital contributions calculated by TD-DFT are shown in Table 2.3. Introduction of solvent to the calculations using the polarisable continuum model (PCM) brings about little change in the predicted absorption bands (< 0.05 eV), which appears to contradict the observed solvatochromism. The large solvent effect is most likely due to a significant structural/solvent reorganisation in the excited triplet state prior to emission, which is difficult to predict

Table 2.2. HOMO, LUMO and LUMO+1 orbital plots of the tris-heteroleptic [IrLL′(acac)] and parent [IrL_2(acac)] complexes as calculated by DFT at the B3LYP/6-31+G/LANL2DZ level of theory. Isovalue: ± 0.02 [$e\ a_0^{-3}$]^{½}. Hydrogen atoms have been omitted for clarity.

Compound	**HOMO** ***E*** **/ eV**	**LUMO** ***E*** **/ eV**	**LUMO+1** ***E*** **/ eV**
[Ir(ppy)$_2$(acac)]	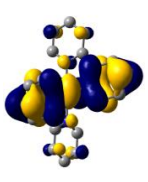 -4.74	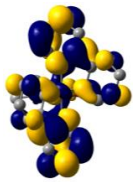 -1.27	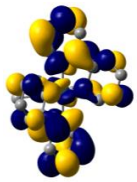 -1.27
[Ir(fppy)$_2$(acac)]	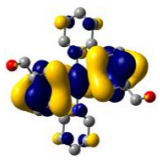 -5.28	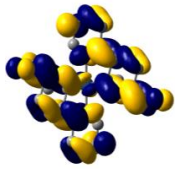 -2.14	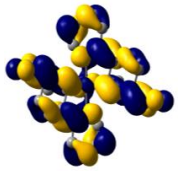 -2.11
[Ir(fppy)(ppy)(acac)]	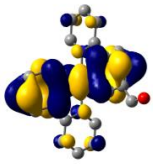 -5.01	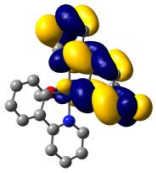 -1.96	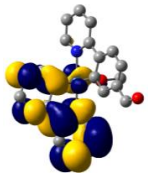 -1.46
[Ir(dppy)$_2$(acac)]	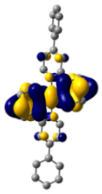 -4.70	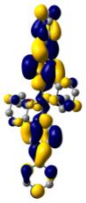 -1.51	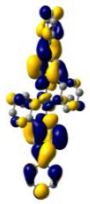 -1.49
[Ir(dppy)(ppy)(acac)]	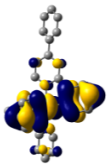 -4.72	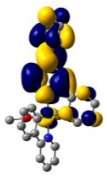 -1.52	 -1.25
[Ir(2-(pep)py)$_2$(acac)]	 -4.89	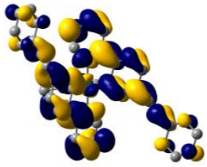 -1.62	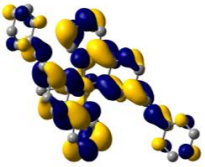 -1.60
[Ir(2-(pep)py)(ppy)(acac)	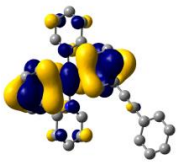 -4.82	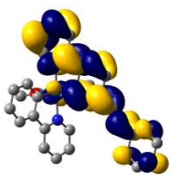 -1.58	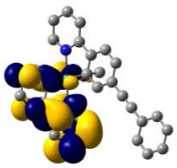 -1.30

Table 2.3. TD-DFT calculated lowest energy transitions for the [IrL_2(acac)] and [IrLL′(acac)] complexes at the CAM-B3LYP/6-31+G/LANL2DZ level of theory.

Compound	Transition	E / eV	λ / nm	Dominant component(s)
[$Ir(ppy)_2$(acac)]	$T_1 \leftarrow S_0$	2.67	464	LUMO+1 ← HOMO
	$T_2 \leftarrow S_0$	2.68	462	LUMO ← HOMO
[$Ir(fppy)_2$(acac)]	$T_1 \leftarrow S_0$	2.37	522	LUMO ← HOMO
				LUMO+1 ← HOMO-2
	$T_2 \leftarrow S_0$	2.38	520	LUMO+1 ← HOMO
				LUMO ← HOMO-2
[Ir(fppy)(ppy)(acac)]	$T_1 \leftarrow S_0$	2.36	526	LUMO ← HOMO
	$T_2 \leftarrow S_0$	2.69	460	LUMO+1 ← HOMO
				LUMO+1 ← HOMO-2
[$Ir(dppy)_2$(acac)]	$T_1 \leftarrow S_0$	2.35	529	LUMO ← HOMO
				LUMO ← HOMO-1
	$T_2 \leftarrow S_0$	2.35	528	LUMO+1 ← HOMO
[Ir(dppy)(ppy)(acac)]	$T_1 \leftarrow S_0$	2.64	470	LUMO ← HOMO
	$T_2 \leftarrow S_0$	2.68	463	LUMO+1 ← HOMO
				LUMO+1 ← HOMO-2
[Ir(2-(pep)py)$_2$(acac)]	$T_1 \leftarrow S_0$	2.29	541	LUMO+1 ← HOMO-1
				LUMO ← HOMO
	$T_2 \leftarrow S_0$	2.29	540	LUMO+1 ← HOMO
				LUMO ← HOMO-1
[Ir(2-(pep)py)(ppy)(acac)]	$T_1 \leftarrow S_0$	2.29	541	LUMO ← HOMO-1
				LUMO ← HOMO
	$T_2 \leftarrow S_0$	2.69	461	LUMO+1 ← HOMO
				LUMO+1 ← HOMO-3

using currently available software packages. The TD-DFT method describes each excitation by the transition between many pairs of occupied and unoccupied MOs; therefore, here, and throughout this work, only the major contribution(s) to the description of the overall process is (are) reported.

For the bis-heteroleptic complexes excitation from S_0 to T_1 and T_2 is isoenergetic, which is a consequence of the quasi-degenerate LUMO and LUMO+1 that contribute significantly to these two transitions. For all tris-heteroleptic complexes, the lowest energy excited state results mainly from excitation from various HOMO-N orbitals (N = 0, 1, 2…) to the LUMO, while the second lowest energy transition is to the LUMO+1 level in all cases. With the notable exception of [Ir(dppy)(ppy)(acac)], the $T_1 \leftarrow S_0$ transition of the tris-heteroleptic systems is similar in energy to the related [IrL_2(acac)] compound, while the $T_2 \leftarrow S_0$ energy in all cases, that is excitation to the ppy^- localised LUMO+1, is of very similar energy to that observed for the $T_1 \leftarrow S_0$

transition of [Ir(ppy)$_2$(acac)]. This provides support for the hypothesis that the excitation is primarily located onto a single ligand, with the cyclometalating ligand that gives rise to the lowest energy excited state being the most readily reduced ligand that controls the emissive properties of the complexes, which in these examples, is the substituted phenylpyridine.

In conclusion, complexes of the general form [IrLL′(acac)] have been synthesised and it is observed that they exhibit subtle differences in their photophysics when compared to the related [IrL$_2$(acac)] species. The lowest energy ligand is found both experimentally and computationally to dominate the emission properties and this may allow exploitation of the remaining two ligands for ancillary purposes. This class of cyclometalated iridium complex also affords the opportunity to have finer control over the photophysical properties for a wide variety of applications.

* * * *

Following the publication of the above work, Baranoff and co-workers[18] have criticised our method for being low yielding and claim that an essentially identical statistical procedure starting from an Ir(I) precursor, [{Ir(η^4-COD)(μ-Cl)}$_2$], where COD is cycloocta-1,5-diene, is more efficient. In their paper they report a yield of 44% of [Ir(F$_2$ppy)(ppy)(acac)] using a 1:1 mixture of the two cyclometalating ligands. If, for simplicity, one considers the situation where the two ligands cyclometalate at the same rate and, due to the large number of molecules in the reaction mixtures, there is an essentially independent probability as to which ligand is incorporated in any one cyclometalation event, then the maximum possible yield has to be 50%. However, one might expect the two ligands selected by Baranoff not to cyclometalate at the same rate, due to the strongly electron-withdrawing fluorine substituents on F$_2$ppyH modulating the reactivity of this ligand relative to ppyH. Any deviation from an equal rate would lead to a lowering of this theoretical yield because it is more likely that the higher reactivity ligand will cyclometalate twice on the same metal centre at the beginning of the reaction, depleting this ligand from the reaction mixture. Therefore, they claim to have isolated close to all of the possible material by simple column chromatography, separating three compounds of very similar composition. This is also notwithstanding their interesting observation in the same paper of significant degradation of [IrL$_2$(acac)] complexes during chromatography on silica gel, eluted with chlorinated solvents, when here they used CH_2Cl_2. However, they do repeat and confirm the observation outlined

above that a positive effect on k_{nr} is achieved by using tris-heteroleptic complexes and they also similarly conclude that these complexes may be useful for multifunctional materials. In a further publication, Baranoff and co-workers have described the construction of an improved efficiency LEC using a tris-heteroleptic complex, finding that the lowest energy cyclometalated ligand essentially controls the emission colour, although they did not cite our work.[19]

Williams and co-workers[20] have since published the synthesis of a related class of tris-heteroleptic complex of the type [Ir(C^N)(N^C^N)A] containing two different cyclometalating ligands, one of which is bidentate (C^N) and the other terdentate (N^C^N), and where A is a monodentate anionic ligand, for example, Cl^-. Whilst they also criticise the statistical method outlined above for being low yielding, and assert that the similar method proposed by Baranoff[18] is superior due to its purported higher yield, they do not themselves propose a method that would be suitable for the synthesis of the complexes reported here.

2.2. Syntheses, structures and comparison of the photophysical properties of cyclometalated iridium complexes containing the isomeric 1- and 2-(2′-pyridyl)pyrene ligands

In this section, two cyclometalated iridium complexes of the form $[IrL_2(acac)]$, where L is either of the isomeric ligands 1- or 2-(2′-pyridyl)pyrene (1-pypyrH or 2-pypyrH), have been investigated (Figure 2.7). It was initially conceived that the introduction of cyclometalated pyrene into an iridium complex would produce species with interesting photophysical properties. In addition, it was considered interesting to probe the influence of substitution pattern in pyrene-based organometallic systems and its subsequent effect on the observed photophysical behaviour.

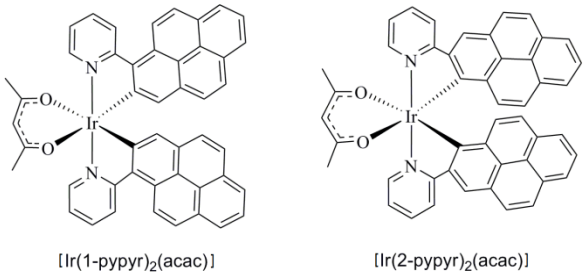

Figure 2.7. The structures of the isomeric complexes $[Ir(1\text{-pypyr})_2(acac)]$ and $[Ir(2\text{-pypyr})_2(acac)]$.

Pyrene is a polycyclic aromatic hydrocarbon exhibiting interesting photophysical properties, such as a long fluorescence lifetime ($\tau = 410$ ns in ethanol),[21] excimer emission[22] and a high PLQY ($\Phi = 0.65$ in cyclohexane),[23] and its utilisation for organic electronics has recently been extensively reviewed.[24] The photophysical properties of pyrene derivatives are particularly sensitive to the position of substitution, attributed to differences in orbital overlap and, importantly, symmetry.[25]

Most studies of the incorporation of pyrene into metal complexes have focused on attaching the pyrene as a pendant to a common ligand, for example onto an iridium complex with a terpyridine ligand,[26] a Pt acetylide[27] or several Ru bi-[28] and terpyridine[29] complexes. Other recent examples include a neutral cyclometalated iridium complex in which energy transfer to a pyrene-conjugated acetylacetonato (acac) ancillary ligand was investigated in detail[30] and an ionic iridium complex with energy transfer to a pyrene substituted bipyridyl ligand.[31] The majority of these studies mentioned have

centered on 1-pyrenyl derivatives due to the ease of their synthesis. There have only been a few studies of organometallic pyrene complexes and the effect of metal coordination directly onto pyrene, which have included examples of *σ*-bonded Au(I),[32, 33] Ru(II),[34] Pd(II) and Pt(II)[35] complexes. Ionkin and co-workers[36] have shown that 1-(2′-pyridyl)pyrene (1-pypyrH) can be cyclometalated with Ir(III) at the 2-position of the pyrene ring; however, no photophysical properties of these materials were reported. More recently, this ligand has been used to prepare a cyclometalated Pt(II) complex, which was shown to be a weakly red-emitting species (λ_{em} = 680 nm, Φ = 0.005 in degassed CH_2Cl_2 solution) with a multi-component emission profile.[37] In addition, an isoquinoline analogue of 1-pypyrH (*i.e.* 1-(1′-isoquinolinyl)pyrene) has been reported as a cyclometalating ligand for Ir(III), although emission was not observed in solution.[38] The isomeric 2-(2′-pyridyl)pyrene (2-pypyrH) ligand has not been reported previously.

Pyrene is most commonly functionalised at the 1-position, which is the site susceptible to electrophilic substitution. Traditionally, the synthesis of 2-substituted derivatives required the reduction of pyrene to 4,5,9,10-tetrahydropyrene, substitution and reoxidation,[39] which is both laborious and low yielding. Recently it has become possible to readily functionalise the 2-position through an Ir(I)-catalysed C–H borylation,[40-42] with the steric demand of the catalyst favouring substitution at the 2-position, allowing the regioselective synthesis of both of the precursors 1- and 2-bromopyrene through published methods.[41, 43] More specifically, 2-bromopyrene was synthesised using iridium-catalysed C–H bond activation and borylation[44] to afford 2-(Bpin)pyrene (pin = pinacolato, $[OCMe_2CMe_2O]^{2-}$) and subsequent treatment with copper(II) bromide.[41] The active catalyst for this reaction is synthesised *in situ* from the Ir(I) precatalyst [{Ir(η^4-COD)(μ-OMe)}$_2$], 4,4′-di-*tert*-butyl-2,2′-bipyridine (dtbpy) and B_2pin_2. Using NMR experiments with isotopically labelled reagents, isolation of intermediates and synthesis of model compounds, the resting state of the catalyst has been elucidated to be a *fac*-tris-boryl(dtbpy)iridium(III) species.[45-47] The unusual Ir(III)/Ir(V) catalytic cycle for the reaction is shown in Figure 2.8 for the generic case of benzene. Note that here [{Ir(η^2-COE)$_2$(μ-OMe)}$_2$] was used as an alternative precatalyst, but the same cycle is expected to apply.

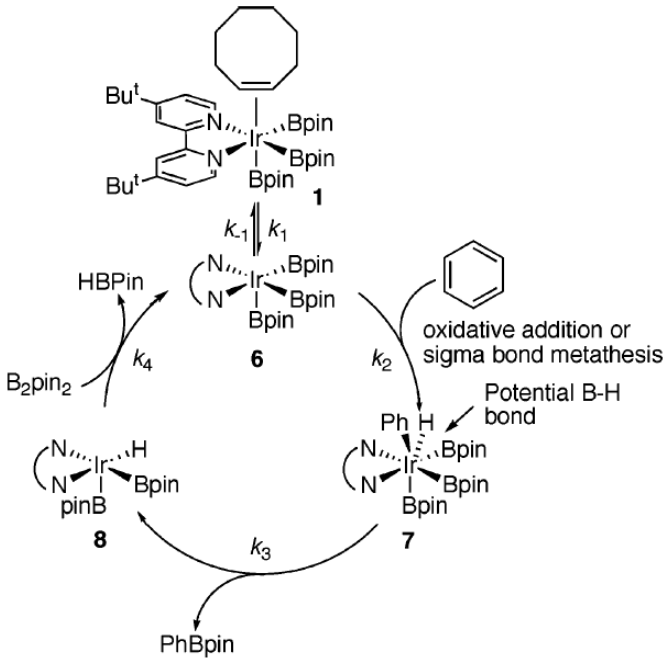

Figure 2.8. Catalytic cycle of the iridium-catalysed aromatic C–H borylation reaction shown for the generic case of benzene. Reproduced from ref. 47.

The regioselectivity of this catalyst towards the 2-position of pyrene is believed to be sterically controlled. It has been observed that borylation cannot be achieved with this catalyst system adjacent to a ring junction or a substituent due to the steric bulk of the [Ir(N^N)(Bpin)$_3$] active catalyst. The only sites of pyrene for which there is not such a ring junction are the 2- and 7-positions, thus selectivity for these sites is achieved.[40] By simply controlling the reagent ratio, 2-(Bpin)pyrene can be synthesised as the major product and converted to the bromo analogue. This was achieved in a one-pot reaction without the separation of pyrene and 2,7-bis(Bpin)pyrene from 2-(Bpin)pyrene.

The two isomeric ligands were synthesised by Stille coupling of the respective 1- or 2-bromopyrene with 2-(tri-*n*-butylstannyl)pyridine in toluene at reflux for 20 h using [Pd(PPh$_3$)$_2$Cl$_2$] or [Pd(PPh$_3$)$_4$] as catalyst. Previously, the 1-pypyrH ligand had been synthesised using Suzuki-Miyaura coupling of 1-pyrenylboronic acid and 2-bromopyridine in 47% yield.[37] The Stille coupling used here affords this ligand in an improved yield of 70% and the novel 2-pypyrH in 82% yield. Cyclometalation of pyrene-containing ligands at the 2-position of the pyrene ring has been described as occurring with difficulty,[34] while it has been shown that 1-pypyrH can be complexed to iridium when trimethyl phosphate is used as the solvent.[36] Ionkin has proposed that using this particular solvent increases the rate of cyclometalation for otherwise low

reactivity ligands by removing the hydrogen chloride generated in the reaction, as well as by improving the solubility of the reactants, and has shown it to be effective for a range of examples.[36, 48-50] Following this procedure, the diiridium μ-chloro-bridged dimer was obtained from 1-pypyrH in a yield of 75% after heating at 90 °C for 36 h. A standard protocol for cyclometalation was used for the analogous dimer of the 2-pypyrH ligand, using a 2:1 mixture of 2-ethoxyethanol and water as the solvent, with a shorter reaction time of 6 h at 110 °C, yielding the desired dimer in 65% yield. Surprisingly, the more sterically hindered 1-(1′-isoquinolinyl)pyrene has been reported to cyclometalate in 3:1 2-ethoxyethanol:water mixture within 6-7 h.[38] The absence of an X-ray structure for this complex, however, means that the possibility of this product being the less sterically demanding 6-membered chelate, cyclometalated at the 10-position, cannot be ruled out. The dimers proved to be highly insoluble in common solvents, making their full characterisation difficult, as reported previously for $[Ir(1\text{-pypyr})_2(\mu\text{-Cl})]_2$.[36] The crude dimers were reacted on further with acetylacetone in the presence of K_2CO_3 as a base to afford the more soluble $[IrL_2(acac)]$ complexes in high yields (83-87%). The synthetic pathways are summarised in Scheme 2.2.

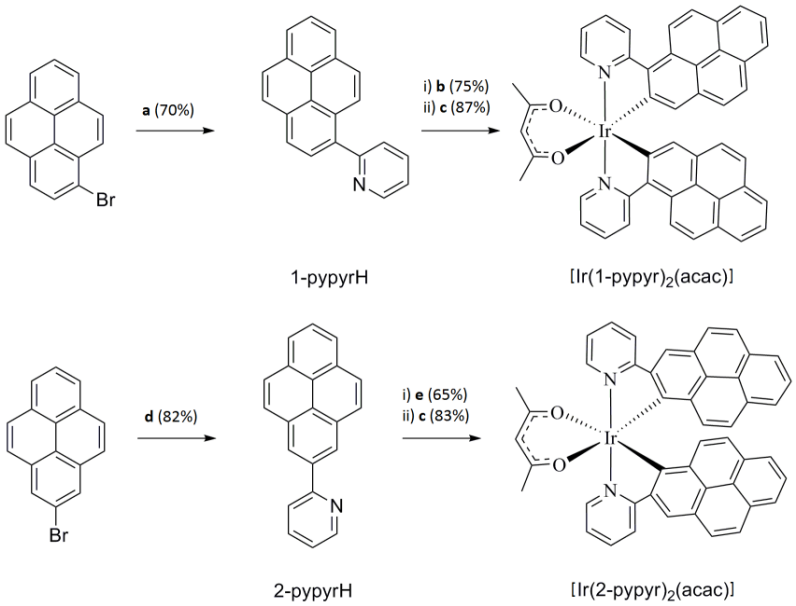

Scheme 2.2. Syntheses of the cyclometalated iridium complexes $[Ir(1\text{-pypyr})_2(acac)]$ and $[Ir(2\text{-pypyr})_2(acac)]$. (**a**) 2-(Tri-*n*-butylstannyl)pyridine, $[Pd(PPh_3)_2Cl_2]$ (4 mol%), N_2, 110 °C, 20 h. (**b**) $IrCl_3{\cdot}3H_2O$, trimethyl phosphate, 90 °C, 36 h. (**c**) Acetylacetone, K_2CO_3, 1:1 ethanol:acetone, 60 °C, 4 h. (**d**) 2-(Tri-*n*-butylstannyl)pyridine, $[Pd(PPh_3)_4]$ (4 mol%), N_2, 110 °C, 20 h. (e) $IrCl_3{\cdot}3H_2O$, 2:1 2-ethoxyethanol: H_2O, 110 °C, 6 h.

The molecular structures of the ligands 1-pypyrH and 2-pypyrH and the complexes [Ir(1-pypyr)$_2$(acac)] and [Ir(2-pypyr)$_2$(acac)] were determined by SC-XRD. The structures of the two ligands are shown in Figure 2.9. Details of the crystallisation procedures and the important crystallographic parameters can be found in Chapter 5. Both ligands crystallise in the $P2_1/c$ space group and both structures show disorder in the orientation of the pyridine rings, which was modeled across two sites at 50% occupancy each. This is likely to be due to the similarity in size of CH and N and the lack of intermolecular interactions, in particular the absence of a hydrogen bond donor group, which might be predicted to lead to a preference of one site over the other. In 1-pypyrH there is a 41° torsional twist between the planes of the pyridine and pyrene rings that is absent in 2-pypyrH (torsion angle of 0°). Although this twist could be brought about by crystal packing forces, it is likely that it is a result of a steric interaction between the hydrogen in the 3-position of the pyridine and those at the 1- and/or 10-position of the pyrene ring (*vide infra*). The crystal packing shows the expected π–π stacking, with pyrene–pyrene interplanar distances of 3.53 and 3.45 Å for 1- and 2-pypyrH, respectively, where the slightly longer distance for 1-pypyrH is attributable to its twisted conformation.

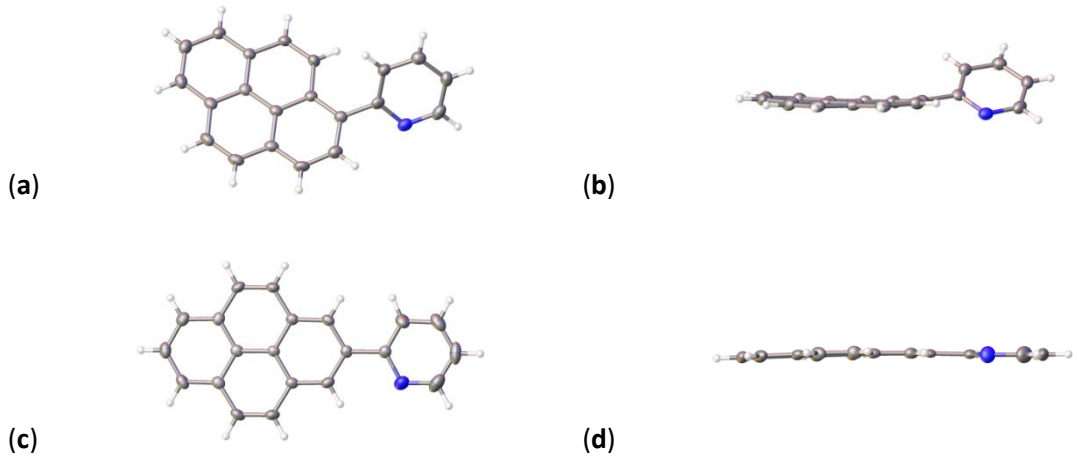

Figure 2.9. Molecular structures of the isomeric ligands 1-pypyrH and 2-pypyrH as obtained by single crystal X-ray diffraction: (**a**) 1-pypyrH front view; (**b**) 1-pypyrH side view; (**c**) 2-pypyrH front view; (**d**) 2-pypyrH side view. Atomic displacement parameters are illustrated as 50% probability surfaces. Element (colour): carbon (grey), nitrogen (blue), hydrogen (white). In both structures the pyridine rings are disordered over two sites and have been modelled with 50% occupancy of the two orientations. Only one orientation is shown here for clarity.

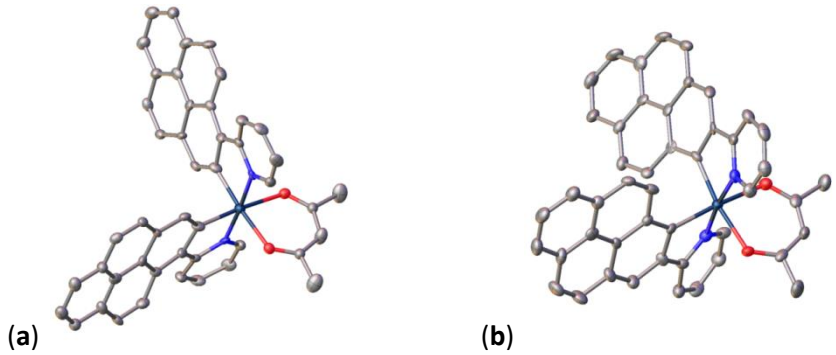

Figure 2.10. Molecular structures of (**a**) [Ir(1-pypyr)$_2$(acac)] and (**b**) [Ir(2-pypyr)$_2$(acac)] as obtained by single crystal X-ray diffraction. Atomic displacement parameters are illustrated as 50% probability surfaces. Element (colour): iridium (dark green), carbon (grey), oxygen (red), nitrogen (blue). The structure of [Ir(1-pypyr)$_2$(acac)] contains a disordered CH_2Cl_2 solvate molecule (not shown) that was modelled with 50% occupancy in two orientations. Hydrogen atoms have been omitted for clarity.

The structures of the two iridium complexes are shown in Figure 2.10. Both complexes have mutually *trans* pyridines, as is common in this class of complex, a fact also revealed by the single set of resonances for the magnetically equivalent cyclometalated ligands in both the ^{1}H and ^{13}C{^{1}H} NMR spectra. The structure of [Ir(1-pypyr)$_2$(acac)] has a twist of 18° between the planes of the pyridine and pyrene rings due to a steric interaction, analogous to that observed in the structure of the free ligand, which is again not present in [Ir(2-pypyr)$_2$(acac)] (dihedral angle of 0°). Complexation of the 1-pypyrH ligand has therefore reduced the torsional angle between the rings compared to the free ligand and thus increased the steric interaction between the hydrogen atoms at the 3-position of the pyridine ring and the 10-position of the pyrene. This increase in steric interaction, coupled with the greater reactivity of pyrene at the 1-position, may account for the more unusual conditions required to complex the 1-pypyrH ligand,[36] compared to those employed for 2-pypyrH. A similar explanation has been invoked for the difficulty of cyclometalating 1-(2′-quinolinyl)pyrene with ruthenium.[34]

Unlike the reported structures of the related heteroleptic complex with the ligand 1-(2′-(4′-methylpyridyl))pyrene and an anionic P^N chelating ancillary ligand,[36] the pyrene rings do not exhibit π–π stacking. [Ir(1-pypyr)$_2$(acac)] forms a CH_2Cl_2 monosolvate in which the solvent molecule fills voids in the structure rather than intercalating between layers of pyrene rings as was seen previously in both the CH_2Cl_2

and acetone solvates of the related compound (CSD Refcodes: OCOTOQ and ODELAL, respectively).

2.2.1. Photophysical study

The photophysical properties of the two ligands are summarised in Table 2.4 and Figure 2.11. In analogy with the parent compound pyrene and other substituted derivatives,[25] the intense absorption bands at *ca.* 340 nm present for both compounds are assigned as the ^1L_a transitions (essentially LUMO ← HOMO). The 2-pypyrH ligand shows pronounced vibrational structure to this band with an energy spacing of 1470 cm^{-1}, while for 1-pypyrH this band is broad and structureless, with the exception of a poorly resolved high energy shoulder. This can be attributed to a combination of two factors. The symmetry along the long axis where the ^1L_a transition dipole moment lies in pyrene is maintained in 2-pypyrH whereas in the 1-pypyrH compound this symmetry is broken, leading to a mixing of states. In the 1-pypyrH compound there is better orbital overlap, allowing charge transfer transitions to the pyridine from the pyrene that additionally broaden the band.[37] Charge transfer is moderated in 2-pypyrH due to the nodal plane that lies along the long axis of pyrene and through the 2-position in both the HOMO and

Table 2.4. Photophysical data for the ligands 1-pypyrH and 2-pypyrH in CH_2Cl_2

Ligand	λ_{abs} / nm[a] ($\log(\varepsilon$ / M^{-1} cm^{-1}))	λ_{em} / nm[b,c]	Φ[b,d] aerated / degassed	τ / ns[e] aerated / degassed
1-pypyrH	271 (4.08), 280 (4.25), 345 (4.18)	389*, 403 483 (excimer)	0.43[f] / 0.55	9.8[g] / 12.9
2-pypyrH	264 (sh., 4.09), 288 (4.24), 308 (3.77), 323 (3.86), 339 (4.12), 385 (2.00)	401*, 423, 446, 476 475 (excimer)	0.20 / 0.36	12.0 / 21.2

[a] sh. = shoulder; [b] Excitation at 340 nm; [c] Peaks assigned as excimer are observed only at high (*ca.* 10^{-4} mol dm^{-3}) concentration. All other peaks are observed at high and low (*ca.* 10^{-6} mol dm^{-3}) concentrations. Starred value is the emission maximum at low concentration; [d] Estimated error: 10% of the value; [e] Excitation at 300 nm. Decay monitored at 400 nm. Estimated error: 5% of the value; [f] Reported previously as 0.41 (Ref. 37); [g] Reported previously as 3 ns (Ref. 37).

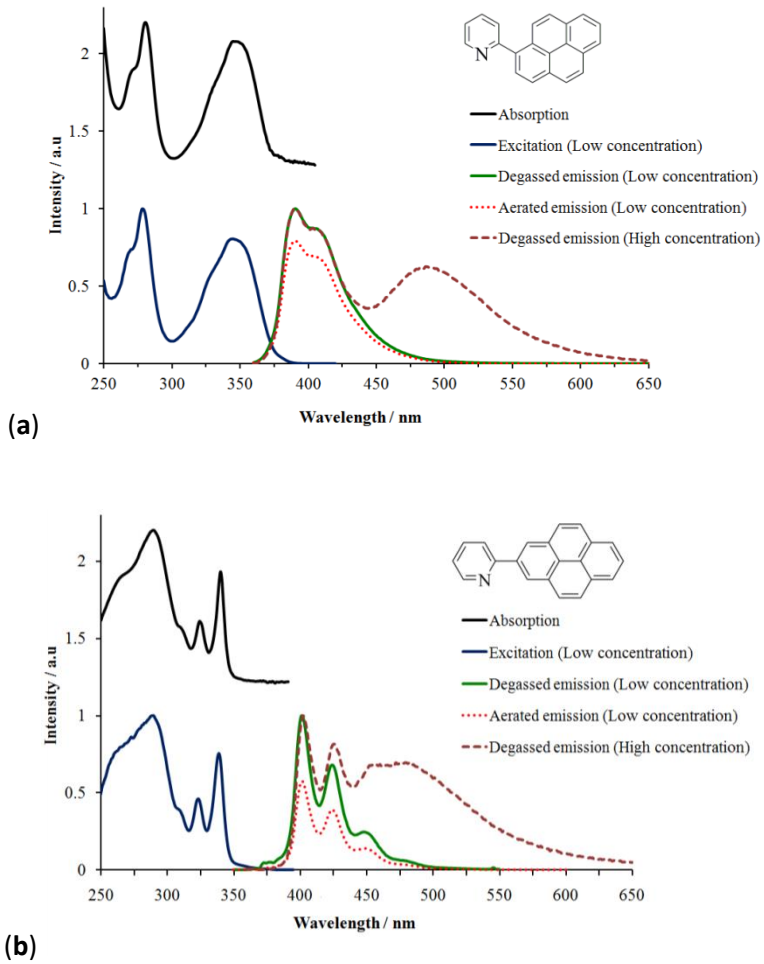

Figure 2.11. Room temperature normalised absorption, excitation and emission (λ_{ex} = 340 nm) spectra of (**a**) 1-pypyrH and (**b**) 2-pypyrH in CH_2Cl_2. Excitation spectra of 1- and 2-pypyrH were independent of λ_{em} (λ_{em} = 425 nm shown). Aerated emission spectra are normalised relative to the degassed emission spectra recorded under identical conditions. The absorption spectra have been offset for clarity. Low concentration and high concentration refer to low (*ca.* 10^{-6} mol dm^{-3}) and high (*ca.* 10^{-4} mol dm^{-3}) concentrations, respectively.

the LUMO. Absorption bands are observed at *ca.* 290 nm for both compounds with differing intensity and spectral width. The weakly allowed ^1L_b (mixed LUMO ← HOMO-1 and LUMO+1 ← HOMO) transitions are poorly resolved and are located at lower energy than the ^1L_a band for 2-pypyrH and coincidental with this band for 1-pypyrH. Justification for this assignment can be found in the computational study section (*vide infra*).

The compound 2-pypyrH shows emission with well resolved vibrational structure, whereas the 1-pypyrH ligand, in which the symmetry is broken and CT transitions are feasible, exhibits a broader profile. The emission spectra are also oxygen

sensitive as can be seen by the diminished intensity under aerated conditions, although the spectral profile is unaffected. The sensitivity of the 2-pypyrH ligand to oxygen is greater than that of 1-pypyrH, which can be attributed to the longer lifetime of the 2-substituted pyrene compound, as observed for other derivatives.[25] Both ligands show excimer emission at high concentration (*ca.* 10^{-4} mol dm^{-3}) with a band centered at 483 and 475 nm for 1-pypyrH and 2-pypyrH, respectively. This is similar to the excimer emission of pyrene, which is centered at 480 nm and is observed at concentrations above 10^{-5} mol dm^{-3}.[22]

The absorption spectra of [Ir(1-pypyr)$_2$(acac)], in a range of solvents, are displayed overleaf in Figure 2.12. In these spectra, there is an intense absorption band at higher energy than 350 nm, which would typically be assigned as the ^{1}LC transition, and this convention is followed here. The band centered at approximately 400 nm is structured, which would imply significant ^{1}LC character for this transition as well. Of particular note is the modest negative solvatochromic shift of this band that can be interpreted as a stabilisation of the ground state in more polar solvents. Not only is there a blue-shift of the peak of this band by approximately 450 cm^{-1} from cyclohexane to acetonitrile, but there is also a change in profile. In cyclohexane, there are three resolved vibronic bands with approximately 1240 cm^{-1} spacing, the lowest energy of which is reduced in intensity in toluene, further reduced to a shoulder in CH_2Cl_2 and is completely absent in acetonitrile. Acetone and acetonitrile solutions produce almost identical features in this region, and thus no further stabilisation is achieved with solvents having a greater polarity than acetone. This broadening of the absorption band in more polar solvents is potentially an indication of the greater charge-transfer (CT) character (either ^{1}MLCT or ^{1}I^{ra}LCT type) of the transition in these solvents. At lower energy, centered at 520 nm, is a second structured band that again broadens in profile with increasing solvent polarity and is also assigned as having mixed ^{3}LC and generic ^{3}CT character dependent on solvent environment, with its lower extinction coefficient an indication that it is likely a triplet transition partially facilitated by the Ir atom.

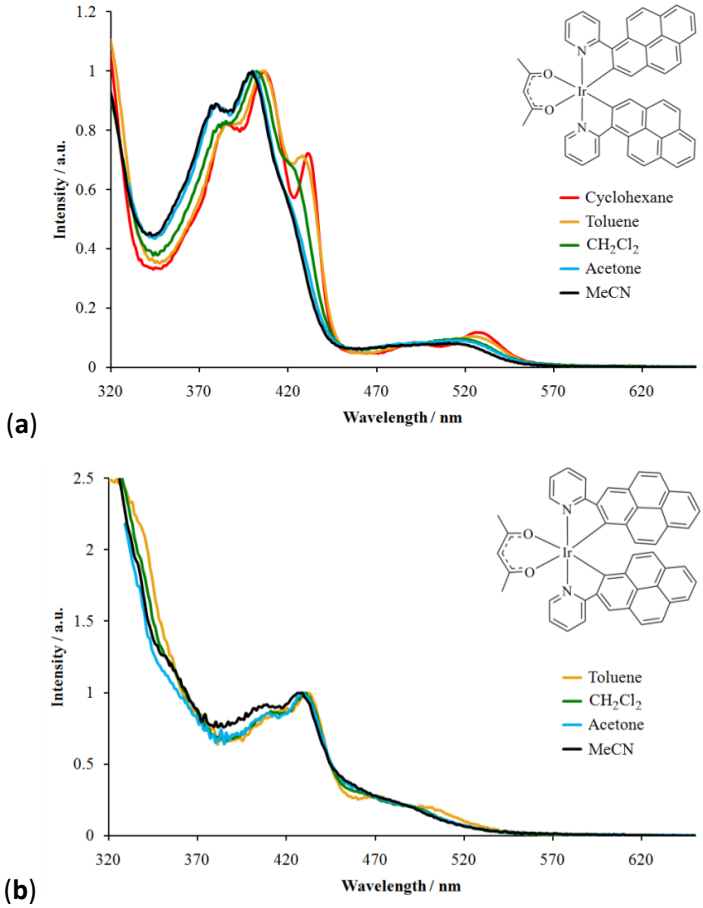

Figure 2.12. Absorption spectra of (**a**) [Ir(1-pypyr)$_2$(acac)] (**b**) and [Ir(2-pypyr)$_2$(acac)] in a range of solvents of different polarity. The spectra have been normalised to the bands centered at 400 and 430 nm, respectively. *N.B.* Due to low solubility, the absorption spectrum of [Ir(2-pypyr)$_2$(acac)] was not measured in cyclohexane.

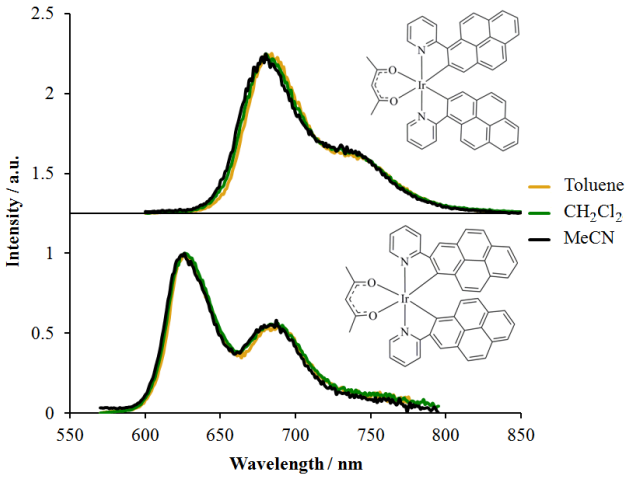

Figure 2.13. Normalised room temperature emission spectra of (**a**) [Ir(1-pypyr)$_2$(acac)] (λ_{ex} = 400 nm) and (**b**) [Ir(2-pypyr)$_2$(acac)] (λ_{ex} = 430 nm) in a range of solvents of different polarity.

The [Ir(2-pypyr)$_2$(acac)] isomer exhibits an absorption profile much broader and less structured than the previously discussed isomer due to the greater overlap of the various bands. However, it does still have bands that can be identified as ^{1}LC-type at wavelengths below 370 nm, a combination ^{1}LC and ^{1}CT band at around 430 nm and a less intense feature centered at 490 nm that is described as an admixture of ^{3}LC and ^{3}CT. The 430 nm centered band is bathochromically shifted by approximately 1700 cm^{-1} compared to the 1-substituted isomer, while the lowest energy band does not extend as far towards the red end of the spectrum. In addition, this isomer does not show such a dramatic solvent dependence; the band shape is predominantly maintained and there is a smaller negative solvatochromic shift of 200 cm^{-1} of the 430 nm centered band.

Comparing the room temperature emission spectra (Figure 2.13) of the two complexes in acetonitrile, there is an energy difference in the emission maxima of 1350 cm^{-1} (λ_{em} = 623 nm for [Ir(2-pypyr)$_2$(acac)] and λ_{em} = 680 nm for [Ir(1-pypyr)$_2$(acac)]). In both cases, the emission spectra are almost solvent independent (< 100 cm^{-1} negative solvatochromic shift between toluene and acetonitrile), implying that the transition can be described as predominantly ^{3}LC. The assignment of a ^{3}LC-type transition is further supported by the structured emission for [Ir(2-pypyr)$_2$(acac]) with a vibrational spacing of 1350 cm^{-1}. The emission spectrum of [Ir(1-pypyr)$_2$(acac)] is similar in profile, but shows a less well resolved vibronic band as a shoulder. This implies that this isomer has a more pronounced geometry change in the excited state, which can be attributed to electronic coupling between the pyridyl and pyrenyl moieties leading to a degree of ^{3}I^{ra}LCT. For comparison, the inclusion of either isomer of the pyrenyl unit in place of a phenyl ring leads to significantly bathochromically shifted emission relative to the parent complex [Ir(ppy)$_2$(acac)], which has an emission maximum at 520 nm in CH_2Cl_2;[1] this corresponds to a shift of 4500 cm^{-1} for [Ir(1-pypyr)$_2$(acac)] and 3300 cm^{-1} for [Ir(2-pypyr)$_2$(acac)]. [Ir(ppy)$_2$(acac)] is also much more solvatochromic due to the predominantly ^{3}MLCT nature of its emission.[6]

Emission and excitation spectra for both complexes were additionally obtained at 77 K in the optically transparent mixed solvent glass EPA (5:5:2 diethyl ether:2-methylbutane:ethanol) (Figure 2.14 overleaf). For both complexes the emission maximum is temperature independent, giving T_1-S_0 $E_{0''\text{-}0'}$ = 14,700 cm^{-1} and 16,100 cm^{-1}, respectively. The negligible temperature-induced shift of the emission lends further support for the assignment of a large ^{3}LC component to the transition.

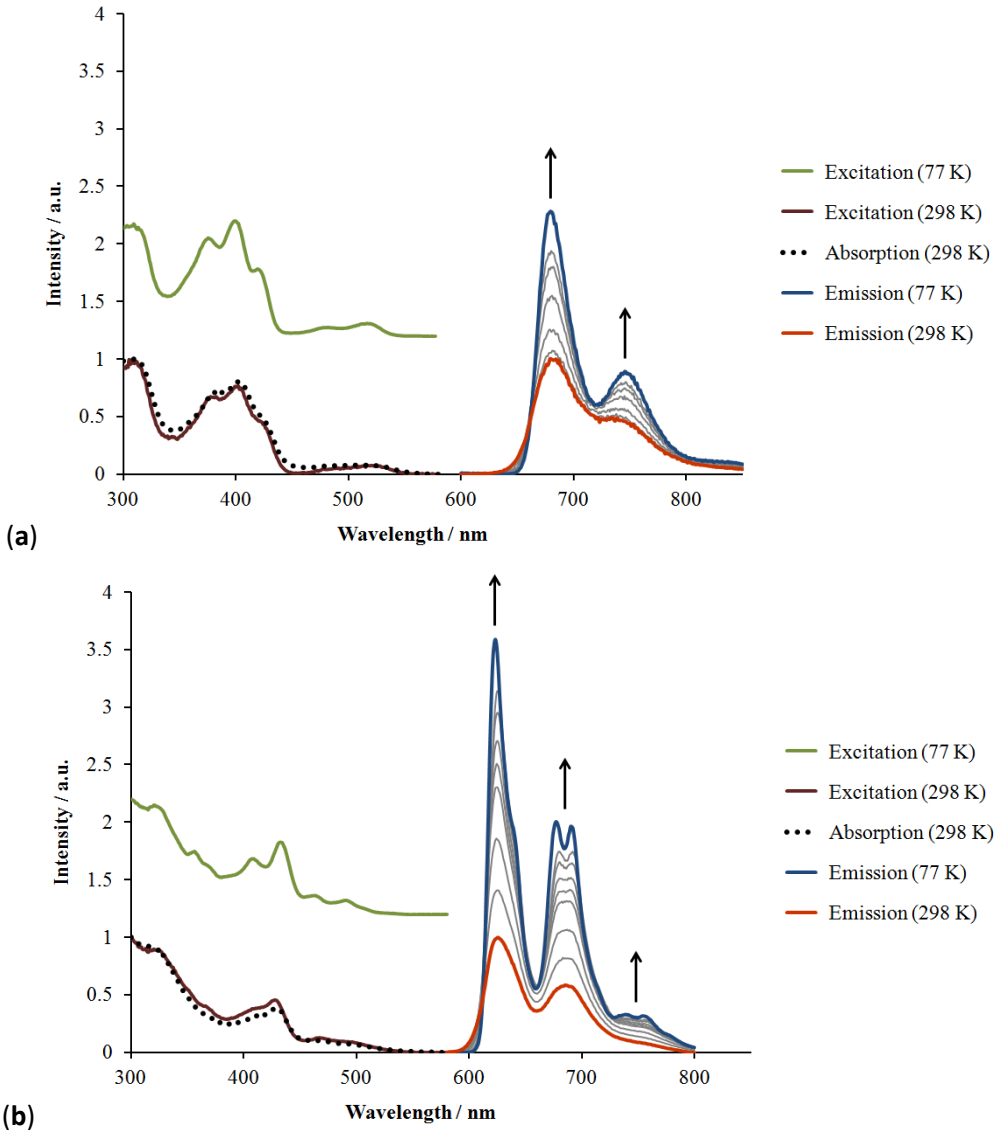

Figure 2.14. Normalised room temperature absorption and variable temperature excitation and emission spectra of (**a**) [Ir(1-pypyr)$_2$(acac)] (λ_{em} = 680 nm, λ_{ex} = 400 nm) and (**b**) [Ir(2-pypyr)$_2$(acac)] (λ_{em} = 630 nm, λ_{ex} = 430 nm) in the solvent mixture EPA. Variable temperature emission spectra are normalised relative to the 298 K spectrum and the spectra in grey were recorded at intervals during the cooling of the sample to 77 K. The excitation spectra at 77 K are offset for clarity. The arrows indicate the change in intensity with decreasing temperature (*N.B.* the volume contraction of EPA ($V_{77\,K}/V_{298\,K}$ = 0.77)[51] only partially accounts for the increase in intensity). Note that the absorption and excitation spectra at 298 K are in good agreement, as expected.

Other features of the low temperature spectra include the expected sharpening of the high energy edge of the emission band and an increase in the resolution of the vibronic structure. This is most notable for [Ir(2-pypyr)$_2$(acac)] where the second vibrational band at room temperature, splits into two peaks of approximately 350 cm^{-1}

spacing at 77 K, potentially indicating a low energy vibrational mode coupling the excited and ground states. Further structure to the low energy tail of the emission spectrum becomes apparent, also with an energy spacing of *ca*. 350 cm^{-1}. Both compounds exhibit a moderate increase in intensity at 77 K, which was monitored during the cooling process. The excitation spectra of both complexes becomes more structured at 77 K, which is particularly noticeable for [Ir(2-pypyr)$_2$(acac)] due to its relatively broader spectrum at room temperature.

Observed phosphorescence lifetimes, τ_P, of [Ir(1-pypyr)$_2$(acac)] (Table 2.5 overleaf) are virtually solvent independent, with an average value of 2.8 μs, which is typical for a cyclometalated Ir complex with low energy ^{3}LC emission. Interestingly, the PLQY increases with solvent polarity, which is a result of a shorter pure radiative lifetime, τ_0, in more polar solvents. The non-radiative decay rate, k_{nr}, is, however, independent of solvent polarity. In contrast, the observed lifetime of [Ir(2-pypyr)$_2$(acac)] varies significantly with the solvent environment, being almost five times longer in toluene than in acetonitrile. Indeed, the observed lifetimes in toluene (52.9 μs) and in EPA at r.t. (67.1 μs), are more than 20 times longer than for the other isomer, and are extraordinarily long compared to other common neutral cyclometalated iridium complexes, although not quite as long as some recently reported charged complexes by Zhao and co-workers[52] and Nazeeruddin and co-workers[53] that have lifetimes of 68 and 84 μs, respectively. The PLQY values are also approximately an order of magnitude greater than those of [Ir(1-pypyr)$_2$(acac)]. These two observations are consistent with the energy gap law in which k_{nr} is greater for the lower energy emitting species.[54, 55] The long pure radiative lifetimes of both complexes are hypothesised to be a consequence of the small Ir contribution to the $T_1 \leftarrow S_o$ transitions, which, in combination with the small orbital change associated with the localised ^{3}LC/^{3}I^{ra}LCT nature of these transitions, leads to a small degree of SOC (similar to the rationalisation of the low radiative rate of some Ru(II)[56] and Ir(III)[57] complexes with ^{3}LC transitions on π-extended ligands). The solvent dependence of τ_0 may be a result of changing the configurational mixing of ^{3}LC, ^{3}I^{ra}LCT and the very minor ^{3}MLCT contributions to include more charge transfer (of either type, stabilised by more polar solvents), facilitating a slight increase in SOC, making the transition more allowed in more polar solvents. In addition, it is suggested that the strain induced by the twist in the cyclometalated ligand of [Ir(1-pypyr)$_2$(acac)] may provide an additional low energy

Table 2.5. Photophysical data for the complexes [Ir(1-pypyr)$_2$(acac)] and [Ir(2-pypyr)$_2$(acac)]

[IrL$_2$(acac)] L	**λ_{abs} / nm (log(ε / M^{-1} cm^{-1})) [a,b]**	**Solvent [c]**	**λ_{em} / nm [b,d]**	**τ / µs [e]**	**Φ [f]**	**τ_0 / ms [g]**	**k_r / s^{-1} [h]**	**k_{nr} / s^{-1} [i]**
1-pypyr	272 (4.55), 309 (4.60), 386 (sh. 4.51), 404 (4.58), 423 (sh. 4.40), 519 (3.55)	Toluene	684*, 734 (sh.)	2.5	0.0013	1.9	520	4.0 x 10^5
		CH_2Cl_2	680*, 734 (sh.)	2.7	0.0056	0.48	2100	3.7 x 10^5
		MeCN	680*, 734 (sh.)	2.5	0.0088	0.28	3600	4.0 x 10^5
		EPA	680*, 738	3.6	-	-	-	-
		EPA (77 K)	679*, 745	5.1	-	-	-	-
2-pypyr	274 (4.98), 296 (4.97), 321 (4.95), 411 (4.45), 432 (4.54), 464 (3.99), 493 (3.82)	Toluene	626*, 680	52.9	0.021	2.5	400	1.9 x 10^4
		CH_2Cl_2	626*, 683	37.0	0.063	0.59	1700	2.5 x 10^4
		MeCN	623*, 685	11.6	0.060	0.19	5200	8.1 x 10^4
		EPA	623*, 685	67.1	-	-	-	-
		EPA (77 K)	622*, 636 (sh.) 676, 692	125	-	-	-	-

[a] Measured in CH_2Cl_2 solution; [b] sh. = shoulder; [c] Degassed samples. 298 K, except where stated otherwise. EPA is the solvent mixture 5:5:2 diethyl ether:2-methylbutane:ethanol; [d] Excitation at 400 and 430 nm for [Ir(1-pypyr)$_2$(acac)] and [Ir(2-pypyr)$_2$(acac)], respectively. Starred value is the emission maximum; [e] Excitation at 337 nm. Decay monitored at 680 and 630 nm for [Ir(1-pypyr)$_2$(acac)] and [Ir(2-pypyr)$_2$(acac)], respectively. Estimated error: 5% of the value; [f] Estimated error: 10% of the value; [g] $\tau_0 = \tau.\Phi_T/\Phi$ and assuming the quantum yield of triplet formation, Φ_T, = 1; [h] $k_r = 1/\tau_0$; [i] $k_{nr} = 1/\tau - k_r$.

vibrational deactivation pathway that further increases k_{nr}. Steric crowding has been implicated in increasing k_{nr} for other polyaromatic hydrocarbon-based cyclometalating ligands, although in these examples the interaction is between a pendant phenyl group and a pyridyl moiety, rather than with the cyclometalated ring as found here.[58] Ruthenium complexes with bipyrimidine ligands have been shown to exhibit a similar phenomenon.[59]

It is worth comparing [Ir(1-pypyr)$_2$(acac)] to the previously reported [Pt(1-pypyr)(acac)] complex that was reported to have a very similar emission maximum of 680 nm and PLQY of 0.005, but a longer lifetime of 6.2 μs (therefore longer pure radiative lifetime of 1.2 ms) in degassed CH_2Cl_2 solution.[37] This Pt complex was described as having a pyrene localised excited state, and the similarity of the photophysical data imply the same for the Ir complex.

2.2.2. Electrochemical study

Cyclic voltammetry (CV) of the two complexes was carried out in dry 0.1 M CH_2Cl_2 [*n*-Bu$_4$N]PF$_6$ supporting electrolyte with decamethylferrocene/decamethylferrocenium (Fc*/Fc*$^+$) as the reference redox couple and are reported relative to the more common ferrocene/ferrocenium (Fc/Fc$^+$) couple. Electrochemical data are summarised in Table 2.6 and the recorded voltammograms are shown in Figure 2.15 for the range within which redox events were observed. Both isomers exhibit reversible first oxidation waves, with [Ir(2-pypyr)$_2$(acac)] showing a second wave (0.64 V) within the solvent window. A second oxidation wave was not observed for [Ir(1-pypyr)$_2$(acac)], even when a more strongly interacting electrolyte, [*n*-Bu$_4$N]Cl, was used. The difference in anodic and cathodic peaks ($|E_{pc} - E_{pa}|$) indicates that all observed oxidations are one electron and are diffusion controlled under the conditions employed. The first oxidation wave of [Ir(1-pypyr)$_2$(acac)] (0.32 V) is shifted positively by 190 mV compared to that of [Ir(2-pypyr)$_2$(acac)] (0.13 V), indicating a lower lying HOMO level, assuming relaxation and electron correlation effects are similar in both compounds. For comparison, [Ir(ppy)$_2$(acac)] has an oxidation potential of 0.40 V *vs.* Fc/Fc$^+$ when measured under similar conditions.[6, 60] The introduction of the pyrenyl moiety has therefore destabilised the HOMO of both isomers of the complexes studied here, to varying extents, relative to [Ir(ppy)$_2$(acac)], which contributes in part to the bathochromically-shifted absorption and emission. No reduction waves were observed.

Table 2.6. Electrochemical data for [Ir(1-pypyr)$_2$(acac)] and [Ir(2-pypyr)$_2$(acac)][a]

	$E_{1/2}$ / V	$\lvert E_{pc} - E_{pa} \rvert$ / mV
[Ir(1-pypyr)$_2$(acac)]	0.32	51
[Ir(2-pypyr)$_2$(acac)]	0.13	56
	0.64	66

[a] N_2 saturated CH_2Cl_2/0.1 M [*n*-Bu_4N]PF_6, r.t., v = 0.10 V s^{-1}, all Pt electrodes, reported *vs*. Fc/Fc$^+$ using the internal reference redox couple Fc*/Fc*$^+$ at $E_{1/2}$ = -0.59 V.[61]

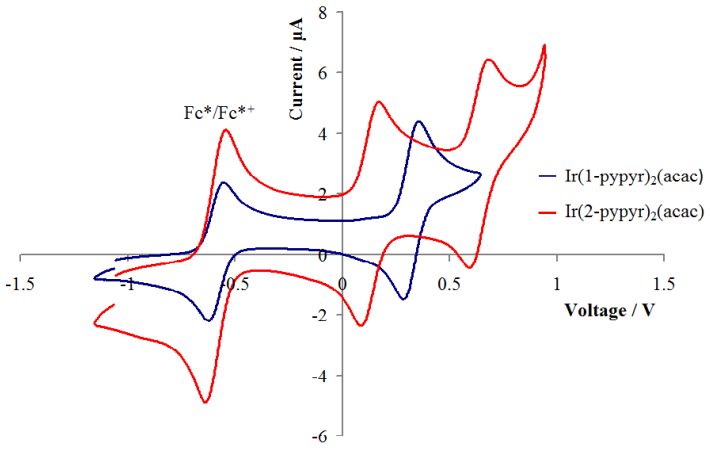

Figure 2.15. Room temperature cyclic voltammograms of [Ir(1-pypyr)$_2$(acac)] and [Ir(2-pypyr)$_2$(acac)] in N_2 saturated 0.1 M [*n*-Bu_4N]PF_6 CH_2Cl_2 solution, recorded at a scan rate of 0.10 V s^{-1} with all platinum electrodes. Reported *vs*. Fc/Fc$^+$ using the internal reference redox couple Fc*/Fc*$^+$ ($E_{1/2}$ = -0.59 V *vs*. Fc/Fc$^+$).[61]

2.2.3. Computational study

The cyclometalation of 1-pypyrH with Ir has been described previously as occurring reluctantly, and has therefore necessitated the use of unusual reaction conditions, in particular, the use of trimethyl phosphate as the solvent.[36] The 2-pypyrH isomer, however, cyclometalates under conventional conditions, an observation partially ascribable to the greater barrier present for 1-pypyrH to form the required planar conformation for cyclometalation than for 2-pypyrH. The difference in the magnitude of this planarisation barrier is manifested in the X-ray crystal structures of the two ligands, in which 2-pypyrH is almost planar, while 1-pypyrH has a dihedral angle of approximately 41° between the pyrene and pyridine moieties. To estimate the size of

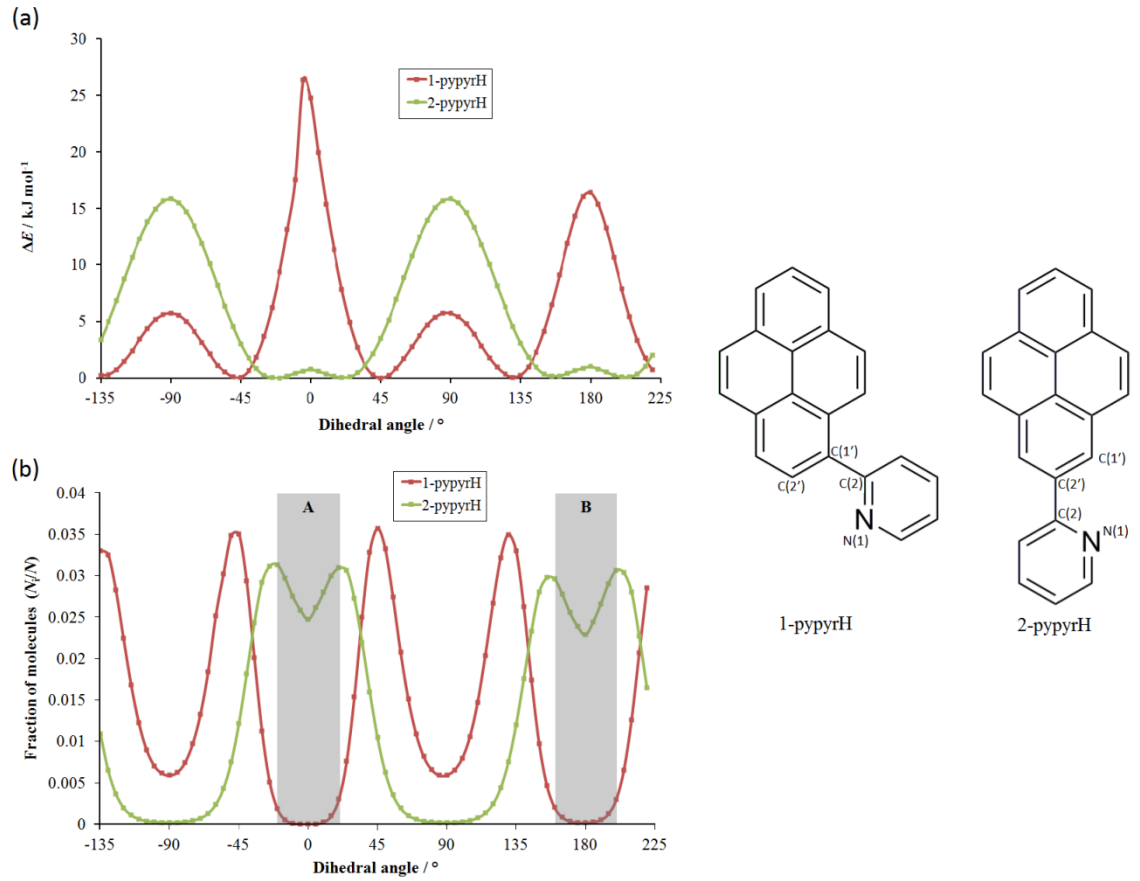

Figure 2.16. (**a**) Potential energy surfaces of 1-pypyrH and 2-pypyrH showing the difference in total energy, Δ*E*, as a function of the dihedral angle between the pyrene and pyridine rings. Calculations were performed using DFT at the B3LYP/6-31+G(d) level of theory. To construct these surfaces, the pyrene-pyridine dihedral angles of the two isomers (N(1)-C(2)-C(1′)-C(2′) for 1-pypyrH and N(1)-C(2)-C(2′)-C(1′) for 2-pypyrH, where 0° corresponds to the planar conformations shown), were changed in 5° steps with optimisation of all other degrees of freedom. (**b**) Boltzmann distribution (383 K) of conformers of 1-pypyrH and 2-pypyrH as a function of the dihedral angle between the pyrenyl and pyridyl rings. [Ir(1-pypyr)$_2$(acac)] has an experimental inter-ring dihedral angle of ≈18°. If the range of dihedral angles suitable for cyclometalation is assumed to be -20° to 20°, it is found that 1-pypyrH has ≈ 0.5% (shaded area **A**) of the molecules in this range at 383 K, *i.e.* at the standard cyclometalation temperature. In the case of 2-pypyrH, the ranges -20° to 20° and 160° to 200° are equivalent by symmetry and in total ≈ 50% of the molecules at any one time are expected to be in conformations suitable for cyclometalation (shaded areas **A** and **B**), indicating a large difference in the distribution of the conformers of the two isomers.

this barrier, energy calculations stepped around this dihedral angle were performed on both isomers. Firstly, the structures were optimised *via* DFT calculations at the

B3LYP/6-31+G(d) level of theory using the ligand structures obtained from the X-ray crystallographic study as the initial input geometry. This was followed by a scan of the dihedral angle between the pyridine and pyrene rings in 5° steps, with full optimisation of the structure in all other degrees of freedom. From these results, the potential energy surfaces (PES) along this coordinate were constructed, and are plotted as the change in total energy from the fully optimised structure as a function of dihedral angle (Figure 2.16a). These calculations indicate that in both isomers there is an unfavorable steric interaction between the hydrogen atom at the 3-position of the pyridine and the proximal hydrogen atoms of the pyrene rings. For the 2-pypyrH ligand, this energy barrier is calculated to be 0.8 kJ mol^{-1}, while for 1-pypyrH it is more than 30 times larger at 26 kJ mol^{-1}. Although the minimum energy geometry is calculated for 2-pypyrH at a dihedral angle of 20°, the small planarisation barrier can easily be overcome, and a planar geometry is obtained in the crystal structure, similar to that observed in some biphenyl derivatives.[62] As a consequence of the much larger barrier for 1-pypyrH, the calculated minimum (45°) is in much closer agreement with the 41° dihedral angle found in the crystal structure. It is also observed that the total energy reaches local maxima for both isomers when the two rings are orthogonal (symmetry related -90° and 90° dihedral angles) due to a reduction in conjugation between the rings. In the case of 2-pypyrH, the conjugation must occur *via* orbitals below the pyrene HOMO because of the nodal plane that passes through the 2-position of the pyrene HOMO (*vide infra*) prohibits conjugation at any pyrene-pyridine dihedral angle. The compound 1-pypyrH undergoes significant distortion at dihedral angles close to 0° in order to minimise the steric interaction between the hydrogen atoms described above; this has the effect of a less smooth PES profile around this value. The complex [Ir(1-pypyr)$_2$(acac)] shows an 18° pyrene-pyridine dihedral angle in the crystal structure. Thus, cyclometalation does not fully overcome the barrier, but still represents an approximately 12 kJ mol^{-1} increase in energy compared to the optimised geometry of the uncoordinated ligand. The Boltzmann distribution of the conformers from the calculated PES at the standard cyclometalating temperature of 383 K is included in Figure 2.16b.

For the parent molecule pyrene, the calculated ordering of the two lowest energy singlet excited states, ^1L_b (experimentally the lowest energy of the two) and ^1L_a, is sensitive to the computational method employed. The use of TD-DFT with the common B3LYP exchange-correlation functional leads to a calculated inversion of states,[63] in

which the ^1L_a state is predicted to lie below the ^1L_b state, while the CAM-B3LYP functional achieves the correct state ordering.[25] With this is mind, TD-DFT calculations were performed with both of these functionals and the 6-31+G(d) basis set, starting from the B3LYP/6-31+G(d) optimised geometry to confirm the assignments made for the experimental UV-visible absorption spectra. For the 2-pypyrH ligand, it is calculated with both methods that the ^1L_b is lower in energy than the ^1L_a state, as expected, although both the energy difference and oscillator strength of the two states varies with the method. Both methods, however, predict correctly that excitation to the ^1L_b state is only weakly allowed ($f \approx 0.01$), similar to other 2-substituted pyrene derivatives[25] and matching the experimentally obtained absorption spectrum. For 1-pypyrH, the ordering of these two states is reversed with both methods, and so the $S_1 \leftarrow S_0$ transition is calculated to be to the allowed (f = 0.46-0.56) ^1L_a state, while $S_2 \leftarrow S_0$ is to the ^1L_b state with a very low oscillator strength (f = 0.001-0.005). The ^1L_b state is particularly sensitive to substituents in the 1-position and this reversal is often seen in 1-substituted derivatives.[25]

Geometry optimisations of the ground S_0 and the excited T_1 states of the two Ir complexes were performed using DFT at the B3LYP/6-31G(d)/LANL2DZ level of theory (spin unrestricted for T_1). Frequency calculations confirmed that minima had been obtained in all cases. Comparison of the bond lengths to the Ir atom experimentally determined by X-ray crystallography with those obtained for the S_0 states by DFT show that they are in close agreement, with a maximum/average discrepancy of 2.0/1.4 and 2.7/1.9% for [Ir(1-pypyr)$_2$(acac)] and [Ir(2-pypyr)$_2$(acac)], respectively. This difference is a systematic elongation of these bonds by *ca.* 0.03-0.06 Å, as has been observed previously with other calculations at a similar level of theory.[15] Only minor geometric differences are calculated between the S_0 and T_1 optimised geometries, both in the metal to ligand bond lengths (< 0.02 Å) and in the X–Ir–Y bond angles (< 0.3°) (X and Y are the C, N and O atoms coordinated to the metal). Furthermore, the calculated geometries are only marginally affected by the inclusion of a high dielectric solvent (MeCN) using the PCM.

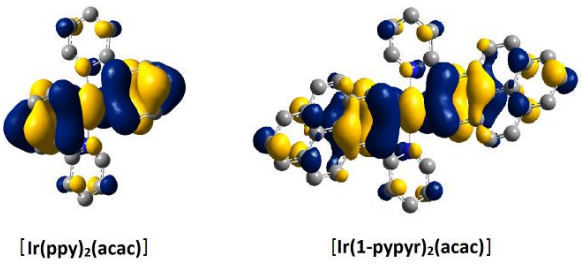

Figure 2.17. A comparison of the HOMOs of [Ir(ppy)$_2$(acac)] and [Ir(1-pypyr)$_2$(acac)]. Isovalue: ± 0.02 [$e\ a_0^{-3}$]$^{1/2}$. Hydrogen atoms are omitted for clarity.

Experimentally the oxidation potential of [Ir(1-pypyr)$_2$(acac)] is greater by 190 mV than that of the [Ir(2-pypyr)$_2$(acac)] analog, and the ordering of the HOMO energies is reproduced here by the calculations, although the calculated energy difference is greater. The HOMO of [Ir(1-pypyr)$_2$(acac)] is distributed over the Ir atom and the single ring of the pyrene system to which it is coordinated and is therefore qualitatively related to the HOMO of [Ir(ppy)$_2$(acac)], which is spread over the metal and the phenyl ring of the ppy$^-$ ligand (Figure 2.17). The first oxidation of the parent [Ir(ppy)$_2$(acac)] has been ascribed to being predominantly an Ir(III)/Ir(IV) process based on its high level of reversibility and the absence of an oxidation event for the free ligand at a similar potential. The somewhat similar oxidation potentials ($\Delta E_{1/2}$ = 0.08 V) and comparable spatial extents of the HOMOs of these two complexes would, upon first inspection, seemingly imply that their first oxidation waves have a similar origin. The HOMO of [Ir(2-pypyr)$_2$(acac)] has a much greater pyrenyl component and a much lower oxidation potential than the parent [Ir(ppy)$_2$(acac)] ($\Delta E_{1/2}$ = 0.27 V). Its origin is therefore described as a ligand-based oxidation with a small amount of metal character. In order to assign the oxidation processes more conclusively, the structure of the mono- and dications of both complexes were optimised at the same level of theory. However, although these calculations converged and frequency calculations indicated that minima had been located, stability calculations revealed instability in the wavefunction due to a non-*aufbau* orbital occupation, a fact not immediately obvious from the initial calculations. Enforcing an exchange of the ordering of the orbital pairs associated with the instabilities resulted in new solutions of marginally lower energy; however, frequency calculations indicated that minima had not been found, suggesting yet lower energy solutions exist. It was not possible to find solutions that were both stable and provided all-positive frequencies. By considering the orbitals from the different

solutions, it was found that very different interpretations of the oxidation procedure could be formulated and thus a definitive description of the oxidation is not available from this method. Therefore, caution is urged when performing calculations to assign electrochemical data by optimisation of the redox products, in particular, advising that both frequency and stability calculations should be routinely run to ensure that erroneous conclusions are not drawn. A more in depth study of the origin of this problem and an investigation of its generality, as well as efforts to identify a more suitable methodology for these types of calculations, are underway.

In order to gain insight into the observed photophysical properties of the Ir complexes, an analysis of the gas phase dipole moment changes between the ground and excited states was first undertaken. From the aforementioned optimised neutral geometries, the dipole moments of the S_0 and T_1 states were obtained. Additional single point energy calculations were performed to evaluate the dipole moment of the triplet state at the ground state geometry, denoted $T_1(S_0)$, and the singlet state at the excited state geometry, $S_0(T_1)$, which correspond to the dipole moments of the Franck-Condon states following absorption and emission, respectively. These data are summarised in Table 4, along with the scalar and vector changes in dipole moment between the optimised S_0 and T_1 states. It can be seen that the scalar change in dipole moment associated with vertical absorption ($T_1(S_0) – S_0$) is larger for [Ir(2-pypyr)$_2$(acac)] than its isomer, indicating a greater degree of charge redistribution following excitation. However, this value is notably smaller than those for chromophores that undergo a significant charge transfer.[64] Following geometric relaxation to the optimised T_1 geometry, the dipole moment has a value close to that calculated for the optimised ground state, S_0. The magnitudes of both the scalar and vector differences between the dipole moments of the optimised T_1 and S_0 states are small, which is consistent with the lack of solvatochromism in the emission, as there is only minimal reorientation of the solvent required following excitation before emission occurs. The difference in the magnitude of the scalar and vector dipole moment changes is due to a minor deviation from collinearity of the ground and excited state dipole moments. It is noted that the change in the dipole moment following emission ($S_0(T_1) – T_1$) is negligible in both cases, indicating even less charge transfer character to the emission than the excitation. The calculated dipole moments were little affected in magnitude by the inclusion of MeCN solvent (< 1 debye).

Table 2.7. DFT (B3LYP/6-31G(d)/LANL2DZ) calculated dipole moments (in debye) for the two isomeric complexes in the gas phase.[a]

	Ir(1-pypyr)$_2$(acac)	**Ir(2-pypyr)$_2$(acac)**
S_0	1.97	4.76
T_1	1.74	4.88
$T_1(S_0)$[b]	3.31	1.12
$S_0(T_1)$[c]	1.79	4.96
$T_1(S_0) - S_0$[d]	1.34	-3.76
$S_0(T_1) - T_1$[d]	0.05	0.08
$T_1 - S_0$[d]	-0.23	0.12
$\|T_1 - S_0\|$[e]	1.30	1.08

[a] Values obtained from SCF energy calculations; [b] T_1 dipole moment at the S_o optimised geometry; [c] S_0 dipole moment at the T_1 optimised geometry; [d] Scalar change in dipole moment; [e] Magnitude of the vector change in dipole moment.

TD-DFT calculations were performed using the same functional and mixed basis set, B3LYP/6+31G(d)/LANL2DZ, from the optimised ground state, to calculate excitation energies to the lowest 10 singlet and 10 triplet excited states. Both singlet and triplet transitions are considered important for these materials: the singlet states are expected to produce the highest oscillator strength transitions, but the triplet transitions gain intensity due to the large SOC of the iridium atom, which makes these formally spin-forbidden transitions partially allowed. The lowest energy transitions of both types are summarised in Table 2.8 and Table 2.9, while the orbitals contributing to these transitions are shown in Table 2.10. Further, TD-DFT calculations from the S_0 state at the optimised T_1 geometry were used to elucidate the nature of the emission (Table 2.8 and Table 2.9 provide a summary of the transitions and Table 2.11 illustrates the main orbitals involved in these transitions). However, the triplet transition energies calculated for both excitation ($T_1 \leftarrow S_0$) and emission ($T_1 \rightarrow S_0$) with this combination of method, functional and basis set are consistently lower than the experimental band maxima by 0.5-0.6 eV. The lowest energy singlet excitations, $S_1 \leftarrow S_0$ and $S_2 \leftarrow S_0$, of both isomers are described by LUMO ← HOMO and LUMO+1 ← HOMO transitions and have significant charge transfer character, being predominantly $^1I^{ra}LCT$, with some additional ^1MLCT character for [Ir(1-pypyr)$_2$(acac)]. However, the low oscillator strengths,

$f < 0.05$, of these transitions make them difficult to identify experimentally, especially as they are expected to overlap with the lower energy triplet bands. The first singlet excitation to have a significant value of f (> 0.10) are the $S_5 \leftarrow S_0$ and $S_4 \leftarrow S_0$ transitions for the 1- and 2-substituted isomers, respectively. These transitions are qualitatively more localised, with ^{1}LC being the dominant descriptor and ^{1}I^{ra}LCT being of secondary importance. The energy difference between the calculated value of these higher energy transitions and the maxima of the experimentally assigned ^{1}LC/^{1}I^{ra}LCT bands of [Ir(1-pypyr)$_2$(acac)] and [Ir(2-pypyr)$_2$(acac)] is 0.17 and 0.03 eV, respectively, representing excellent agreement. In order to identify an alternative method that addressed the greater energy discrepancies in the triplet transition energies, it was first necessary to consider the nature of the excitation and emission in terms of orbital transitions and classification (^{3}LC versus ^{3}CT) described by these initial calculations; thus, such an analysis is now presented.

Table 2.8 Lowest energy transitions of [Ir(1-pypyr)$_2$(acac)] as calculated by the TD-DFT, TDA and ΔSCF methods with the B3LYP and CAM-B3LYP functionals and the 6-31G(d)/LANL2DZ basis set.

Method	State	Transition (*f*)	*E* / eV	*λ* / nm	Dominant component(s)
Excitation					
TD-DFT B3LYP	1	$T_1 \leftarrow S_0$	1.85	674	LUMO ← HOMO-1 LUMO+1 ← HOMO-2
	2	$T_2 \leftarrow S_0$	1.85	674	LUMO ← HOMO-2 LUMO+1 ← HOMO-1
	3	$T_3 \leftarrow S_0$	2.22	558	LUMO+1 ← HOMO
	4	$T_4 \leftarrow S_0$	2.24	554	LUMO ← HOMO
	5	$S_1 \leftarrow S_0$ (0.002)	2.49	498	LUMO+1 ← HOMO
	6	$S_2 \leftarrow S_0$ (0.045)	2.48	496	LUMO ← HOMO
	13	$S_5 \leftarrow S_0$ (0.408)	2.90	428	LUMO ← HOMO-2
	15	$S_6 \leftarrow S_0$ (0.171)	2.97	417	LUMO+1 ← HOMO-2 LUMO ← HOMO-1
TD-DFT CAM-B3LYP	1	$T_1 \leftarrow S_0$	1.64	756	LUMO+1 ← HOMO-1 LUMO ← HOMO-2
	2	$T_2 \leftarrow S_0$	1.64	756	LUMO ← HOMO-1 LUMO+1 ← HOMO-2
	3	$T_3 \leftarrow S_0$	2.58	481	LUMO+1 ← HOMO
	4	$T_4 \leftarrow S_0$	2.60	477	LUMO ← HOMO
TDA B3LYP	1	$T_1 \leftarrow S_0$	2.05	605	LUMO ← HOMO-2 LUMO+1 ← HOMO-1
	2	$T_2 \leftarrow S_0$	2.05	605	LUMO ← HOMO-1 LUMO+1 ← HOMO-2
	3	$T_3 \leftarrow S_0$	2.24	554	LUMO+1 ← HOMO
	4	$T_4 \leftarrow S_0$	2.26	549	LUMO ← HOMO
TDA CAM-B3LYP	1	$T_1 \leftarrow S_0$	2.18	569	LUMO+1 ← HOMO-1 LUMO ← HOMO-2
	2	$T_2 \leftarrow S_0$	2.18	569	LUMO ← HOMO-1 LUMO+1 ← HOMO-2
	3	$T_3 \leftarrow S_0$	2.67	464	LUMO+1 ← HOMO LUMO+1 ← HOMO-2
	4	$T_4 \leftarrow S_0$	2.69	461	LUMO ← HOMO LUMO ← HOMO-2
ΔSCF B3LYP	–	$T_1(S_0)$-S_0	2.30	539	–
Experimental	1	$T_1 \leftarrow S_0$	2.39	519	–
Emission					
TD-DFT B3LYP [a]	1	$T_1 \rightarrow S_0$	1.25	992	LUMO → HOMO
TD-DFT CAM-B3LYP [a]	1	$T_1 \rightarrow S_0$	0.75	1653	LUMO → HOMO
TDA B3LYP [a]	1	$T_1 \rightarrow S_0$	1.51	821	LUMO → HOMO
TDA CAM-B3LYP [a]	1	$T_1 \rightarrow S_0$	1.55	805	LUMO → HOMO
ΔSCF B3LYP	–	T_1-$S_0(T_1)$	1.50	828	–
Experimental	–	$T_1 \rightarrow S_0$	1.82	680	–

[a] Taken as the reverse of the absorption process calculated from the S_0 state at the T_1 geometry

Table 2.9. Lowest energy transitions of [Ir(2-pypyr)$_2$(acac)] as calculated by the TD-DFT, TDA and ΔSCF methods with the B3LYP and CAM-B3LYP functionals and the 6-31G(d)/LANL2DZ basis set.

Method	State	Transition (*f*)	*E* / eV	*λ* / nm	Dominant component(s)
Excitation					
TD-DFT B3LYP	1	$T_1 \leftarrow S_0$	1.99	624	LUMO+2 ← HOMO
					LUMO+3 ← HOMO-1
	2	$T_2 \leftarrow S_0$	2.04	609	LUMO+2 ← HOMO-1
					LUMO+3 ← HOMO
					LUMO+5 ← HOMO
	3	$T_3 \leftarrow S_0$	2.13	582	LUMO ← HOMO
	4	$T_4 \leftarrow S_0$	2.26	549	LUMO+1 ← HOMO
	5	$S_1 \leftarrow S_0$ (0.003)	2.32	534	LUMO ← HOMO
	6	$S_2 \leftarrow S_0$ (0.029)	2.50	497	LUMO+1 ← HOMO
	11	$S_4 \leftarrow S_0$ (0.144)	2.84	436	LUMO+2 ← HOMO
TD-DFT CAM-B3LYP	1	$T_1 \leftarrow S_0$	1.79	693	LUMO+2 ← HOMO
					LUMO+3 ← HOMO-1
	2	$T_2 \leftarrow S_0$	1.81	685	LUMO+3 ← HOMO
					LUMO+2 ← HOMO-1
	3	$T_3 \leftarrow S_0$	2.58	481	LUMO ← HOMO
	4	$T_4 \leftarrow S_0$	2.64	470	LUMO+1 ← HOMO
					LUMO ← HOMO-1
TDA B3LYP	1	$T_1 \leftarrow S_0$	2.14	579	LUMO ← HOMO
	2	$T_2 \leftarrow S_0$	2.20	564	LUMO+2 ← HOMO
					LUMO+1 ← HOMO
	3	$T_3 \leftarrow S_0$	2.27	546	LUMO+3 ← HOMO
					LUMO+2 ← HOMO-1
					LUMO+5 ← HOMO
	4	$T_4 \leftarrow S_0$	2.30	539	LUMO+1 ← HOMO
					LUMO+2 ← HOMO
TDA CAM-B3LYP	1	$T_1 \leftarrow S_0$	2.36	525	LUMO+2 ← HOMO
					LUMO+3 ← HOMO-1
	2	$T_2 \leftarrow S_0$	2.39	519	LUMO+3 ← HOMO
					LUMO+2 ← HOMO-1
	3	$T_3 \leftarrow S_0$	2.66	466	LUMO ← HOMO
	4	$T_4 \leftarrow S_0$	2.73	454	LUMO+1 ← HOMO
					LUMO ← HOMO-1
ΔSCF B3LYP	–	$T_1(S_0)$-S_0	2.27	546	–
Experimental	1	$T_1 \leftarrow S_0$	2.51	493	–
Emission					
TD-DFT B3LYP [a]	1	$T_1 \rightarrow S_0$	1.45	856	LUMO+1 → HOMO
					LUMO+2 → HOMO
TD-DFT CAM-B3LYP [a]	1	$T_1 \rightarrow S_0$	1.02	1216	LUMO+1 → HOMO
					LUMO → HOMO
					LUMO+2 → HOMO
TDA B3LYP [a]	1	$T_1 \rightarrow S_0$	1.72	721	LUMO+1 → HOMO
					LUMO+2 → HOMO
TDA CAM-B3LYP [a]	1	$T_1 \rightarrow S_0$	1.77	700	LUMO+1 → HOMO
					LUMO → HOMO
					LUMO+2 → HOMO
ΔSCF B3LYP	–	T_1-$S_0(T_1)$	1.70	729	–
Experimental	1	$T_1 \leftarrow S_0$	1.99	623	–

[a] Taken as the reverse of the absorption process calculated from the S_0 state at the T_1 geometry.

Table 2.10. Frontier and other orbitals that contribute to the lowest energy transitions of [Ir(1-pypyr)$_2$(acac)] and [Ir(2-pypyr)$_2$(acac)], as calculated by DFT at the B3LYP/6-31G(d)/LANL2DZ level of theory. Isovalue: ± 0.02 [$e\ a_0^{-3}$]^{½}. Hydrogen atoms are omitted for clarity.

Orbital (*E* / eV)	**[Ir(1-pypyr)$_2$(acac)]**	**Orbital (*E* / eV)**	**[Ir(2-pypyr)$_2$(acac)]**
LUMO+1 (-2.10)	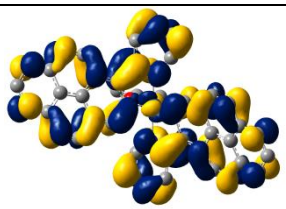	LUMO+5 (-0.84)	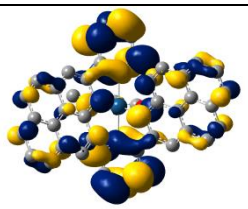
LUMO (-2.11)	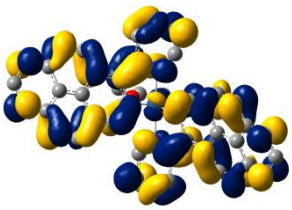	LUMO+3 (-1.08)	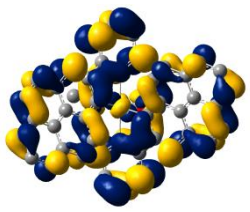
HOMO (-5.14)	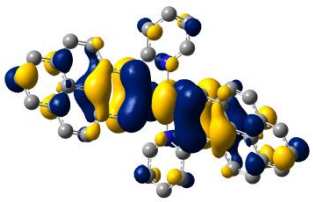	LUMO+2 (-1.18)	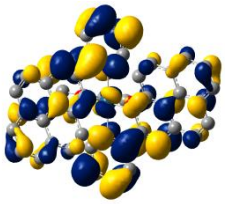
HOMO-1 (-5.28)	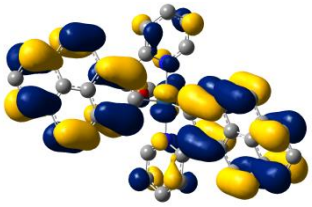	LUMO+1 (-1.40)	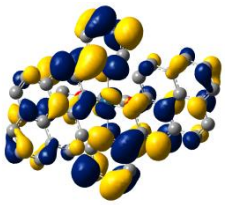
HOMO-2 (-5.29)	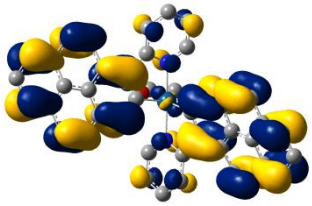	LUMO (-1.58)	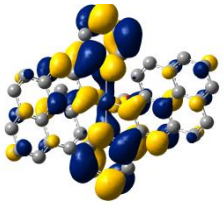
		HOMO (-4.47)	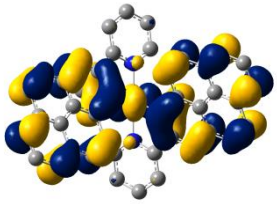
		HOMO-1 (-4.86)	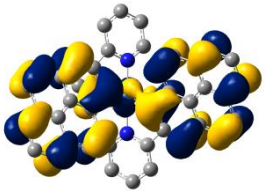

Table 2.11. Frontier and other orbitals that contribute to the emission of [Ir(1-pypyr)$_2$(acac)] and [Ir(2-pypyr)$_2$(acac)] from T_1, as calculated by DFT at the B3LYP/6-31G(d)/LANL2DZ level of theory. Isovalue: ± 0.02 [$e\ a_0^{-3}$]^{½}. Hydrogen atoms are omitted for clarity.

Orbital (*E* / eV)	**[Ir(1-pypyr)$_2$(acac)]**	**Orbital (*E* / eV)**	**[Ir(2-pypyr)$_2$(acac)]**
LUMO (-2.09)	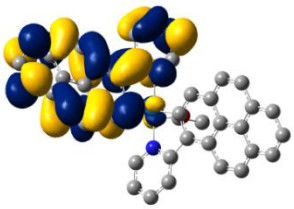	LUMO+2 (-1.32)	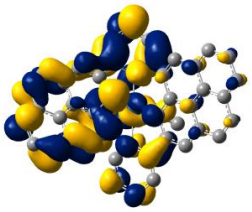
HOMO (-4.78)	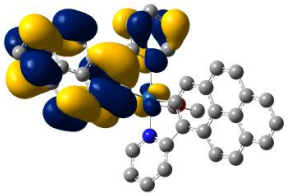	LUMO+1 (-1.46)	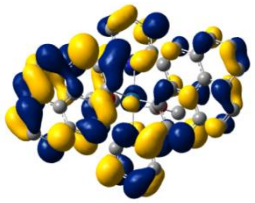
		LUMO (-1.59)	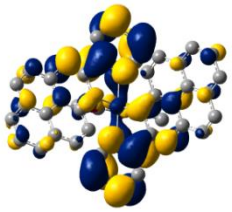
		HOMO (-4.31)	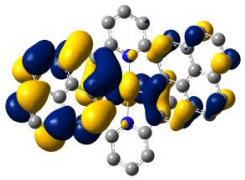

Excitation to the T_1 state of both isomers involves a transition from orbitals based upon the pyrene moiety, with some metal contribution, to one additionally incorporating the pyridine ring. This is similar to that calculated for [Ir(ppy)$_2$(bza)] (bzaH = benzoylacetone),[15] although there is a much greater contribution from the pyrene ring in the excited state compared to the analogous phenyl ring in [Ir(ppy)$_2$(bza)]. Specifically, for [Ir(1-pypyr)$_2$(acac)], T_1 and T_2 are quasi-degenerate and are described by a transition between the quasi-degenerate pairs HOMO-1 and HOMO-2 to LUMO and LUMO+1 (the molecule belongs to the point group C_2 that precludes truly degenerate orbitals). Each of these orbitals contains a nodal plane along the long axis of the pyrene ring through the site of coordination to the iridium, and so there is only a small metal contribution to the transition. Interestingly, the HOMO, which is not involved in the transition, does not contain this nodal plane. For [Ir(2-pypyr)$_2$(acac)], T_1 and T_2 are further separated in energy and involve transitions from HOMO and HOMO-1 to LUMO+2 and LUMO+3. These orbitals have a nodal plane along the long axis of the pyrene ring that reduces

intraligand conjugation between the pyridine and pyrene moieties. This is in contrast to [Ir(1-pypyr)$_2$(acac)], which is conjugated between these two rings, resulting in a calculated 0.15 eV (50 nm) lower energy transition to the T_1 state. This is in agreement with the observed bathochromic shift of the lowest energy absorption band and the emission maximum for this isomer. The best description of the excited state of both of these isomers is an admixture of ^{3}LC, ^{3}I^{ra}LCT and ^{3}MLCT transitions. For [Ir(1-pypyr)$_2$(acac)], this admixture has ^{3}LC (on the pyrene moiety) as the dominant factor, with ^{3}I^{ra}LCT (between the pyrene and pyridine rings) playing a secondary role. Conversely, [Ir(2-pypyr)$_2$(acac)] has somewhat greater ^{3}I^{ra}LCT character to the excitation, with ^{3}LC being less important to the description. This is consistent with the calculated larger change in dipole moment upon excitation for [Ir(2-pypyr)$_2$(acac)], indicative of more charge transfer character. In both complexes, ^{3}MLCT is much less important, although some small component must be included for a full description. This correlates well with the explanation of the observed photophysical measurements.

The higher energy $T_3 \leftarrow S_0$ and $T_4 \leftarrow S_0$ transitions of both complexes are predominantly ^{3}I^{ra}LCT, with some additional ^{3}MLCT character for [Ir(1-pypyr)$_2$(acac)]. The orbital description of these transitions is similar to that of the low energy singlet transitions, $S_1 \leftarrow S_0$ and $S_2 \leftarrow S_0$, which have low oscillator strength; therefore, these related triplet transitions are expected to have vanishingly small oscillator strengths and are not expected to be experimentally observable. The $T_1 \leftarrow S_0$ and $T_2 \leftarrow S_0$ would be expected to have relatively higher oscillator strengths as their character is more akin to the higher oscillator strength singlet states discussed above; although, of course, their triplet nature makes them significantly weaker than the related singlet transitions.

Spin density plots of the T_1 states were constructed and are included in Figure 2.18 (gas phase). Little difference is observable when MeCN solvent is included in the calculation through the PCM. From these plots it can be seen that, following geometric relaxation, the excited state becomes localised on the Ir atom and on a single cyclometalated ligand, as has been seen previously in other derivatives.[65] In the case of [Ir(1-pypyr)$_2$(acac)], the ligand component is delocalised over the conjugated pyridyl and pyrenyl moieties, while for [Ir(2-pypyr)$_2$(acac)], it is localised on the pyrene ring. [Ir(1-pypyr)$_2$(acac)] undergoes emission that can be described by a LUMO → HOMO transition (orbitals used here refer to the S_0 state at the T_1 optimised geometry), which is almost purely ^{3}LC delocalised over both the conjugated pyrenyl and pyridyl components. This is consistent with the observed long pure radiative lifetime in which there is little orbital momentum change and only a small metal contribution to the

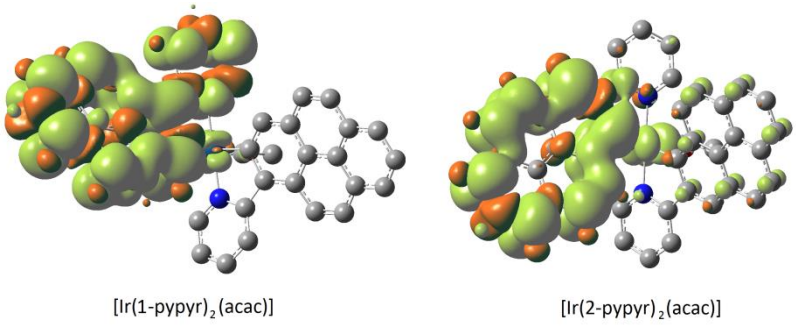

Figure 2.18. Surface plots of the spin density distribution of the optimised T_1 states of [Ir(1-pypyr)$_2$(acac)] and [Ir(2-pypyr)$_2$(acac)]. Calculated using DFT at the (unrestricted) B3LYP/6-31G(d)/LANL2DZ level. Isovalue: $\pm$ 5 x 10^{-4} e a_0^{-3}. Hydrogen atoms are omitted for clarity.

transition. [Ir(2-pypyr)$_2$(acac)] exhibits a much more mixed emissive state, with a combination of ^{3}LC and ^{3}I^{ra}LCT characters. For this isomer, a LUMO → HOMO component would be almost purely ^{3}I^{ra}LCT, but this is considered to provide only a minor contribution to the transition, and therefore mixed ^{3}LC/^{3}I^{ra}LCT offers the best description of the emitting state. Furthermore, the pyrene components of the orbitals involved in the emission of both complexes are pyrene-like, that is the HOMO of both complexes in the T_1 geometry resemble the HOMO of pyrene, and the LUMO of [Ir(1-pypyr)$_2$(acac)] and the LUMO+1 and LUMO+2 of [Ir(2-pypyr)$_2$(acac)] resemble a distorted version of the LUMO of pyrene. Therefore, the pyrene ^{3}LC component is a pseudo-^{3}L$_a$ transition.

The assignment of mixed ^{3}LC/^{3}I^{ra}LCT character for the lowest energy triplet states of both isomers raised two potential issues that were addressed separately. Recently, a connection between a near triplet instability in the ground state wavefunction and an artificial lowering of triplet transitions calculated by TD-DFT using functionals with a significant Hartree-Fock (HF) exchange component has been identified.[66] This effect is particularly important for transitions having significant spatial overlap of the ground and excited state, such as ^{3}LC transitions. B3LYP, the functional initially employed here, contains 20% HF exchange and thus would be susceptible to this problem if a near instability existed; therefore, stability calculations were conducted and the calculated eigenvalues, ω_{STAB}, were assessed. The eigenvectors from these calculations can be associated with particular transitions from the TD-DFT calculations as they are similarly described by transitions between pairs of orbitals. It has been found

previously that, empirically, a value of $\omega_{STAB} < 2$ eV is an indicator of this problem with HF exchange-containing functionals.[67] The lowest triplet transitions of both complexes were found to have ω_{STAB} values that conform to this criterion. It has also been identified that a solution to this error is provided by the Tamm-Dancoff Approximation (TDA) to TD-DFT.[67] In conventional TD-DFT, a combination of both excitation and de-excitation between orbital pairs is used to describe a transition and, while mathematically rigorous, this can lead to underestimation of, in particular, localised triplet transitions. The TDA method sets the matrix elements responsible for the de-excitation components to zero, providing a more physically intuitive solution and also partially correcting the underestimation of the transition energies.

Performing TDA calculations (B3LYP/6-31G(d)/LANL2DZ) improved the correspondence between theory and experiment to 0.34 and 0.27 eV for [Ir(1-pypyr)$_2$(acac)] and [Ir(2-pypyr)$_2$(acac)], respectively (Figure 2.19 and Figure 2.20 overleaf); similarly, emission energies were improved, and are within 0.27-0.34 eV of the experimental value with this method. Next, considering that the $T_1 \leftarrow S_0$ and $T_2 \leftarrow S_0$ transitions have some ^{3}I^{ra}LCT character, the CAM-B3LYP functional was selected, due to its better description of CT.[16, 68] This functional incorporates a variable (distance-dependent) amount of HF exchange, rather than the fixed 20% included in B3LYP. Combining TDA calculations with the CAM-B3LYP functional and the same 6-31G(d)/LANL2DZ basis set provided further improvement, giving energies within 0.21 and 0.15 eV of the experimental lowest energy excitation energies for [Ir(1-pypyr)$_2$(acac)] and [Ir(2-pypyr)$_2$(acac)], respectively. However, due to, and supporting, the assignment of the emission as being nearly pure ^{3}LC, TDA with the CAM-B3LYP functional provided only a very modest improvement over TDA with B3LYP in the emission values (ΔE = 0.04-0.05 eV). The residual difference between experimental and theoretical values is justified by the relatively small basis set, the small perturbation expected upon inclusion of solvent and the inequivalence of the compared values (vertical gas phase compared to the band maximum that may not correspond to the $v = 0'' \leftarrow 0'$ transition). Noticeably, when only the correction to the long range component was performed, that is the CAM-B3LYP functional was used with conventional TD-DFT, a large detrimental effect is observed, with excitation values being *ca.* 0.7 eV and emission values *ca.* 1.0-1.1 eV lower than experiment. This can be rationalised based on the larger HF exchange component of CAM-B3LYP,

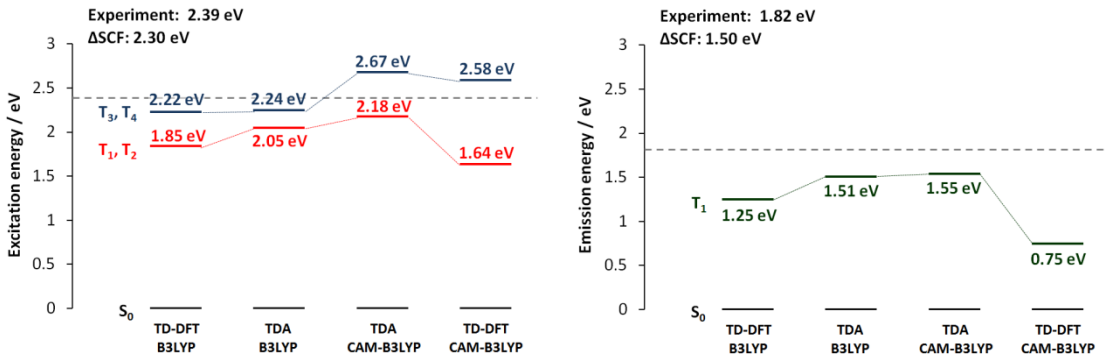

Figure 2.19. A comparison of the calculated excitation (left) and emission (right) transition energies for [Ir(1-pypyr)$_2$(acac)] using the TD-DFT and TDA methods with the B3LYP and CAM-B3LYP exchange-correlation functionals. The mixed 6-31G(d)/LANL2DZ basis set was used in each case. Experimental values are indicated by dashed lines. Energy labels for excitation are those calculated for the $T_1 \leftarrow S_0$ (red) and $T_3 \leftarrow S_0$ (blue) transitions, as defined from the initial TD-DFT/B3LYP calculation.

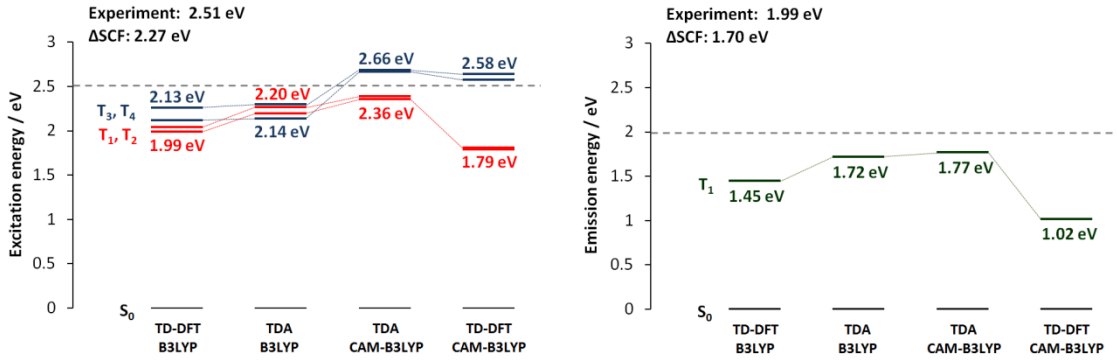

Figure 2.20. A comparison of the calculated excitation (left) and emission (right) transition energies for [Ir(2-pypyr)$_2$(acac)] using the TD-DFT and TDA methods with the B3LYP and CAM-B3LYP exchange-correlation functionals. The mixed 6-31G(d)/LANL2DZ basis set was used in each case. Experimental values are indicated by dashed lines. Energy labels for excitation are those calculated for the $T_1 \leftarrow S_0$ (red) and $T_3 \leftarrow S_0$ (blue) transitions, as defined from the initial TD-DFT/B3LYP calculation.

exacerbating the near triplet instability problem of the local transition component to a greater extent than the CT component is corrected.

The $T_3 \leftarrow S_0$ and $T_4 \leftarrow S_0$ transitions are of much greater charge transfer character and so the transition energies are only marginally affected by the use of the TDA method with B3LYP, while CAM-B3LYP with either TDA or TD-DFT leads to an increase in energy as the long range problem is corrected. Indeed in the case of

[Ir(2-pypyr)$_2$(acac)], the difference in the response of the more localised (T_1 and T_2) and more CT (T_3 and T_4) states to the choice of method leads to a change in state order when TDA/B3LYP is used compared to TD-DFT/B3LYP, which shows that the other low lying states must be considered when choosing a method in order to avoid incorrect state ordering. It is important to note that the orbital pairs describing the transitions provided by the different methods are similar, while the energies are significantly affected, thus the interpretations of the nature of the transitions, based upon the initial TD-DFT/B3LYP calculations, are unaffected. This study thus highlights the need for very careful selection of both the computational method and functional when performing calculations to assess the photophysical properties of phosphorescent organometallic complexes, especially where there is mixed character to the transition. Of particular practical importance is that the TDA/CAMB3LYP combination is of a similar computational cost to TD-DFT/B3LYP with the same basis set, but greatly increases the correspondence in transition energies between theory and experiment in this case. This method will likely be useful for similar complexes when TD-DFT methods with the B3LYP functional predict very low, or even imaginary, values of the transition energies.[69]

The ΔSCF method was also evaluated as an alternative to TD-DFT, taking for excitation the energy difference between the optimised S_0 geometry and the T_1 state at the S_0 geometry (S_0-$T_1(S_0)$) and for emission, the energy difference between the T_1 optimised geometry and the S_0 state at the T_1 geometry (T_1-$S_o(T_1)$). This method is found to give reasonable agreement with experiment, although in most cases slightly worse than the TDA/CAM-B3LYP combination. The ΔSCF method has recently gained renewed interest as a computationally low-cost alternative to TD-DFT with some theoretical justification as the exact solution in the adiabatic limit, although the method often relies heavily on cancellation of errors;[70] therefore, the TDA/CAM-B3LYP approach, which is on arguably firmer theoretical grounding, presents itself as the best method for use with this system and should be considered for other similar compounds.

2.2.4. Conclusion

Two isomeric cyclometalated iridium complexes have been synthesised to investigate the impact of varying the coordination site on the photophysics of pyrene-derived cyclometalating ligands. The greatest factor differentiating the two isomers appears to

be the location of the nodal plane along the long axis of pyrene and whether this reduces orbital overlap between the metal and the ligand or intraligand between the pyridine and pyrene rings. It is found that both isomers exhibit predominantly LC lowest energy triplet excitations with some I^{ra}LCT character, which are sensitive to solvent environment in terms of their observed and pure radiative lifetimes and quantum yields, but do not show solvatochromism in their emission spectra. Lifetime and quantum yield measurements made on this class of material are typically performed in a single solvent, whereas herein it is shown that further effects may be observed when a range of solvents is employed. In addition, crystallographic and DFT analysis has provided a rationale for the more unusual conditions required for the cyclometalation of 1-pypyrH compared to 2-pypyrH, based upon an unfavorable steric interaction in the former. The unfavorable steric interaction present in [Ir(1-pypyr)$_2$(acac)] is also believed to promote non-radiative deactivation through an additional vibrational mode, enhancing k_{nr} for this isomer. DFT, TD-DFT, TDA and ΔSCF calculations have been used to interpret the observed photophysical data, such as the red-shifted absorption of [Ir(1-pypyr)$_2$(acac)]. In addition, these calculations have confirmed that excitation to the lowest energy excited state for both complexes is a mixed $^3I^{ra}$LCT/^{3}LC-type transition with only minor ^{3}MLCT character, whilst the emission is almost purely ^{3}LC for [Ir(1-pypyr)$_2$(acac)] with some additional $^3I^{ra}$LCT character for [Ir(2-pypyr)$_2$(acac)], a finding that is consistent with the measured photophysical data. The TDA method employing the CAM-B3LYP functional is found to be an effective combination for the calculation of the excitation and emission energies of these phosphorescent iridium complexes that have mixed excited state character. The main general conclusion that can be drawn from this combined theoretical and experimental analysis of the photophysical and electrochemical data of these two isomeric complexes is that assignment by analogy with the parent complex [Ir(ppy)$_2$(acac)] is not always reliable for new [IrL$_2$(acac)] complexes, even when, superficially, the experimental data look similar, and therefore each new system should be evaluated individually.

* * * *

During the review of our paper concerning this work, another paper by Pope and co-workers[71] appeared that reported what they claimed to be "…the first examples of cyclometalated pyrene complexes of iridium(III)"; however, Ionkin[36] and Lee[38] provided earlier examples, as detailed in the introduction to this section. The authors describe the

synthesis, structures and use of Ir(III) complexes of some *N*-substituted 1-(2′-benzimidazole)pyrene ligands (Figure 2.21) as "enhanced photooxidation sensitizers". These compounds are described as exhibiting, very unusually, pure fluorescence, which is viewed with considerable scepticism considering the large SOC of Ir. Their finding (SC-XRD structure), however, of cyclometalation at the 10-position of the pyrene ring supports the suggestion of cyclometalation at this position for the 1-(1′-isoquinolinyl)pyrene analogue reported in reference 39.

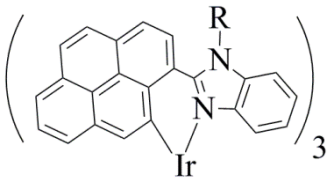

Figure 2.21. Series of iridium complexes having *N*-substituted 1-(2′-benzimidazole)pyrene ligands reported by Pope and co-workers. Notably, the site of cyclometalation is the 10-position, forming a 6-membered chelate.

2.3. Time gated two-photon absorption spectroscopy of iridium-lanthanide dyads

The MC f-f optical transitions of lanthanide (Ln) complexes are formally Laporte (parity) forbidden, resulting in low extinction coefficients and therefore only weak absorption. However, complexes of the visible light emitting lanthanides Eu (red) and Tb (green) are particularly attractive for display and communication technologies,[72] and for imaging and sensing applications.[73-75] They exhibit intense, oxygen insensitive, symmetry sensitive and long lived (μs to ms), atomic-like emission bands that make them suitable for time-gating.[76] As both a strength and a shortcoming, they exhibit only weak perturbation of the perceived emission colour with ligand variation due to the poor overlap of the Ln f and ligand σ-orbitals;[77] however, improvement in properties such as PLQY can be achieved by ligand design.[78] Due to the forbidden nature of the absorption process, it is usually necessary to use a sensitising antenna chromophore in order to generate a significant population of the excited state for emission applications.

The antenna chromophore should exhibit a much higher extinction coefficient and be of a suitable energy to sensitise excitation of the lanthanide of interest (Figure 2.22). Most often, this has been achieved with organic compounds, but recently there has been significant interest in the use of transition metal complexes as sensitising components.[79]

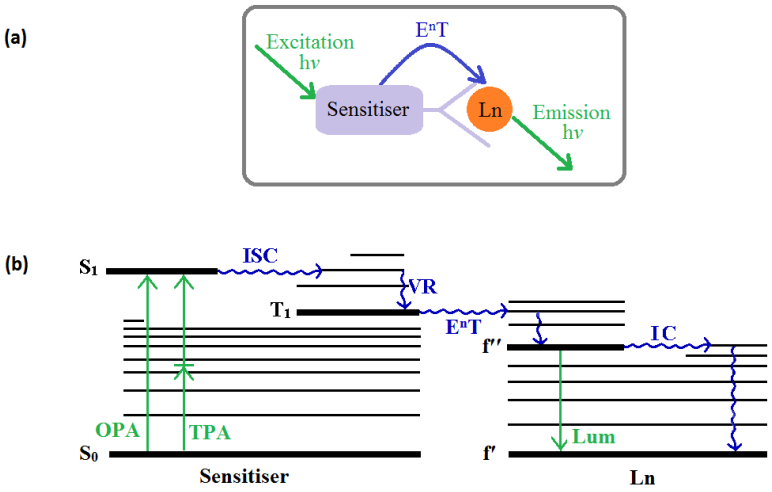

Figure 2.22. (**a**) Schematic of a sensitiser-Ln dyad. (**b**) Jablonski diagram for the sensitisation of a Ln complex by a bound sensitiser. E^nT = energy transfer. Lum = luminescence. All other abbreviations are the same as Figure 1.1 and text.

This is due to their additional desirable properties: efficient emission, which allows incomplete energy transfer to be monitored; oxygen sensitisation; almost limitless possibility for structural variation and tuneable excited states. A molecular dyad comprised of a d-block and an f-block complex is termed a d-f hybrid and in these systems energy transfer (E^nT) from the higher energy transition metal complex occurs either through a Förster or Dexter type mechanism, dependent on the system in question, to the lanthanide, which can then undergo luminescence. While it has been possible to sensitise the near-infrared (NIR) emitting lanthanides ions (Nd(III), Yb(III), Er(III) and Pr(III)) in d-f hybrids with relative ease,[80] with, for instance, Os(II),[81-83] Ru(II),[84-86] Re(I),[87-89] Pt(II)[90-92] and Ir(III)[93-95] complexes, it remains much more of a challenge for the higher energy excited state lanthanides, such as Eu(III)[96-100] and, in particular, Tb(III).

The use of cyclometalated iridium complexes as sensitisers for Eu(III)[94, 101] and Tb(III)[102] has recently been investigated. The ease with which iridium complexes of this type can be synthesised and functionalised for a particular application make them attractive for this purpose. One of the sensitisers reported by Ward and co-workers[101, 102] is the nitrate salt[i] of a blue emitting (λ_{em} = 455 nm) iridium complex with two 2′-(2,4-difluorophenyl)pyridine (F_2ppyH) cyclometalating ligands and a ditopic neutral bis(2-pyridyl-3-pyrazole) (pypz) ancillary ligand. This species, $[Ir(F_2ppy)_2(pypz)]^+$, has a free binding site capable of coordinating to $[Ln(hfac)_3]$ (Ln = Eu, Tb or Gd, hfacH = 1,1,1,5,5,5-hexafluoropentane-2,4-dione) by displacement of two water molecules from $[Ln(hfac)_3(H_2O)_2]$. Titration of the hydrated lanthanide complex into a solution of the Ir complex in non-competitive solvents, such as CH_2Cl_2, forms the bound d-f hybrid and the free complexes in equilibrium ($K_A = 2 \times 10^5$ M^{-1}).[101] The excited state of the complex $[Ir(F_2ppy)_2(pypz)]^+$ is of sufficiently high energy (22,000 cm^{-1}) to sensitise both Eu ($^5D_0$ *ca.* 17,300 cm^{-1}, $^5D_1$ *ca.* 19,000 cm^{-1}) and Tb ($^5D_4$ *ca.* 20,400 cm^{-1}) without significant back energy transfer. Gd cannot be sensitised in this way because its lowest lying excited state is too high in energy ($^6P_{7/2}$ *ca.* 32,000 cm^{-1}); thus, Gd is used as a control for assessing the importance of other quenching mechanisms, for example electron transfer.[101] The dyads with these two lanthanides are denoted $[Ir(F_2ppy)_2(pypz)*Ln(hfac)_3]^+$, where Ln is Eu or Tb, respectively (Figure 2.23).

[i] Henceforth, the nitrate counterion is implied, but is omitted for brevity

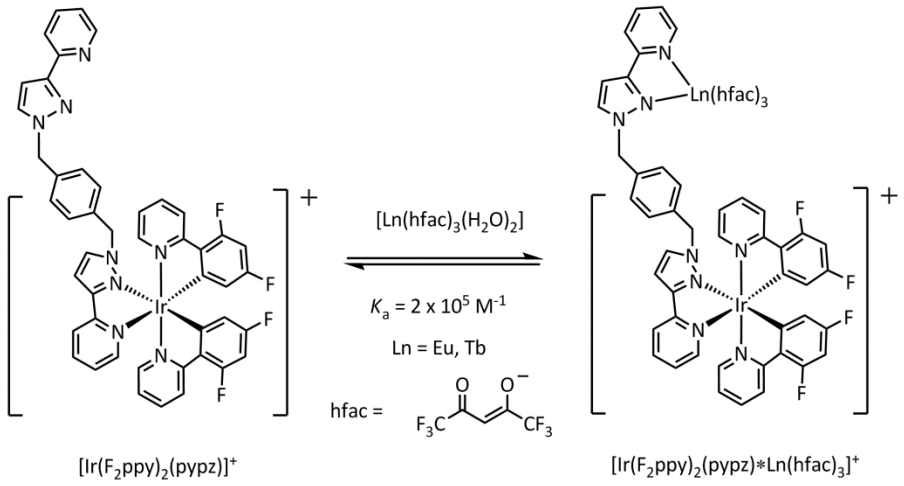

Figure 2.23. The complex $[Ir(F_2ppy)_2(pypz)]^+$ and the d-f hybrids $[Ir(F_2ppy)_2(pypz)*Ln(hfac)_3]^+$ (Ln = Eu or Tb) formed upon titration of $[Ln(hfac)_3(H_2O)_2]$ into a solution of the nitrate salt of $[Ir(F_2ppy)_2(pypz)]^+$ in non-competitive solvents (*e.g.* CH_2Cl_2).

In previous work, the two-photon excitation spectra of some prototypical cyclometalated iridium complexes[55] were reported. Therefore, it was assumed possible to excite the sensitising Ir complex of these d-f hybrids by two-photon excitation. Before the results of this study are presented, a short introduction to the background of two-photon absorption (TPA) and a summary of the results from both our earlier work[55] along with that of others[103-107] is presented in order to put into context the results of the study of the TPA of the $[Ir(F_2ppy)_2(pypz)*Ln(hfac)_3]^+$ dyads.[2]

TPA is a third order non-linear optical technique in which two photons are simultaneously absorbed by a compound to generate an excited state. This process uses photons of lower energy than the gap between the ground and the excited state. The upper state is instead populated *via* an intermediate virtual state, with the energy between the two real states matched by the sum of the energies of the two photons. This process was first described by the Nobel Prize winning physicist Maria Göppert-Mayer in her 1931 PhD thesis ("*Über Elementarakte mit zwei Quantensprüngen*").[108] The unit of the two-photon cross-section (σ_2) has been named in her honour (Göppert-Mayer units where 1 GM = 10^{-50} cm^4 s $photon^{-1}$). The quantity σ_2 indicates the strength and, therefore, how allowed is a particular TPA transition at a specific wavelength. The probability of TPA occurring is dependent on the square of the intensity of the excitation source, which is used experimentally to confirm a two-photon process, but also has the advantage that excitation is highly spatially localised. TPA is increasingly

being studied for use in improved resolution luminescence microscopy, photodynamic therapy, optical power limiting and micro-fabrication, as well as several other realised or hypothetical applications.[109] This has been facilitated by the increased availability of stable, high peak-powered fs excitation sources, principally the Ti:sapphire laser, that operate in the near-infrared region. The use of near-infrared excitation is particularly appealing for biological applications because tissue is more transparent in this part of the spectrum and, subsequently, also less susceptible to photodamage.[110]

In our previous work, complexes of the form $[IrL_3]$, $[IrL_2(acac)]$ and $[IrL_2L']$ were investigated for their TPA activity.[55] It was found that in representative systems there was very little difference in the magnitude of σ_2 between complexes of the form $[Ir(L)_3]$ and $[Ir(L)_2(acac)]$, with both $[Ir(ppy)_3]$ and $[Ir(ppy)_2(acac)]$ having a cross-sections of approximately 20 GM. This value is admittedly small compared to some of the best organic materials, which can have values of hundreds or even thousands of GM,[109] but it is comparable or better than systems of similar structure, such as $[Ru(bpy)_3]^{2+}$, which has σ_2 = 4 GM at 880 nm.[111] Indeed, a Pt complex with a σ_2 of only 20 GM has been successfully employed in TPA microscopy[112] and therefore, in combination with their long lifetimes and high quantum yields, the iridium complexes also present themselves as a readily tuneable class of chromophore for such applications. A new complex with an extended π-system was then constructed and was measured to have a larger σ_2 = 44 GM at 800 nm, rising to 62 GM at 820 nm. Thus, it was demonstrated that improvement of the of σ_2 value for Ir complexes was possible using the standard techniques that have been used in organic materials research, namely, the design of a chromophore that acts as a multipolar system with the ability to undergo a large charge transfer between its ground and excited states.[113] The complex designed had a phenylethynyl unit appended to the phenylpyridine ligand to give the simplest rod-like acceptor-donor-acceptor structure for an iridium complex, making use of the enforced *trans* geometry of the pyridyl moieties, imparted by the mild synthesis of the acac complex from the μ-chloro-bridged dimer. Figure 2.24 shows (a) the designed complex and (b-d) the results of these earlier TPA spectroscopy measurements.[55]

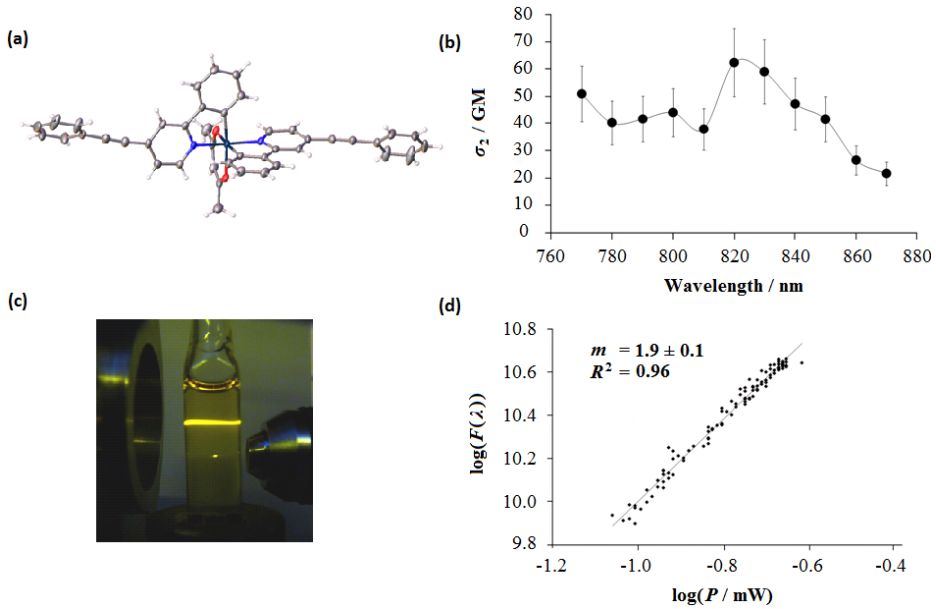

Figure 2.24. (**a**) Molecular structure of [Ir(peppy)$_2$(acac)] designed as a more efficient TPA chromophore. (**b**) Two-photon excitation spectrum of this complex. (**c**) Photograph illustrating the difference in localisation of one photon excitation (λ_{ex} = 396 nm, upper) and two-photon excitation (λ_{ex} = 780 nm, lower). (**d**) Confirmation that a two-photon process had been observed by the quadratic dependence of the emission intensity on excitation power.

Earlier work by Koide *et al*. in this area showed that two-photon induced ligand fluorescence from Ir complexes can occur.[103] In addition, a material for optical power limiting of ns laser pulses based on ESA following TPA by an Ir complex was also reported, but the cross-section of the material was not measured.[104] Natrajan and co-workers have measured values of σ_2 = 11-67 GM for Ir and Ru terpyridine complexes with attached donor-terminated stilbene groups, albeit with low PLQY values of < 0.01.[105] A complex with a strong electron donor (NMe_2) on two ppy-type ligands and a third ppy ligand substituted with a strong electron acceptor ($BMes_2$) has been reported to have a σ_2 value of 350 GM. Interestingly, this complex was found to exclusively stain the Golgi apparatus and could be used in two-photon microscopy to observe these features in detail.[106] Dinuclear Ir complexes have also been studied by two-photon spectroscopy, which is surprising considering their usually limited emission, a property often desired in combination with a large σ_2; however, for this particular example, a moderate PLQY of 0.13 was measured and a σ_2 = 195 nm.[107] These reports all suggested that the iridium-based d-f hybrids discussed above should be susceptible to TPA, and thus it was envisioned that it should be possible to excite the Ln

by sequential TPA of the Ir sensitiser followed by energy transfer. TPA excitation of antennae chromophores of Ln complexes has been reported previously for several examples,[114-117], but observation of a similar process in a d-f hybrid was unknown. Therefore, in collaboration with Prof. M. Ward (University of Sheffield), $[Ir(F_2ppy)_2(pypz)*Ln(hfac)_3]^+$ hybrids were investigated for TPA.

First, as direct excitation of simple Ln complexes was potentially possible and has been reported recently,[118] it was necessary to exclude the possibility that this process was occurring here. Control experiments were undertaken in which CH_2Cl_2 solutions of the $[Ln(hfac)_3(H_2O)_2]$ starting complexes were irradiated at 780 nm under the same conditions (concentration and excitation power) as those planned for the d-f hybrids. No emission was observed for Ln = Tb or Eu, confirming that direct excitation of the Ln would not be a competing, and hence complicating, process.

The emission of the complex $[Ir(F_2ppy)_2(pypz)]^+$ is assigned as occurring from the typical mixed ^{3}MLCT/^{3}LC/^{3}I^{er}LCT state for a charged Ir complex. In the absence of a quenching Ln complex, a lifetime for the iridium complex of 700 ns has been measured in (aerated) CH_2Cl_2.[101] Upon coordination of the Ln unit, however, the excited state lifetime is reduced considerably (to 100 ns with Eu and 70 ns with Tb),

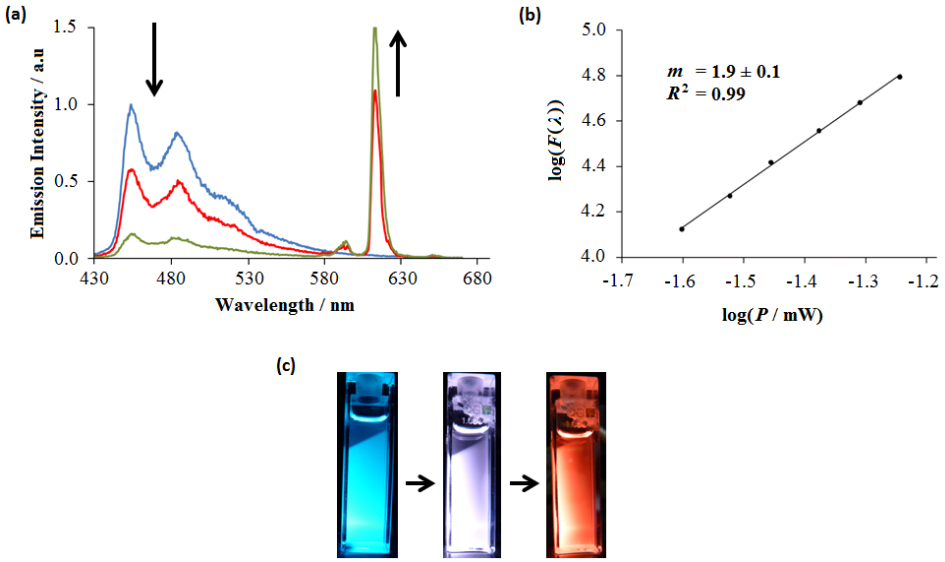

Figure 2.25. (**a**) Emission spectrum of $[Ir(F_2ppy)_2(pypz)*Eu(hfac)_3]^+$ following excitation at 780 nm. (**b**) Two photon excitation is confirmed by the quadratic dependence on laser power. (**c**) Photographs of the emission (λ_{ex} = 396 nm) of a sample of $[Ir(F_2ppy)_2(pypz)]^+$ during titration of $[Eu(hfac)_3(H_2O)_2]$ into a CH_2Cl_2 solution. The emission changes from blue (pure Ir complex) to pseudo-white (balance of Ir and Eu emission) to the endpoint where red (sensitised Eu) emission dominates.

indicating quenching due to energy transfer. While sensitisation of the Ln unit is clearly achieved in these d-f hybrids, the energy-transfer process is incomplete, resulting in dual emission from the partially quenched Ir and the sensitised lanthanide complexes. Therefore, the resultant emission spectra of the d-f hybrids are a combination of the residual Ir (blue) and Eu (red) or Tb (green) emission. In the case of the Ir/Eu hybrid, a correctly balanced ratio of the two colours appears white.[101]

The TPA cross-section of $[Ir(F_2ppy)_2(pypz)]^+$ was measured to be *ca.* 4 GM at 780 nm using the common two-photon induced fluorescence method with femtosecond excitation (*ca.* 150 fs FWHM) from a Ti:sapphire laser. This σ_2 value is clearly smaller than some of the best performing complexes mentioned above, but is in the typical range for un-optimised iridium complexes.[55] The emission spectrum following TPA is shown in blue in Figure 2.25a. A quadratic dependence of the integrated emission intensity on the excitation laser power was found, confirming that a two-photon process is occurring (Figure 2.25b). Solutions of the Ir/Eu and Ir/Tb d-f hybrids, produced from 2:1 ratios of the Ln and Ir complexes to ensure > 95% formation of $[Ir(F_2ppy)_2(pypz)*Ln(hfac)_3]^+$, following TPA at 780 nm were found to have emission spectra exactly the same as those obtained by conventional emission spectroscopy (λ_{ex} = 390 nm). The two-photon induced emission spectra of the Ir/Eu d-f hybrid with one or two equivalents of Eu are shown in red and green, respectively, in Figure 2.25a.

The lanthanide components of the dual emission spectra have lifetimes several orders of magnitude longer than the residual Ir component (*ca.* 0.65 ms for Eu and 5 ms for Tb). Therefore, it was clear that the two components of each emission spectrum should be separable in the time-domain by time-gating. The standard set-up for recording two-photon induced emission spectra was modified to achieve this. The laser was reduced to a repetition rate of 25 kHz, giving a time window of 40 μs between each excitation pulse. A scanning monochromator and photomultiplier tube replaced the CCD detector routinely used on this set-up to improve spectral quality and to allow time-gated detection. In addition, as a consequence of the weak emission of from the d-f hybrids following TPA, a 1 s integration time was used and spectra were averaged over 16 scans to ensure good signal-to-noise ratios. Employing a variable electronic pulse sequence, triggered from the cavity dumper control, and an AND gate, the signal from the photomultiplier tube could be gated in a controlled manner, with both the delay before detection and the gate width being variables.

Figure 2.26 overleaf shows the effects of time-gating. Due to the short lifetime of the iridium component, a gate width of 1 μs and no delay was sufficient to almost completely exclude the Ln emission (Figure 2.26, spectrum b for both Eu and Tb). This is additionally helped in the Ir/Eu complex by the rise time of *ca*. 1.2 μs for the Eu component. Instead, when a 3 μs delay was applied before a 21 μs gate (limited in duration only by the signal generator used), the blue emission of the Ir complex could be eliminated and the Ln emission selected (Figure 2.26, spectrum c for both Eu and Tb). It is expected that the balance of colour detected could be modified easily upon adaption of the gating sequence. It is believed that a system from which the emission colour can be selected at will, may be of interest in biological imaging applications.

To conclude, a known d-f hybrid, constructed from an Ir sensitising complex and a coordinating lanthanide unit ([Eu(hfac)$_3$] or [Tb(hfac)$_3$]), has been investigated by time-gated two-photon spectroscopy. The dual emission of the Ir/Eu and Ir/Tb d-f hybrids has been recorded following TPA of the Ir complex at 780 nm, even though the cross-section for this antenna complex is low (4 GM). Furthermore, using a simple time-gating routine, the emission colour balance has been selectively detected, providing an unusual example of variable (recorded) emission colour following two-photon excitation.

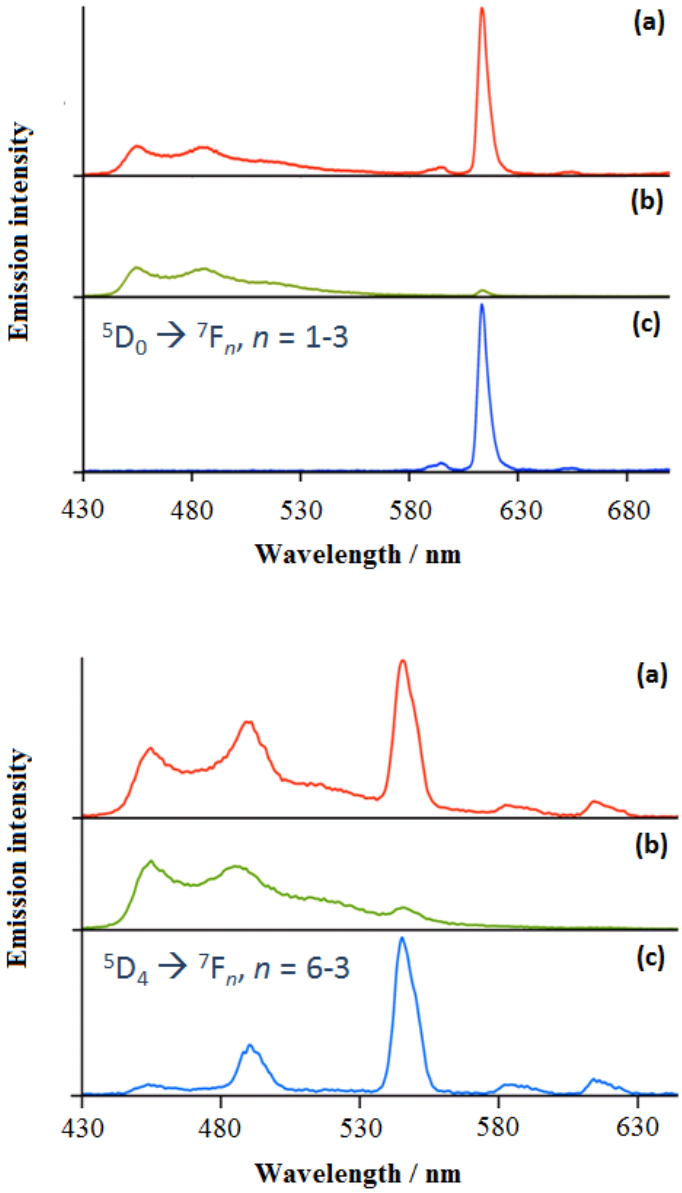

Figure 2.26. Time-gated emission spectra of $[Ir(F_2ppy)_2(pypz)*Eu(hfac)_3]^+$ (**top**) and $[Ir(F_2ppy)_2(pypz)*Tb(hfac)_3]^+$ (**bottom**) following two-photon excitation (λ_{ex} = 780 nm). (**a**) Total emission spectrum. (**b**) Emission spectrum following a 0 μs delay and a 1 μs gate. (**c**) Emission spectrum following a 3 μs delay and a 21 μs gate. Spectra (**b**) and (**c**) are normalised relative to the Ir and Ln components of (**a**), respectively. The observed Ln transitions are indicated on spectra (**c**). All measurements were obtained in aerated solvent at 298 K.

2.4. Derivatives of [Ir(peppy)$_2$(acac)]

As outlined above, the compound [Ir(ppy)$_2$(acac)] has $\sigma_2 \approx 20$ GM at 800 nm, which can be enlarged to 39 GM using the ligand 2-phenyl-4-(phenylethynyl)pyridine (peppyH) in the complex [Ir(peppy)$_2$(acac)] (Figure 2.27, X = H).[55] The usual criterion for organic materials to have large values of σ_2 is extensive charge transfer in a multipole system.[109] Therefore, using this knowledge, the design rationale for [Ir(peppy)$_2$(acac)] was that to lower the energy and enhance the contribution of the ^{3}MLCT state, and increase the CT distance, conjugation *para* to the metal should be augmented because that is the location of the LUMO in [Ir(ppy)$_2$(acac)].[15]

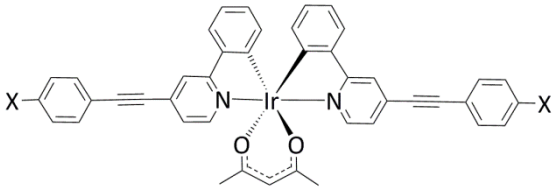

Figure 2.27 Previously synthesised [Ir(peppy)$_2$(acac)] (X = H) and the proposed derivatives (X = OMe or CN).

A series of derivatives were designed based around the peppyH ligand, initially with the intention of trying to further enhance the value of σ_2. This included substitution at the *para* position (X substitution, Figure 2.27) of the terminal phenyl group with methoxy donor (peppyH-OMe) or cyano acceptor (peppyH-CN) groups. However, the synthesis of these derivatives proved more challenging than expected. The ligand peppyH-OMe could be produced in relatively low yield *via* a four step synthesis, with minimal adaption of the synthesis of peppyH. Thus, the intermediate compound 4-(4′-methoxyphenylethynyl)pyridine was synthesised in two steps by two sequential Sonogashira coupling reactions, with the second being a one-pot TMS acetylene deprotection and coupling. The reaction of this compound with phenyllithium was low yielding, as had been the case in the original synthesis of peppyH.[55] Purification by formation of the HCl salt and filtration allowed separation of peppyH-OMe from the crude mixture. The synthetic protocol is summarised in Scheme 2.3.

Slow evaporation of a CH_2Cl_2 solution of peppyH-OMe produced colourless, plate-habited crystals suitable for SC-XRD. The molecular structure of peppyH-OMe is shown in Figure 2.28a. The crystal structure of peppyH-OMe can be compared to that

of the styryl analogue that has been reported previously (CIGSOB).[119] A comparison of the crystal packing of the two compounds can be seen in Figure 2.28b, showing that they are isostructural. The alkene analogue has a higher *Z′* of 2, with two distinct OMe orientations (synperiplanar and antiperiplanar with respect to the pyridyl-bonded phenyl ring), resulting in a doubled crystallographic *c*-axis compared to peppyH-OMe. The two compounds both have a twist in the solid state between the pyridyl moiety and the phenyl ring in the 2-position with a torsion angle of 39° for peppyH-OMe and 41° for its alkene analogue.

Attempts to form the μ-chloro-bridged diiridium dimer from peppyH-OMe using standard conditions were unsuccessful; instead, a different approach to complexes of this family was sought. An alternative strategy was also required to synthesise examples with functional groups sensitive to the basic and nucleophilic reagent PhLi. For instance, the synthesis of peppyH-CN using an analogous reaction of PhLi with 4-(4′-cyanophenylethynyl)pyridine would not be viable: PhLi would react with the

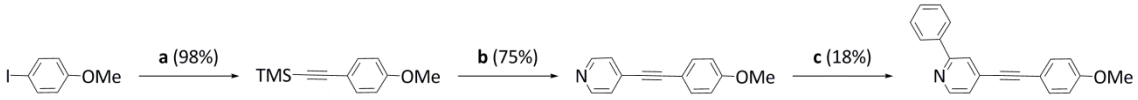

Scheme 2.3. Synthesis of the ligand peppyH-OMe. (**a**) TMSA, NEt_3, $Pd(PPh_3)_4$ (1 mol%), CuI (1 mol%), 65 °C, 4.5 h. (**b**) 4-bromopyridine hydrochloride, 1:1:2 NEt_3:MeOH:MeCN, K_2CO_3, $Pd(PPh_3)_4$ (1 mol%), CuI (1 mol%), 60 °C, 20 h. (**c**) i) PhLi (1 eq.), toluene, 0 °C, 1 h; ii) H_2O, r.t., 10 min.

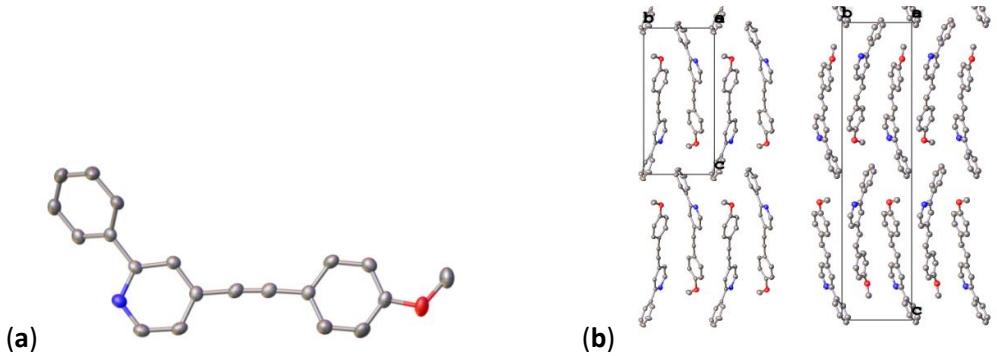

Figure 2.28. (**a**) Molecular structure of 4-(4′-methoxyphenylethynyl)pyridine (peppy-OMeH) as determined by SC-XRD. Element (colour): carbon (grey), nitrogen (blue), oxygen (red). Atomic displacement parameters are shown at 50% probability Hydrogen atoms are omitted for clarity. (**b**) A comparison of the crystal packing of peppy-OMeH (left) and its alkene analogue (right) viewed down the (1 0 0) direction.

nitrile group to give the corresponding ketone or alcohol upon work-up. A late stage introduction of the substituted ring onto the alkyne through a "chemistry on the complex" methodology[120] was thus explored. Protected 4-ethynylpyridines were considered as starting materials for this purpose. Initially, the compound 4-(trimethylsilylethynyl)pyridine was targeted as a substrate for phenylation, synthesised by the Sonogashira coupling of TMSA and 4-bromopyridine hydrochloride; however, subsequent reaction with PhLi only resulted in (quantitative) deprotection of the acetylene, even at low temperature (-78 °C), as observed by GC-MS. The protected 4-ethynylpyridine with the bulkier and more robust triisopropylsilyl (TIPS) protecting group was synthesised in a similar manner and phenylation of this analogue was successful with no deprotection observed, even when the reaction was conducted at room temperature. It was therefore possible to produce the desired intermediate ligand TIPSeppyH.

However, very variable yields of the phenylation were achieved (10-30%) with the formation of biphenyl also observed by GC-MS and ^{1}H NMR. It was later found that the 4-((triisopropylsilyl)ethynyl)pyridine contained a small quantity of an impurity that could be isolated as a bright yellow solid. The SC-XRD structure of the complex was determined and it was found that it comprised a μ-diiodide-bridged dicopper core, ligated by four of the substituted pyridines (Figure 2.29). This compound packs by interdigitation of each TIPS-ethynylpyridine ligand of one complex with two of these ligands from its nearest neighbours, as viewed down (0 1 0). This is similar to that seen in some picoline derivatives[121] and is presumably stabilised by C–H$\cdots\pi$ interactions.[122] The Cu–Cu distance of 2.625(2) Å and other bond distances are unremarkable when compared to other substituted pyridine adducts of Cu_2I_2 that have been structurally characterised.[121]

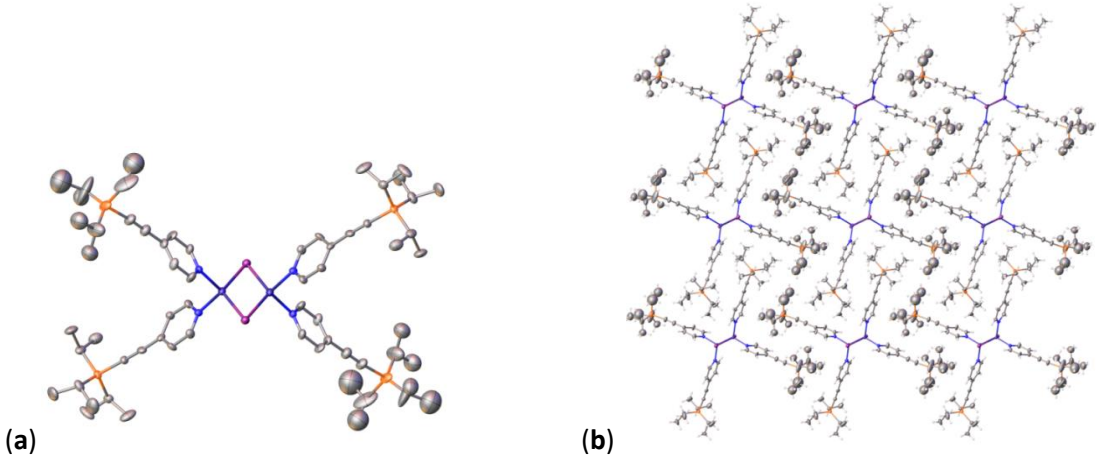

Figure 2.29. (a) Molecular structure of $[Cu(TIPSepy)_2(\mu\text{-}I)]_2$ as determined by SC-XRD. Element (colour): carbon (grey), nitrogen (light blue), copper (dark blue), iodine (purple), silicon (orange). Hydrogen atoms are omitted for clarity. Atomic displacement parameters are shown at 50% probability. **(b)** Packing of $[Cu(TIPSepy)_2(\mu\text{-}I)]_2$ as viewed down (0 1 0).

The ^1H NMR spectrum (400 MHz) of the Cu complex at room temperature in $CDCl_3$ is broadened to such an extent, due to fast exchange of the ligands on the ^1H NMR timescale, that no signal is observable. NMR spectra of TIPSepy containing the copper complex are broadened to varying extents, without changing the peak positions; in particular, the signals for the hydrogen atoms in the equivalent 2- and 6-positions of the pyridine ring are affected. The ESI^+ and $ASAP^+$ mass spectra (from both solution and the solid) showed the free substituted pyridine as the heaviest identifiable fragment, and so it was not immediately obvious that the complex was present. In addition, the solid complex is soluble in the bulk ligand. Under the typical work-up conditions employed here for Sonogashira reactions, the CuI was removed by passage through a short column of silica; however, the non-polar complex readily passed through the column.

The traces of free CuI formed from the labile complex, or indeed the complex itself, are presumed to be responsible for oxidatively homocoupling the phenyllithium to biphenyl under the non-rigorously anaerobic conditions employed for the phenylation reaction (nitrogen purge as opposed to freeze-pump-thaw or vacuum-backfill cycles). Once the presence of this complex had been established, it could be removed by careful chromatography. In subsequent reactions, biphenyl was no longer observed while the yield of the phenylated product became more consistent (maximum 53%). It may well

be that the syntheses of peppyH and peppyH-OMe were hampered by a similar impurity and thus their synthesis could be improved if repeated.

It is interesting to note that the isolated complex consisted of only the μ-diiodo-bridged species when, in solution, an approximately 100-fold excess of bromide and chloride (from the 4-bromopyridine hydrochloride) over iodide was present. This could simply be a matter of solubility, in which the chloride and bromide precipitated as the NEt_3HX salt formed in the reaction; however, it does raise the question of the exact role of the copper iodide in the Sonogashira reaction. The mechanism of the reaction, as it is commonly drawn, indicates that the amine (NR_3) base deprotonates the η^2-copper bound terminal acetylene and forms a copper acetylide *in situ*, with concomitant formation of NR_3HI. This copper acetylide is then proposed to transmetalate with the palladium catalyst to form the palladium acetylide and regeneration of copper halide (bromide in the present case).[123] That the iodide is still associated with the copper, even in such a competitive environment where other halides are present in vast excess, is perhaps indicative of a more complicated mechanism. Further studies are clearly required to understand this result.

Formation of the μ-dichloro-bridged diiridium complex of TIPSeppyH proceeded under standard conditions. Subsequent reaction with acetylacetone in the presence of base (K_2CO_3) afforded the monomeric complex. Similarly, the ligand could used to make the tris-heteroleptic complex [Ir(TIPSeppy)(ppy)(acac)]. In contrast with the tris-heteroleptic complexes reported in Section 2.1, the substituted bis-heteroleptic complex [Ir(TIPSeppy)$_2$(acac)] separated very easily as the fore-running fraction, while the mixed system ran with an R_f more similar to [Ir(ppy)$_2$(acac)]. The conditions used for the synthesis of [Ir(TIPSeppy)(ppy)(acac)] are summarised in Scheme 2.4. Unfortunately, it was not possible to obtain crystals of the tris-heteropleptic complex suitable for SC-XRD; however, the bis-heteroleptic complex [Ir(TIPSeppy)$_2$(acac)] did crystallise well, and its structure is shown in Figure 2.30. The difficulty in producing single crystals of the tris-heteroleptic complexes so far synthesised, with the exception of [Ir(fppy)(ppy)(acac)], is ascribed to their lower symmetry and, presumably, less favourable packing in the solid state.

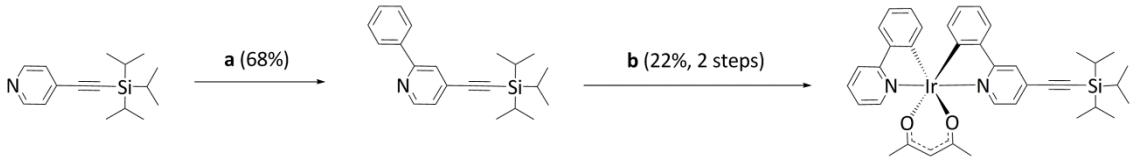

Scheme 2.4. Conditions for the synthesis of the TIPS protected ligand TIPSeppyH and the tris-heteroleptic complex [Ir(TIPSeppy)(ppy)acac]. (**a**) PhLi (1 eq.), toluene, r.t., 2 h. (**b**) i) ppyH (3 eq.), $IrCl_3 \cdot 3H_2O$, 2:1 $EtO(CH_2)_2OH$:H_2O, 110 °C, 16 h; ii) AcacH, K_2CO_3, 1:1 acetone:EtOH, 60 °C, 4 h.

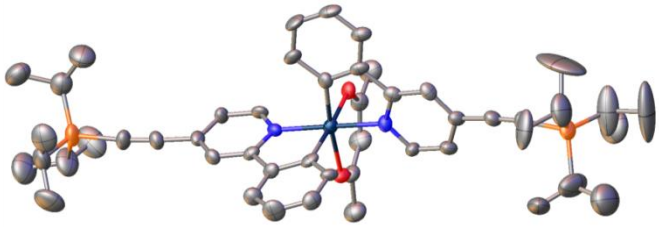

Figure 2.30. Molecular structure of $[Ir(TIPSeppy)_2(acac)]$ as determined by SC-XRD. Element (colour): carbon (grey), nitrogen (blue), oxygen (red), iridium (dark green), silicon (orange). Hydrogen atoms, a second symmetry independent molecule and half a molecule of acetonitrile solvent are omitted for clarity. Atomic displacement parameters are shown at 50% probability.

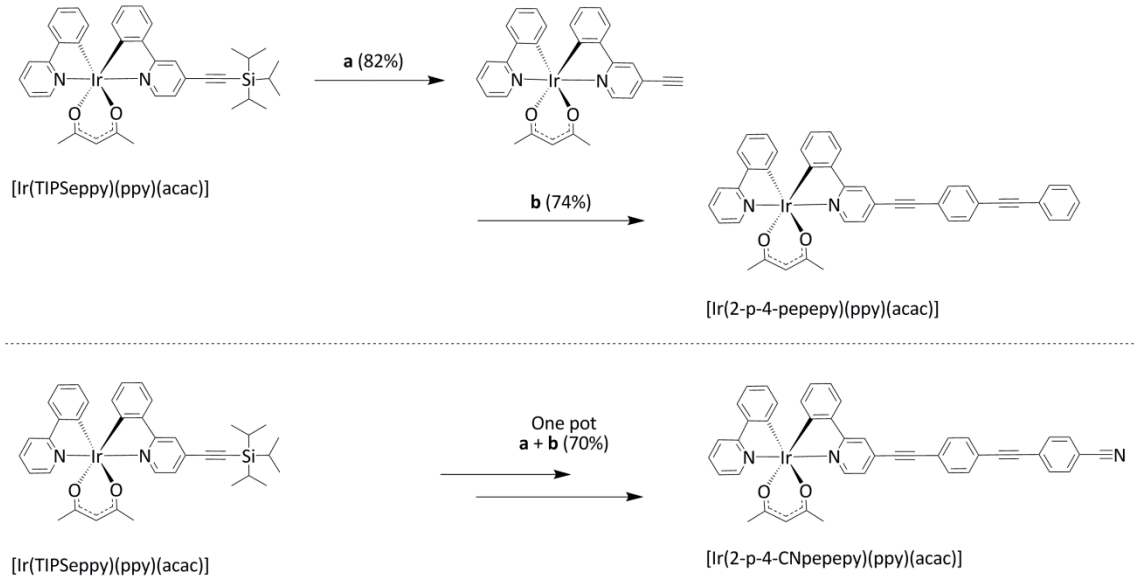

Scheme 2.5. Conditions used for the synthesis of the extended iridium complexes from [Ir(TIPSeppy)(ppy)acac]. (**a**) TBAF (3 eq.), THF, r.t., 16 h (complete after 2 h by TLC). (**b**) Aryliodide (4-iodotolan or 4-cyano-4′-iodotolan), 1:1 NEt_3:THF, $Pd(PPh_3)_4$ (2 mol%), CuI (2 mol%), 60 °C, 6 h.

Standard conditions for deprotection, namely tetra-*n*-butylammonium fluoride in dry tetrahydrofuran, could be used with the complexes to afford the terminal acetylene of either the mono or bis substituted complex.[124] While the deprotection was high yielding and occurred without reaction with the rest of the complex, significant degradation was observed if the compound was heated to remove the last traces of the solvent. Sonogashira coupling of the tris-heteroleptic complex with aryl halides was possible with the yield being maximised by using two or more equivalents of the coupling partner, the excess of which could be recovered easily by chromatography (Scheme 2.5). In particular, aryliodides were chosen due to their higher reactivity, which is important for a valuable intermediate such as this. This two-step procedure of deprotection and coupling was made more efficient by using a one-pot approach; the deprotection was monitored by TLC until completion was observed (*ca*. 2 h), before the arylhalide and base were added, the solution fully degassed and the catalysts added. The excess TBAF does not seem to hamper the Sonogashira coupling in any way. This method gave a better yield overall (by *ca.* 10% over the two steps) in a shorter time without making the operation of the reaction or the separation of the product more difficult. In fact, the use of a one-pot deprotection-coupling procedure is suitable for many Sonogashira couplings and should be used more regularly.

The TIPS-protected complex, [Ir(TIPSeppy)(ppy)acac], has a large quantum yield of 0.76 and a lifetime of 1.5 μs. The pure radiative lifetime is therefore *ca.* 2.0 μs and is thus relatively short, indicative of a considerable ^{3}CT component to the emission. Moreover, from the molecular design, ^{3}MLCT is expected to be the prominent component, which also is consistent with high quantum yield emission from the triplet state due to efficient SOC by the metal. The TIPS group probably plays two additional roles: as an electron accepting moiety and as a bulky group that can buffer the excited complex from non-radiative collisional deactivation. Once the π-system is extended to give complex [Ir(2-p-4-pepepy)$_2$(acac)], the value of the PLQY drops to 0.16 and the lifetime is considerably shorter at 0.36 μs. The pure radiative lifetime, however, is not significantly altered, having a value of 2.3 μs, thus indicating that a similar excited state is formed; instead, non-radiative decay must be increased. This is most likely a result of additional modes for rotation around the relatively free-rotor of the acetylene ligand that can couple the excited and ground state surfaces and the removal of the steric bulk imparted by the TIPS group. Upon introduction of the cyano accepting group in the complex [Ir(2-p-4-CNpepepy)$_2$(acac)], the quantum yield is relatively unaffected, with

this complex having a PLQY of 0.14. The lifetime, however, is shorter at 0.18 μs, a value that is considered very small for an Ir complex in degassed solution. The value of τ_0 is 1.29 μs and so an even greater contribution from the ^{3}MLCT state is expected.

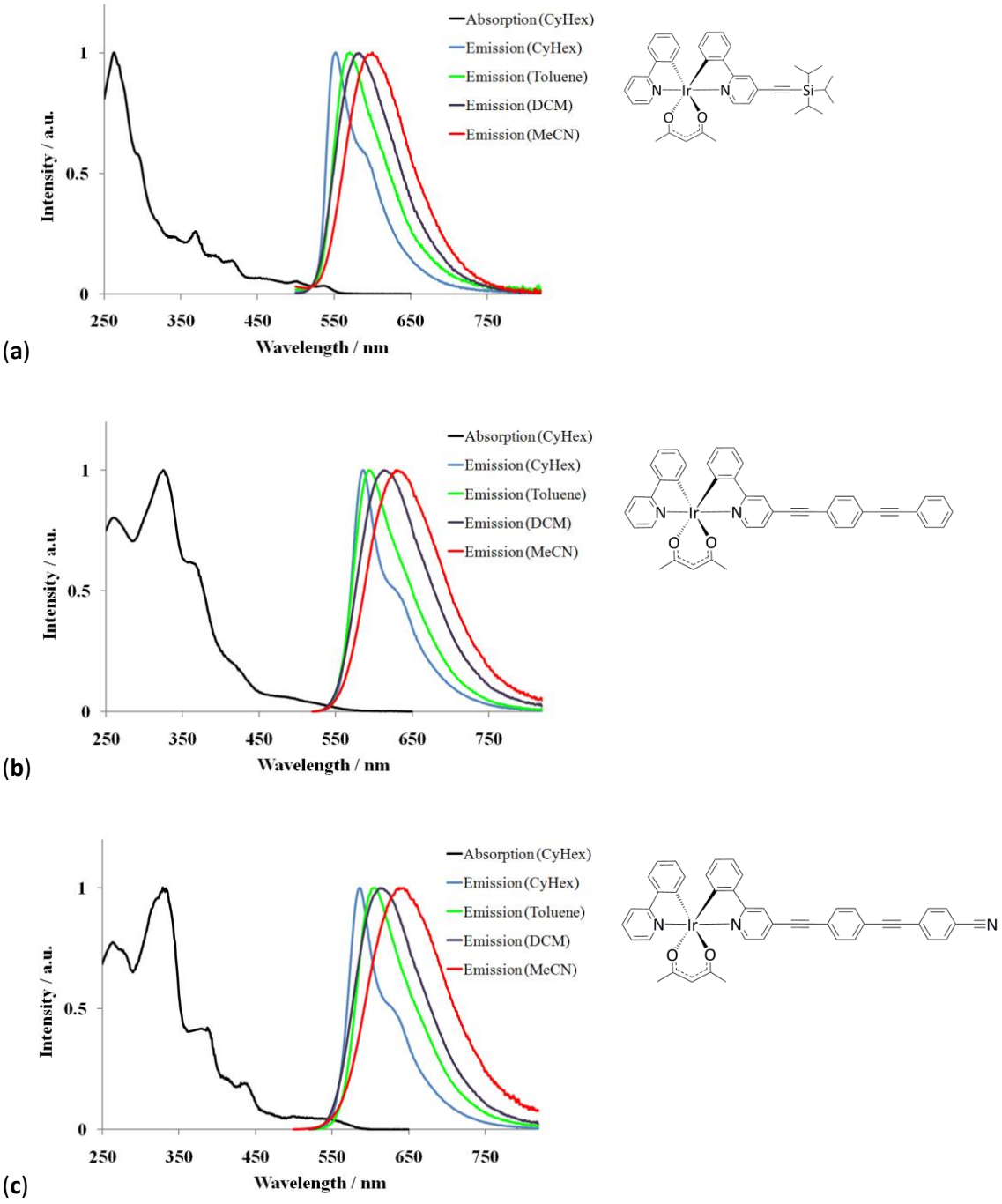

Figure 2.31. Normalised absorption and emission spectra of the tris-heteroleptic cyclometalated iridium complexes (**a**) [Ir(TIPSeppy)(ppy)(acac)], (**b**) [Ir(2-p-4-pepepy)(ppy)(acac)] and (**c**) [Ir(2-p-4-CNpepepy)(ppy)(acac)]. λ_{ex} = 475 nm. All measurements were obtained in degassed solvent at 298 K.

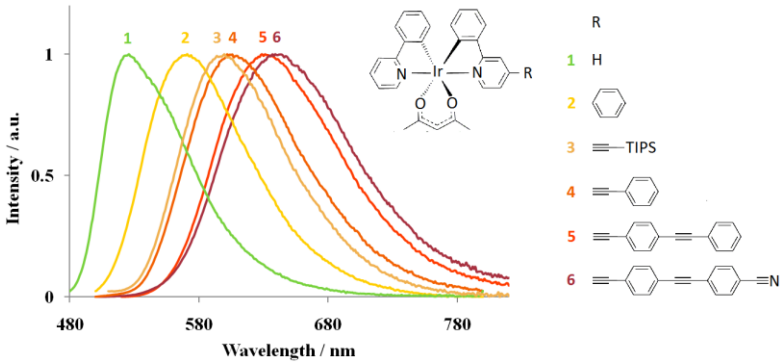

Figure 2.32. A summary of the emission spectra of the synthesised tris-heteroleptic iridium complexes that have π-conjugated substituents at the 4-position of a single ppy-type ligand. Spectra were recorded with excitation at their respective absorption band maxima (see Figure 2.5 and Figure 2.31Error! Reference source not found. for further details) at room temperature in degassed acetonitrile.

A systematic red-shift of the emission maxima upon π-extension of the substituent in the 4-position of the ppy-type ligand is evident when the emission spectra of [Ir(ppy)$_2$(acac)] is compared to [Ir(dppy)(ppy)(acac)] (from Section 2.1), [Ir(peppy)(ppy)acac] (from Section 2.3) and the complexes of Section 2.4 (Figure 2.31). It is relatively easy to tune the low energy emission of these Ir complexes (Figure 2.32).

DFT calculations have been performed on this series of complexes, optimising the structures with B3LYP/6-31G(d)/LANL2DZ and using the CAM-B3LYP functional for TD-DFT calculations due to the expected CT nature of the transitions. The frontier orbitals and those relevant to the $T_1 \leftarrow S_0$ transitions for the two complexes (with transition components) are included in Table 2.12. In both cases, the HOMO distribution is unperturbed from that calculated for [Ir(ppy)$_2$(acac)] and other tris-heteroleptic complexes with an unsubstituted phenyl ring. The LUMO distribution, however, is delocalised along the substituent in the 4-position of the pyridine ring. TD-DFT calculations confirm the importance of ^{3}CT to the $T_1 \leftarrow S_0$ transition of both complexes with some minor ^{3}LC character. The emission properties of these complexes have not been investigated computationally in detail but a preliminary TD-DFT calculation for [Ir(2-p-4-CNpepepy)$_2$(acac)] from $S_0(T_1)$ gave an energy of 1.85 eV (671 nm) for the emission, in moderately good agreement with experiment, and indicated significant ^{3}CT-character. Furthermore, in order to understand the effect on orbital and transition energies, TD-DFT calculations of additional complexes with intermediate degrees of π-conjugation have been performed. The results of these

calculations are summarised in Table 2.13. The calculations reproduce the red-shifted absorption across the series and indicate that, as expected, the LUMO energy is lowered upon extension of the pyridyl moiety, while the HOMO is only slightly stabilised.[ii]

To conclude, a versatile and divergent intermediate tris-heteroleptic complex, [Ir(TIPSeppy)(ppy)acac], has been synthesised that is amenable to further functionalisation at the important 4-position of the pyridyl ring of one ppy^- ligand. Using a one-pot method, it is possible to deprotect this intermediate complex *in situ* and perform Sonogashira couplings with aryliodides. The photophysical properties of the synthesised compounds follow the expected trend of red-shifted absorption and emission, with DFT calculations corroborating the former. It should be possible to use this simple intermediate in a multitude of ways, a few examples of which will be outlined in the future work section.

Table 2.12. Frontier and other orbitals that contribute to the $T_1 \leftarrow S_0$ transitions of $[Ir(2\text{-p-4-pepepy})_2(acac)]$ and $[Ir(2\text{-p-4-CNpepepy})_2(acac)]$ as calculated by DFT at the B3LYP/6-31G(d)/LANL2DZ level of theory. Isovalue: ± 0.02 $[e\ a_0^{-3}]^{½}$. Hydrogen atoms are omitted for clarity.

Orbital (*E* / eV)	**$[Ir(2\text{-p-4-pepepy})_2(acac)]^a$**	**Orbital (*E* / eV)**	**$[Ir(2\text{-p-4-CNpepepy})_2(acac)]^b$**
LUMO (-2.14)	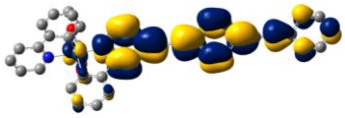	LUMO (-2.51)	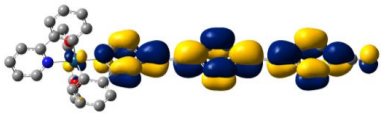
HOMO (4.81)		HOMO (-4.89)	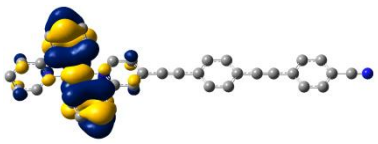
HOMO-1 (-5.26)	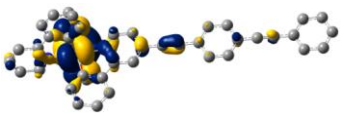	HOMO-3 (-5.86)	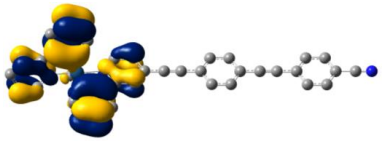
HOMO-2 (-5.62)	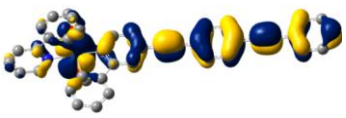	HOMO-4 (-6.03)	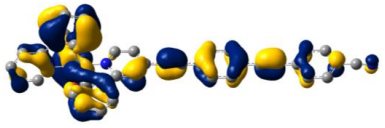

[a] $T_1 \leftarrow S_0$ mainly LUMO ← HOMO-1 (^{3}MLCT) and minor LUMO ← HOMO-2 (^{3}LC);

[b] $T_1 \leftarrow S_0$ mainly LUMO ← HOMO-4 (^{3}I^{er}LCT) and minor LUMO ← HOMO-3 (^{3}LC/^{3}CT)

[ii] The potential basis set superposition error has not been accounted for in the calculations.

Table 2.13. TD-DFT calculated $T_1 \leftarrow S_0$ transitions for tris-heteroleptic complexes with π-extended substituents at the 4-position of a ppy-type like ligand. Calculations were performed at the CAM-B3LYP/6-31G(d)/LANL2DZ level of theory. Where applicable, the TIPS group required for synthetic reasons is replaced by TMS here to reduce computational cost.

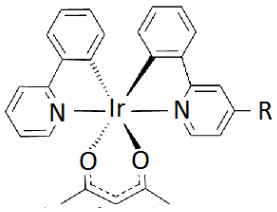

R	HOMO *E* / eV	LUMO *E* / eV	*E* / eV	*λ* / nm
H[a]	-4.74	-1.27	2.67	464
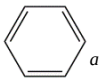	-4.70	-1.51	2.64	470
	-4.83	-1.74	2.53	490
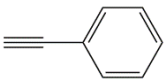	-4.75	-1.89	2.41	515
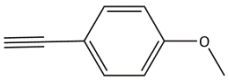	-4.66	-1.74	2.40	518
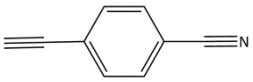	-4.85	-2.41	2.31	536
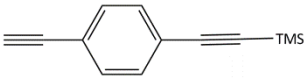	-4.78	-2.07	2.26	547
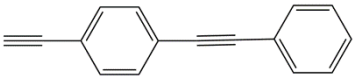	-4.81	-2.14	2.14	579
	-4.72	-2.04	2.15	575
	-4.89	-2.51	2.09	592

[a] The basis set used was 6-31+G/LANL2DZ (see section 2.1)

2.5. Future work

The aim of this section is to provide a flavour of the type of work that could be undertaken to extend and develop the work outlined above and to apply it in new ways.

In section 2.1, the first synthesis and separation of tris-heteroleptic cyclometalated Ir(III) complexes was described. As postulated in that work, this class of compound could be utilised in multi-functional materials: two of the ligands could be used to modify the physical characteristics, alter the bio-compatability or bind substrates, while the third ligand principally tunes the emission characteristics. This is clearly an area that needs to be explored further. In view of biological imaging or singlet oxygen generation applications, water solubility is of concern. Possibly the easiest way to do this would be to use a neutral ancillary ligand, such as bpy, to afford a charged tris-heteroleptic complex. While charged Ir complexes are often used for these applications, their photophysical properties, in general, are inferior; thus, it would be of interest to explore ligands that are solublising, for instance those with alkyl sulfanate salt or poly(ethylene glycol) groups. This should preserve the desired spectroscopic properties, while alleviating the poor water solubility. Tris-heteroleptic complexes tend to have larger PLQYs and therefore their use in OLEDs should be explored, especially considering that they have been subsequently described as having favourable attributes for the related LECs.[19]

It is of interest, from a more fundamental point of view, to make the tris-heteroleptic complexes based on the isomeric pyridylpyrene ligands of Section 2.2, namely [Ir(1-pypyr)(ppy)(acac)] and [Ir(2-pypyr)(ppy)(acac)]. These pyridylpyrene complexes should be a good test of the hypothesis that the increase in quantum yield for tris-heteroleptic complexes relative to their bis-heteroleptic congers is due to a reduction in k_{nr} from a lowering of the number of vibrational modes coupling the ground and excited states. The bis-heteroleptic complexes have k_{nr} values considerably larger than their k_r values and those of conventional ppy^- ligand systems; thus, it would be expected that these complexes should be particularly affected by this effect.

The terminal alkyne Ir complex described in Section 2.4 can be exploited in many different ways. It could be used in further Sonogashira coupling reactions, including making some of the products upon which calculations were run (Table 2.13). The best charge transfer compounds should be measured for their TPA to explore and to challenge the design strategies for high σ_2 materials, the original aim of the project. The

intermediate complex could also be coupled with an alkyl or aryl azide in the now ubiquitous Huisgen [3+2] cycloaddition, which was popularised by Sharpless as an example of "click chemistry".[125, 126] This copper-catalysed reaction affords 1,2,3-triazole products and can be used to link the complex to other chromophores or accepting moieties. One intriguing possibility is to use the Ir complex as a sensitising antenna for a lanthanide complex, in an extension of the work of Section 2.3. Coupling with an azide terminated Ln complex would allow facile coupling of the two units and would likely be suitable for sensitising NIR emitting lanthanides (the conjugated linker will lower the energy of the Ir complex too much to be suitable for Eu and Tb sensitisation).

Reaction of the complex in a Sonogashira or Cadiot-Chodkiewicz cross-coupling (copper-catalysed reaction with a terminal bromoalkyne to form a diyne) and then reduction of the unsaturated linker with Pd/C and H_2 would be a simple method to effectively introduce [Ir(ppy)$_2$(acac)] tethered onto another substrate by an alkyl chain. Thus, the chromophore could be attached *via* a flexible, saturated linker that inhibits chromophore coupling or electronic communication. One example might be Sonogashira reaction with 4-iodophenylalanine and reduction to give the complex on an amino acid for further bioconjugation.

In section 2.4, initial attempts at inducing greater charge transfer in an [IrL$_2$(acac)]-type complex were outlined. There, the 4-position of the pyridine ring was functionalised by π-conjugated substituents. While ancillary ligands, by their very nature, are usually considered innocent towards determining the excited state properties of transition metal complexes, the popular ligand picolinate is involved in the LUMO of [Ir(ppy)$_2$(pic)]. This could act as another channel through which to funnel excited state charge transfer and generate a charge separated state, pertinent to solar harvesting.

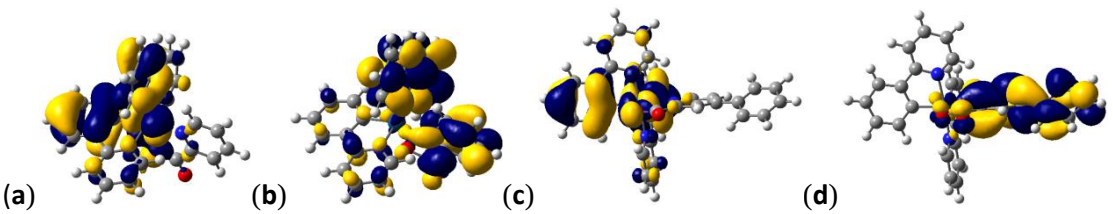

Figure 2.33. DFT B3LYP/6-31G(d) calculated frontier orbitals. (**a**) HOMO of [Ir(ppy)$_2$(pic)]; (**b**) LUMO of [Ir(ppy)$_2$(pic)]; (**c**) HOMO of [Ir(ppy)$_2$(Phpic)]; (**d**) LUMO of [Ir(ppy)$_2$(Phpic)].

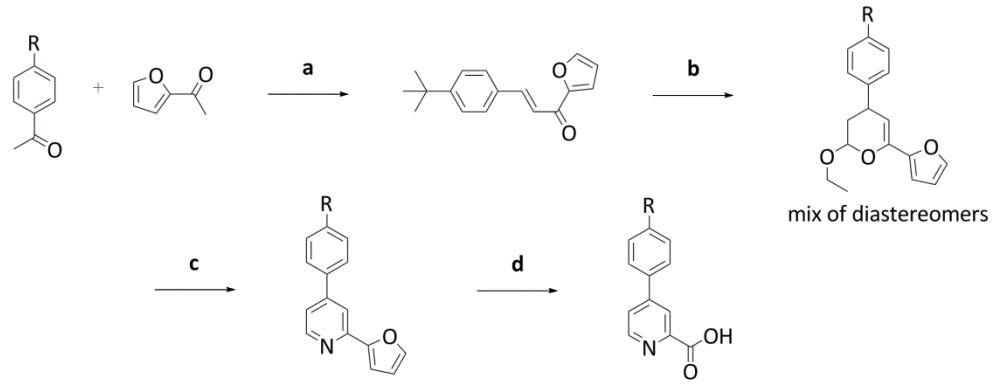

Scheme 2.6. Synthetic route to a series of extended pic^- ligands. (**a**) KOH, ethanol/H_2O, 0 °C → r.t. (**b**) Ethyl vinyl ether, [Yb(fod)$_3$], $(CH_2Cl)_2$, 90 °C. (**c**) $NH_2OH{\cdot}H_2O$, ethanol. (**d**) $KMnO_4$, 1:1 acetone: H_2O or ozone.

Preliminary DFT calculations indicate that by extending the π-conjugation of the pyridine moiety in the 4-position with an addition phenyl ring (Phpic), the location of the LUMO of [Ir(ppy)$_2$(pic)] can be shifted completely onto this component (Figure 2.33). During the course of this work, a single attempt was made at the synthesis of the 4-*tert*-butylphenyl derivative, using furan as a masked or 'latent' carboxylic acid.[127] The synthetic route is shown in Scheme 2.6. Briefly, this comprised an aldol reaction of 4-*tert*-butylbenzaldehyde and 2-furyl methyl ketone with $KOH_{(aq)}$ base followed by an [Yb(fod)$_3$] Lewis acid-catalysed hetero Diels-Alder cycloaddition with ethyl vinyl ether as the dienophile using a close modification of a literature method.[128] Reaction of this intermediate dihydropyran with hydroxylamine hydrochloride in ethanol afforded the corresponding pyridine.[128] Unfortunately, $KMnO_4$ oxidation of the furan to the carboxylic acid didn't work in our hands in the initial attempt; however, this reported reaction[129, 130] should be viable, and thus with some optimisation of the conditions it should be possible. Another method of completing this conversion could be ozonolysis.[131] As alluded to above, such a system, in which charge is transferred from the metal to the terminus of the π-conjugated ligand, may be of use for photoinduced charge injection in a DSSC. To achieve this, the dye must also be surface-bound to TiO_2 and so anchoring groups such as carboxylic acid need to be considered.

Thus, although cyclometalated iridium complexes have elicited a large body of work over recent years, there is still yet more to learn and new avenues to explore in order to take full advantage of their rich photophysics.

2.6. References

1. R. M. Edkins, A. Wriglesworth, K. Fucke, S. L. Bettington and A. Beeby, *Dalton Trans.*, 2011, **40**, 9672.
2. R. M. Edkins, D. Sykes, A. Beeby and M. D. Ward, *Chem. Commun.*, 2012, **44**, 9977.
3. M. Nonoyama, *Bull. Chem. Soc. Jpn.*, 1974, **47**, 767.
4. A. Beeby, S. Bettington, I. D. W. Samuel and Z. Wang, *J. Mater. Chem.*, 2003, **13**, 80.
5. G. Y. Park, Y. Kim and Y. Ha, *Mol. Cryst. Liq. Cryst.*, 2006, **462**, 179.
6. S. Lamansky, P. Djurovich, D. Murphy, F. Abdel-Razzaq, R. Kwong, I. Tsyba, M. Bortz, B. Mui, R. Bau and M. E. Thompson, *Inorg. Chem.*, 2001, **40**, 1704.
7. M. Felici, P. Contreras-Carballada, J. M. M. Smits, R. J. M. Nolte, R. M. Williams, L. De Cola and M. C. Feiters, *Molecules*, 2010, **15**, 2039.
8. E. Baranoff, I. Jung, R. Scopelliti, E. Solari, M. Grätzel and M. K. Nazeeruddin, *Dalton Trans.*, 2011, **40**, 6860.
9. K. A. King, P. J. Spellane and R. J. Watts, *J. Am. Chem. Soc.*, 1985, **107**, 1431.
10. H. Andersson, F. Almqvist and R. Olsson, *Org. Lett.*, 2007, **9**, 1335.
11. K. R. Roesch and R. C. Larock, *Org. Lett.*, 1999, **1**, 553.
12. C. Sicre, J. L. Alonso-Gómez and M. M. Cid, *Tetrahedron*, 2006, **62**, 11063.
13. S. Sprouse, K. A. King, P. J. Spellane and R. J. Watts, *J. Am. Chem. Soc.*, 1984, **106**, 6647.
14. Y. You and S. Y. Park, *Dalton Trans.*, 2009, 1267.
15. P. J. Hay, *J. Phys. Chem. A*, 2002, **106**, 1634.
16. T. Yanai, D. P. Tew and N. C. Handy, *Chem. Phys. Lett.*, 2004, **393**, 51.
17. M. J. G. Peach, T. Helgaker, P. Salek, T. W. Keal, O. B. Lutnaes, D. J. Tozer and N. C. Handy, *Phys. Chem. Chem. Phys.*, 2006, **8**, 558.
18. E. Baranoff, B. F. E. Curchod, J. Frey, R. Scopelliti, F. Kessler, I. Tavernelli, U. Rothlisberger, M. Grätzel and M. K. Nazeeruddin, *Inorg. Chem.*, 2012, **51**, 215.
19. D. Tordera, M. Delgado, E. Ortí, H. J. Bolink, J. Frey, M. K. Nazeeruddin and E. Baranoff, *Chem. Mater.*, 2012, **24**, 1896.

20. P. Brulatti, R. J. Gildea, J. A. K. Howard, V. Fattori, M. Cocchi and J. A. G. Williams, *Inorg. Chem.*, 2012, **51**, 3813.
21. A. Nakajima, *Bull. Chem. Soc. Jpn.*, 1973, **46**, 2602.
22. J. B. Birks, D. J. Dyson and I. H. Munro, *Proc. R. Soc. London, Ser. A*, 1963, **275**, 575.
23. D. S. Karpovich and G. J. Blanchard, *J. Phys. Chem.*, 1995, **99**, 3951.
24. T. M. Figueira-Duarte and K. Müllen, *Chem. Rev.*, 2011, **111**, 7260.
25. A. G. Crawford, A. D. Dwyer, Z. Liu, A. Steffen, A. Beeby, L.-O. Pålsson, D. J. Tozer and T. B. Marder, *J. Am. Chem. Soc.*, 2011, **133**, 13349.
26. W. Leslie, R. A. Poole, P. R. Murray, L. J. Yellowlees, A. Beeby and J. A. G. Williams, *Polyhedron*, 2004, **23**, 2769.
27. I. E. Pomestchenko, C. R. Luman, M. Hissler, R. Ziessel and F. N. Castellano, *Inorg. Chem.*, 2003, **42**, 1394.
28. D. V. Kozlov, D. S. Tyson, C. Goze, R. Ziessel and F. N. Castellano, *Inorg. Chem.*, 2004, **43**, 6083.
29. C. Goze, C. Sabatini, A. Barbieri, F. Barigelletti and R. Ziessel, *Inorg. Chem.*, 2007, **46**, 7341.
30. F. Spaenig, J.-H. Olivier, V. Prusakova, P. Retailleau, R. Ziessel and F. N. Castellano, *Inorg. Chem.*, 2011, **50**, 10859.
31. E. C. Constable, M. Neuburger, P. Rösel, G. E. Schneider, J. A. Zampese, C. E. Housecroft, F. Monti, N. Armaroli, R. D. Costa and E. Ortí, *Inorg. Chem.*, 2012, **52**, 885.
32. W. Y. Heng, J. Hu and J. H. K. Yip, *Organometallics*, 2007, **26**, 6760.
33. L. Gao, M. A. Peay, D. V. Partyka, J. B. Updegraff, T. S. Teets, A. J. Esswein, M. Zeller, A. D. Hunter and T. G. Gray, *Organometallics*, 2009, **28**, 5669.
34. C. Bonnefous, A. Chouai and R. P. Thummel, *Inorg. Chem.*, 2001, **40**, 5851.
35. J. Hu, J. H. K. Yip, D.-L. Ma, K.-Y. Wong and W.-H. Chung, *Organometallics*, 2008, **28**, 51.
36. A. S. Ionkin, W. J. Marshall and B. M. Fish, *Organometallics*, 2006, **25**, 1461.
37. W. T. Wu, W. H. Wu, S. M. Ji, H. M. Guo and J. Z. Zhao, *Eur. J. Inorg. Chem.*, 2010, 4470.

38. W. Lee, T.-H. Kwon, J. Kwon, J.-y. Kim, C. Lee and J.-I. Hong, *New J. Chem.*, 2011, **35**, 2557.
39. R. G. Harvey, S. Schmolka, C. Cortez and H. M. Lee, *Synth. Commun.*, 1988, **18**, 2207.
40. D. N. Coventry, A. S. Batsanov, A. E. Goeta, J. A. K. Howard, T. B. Marder and R. N. Perutz, *Chem. Commun.*, 2005, 2172.
41. A. G. Crawford, Z. Liu, I. A. I. Mkhalid, M.-H. Thibault, N. Schwarz, G. Alcaraz, A. Steffen, J. C. Collings, A. S. Batsanov, J. A. K. Howard and T. B. Marder, *Chem. Eur. J.*, 2012, **18**, 5022.
42. A. S. Batsanov, J. A. K. Howard, D. Albesa-Jové, J. C. Collings, Z. Liu, I. A. I. Mkhalid, M.-H. Thibault and T. B. Marder, *Cryst. Growth Des.*, 2012, **12**, 2794.
43. P. V. Vyas, A. K. Bhatt, G. Ramachandraiah and A. V. Bedekar, *Tetrahedron Lett.*, 2003, **44**, 4085.
44. I. A. I. Mkhalid, J. H. Barnard, T. B. Marder, J. M. Murphy and J. F. Hartwig, *Chem. Rev.*, 2010, **110**, 890.
45. T. Ishiyama, J. Takagi, K. Ishida, N. Miyaura, N. R. Anastasi and J. F. Hartwig, *J. Am. Chem. Soc.*, 2001, **124**, 390.
46. J.-Y. Cho, M. K. Tse, D. Holmes, R. E. Maleczka and M. R. Smith, *Science*, 2002, **295**, 305.
47. T. M. Boller, J. M. Murphy, M. Hapke, T. Ishiyama, N. Miyaura and J. F. Hartwig, *J. Am. Chem. Soc.*, 2005, **127**, 14263.
48. A. S. Ionkin and W. J. Marshall, *Inorg. Chem.*, 2005, **44**, 6244.
49. A. S. Ionkin, W. J. Marshall and Y. Wang, *Organometallics*, 2005, **24**, 619.
50. A. S. Ionkin, W. J. Marshall, D. C. Roe and Y. Wang, *Dalton Trans.*, 2006, 2468.
51. R. Passerini and I. G. Ross, *J. Sci. Instrum.*, 1953, **30**, 274.
52. L. Ma, H. Guo, Q. Li, S. Guo and J. Zhao, *Dalton Trans.*, 2012, **41**, 10680.
53. N. M. Shavaleev, F. Monti, R. D. Costa, R. Scopelliti, H. J. Bolink, E. Ortí, G. Accorsi, N. Armaroli, E. Baranoff, M. Grätzel and M. K. Nazeeruddin, *Inorg. Chem.*, 2012, **51**, 2263.
54. M. Xu, G. Wang, R. Zhou, Z. An, Q. Zhou and W. Li, *Inorg. Chim. Acta*, 2007, **360**, 3149.

55. R. M. Edkins, S. L. Bettington, A. E. Goeta and A. Beeby, *Dalton Trans.*, 2011, **40**, 12765.
56. G. Pourtois, D. Beljonne, C. Moucheron, S. Schumm, A. Kirsch-De Mesmaeker, R. Lazzaroni and J.-L. Brédas, *J. Am. Chem. Soc.*, 2003, **126**, 683.
57. S. Kammer, I. Starke, A. Pietrucha, A. Kelling, W. Mickler, U. Schilde, C. Dosche, E. Kleinpeter and H.-J. Holdt, *Dalton Trans.*, 2012, **41**, 10219.
58. M. Velusamy, K. R. J. Thomas, C.-H. Chen, J. T. Lin, Y. S. Wen, W.-T. Hsieh, C.-H. Lai and P.-T. Chou, *Dalton Trans.*, 2007, 3025.
59. D. P. Rillema, C. B. Blanton, R. J. Shaver, D. C. Jackman, M. Boldaji, S. Bundy, L. A. Worl and T. J. Meyer, *Inorg. Chem.*, 1992, **31**, 1600.
60. A. Kapturkiewicz, J. Nowacki and P. Borowicz, *Electrochim. Acta*, 2005, **50**, 3395.
61. N. G. Connelly and W. E. Geiger, *Chem. Rev.*, 1996, **96**, 877.
62. C. P. Brock and R. P. Minton, *J. Am. Chem. Soc.*, 1989, **111**, 4586.
63. M. Parac and S. Grimme, *Chem. Phys.*, 2003, **292**, 11.
64. L. Weber, D. Eickhoff, T. B. Marder, M. A. Fox, P. J. Low, A. D. Dwyer, D. J. Tozer, S. Schwedler, A. Brockhinke, H. G. Stammler and B. Neumann, *Chem. Eur. J.*, 2012, **18**, 1369.
65. X. Gu, T. Fei, H. Zhang, H. Xu, B. Yang, Y. Ma and X. Liu, *J. Phys. Chem. A*, 2008, **112**, 8387.
66. M. J. G. Peach, M. J. Williamson and D. J. Tozer, *J. Chem. Theory Comput.*, 2011, **7**, 3578.
67. M. J. G. Peach and D. J. Tozer, *J. Phys. Chem. A*, 2012, **116**, 9783.
68. M. J. G. Peach, P. Benfield, T. Helgaker and D. J. Tozer, *J. Chem. Phys.*, 2008, **128**, 044118.
69. G. Volpi, C. Garino and C. Nervi, *Dalton Trans.*, 2012, **41**, 7098.
70. T. Kowalczyk, S. R. Yost and T. Van Voorhis, *J. Chem. Phys.*, 2011, **134**, 054128.
71. A. J. Hallett, N. White, W. Wu, X. Cui, P. N. Horton, S. J. Coles, J. Zhao and S. J. A. Pope, *Chem. Commun.*, 2012, **48**, 10838.
72. A. de Bettencourt-Dias, *Dalton Trans.*, 2007, 2229.
73. D. Parker, *Coord. Chem. Rev.*, 2000, **205**, 109.

74. S. Faulkner, S. J. A. Pope and B. P. Burton-Pye, *Appl. Spectrosc. Rev.*, 2005, **40**, 1.
75. J. C. G. Bunzli, *Chem. Rev.*, 2010, **110**, 2729.
76. J. C. G. Bunzli and C. Piguet, *Chem. Soc. Rev.*, 2005, **34**, 1048.
77. E. G. Moore, A. P. S. Samuel and K. N. Raymond, *Acc. Chem. Res.*, 2009, **42**, 542.
78. E. S. Andreiadis, R. Demadrille, D. Imbert, J. Pecaut and M. Mazzanti, *Chem. Eur. J.*, 2009, **15**, 9458.
79. S. Faulkner, L. S. Natrajan, W. S. Perry and D. Sykes, *Dalton Trans.*, 2009, 3890.
80. M. D. Ward, *Coord. Chem. Rev.*, 2007, **251**, 1663.
81. S. J. A. Pope, B. J. Coe, S. Faulkner, E. V. Bichenkova, X. Yu and K. T. Douglas, *J. Am. Chem. Soc.*, 2004, **126**, 9490.
82. S. G. Baca, S. J. A. Pope, H. Adams and M. D. Ward, *Inorg. Chem.*, 2008, **47**, 3736.
83. T. Lazarides, N. M. Tart, D. Sykes, S. Faulkner, A. Barbieri and M. D. Ward, *Dalton Trans.*, 2009, 3971.
84. J. M. Herrera, S. J. A. Pope, H. Adams, S. Faulkner and M. D. Ward, *Inorg. Chem.*, 2006, **45**, 3895.
85. A. M. Nonat, S. J. Quinn and T. Gunnlaugsson, *Inorg. Chem.*, 2009, **48**, 4646.
86. Q.-H. Wei, Y.-F. Lei, W.-R. Xu, J.-M. Xie and G.-N. Chen, *Dalton Trans.*, 2012, **41**, 11219.
87. F. Kennedy, N. M. Shavaleev, T. Koullourou, Z. R. Bell, J. C. Jeffery, S. Faulkner and M. D. Ward, *Dalton Trans.*, 2007, 1492.
88. T. Koullourou, L. S. Natrajan, H. Bhavsar, S. J. A. Pope, J. Feng, J. Narvainen, R. Shaw, E. Scales, R. Kauppinen, A. M. Kenwright and S. Faulkner, *J. Am. Chem. Soc.*, 2008, **130**, 2178.
89. M. Tropiano, C. J. Record, E. Morris, H. S. Rai, C. Allain and S. Faulkner, *Organometallics*, 2012, **31**, 5673.
90. T. K. Ronson, T. Lazarides, H. Adams, S. J. A. Pope, D. Sykes, S. Faulkner, S. J. Coles, M. B. Hursthouse, W. Clegg, R. W. Harrington and M. D. Ward, *Chem. Eur. J.*, 2006, **12**, 9299.

91. X.-L. Li, L.-X. Shi, L.-Y. Zhang, H.-M. Wen and Z.-N. Chen, *Inorg. Chem.*, 2007, **46**, 10892.

92. H. B. Xu, L. Y. Zhang, Z. H. Chen, L. X. Shi and Z. N. Chen, *Dalton Trans.*, 2008, 4664.

93. F. F. Chen, Z. Q. Bian, B. Lou, E. Ma, Z. W. Liu, D. B. Nie, Z. Q. Chen, J. Bian, Z. N. Chen and C. H. Huang, *Dalton Trans.*, 2008, 5577.

94. N. M. Tart, D. Sykes, I. Sazanovich, I. S. Tidmarsh and M. D. Ward, *Photochem. Photobiol. Sci.*, 2010, **9**, 886.

95. J. E. Jones, R. L. Jenkins, R. S. Hicks, A. J. Hallett and S. J. A. Pope, *Dalton Trans.*, 2012, **41**, 10372.

96. P. Coppo, M. Duati, V. N. Kozhevnikov, J. W. Hofstraat and L. De Cola, *Angew. Chem., Int. Ed.*, 2005, **44**, 1806.

97. R. Ziessel, S. Diring, P. Kadjane, L. Charbonniere, P. Retailleau and C. Philouze, *Chem. Asian J.*, 2007, **2**, 975.

98. F.-F. Chen, Z.-Q. Bian, Z.-W. Liu, D.-B. Nie, Z.-Q. Chen and C.-H. Huang, *Inorg. Chem.*, 2008, **47**, 2507.

99. L. Moriggi, A. Aebischer, C. Cannizzo, A. Sour, A. Borel, J. C. G. Bunzli and L. Helm, *Dalton Trans.*, 2009, 2088.

100. W. Jiang, B. Lou, J. Wang, H. Lv, Z. Bian and C. Huang, *Dalton Trans.*, 2011, **40**, 11410.

101. D. Sykes, I. S. Tidmarsh, A. Barbieri, I. V. Sazanovich, J. A. Weinstein and M. D. Ward, *Inorg. Chem.*, 2011, **50**, 11323.

102. D. Sykes and M. D. Ward, *Chem. Commun.*, 2011, **47**, 2279.

103. Y. Koide, S. Takahashi and M. Vacha, *J. Am. Chem. Soc.*, 2006, **128**, 10990.

104. K.-Y. Kim, R. T. Farley and K. S. Schanze, *J. Phys. Chem. B*, 2006, **110**, 17302.

105. L. S. Natrajan, A. Toulmin, A. Chew and S. W. Magennis, *Dalton Trans.*, 2010, **39**, 10837.

106. C. L. Ho, K. L. Wong, H. K. Kong, Y. M. Ho, C. T. L. Chan, W. M. Kwok, K. S. Y. Leung, H. L. Tam, M. H. W. Lam, X. F. Ren, A. M. Ren, J. K. Feng and W. Y. Wong, *Chem. Commun.*, 2012, **48**, 2525.

107. W.-J. Xu, S.-J. Liu, X. Zhao, N. Zhao, Z.-Q. Liu, H. Xu, H. Liang, Q. Zhao, X.-Q. Yu and W. Huang, *Chem. Eur. J.*, 2013, **19**, 621.

108. M. Göppert-Mayer, *Annalen der Physik*, 1931, **401**, 273.
109. G. S. He, L.-S. Tan, Q. Zheng and P. N. Prasad, *Chem. Rev.*, 2008, **108**, 1245.
110. M. R. Detty, S. L. Gibson and S. J. Wagner, *J. Med. Chem.*, 2004, **47**, 3897.
111. F. N. Castellano, H. Malak, I. Gryczynski and J. R. Lakowicz, *Inorg. Chem.*, 1997, **36**, 5548.
112. S. W. Botchway, M. Charnley, J. W. Haycock, A. W. Parker, D. L. Rochester, J. A. Weinstein and J. A. G. Williams, *Proc. Nat. Acad. Sci.*, 2008, **105**, 16071.
113. F. Terenziani, C. Katan, E. Badaeva, S. Tretiak and M. Blanchard-Desce, *Adv. Mater. (Weinheim, Ger.)*, 2008, **20**, 4641.
114. M. H. V. Werts, N. Nerambourg, D. Pélégry, Y. L. Grand and M. Blanchard-Desce, *Photochem. Photobiol. Sci.*, 2005, **4**, 531.
115. L.-O. Pålsson, R. Pal, B. S. Murray, D. Parker and A. Beeby, *Dalton Trans.*, 2007, 5726.
116. A. Picot, A. D'Aléo, P. L. Baldeck, A. Grichine, A. Duperray, C. Andraud and O. Maury, *J. Am. Chem. Soc.*, 2008, **130**, 1532.
117. X. Xiao, J. P. Haushalter, K. T. Kotz and G. W. Faris, *Biomed. Opt. Express*, 2011, **2**, 2255.
118. T. J. Sørensen, O. A. Blackburn, M. Tropiano and S. Faulkner, *Chem. Phys. Lett.*, 2012, **541**, 16.
119. M. Lepeltier, T. K.-M. Lee, K. K.-W. Lo, L. Toupet, H. Le Bozec and V. Guerchais, *Eur. J. Inorg. Chem.*, 2007, **2007**, 2734.
120. C. J. Aspley and J. A. G. Williams, *New J. Chem.*, 2001, **25**, 1136.
121. P. C. Healy, C. Pakawatchai and A. H. White, *J. Chem. Soc., Dalton Trans.*, 1983, 1917.
122. J. C. Dyason, L. M. Engelhardt, P. C. Healy, C. Pakawatchai and A. H. White, *Inorg. Chem.*, 1985, **24**, 1950.
123. C. He, J. Ke, H. Xu and A. Lei, *Angew. Chem. Int. Ed.*, 2013, **52**, 1527.
124. P. G. M. Wuts and T. W. Greene, *Greene's Protective Groups in Organic Synthesis*, 4th edn. edn., John Wiley & Sons Inc., Hoboken, New Jersey, 2007.
125. H. C. Kolb, M. G. Finn and K. B. Sharpless, *Angew. Chem. Int. Ed.*, 2001, **40**, 2004.

126. V. V. Rostovtsev, L. G. Green, V. V. Fokin and K. B. Sharpless, *Angew. Chem. Int. Ed.*, 2002, **41**, 2596.

127. S. Sasaki, Y. Hamada and T. Shioiri, *Tetrahedron Lett.*, 1997, **38**, 3013.

128. M. A. Ciufolini and N. E. Byrne, *J. Chem. Soc., Chem. Commun.*, 1988, 1230.

129. J. Husson, M. Beley and G. Kirsch, *Tetrahedron Lett.*, 2003, **44**, 1767.

130. J. Husson and M. Knorr, *Beilstein J. Org. Chem.*, 2012, **8**, 379.

131. B. A. Pearlman, A. G. Padilla, J. T. Hach, J. L. Havens and M. D. Pillai, *Org. Lett.*, 2006, **8**, 2111.

Chapter 3

Photochromic Materials:

Introduction

3. Introduction

This chapter will introduce the phenomenon of photochromism, including a short overview of some of the classes of materials that exhibit this effect. The main focus is upon the triphenylimidazolyl radical-dimer systems and dihydropyrenes that feature in the results and discussion of Chapter 4.

3.1. Photochromic compounds

Photochromism describes a reversible colour change of a material when exposed to light.[1] This phenomenon has been recognised for some 145 years, with the earliest known report attributable to Fritzsche, who noted that when a solution of tetracene was exposed to daylight its usual orange colour bleached.[2] This was later demonstrated to be a result of photodimerisation of the acene that disrupts its conjugation and shifts the absorption maximum into the ultraviolet region.[3]

Photochromism has been defined above as being a reversible process; therefore, irreversible photochemical reactions, even if they include a change in colour, such as the conversion of white AgCl to colloidal brown/black Ag, are not considered forms of photochromism. A second stimulus is required to induce the reverse process: this can either be *via* a thermal (T-type) or photo (P-type) mechanism, with the latter typically at a different wavelength to that used for the forward reaction. Reversibility is also a desirable quality for technological applications. These applications range from the relatively mundane, such as spectacles which change colour upon exposure to bright light,[4] to more advanced, prototypically realised, optoelectronic memory devices for data storage wherein a molecule is 'written' into one state by an input photon and 'read' by a second (for instance, by a change in its UV-visible absorption or infra-red spectrum).[5] The use of TPA could even result in 3D optical data storage due to localised excitation of the photochromic material.[6]

If a photochromic compound is to find use in a particular application then the material has to be stable upon transformation between the two or more forms of interest, typically for extended periods of time and over multiple cycles.[1] A complicating factor is that of additional photochemical pathways that deplete the sample by producing non-photochromic side-products. Such fatigue pathways affect many photochromic systems: if the alternative processes are sufficiently competitive with the desired conversion, the

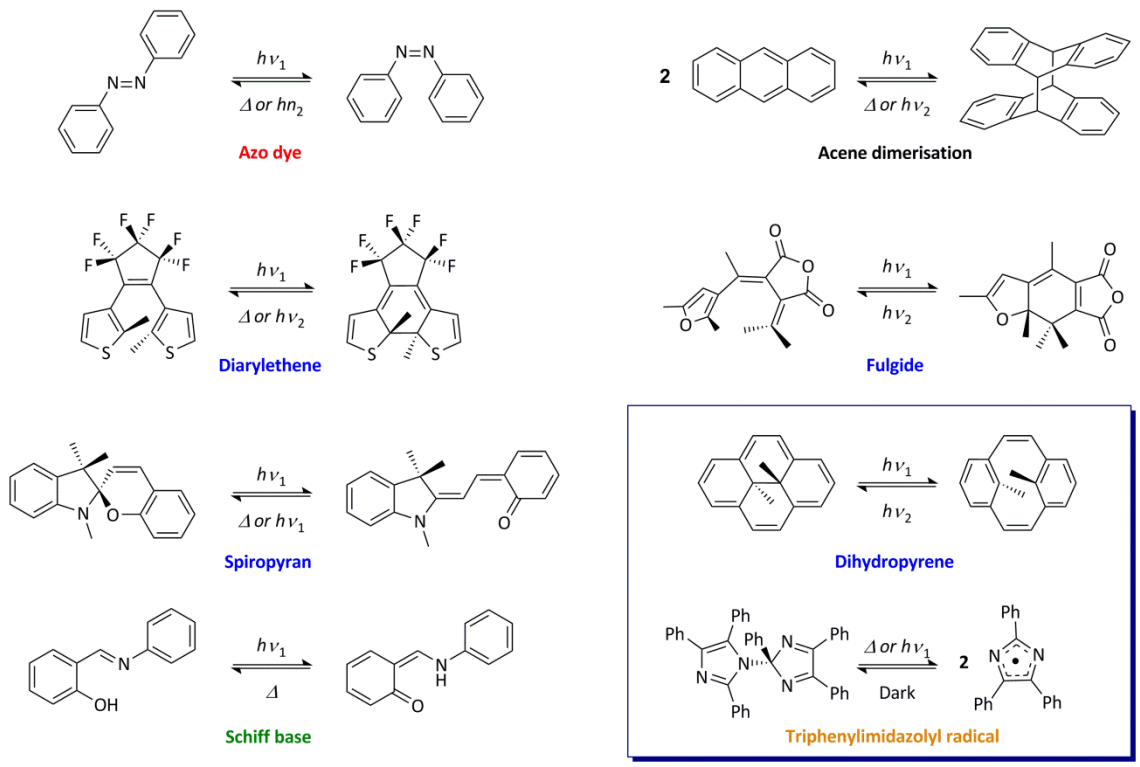

Figure 3.1. Common photochromic materials and their classifications. The compounds bound within the blue rectangle to the lower right corner of the figure are those that are explored in this work. The photochromic mechanism of each class is indicated by the colour of their name: *trans-cis* isomerism (red), cycloaddition (black), electrocyclisation (blue), excited state intramolecular proton transfer (green) and radical-dimer equilibrium (orange).

material is rendered essentially useless under certain operating conditions. These pathways depend on the molecule of interest, but may include reaction with oxygen or adventitious water, proton abstraction from solvent or the formation of non-photochromic isomers. It is therefore important to study not only the properties of direct importance to the photochromism, such as the quantum yield, rate of transformation and net change in colouration, but also to identify and understand such deleterious pathways.

There are several general classes of molecules that undergo photochromism, with some of the most common illustrated in Figure 3.1. The tetracene dimerisation observed by Fritzsche is an example of a cycloaddition. Photochemical inter- or intramolecular concerted cycloaddition reactions are observed for [2*n*+2*m*] processes, where *n* and *m* are the number of π-electrons of the two components and are positive integers having an even sum. These reactions are a subset of the processes that can occur according to the Woodward-Hoffmann Rules. The inherent reversibility of

cycloaddition reactions makes them suitable as a mechanism for photochromic materials. The dimerisation of tetracene described above is a [4+4] cycloaddition. The extension of this concept to other acenes, such as anthracene, is obvious.[7] Acene dimerisation still receives attention with new derivatives of tetracene being investigated.[8] The dimerisation of tetracene has the complication that it can produce a mixture of two isomers. Of the other possible photocycloadditions that could lead to photochromism, the [2+2] reaction of two alkenes is the most studied. Such studies include pre-organised tethered systems and solid-state structures that orientate the two molecules into a suitable mutual arrangement to facilitate a topochemical cycloaddition.[9]

A somewhat related process to that described above is electrocyclisation, wherein one new bond is formed in an intramolecular reaction. Some examples of molecules that undergo photochromic isomerisation through this mechanism are indicated in Figure 3.1. These include the spiropyran,[10] fulgide,[11] diarylethene[12] and dihydropyrene[i] (DHP)[13] classes, with the last of these occurring *via* a retro-electrocyclisation in the forward direction of the photochromism.[13] Arguably, the most well studied class are the diarylethene derivatives developed by Irie.[12] The bisthiophene analogue shown is the most common, with the perfluorocyclopentene ring required for both rigidity, to hinder isomerism, and for inhibition of fatigue by oxidation at the pseudo-benzylic positions. In the open form, conjugation is limited to each individual thiophene ring, whereas upon electrocyclisation, conjugation occurs also through the bridge. The diarylethene photochromic-unit has been incorporated into many organic[14-16] and organometallic[17-19] systems to induce a change in electronic communication between two moieties. Furthermore, development of the system through variation of the arene has lead to tuning of both the colour and switching rates of diarylethene molecules.[12] The spiropyran and fulgide systems are similar in their mechanism and utility, although they perhaps have more restricted opportunity for derivatisation. DHPs will be considered in more detail later in Section 3.3.

Another mechanism for photochromic materials to operate *via* is a *trans* to *cis* isomerism, such as the azo dyes.[20] Excitation to the S_1 $\pi^* \leftarrow \pi$ state of a diarylazo compound reduces the bond order of the azo linkage, allowing rotation about this bond and formation of the metastable *cis* form that has a different absorption spectrum. The

[i] In full, the unsubstituted derivative is *trans*-10b,10c-dimethyl-10b,10c-dihydropyrene. Numbering of substituents is the same as for pyrene used in Chapter 2.

cis form can be reverted to the thermodynamically more stable *trans* form by either irradiation or heat. Schiff bases (imines) may also undergo a similar isomerism; however, in the case of substituted 2-phenolimines, excited state intramolecular proton transfer from the hydroxyl group to the nitrogen atom of the imine is a competitive process, with concomitant redistribution of the π-system and a change in conjugation.[21] Thus, Schiff bases are an interesting example whereby two different mechanisms could result in different photochromic behaviour.

The final mechanism of photochromism to be discussed here is the dimerisation of a radical, as exemplified by the triphenylimidazolyl radical (TPIR). Radicals, in general, have low energy absorption bands due to the small energy gap between their highest doubly occupied molecular orbital and their yet higher energy singly occupied molecular orbital (SOMO). Upon dimerisation, a closed-shell species is formed that has an absorption spectrum more akin to a typical organic material. Thus, a significant colour change is observed upon dimerisation. If the radical dimerisation is reversible, then photochromism can be achieved. The TPIR system is considered in some more detail in the next section.

3.2. 2,4,5-Triphenylimidazolyl radicals and their dimers

The extraordinary optical and structural properties of TPIR materials have been studied for more than 50 years.[22] They were first reported by Hayashi and Maeda[22] in 1960 and they continue to attract significant attention.[23-29] These radical species have been shown to reversibly form various dimers[30] that exhibit photo-, thermo- and piezochromism.[31,ii] Recently, the focus has been to identify methods to tune the colour of these materials and to increase the rate of switching for a range of applications.[24] They are considered potentially of use in display screens and other devices requiring a fast change between coloured materials,[29] as well as for optical data storage and for use as molecular switches. They have also been used as polymerisation initiators, in particular 2-(2′-chlorophenyl)-4,5-diphenylimidazole.[32]

The various forms of chromism that these materials exhibit have a common origin: reversible formation of two coloured TPIRs from a colourless dimer.[33] The

[ii] Thermochromism and piezochromism refer to a reversible change in colour upon application of heat or pressure, respectively.

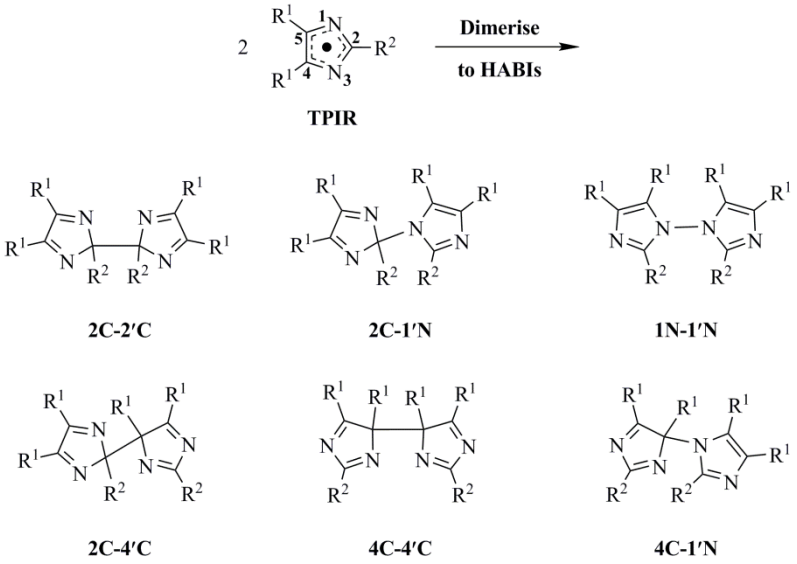

Scheme 3.1. Potential dimerisation modes of two TPIRs bound through combinations of the atoms of the imidazole rings to form HABIs.

dimer is a HABI that has six potential isomeric modes (Scheme 3.1).[31] Early studies attempted to establish the HABI speciation in both the solution and solid states and to correlate this to a particular type of chromism, with some conflicting results.[34-38] Thus, it was initially assumed that the 1N-1′N mode was that which is formed, although no convincing evidence for this was presented.[35] More recent assessments suggest that the most common HABIs are the 2C-1′N mode, which is both photo- and thermochromic, and the 4C-4′C mode, for which thermo- or piezochromic materials have been described.[23, 39] Modes other than these six have been observed occasionally in sterically hindered systems.[26]

TPIRs were extensively investigated in the 1970s and 1980s by the DuPont chemical company, among others, for use in colour photography. Although the materials were not particularly successful for this application, they found use in *Dylux* copy paper produced by the same company. The history of this work has been discussed in detail in a book concerning these materials.[23] This industrial research into the applications of TPIRs also led to several advances in the understanding of their properties, including that derivatives substituted in the *ortho* position of the phenyl ring in the 2-position dimerise more quickly than other isomers, as do those bearing electron-withdrawing substituents.[40, 41]

Following the end of work on these materials by DuPont, there was something of a hiatus before they were re-discovered by the academic community. Jiro Abe

(Aoyama Gakuin University, Japan) has rekindled some interest in these materials by producing species that can switch at a fast rate for more modern applications, such as data storage and holographic display screens.[42] This recent work has been centred on tethered systems in which two TPIRs are constrained in their relative orientations and are limited in their extent of separation, both of which make dimerisation more favourable.[24, 26]

SC-XRD studies have been indispensible in furthering the understanding of the dimerisation of TPIRs, which otherwise has relied principally on the less definitive method of IR spectroscopy.[31, 35] Several 2C-1′N dimers have been characterised by SC-XRD[iii] and it has been concluded that this is usually the most stable form. The SC-XRD structure of the 2-(2′-chlorophenyl)-4,5-diphenylimidazolyl TPIR has been obtained following *in situ* UV irradiation of a single crystal of its 2C-1′N dimer, even with only 10% conversion of one of two symmetry independent dimers in the asymmetric unit (BARCOM).[43, 44] Lowering the temperature to < 30 K gave a higher conversion of 24% (BARCOM02).[45] Irradiation of a crystal of the 2C-1′N dimer of the unsubstituted TPIR lead to partial conversion through a "molecular swapping" process to a mixture of the radical and its 2C-2′C HABI (QIWXID).[46] However, the low conversion (14%) for this process made structural analysis of the dimer challenging; hence, isolation of a crystalline sample of a 2C-2′C HABI is still required. The radical nature of the TPIRs has been demonstrated for several derivatives by EPR measurements.[22, 44, 47, 48]

3.3. Dihydropyrene

Similar to the TPIR system, DHPs have a long history dating back nearly 50 years to when they were first reported to be photochromic by Boekelheide and co-workers.[49] In its closed form, conjugation is present around the perimeter of the polycyclic aromatic (14π, $4n + 2$ where $n = 3$) hydrocarbon making the unsubstituted derivative dark green in colour. As stated above, the mechanism of DHP photochromism is a retro-electrocyclisation reaction that results in the formation of a partially conjugated system that has little to no absorption in the visible region in its open form. This is unusual

[iii] 13 structures of 2C-1′N HABIs (excluding redeterminations and additional solvate structures) have been deposited in the CSD (WebCSD *ver.* 1.1.1, January 2013 update).

because most photochromic systems form a species that absorbs at lower energy upon irradiation. DHPs are therefore referred to as negative photochromic materials.[1]

The majority of the work on this system has been performed by the group of Mitchell, who has also reviewed the topic.[13] For simple derivatives, the energy barrier to conversion between the open and closed forms is relatively large (*ca.* 80-90 kJ mol^{-1}) compared to the enthalpic energy difference between the forms (*ca.* 12 kJ mol^{-1} in favour of the closed form).[50] The ring opening occurs *via* the S_1 state of the closed DHP with some evidence of participation of the T_1 state.[51] The photochemical back-reaction is often much more efficient ($\Phi \sim 0.1$) than the forward reaction ($\Phi \sim 0.02$) making the choice of excitation wavelength important to avoid a photostationary state favouring the closed form. In general, when the aromatic ring system is expanded by annulation, the rate of both the forward reaction and cycloreversion to the closed form is increased.[52, 53] The thermal ring closure can be slowed considerably by exchange of the internal methyl groups to cyano substituents.[54] Making this seemingly small change increases the half-life of thermal conversion of the open to closed forms from 42 h to an extrapolated 30 years at 20 °C. Clearly for reversibility, finer tuning of the rate is required and, in addition, this derivative undergoes a rearrangement to give the cyano substituent *exo* to the DHP ring when heated above 50 °C. A similar process occurs with internal fluorine substituents.[55] A system for which isomerisation is avoided but still has a slow thermal back reaction (2 years at 20 °C) has been described using *iso*-butenyl substituents as the internal groups.[56] Changing the substituent at the 2-position to a formyl group increases the ring-opening quantum yield, but at the expense of also increasing the quantum yield for ring closure by an even greater amount.[50] Unsubstituted DHP is weakly fluorescent at *ca.* 640 nm in its closed form ($\Phi = 0.6 \times 10^{-3}$, $\tau = 5$ ns),[52] which can be increased by a pyrenoyl substituent in the 4-position; however, any emission is detrimental to efficient photochromism because the excited state is depleted before isomerisation can occur.[57]

3.4. Summary and aims

Photochromic materials are interesting both as a curiosity and for their potential applications. Many classes of these materials are known that operate by a variety of mechanisms, allowing a particular type to be selected when a certain property is desired. Despite sustained interest in the synthesis and study of photochromic materials, there are still some specific aspects of the photochemistry to be addressed and the potential properties of many of the systems have yet to be fully exploited. One of the aims of this

work has been to explore the colour-tuning of the TPIR class of photochromic materials and to better understand their dimerisation and potential fatigue processes. The DHP system has also been investigated, initially with the aim of establishing the structure of its open form, but subsequently with a view to using the DHP ring as a photochemical switch for modulating charge transfer between electron donating and accepting groups.

3.5. References

1. H. Bouas-Laurent and H. Durr, *Pure Appl. Chem.*, 2001, **73**, 639.
2. J. Fritzsche, *Comptes Rendus Acad. Sci., Paris*, 1867, **69**, 1035.
3. J. A. Katul and A. B. Zahlan, *J. Chem. Phys.*, 1967, **47**, 1012.
4. R. J. Araujo, *J. Chem. Educ.*, 1985, **62**, 472.
5. Y.-C. Jeong, S. H. Kim, H. Ko, K. Song, K.-H. Ahn and S. I. Yang, *Photochem. Photobiol. Sci.*, 2009, **8**, 1590.
6. E. Walker, A. Dvornikov, K. Coblentz and P. Rentzepis, *Appl. Opt.*, 2008, **47**, 4133.
7. M. O'Donnell, *Nature*, 1968, **218**, 460.
8. A. G. L. Olive, A. Del Guerzo, J.-L. Pozzo, J.-P. Desvergne, J. Reichwagen and H. Hopf, *J. Phys. Org. Chem.*, 2007, **20**, 838.
9. K. Biradha and R. Santra, *Chem. Soc. Rev.*, 2013, **42**, 950.
10. S. V. Paramonov, V. Lokshin and O. A. Fedorova, *J. Photochem. Photobiol. C-Photochem. Rev.*, 2011, **12**, 209.
11. H. Koshima, H. Nakaya, H. Uchimoto and N. Ojima, *Chem. Lett.*, 2012, **41**, 107.
12. M. Irie, *Chem. Rev.*, 2000, **100**, 1685.
13. R. H. Mitchell, *Eur. J. Org. Chem.*, 1999, 2695.
14. H.-h. Liu, X. Zhang, Z. Gao and Y. Chen, *J. Phys. Chem. A*, 2012, **116**, 9900.
15. S. Chen, L.-J. Chen, H.-B. Yang, H. Tian and W. Zhu, *J. Am. Chem. Soc.*, 2012, **134**, 13596.
16. A. Perrier, F. Maurel and D. Jacquemin, *Acc. Chem. Res.*, 2012, **45**, 1173.
17. W. Tan, Q. Zhang, J. Zhang and H. Tian, *Org. Lett.*, 2008, **11**, 161.
18. J. C.-H. Chan, W. H. Lam, H.-L. Wong, N. Zhu, W.-T. Wong and V. W.-W. Yam, *J. Am. Chem. Soc.*, 2011, **133**, 12690.
19. H.-M. Wen, B. Li, J.-Y. Wang, L.-X. Shi, C.-N. Chen and Z.-N. Chen, *Organometallics*, 2013, **32**, 1759.
20. J. García-Amorós and D. Velasco, *Beilstein J. Org. Chem.*, 2012, **8**, 1003.
21. E. Hadjoudis and I. M. Mavridis, *Chem. Soc. Rev.*, 2004, **33**, 579.
22. T. Hayashi and K. Maeda, *Bull. Chem. Soc. Jpn.*, 1960, **33**, 565.

23. R. Dessauer, *Photochemistry, History and Commercial Applications of Hexaarylbiimidazoles: All About HABIs, 1st edn.*, Elsevier, Amsterdam, 2006.
24. Y. Kishimoto and J. Abe, *J. Am. Chem. Soc.*, 2009, **131**, 4227.
25. H. Miyasaka, Y. Satoh, Y. Ishibashi, S. Ito, Y. Nagasawa, S. Taniguchi, H. Chosrowjan, N. Mataga, D. Kato, A. Kikuchi and J. Abe, *J. Am. Chem. Soc.*, 2009, **131**, 7256.
26. Y. Harada, S. Hatano, A. Kimoto and J. Abe, *J. Phys. Chem. Lett.*, 2010, **1**, 1112.
27. K. Mutoh and J. Abe, *Chem. Commun.*, 2011, **47**, 8868.
28. K. Mutoh and J. Abe, *J. Phys. Chem. A*, 2011, **115**, 4650.
29. H. Yamashita and J. Abe, *J. Phys. Chem. A*, 2011, **115**, 13332.
30. Y. H. Zhou, W. E. Baker, P. M. Kazmaier and E. Buncel, *Can. J. Chem.*, 1998, **76**, 884.
31. D. M. White and J. Sonnenberg, *J. Am. Chem. Soc.*, 1966, **88**, 3825.
32. A. D. Liu, A. D. Trifunac and V. V. Krongauz, *J. Phys. Chem.*, 1992, **96**, 207.
33. K. Maeda and T. Hayashi, *Bull. Chem. Soc. Jpn.*, 1970, **43**, 429.
34. T. Hayashi and K. Maeda, *Bull. Chem. Soc. Jpn.*, 1962, **35**, 2057.
35. D. M. White and J. Sonnenberg, *J. Org. Chem.*, 1964, **29**, 1926.
36. H. Tanino, T. Kondo, K. Okada and T. Goto, *Bull. Chem. Soc. Jpn.*, 1972, **45**, 1474.
37. T. Goto, H. Tanino and T. Kondo, *Chem. Lett.*, 1980, **9**, 431.
38. A. Kimoto, S. Niitsu, F. Iwahori and J. Abe, *New J. Chem.*, 2009, **33**, 1339.
39. E. Kiepek, Y. Zhou, S. Hoz, E. Rozental, P. M. Kazmaier and E. Buncel, *Can. J. Chem.*, 2005, **83**, 1448.
40. G. R. Coraor, L. A. Cescon, R. Dessauer, A. S. Deutsch, H. L. Jackson, A. MacLachlan, K. Marcali, E. M. Potrafke and R. E. Read, *J. Org. Chem.*, 1971, **36**, 2267.
41. G. R. Coraor, L. A. Cescon, R. Dessauer, E. F. Silversmith and E. J. Urban, *J. Org. Chem.*, 1971, **36**, 2262.
42. N. Ishii, T. Kato and J. Abe, *Sci. Rep.*, 2012, **2**.
43. M. Kawano, T. Sano, J. Abe and Y. Ohashi, *J. Am. Chem. Soc.*, 1999, **121**, 8106.

44. J. Abe, T. Sano, M. Kawano, Y. Ohashi, M. M. Matsushita and T. Iyoda, *Angew. Chem. Int. Ed.*, 2001, **40**, 580.
45. M. Kawano, Y. Ozawa, K. Matsubara, H. Imabayashi, M. Mitsumi, K. Toriumi and Y. Ohashi, *Chem. Lett.*, 2002, **31**, 1130.
46. M. Kawano, T. Sano, J. Abe and Y. Ohashi, *Chem. Lett.*, 2000, **29**, 1372.
47. S. Hatano and J. Abe, *Phys. Chem. Chem. Phys.*, 2012, **14**, 5855.
48. A. Kikuchi, T. Iyoda and J. Abe, *Chem. Commun.*, 2002, 1484.
49. H. R. Blattmann, D. Meuche, E. Heilbronner, R. J. Molyneux and V. Boekelheide, *J. Am. Chem. Soc.*, 1965, **87**, 130.
50. H. R. Blattmann and W. Schmidt, *Tetrahedron*, 1970, **26**, 5885.
51. R. S. Murphy, Y. Chen, T. R. Ward, R. H. Mitchell and C. Bohne, *Chem. Commun.*, 1999, **0**, 2097.
52. M. A. L. Sheepwash, R. H. Mitchell and C. Bohne, *J. Am. Chem. Soc.*, 2002, **124**, 4693.
53. M. A. L. Sheepwash, T. R. Ward, Y. Wang, S. Bandyopadhyay, R. H. Mitchell and C. Bohne, *Photochem. Photobiol. Sci.*, 2003, **2**, 104.
54. K. Ayub, R. Zhang, S. G. Robinson, B. Twamley, R. V. Williams and R. H. Mitchell, *J. Org. Chem.*, 2007, **73**, 451.
55. V. Boekelheide and P. H. Anderson, *J. Org. Chem.*, 1973, **38**, 3928.
56. K. Ayub, R. Li, C. Bohne, R. V. Williams and R. H. Mitchell, *J. Am. Chem. Soc.*, 2011, **133**, 4040.
57. R. H. Mitchell, C. Bohne, S. G. Robinson and Y. Yang, *J. Org. Chem.*, 2007, **72**, 7939.

Chapter 4

Photochromic Materials:

Results and Discussion

4. Introduction

This chapter outlines the work conducted on photochromic sytems, including a discussion of the synthesis of the materials and their properties. In particular, the focus is on the structural properties of the TPIR system, including the isolation of a previously structurally uncharacterised dimerisation mode and the formation of peroxides by these materials. A photocrystallisation method to produce single crystals of the 2C-2′C dimer of a novel TPIR derivative is described. Finally, the dihydropyrene (DHP) photochromic system is considered and the challenges in making new derivatives of this intriguing molecule are outlined.

4.1. Dimerisation modes of a novel TPIR system

A TPIR with a vinylbithiophene substituent has been reported to exhibit colour-tuned chromism, relative to its well known parent compound.[1] The colour tuning effect on the chromism of such systems was identified as an area requiring further study. To do this, an acetylenic TPIR derivative, ETPI, with a rigid, π-conjugated 4-*tert*-butylphenylethynylphenyl substituent at the 2-position of the imidazole ring (Scheme 4.1) was chosen. The synthesis of ETPI comprised four steps. The intermediate 4′-(4-*tert*-butylphenylethynyl) benzaldehyde (EBA) was synthesised by conventional Sonogashira cross-coupling and deprotection methodology in 63% yield (two steps). This compound was then condensed with benzil and ammonium acetate in a microwave-heated reaction[2] to give the imidazole ETPI-H in 64% yield; this compound was characterised fully, including the SC-XRD structure of its ethanol disolvate (Figure 4.1). Interestingly, the inclusion of ethanol into the crystal structure disrupts the standard N-H···N hydrogen bonding chain motif that exists in the crystal structures most imidazole derivatives by forming an alternative O-H···O-H···N triad (*cf.* the structures presented in Section 4.2 below). Finally, ETPI-H was oxidised by $K_3[Fe(CN)_6]$ in a biphasic mixture of CH_2Cl_2 and aqueous KOH, forming initially a dark green solution, from which a light green solid was isolated.

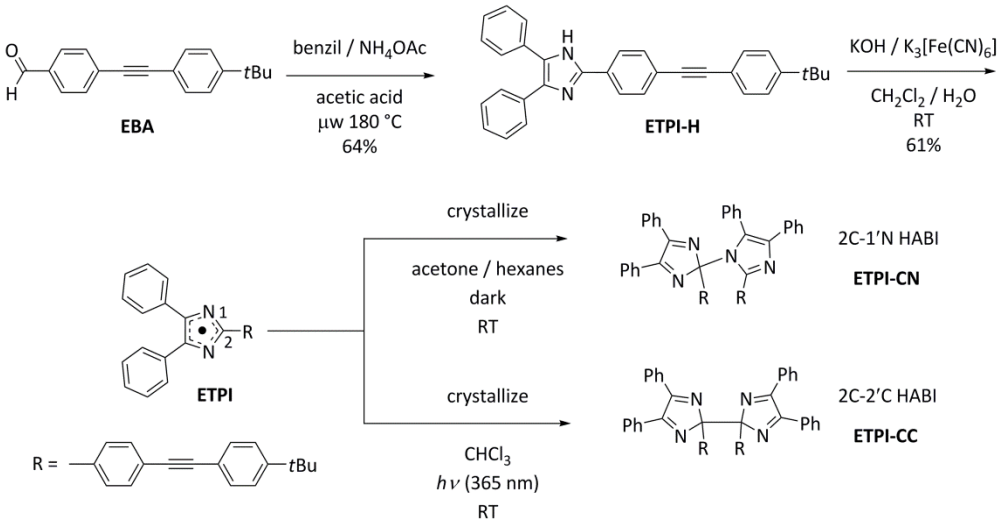

Scheme 4.1. Synthesis of extended TPIR derivative ETPI and the conditions used to obtain single crystals of its isomeric dimers ETPI-CN and ETPI-CC.

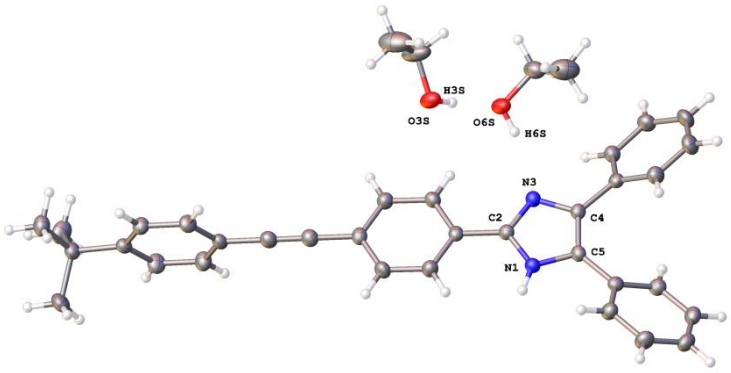

Figure 4.1. The molecular structure of ETPI-H ethanol disolvate obtained by SC-XRD. The two ethanol solvent molecules are hydrogen bonded to each other and then to N3 of the imidazole ring in an O3S-H3S···O6S-H6S···N3 sequence. The potential N1-H donor is not involved in any hydrogen bonding. Element (colour): carbon (grey), hydrogen (white), nitrogen (blue), oxygen (red). Atomic displacement parameters are shown at 50% probability.

The *tert*-butyl group was selected for two purposes: to increase solubility and to provide a readily interpretable set of NMR signals, characteristic of the HABI symmetry in solution. Signals corresponding to two inequivalent *tert*-butyl groups were observed by ^{1}H and ^{13}C{^{1}H} NMR, and two inequivalent acetylene groups were identified by ^{13}C{^{1}H} NMR, indicating an asymmetric dimerisation mode (Figure 4.2). SC-XRD of pale green crystals grown in the dark from acetone/hexanes (anti-solvent), confirmed

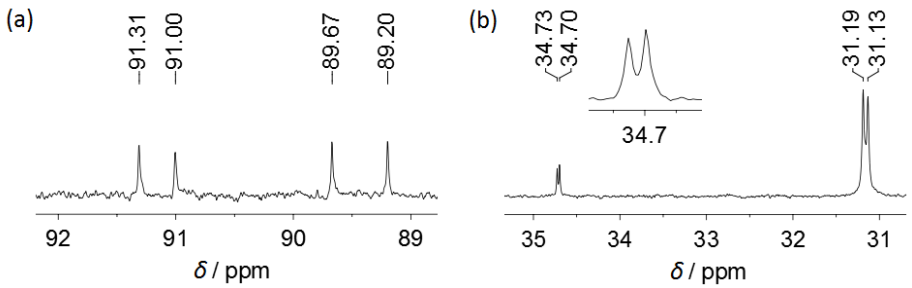

Figure 4.2. The inequivalent (**a**) acetylene and (**b**) *tert*-butyl signals in the 101 MHz $^{13}C\{^{1}H\}$ NMR (C_6D_6) spectrum of the initial ETPI dimer, consistent with the asymmetric 2C-1′N HABI dimer ETPI-CN.

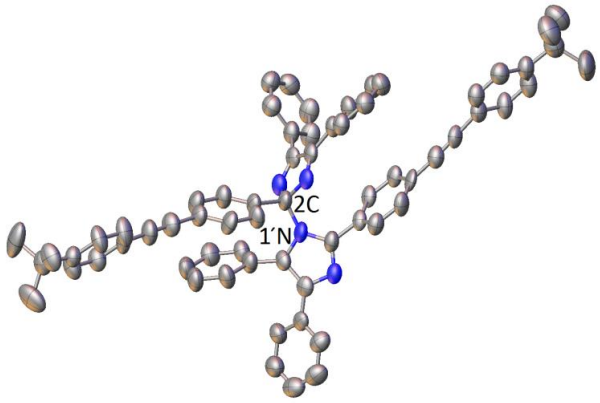

Figure 4.3. Molecular structure of ETPI-CN obtained by SC-XRD from a crystal grown in the absence of light from acetone/hexanes. As a result of poor diffraction quality and the inclusion of highly disordered solvent, the structure is used only to confirm connectivity. Hydrogen atoms are omitted for clarity. Element (colour): carbon (grey), nitrogen (blue). Atomic displacement parameters are shown at 50% probability.

this compound to be the common 2C-1′N HABI (ETPI-CN) (Figure 4.3). This compound was found to be both photo- and thermochromic in CH_2Cl_2 solution, but exhibited no obvious piezochromism in the solid state, consistent with other 2C-1′N derivatives. Figure 4.4 shows the change in the UV-visible absorption spectrum during irradiation at 365 nm. The coloured species generated has two additional bands in the visible region: a structured, but very broad, band between 500-800 nm (λ_{max} = 721 nm) with an energy spacing of *ca.* 2000 cm^{-1} between the two vibronic features, and a higher

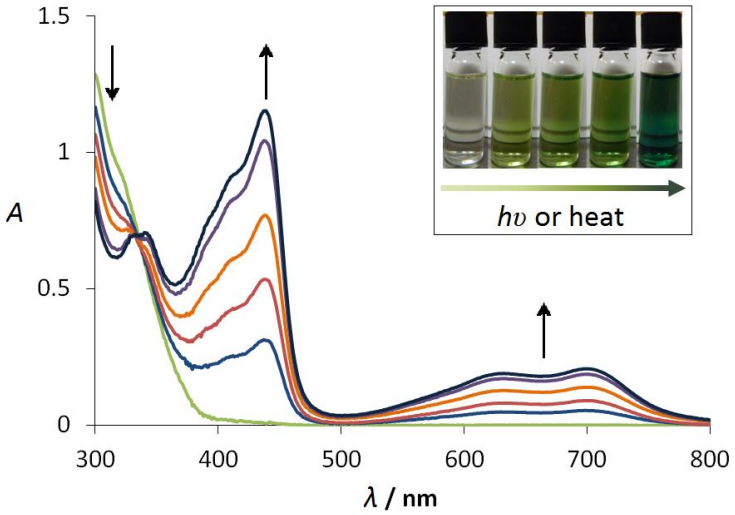

Figure 4.4. UV-visible absorption spectra recorded during the conversion of ETPI-CN (*ca.* 5 x 10^{-6} M) to ETPI in CH_2Cl_2 by UV (365 nm) irradiation at room temperature. Interval of *ca.* 30 s. Inset: photograph of the visible colour change from colourless to dark green.

energy peak at λ_{max} = 445 nm. Compared to the unsubstituted TPIR radical,[3] there is a bathochromic shift of *ca.* 170 nm (4310 cm^{-1}) in the low energy band, demonstrating the colour tuning of these photochromic materials (from violet to green in this case). The spectral tuning relative to the parent TPIR is intermediate to that of the vinylbithiophene derivative.[1] An isosbestic point, indicative of only two species present in equilibrium in solution, was observed at *ca.* 330 nm.

Irradiation (365 nm) of an ethyl acetate solution of ETPI-CN at room temperature generated a dark green deposit at the point of irradiation on the wall of the vial. Abe and co-workers reported previously the structure of the quinoidal form of a bisimidazole diradical from a crystal obtained during low temperature (200 K) irradiation of a toluene solution of the parent dimer.[4, 5] Similarly, during the study of phenalenyl neutral radicals, Haddon and co-workers obtained a novel dimerisation mode when a sample crystallised under ambient visible light conditions.[6] These reports of unusual materials being formed under irradiation encouraged us to elucidate the structure of the solid. After considerable experimentation, single crystals suitable for diffraction were produced from a *ca.* 10 mM $CHCl_3$ solution of ETPI-CN by 365 nm irradiation focused on the vial wall. The structure of the crystallised material was determined by SC-XRD to be the 2C-2′C HABI (ETPI-CC) (Figure 4.5), previously only observed as a small proportion of an irradiated crystal (*vide supra*).[7] Importantly, the SC-XRD structure and NMR spectra of ETPI-CN from the bulk sample confirm that

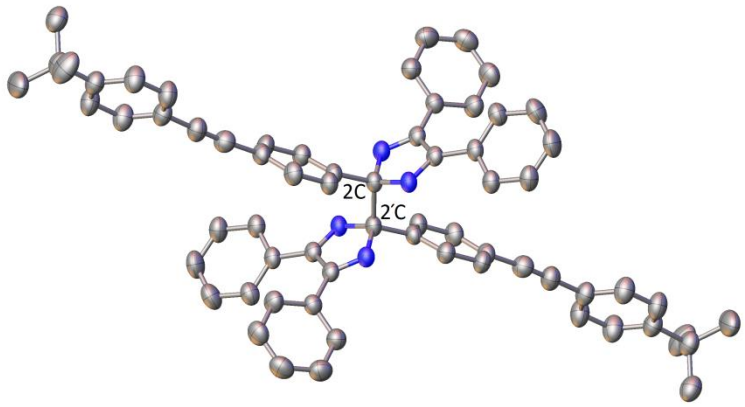

Figure 4.5. Molecular structure of ETPI-CC obtained by SC-XRD of a crystal grown under irradiation at 365 nm in $CHCl_3$ solution. Hydrogen atoms are omitted for clarity. Element (colour): carbon (grey), nitrogen (blue). Atomic displacement parameters are shown at 50% probability. Primed atom generated by the symmetry operation (1-*x*, 1-*y*, 1-*z*).

the 2C-2′C dimer is *not* the favoured mode for this derivative under standard conditions. To the best of the knowledge of the author, this is the first conclusive evidence for a pure form of this dimerisation mode for any TPIR derivative. It is noted that a metal organic framework comprised of 2C-2'C dimers stabilised by coordination through all four N atoms to $CuBr_4$ units has been reported.[8]

The 2C–2′C bond length of ETPI-CC is 1.601(4) Å, which is relatively long compared to the typical C(sp^3)–C(sp^3) bond length of 1.54 Å.[9] Long C–C bonds are of considerable interest for furthering our understanding of chemical bonding,[10] and while this bond is not as long as previously reported systems designed to induce long bonds though ring strain (1.72 Å)[11, 12] or steric bulk (1.63-1.65 Å),[13] it is unusual in that it is a system where neither of these driving forces are overtly present.[6, 14] Dispersion interactions have been used to stabilise a bulky alkane with a bond length of 1.71 Å, but this does not seem an obvious stabilising factor for ETPI-CC.[15, 16] A radical cation dimer with a bond length of 1.637(5) Å has also been reported very recently, which highlights the continued interest in this area.[17] The long bond is suggestive of weak association between the constituent parts of the dimers. Consistent with this, dissolution of ETPI-CC in CH_2Cl_2 immediately produced a dark green solution. The UV-visible absorption spectrum of this solution was indistinguishable from an irradiated solution of ETPI-CN, suggesting that ETPI-CC dissociates rapidly to give ETPI. After leaving the solution of ETPI-CC in the dark for *ca*. two hours, the colour completely disappeared

and the absorption spectrum matched that of freshly dissolved ETPI-CN. This is very similar behaviour to that described for the 4C-4′C mode, which is said to be only stable in the solid state, dissociating to the radical when dissolved. It is noted that the structure of a 4C-4′C mode has never been verified by SC-XRD, with only IR spectra presented as verification. No evidence for the existence of this, or any other, additional dimerisation mode of ETPI was observed.

ETPI-CC and ETPI-CN have strong Raman acetylenic stretches centred at 2217 and 2214 cm^{-1}, respectively, and ring modes at 1602 and 1605 cm^{-1}, respectively. Both have bands at 1115 cm^{-1}. Characteristically, ETPI-CC has a weak band at 910 cm^{-1}, absent for ETPI-CN, while ETPI-CN has additional aromatic stretches at 1472 and 1538 cm^{-1} due to its lower symmetry. Raman spectra of CH_2Cl_2 solutions of ETPI-CN before and after irradiation are indistinguishable, both from each other and from a solution of ETPI-CC immediately following dissolution. The instability of ETPI-CC in solution and the absence of a bulk quantity inhibited further spectroscopic investigation.

DFT geometry optimisations of ETPI (unrestricted), ETPI-CN and ETPI-CC (both restricted) using the B3LYP and M06-2X (which provides a good description of non-covalent interactions, important in large systems such as these, and has been used recently to model effectively systems with long C-C bonds[16]) functionals and 6-31+G(d) basis set have been performed (*tert*-butyl substituted for Me groups on the dimers). The connecting C–C bond length of ETPI-CC is calculated to be 1.618 Å (B3LYP) / 1.633 Å (M06-2X), reproducing moderately well the experimentally observed long bond of this isomer. The calculated elongation of 0.02-0.03 Å may be a result of the difference between the structure in the solid state and the gas phase or be due to a deficiency in the method. The Wiberg Bond Index[18] of this C–C bond is 0.81 (M06-2X) / 0.85 (B3LYP), indicating a relatively weak bond (the other three bonds to these carbon atoms have Wiberg Bond Indices of 0.97-0.98). According to previous calculations on a related phenanthroline fused-TPIR system,[19] the order of thermodynamic stability of the dimers is 1N-1′N > 2C-1′N > 2C-2′C > all other potential modes, and it is calculated, in agreement with this, that ETPI-CN is lower in energy than ETPI-CC by 27 kJ mol^{-1} (B3LYP) / 35 kJ mol^{-1} (M06-2X). Dimerisation through the 2-position of the imidazolyl ring disrupts conjugation with the phenylethynyl moiety; therefore, the lower energy of ETPI-CN compared to ETPI-CC is rationalised as loss of conjugation in one half *versus* both halves of the respective dimers.

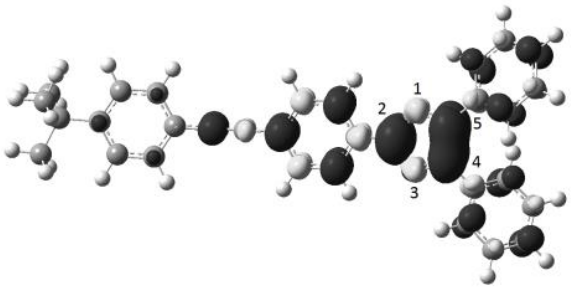

Figure 4.6. (Unrestricted) B3LYP/6-31+G(d) DFT calculated spin density distribution of ETPI. Black and white shading show positive and negative spin density, respectively. Isovalue: $\pm$ 5 x 10^{-4} e a_0^{-3}.

Due to the radical nature of ETPI, its spin density distribution must be considered in order to understand its dimerisation behaviour. The DFT calculated spin density of ETPI is shown in Figure 4.6. It can be seen that there is significant spin density at the 2-position of the imidazolyl ring through which both ETPI-CN and ETPI-CC dimerise. The radical is delocalised onto the 4-phenylethynyl moiety in the 2-position, but the terminal phenyl ring shows only a minor contribution. The symmetry related 4- and 5-positions also carry significant spin density, but dimerisation through these positions was not observed, tentatively ascribed to steric hindrance. The low spin density on the nitrogen atoms has been suggested to kinetically inhibit the formation of the 1N-1′N mode.[19] It would, however, also be expected to contribute to a lower rate of formation of ETPI-CN than of ETPI-CC. Under the non-equilibrium conditions of constant irradiation used in the crystallisation of ETPI-CC, a high local concentration of ETPI is produced, which potentially could form either of these dimer modes; however, kinetic dimerisation leads to a greater proportion of ETPI-CC, and it is thus this mode that crystallises, localised at the site of irradiation. This method of producing crystalline material also relies on the relative difference in the solubility of the photogenerated species and the initial compound in the particular solvent.

Crystallisation following a photochemical reaction has precedence, both in the gas phase[20] and in solution, having been used in the crystallisation of the photochemical product of benzophenone (benzopinacol)[21] and of proteins.[22, 23] Photocrystallisation has also been used to form charge transfer salts following photoreduction of tetracyanoquinodimethane (TCNQ) in the presence of a sacrificial electron donor.[24, 25] However, these prior reports resulted in non-reversible formation of a photoproduct

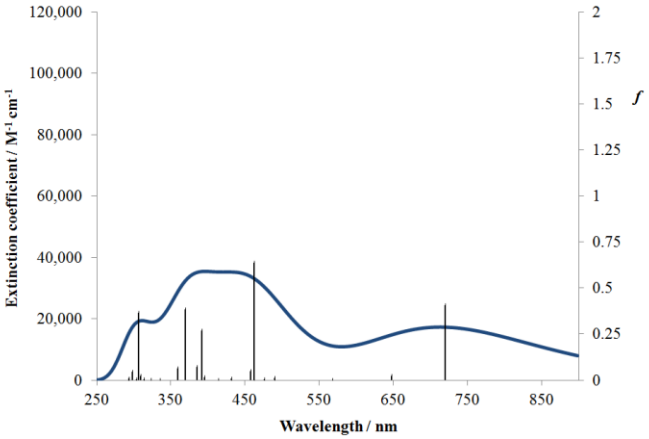

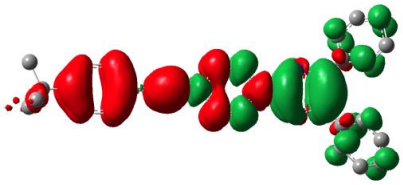

D$_1$ ← **D$_0$**; β-LUSO ← β-HOSO (90%)

f = 0.405; 720 nm (1.72 eV)

Assignment: ^{1}CT

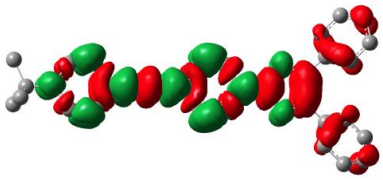

D$_6$ ← **D$_0$**; α-LUSO ← α-HOSO (58%) and β-LUSO+1 ← β-HOSO (15%)

f = 0.638; 463 nm (2.68 eV)

Assignment: $^1\pi$-π*

Figure 4.7. TD-DFT calculated UV-visible absorption spectra (2700 cm^{-1} FWHM), EDDMs (constructed from components with > 10% contribution), transition details and assignments for ETPI, all at the (unrestricted) B3LYP/6-31+G(d) level of theory. The transitions listed are the lowest energy and the next highest with f > 0.2. Green and red shading show increase and decrease in electron density, respectively. Hydrogen atoms are omitted for clarity. Isovalue: ± 4 x 10^{-4} e a_0^{-3}.

rather than perturbing an equilibrium as demonstrated here for the formation of ETPI-CC. Non-photochemical irradiation has also been used to induce nucleation of both inorganic[26-29] and organic materials,[30-34] although the suggested origin of this effect differs greatly. In this method, clusters are aligned into a nucleation seed by the electric field of a high intensity laser focused using the optical Kerr effect. The adaption of the photocrystallisation method outlined here should be a viable route to single crystals for many systems that switch between different structural forms following irradiation.

An unrestricted TD-DFT calculation (UB3LYP/6-31+G(d)) was used to assign the broad, low energy band observed in the absorption spectrum of ETPI as the

$D_1 \leftarrow D_0$ transition. This transition is described by a β-LUSO ← β-HOSO excitation (calculated 720 nm, observed 721 nm), whilst the higher energy band (calculated 462 nm, observed 445 nm) is assigned as an α-LUSO ← α-HOSO transition. The band at *ca.* 720 nm is classified as predominantly charge-transfer (CT) in character; in contrast, the more intense band at *ca.* 445 nm is identified as a π,π^* transition. The difference in the transition type can be seen most clearly in the electron density difference maps (EDDMs) (Figure 4.7). TD-DFT calculations of both dimers predict, as expected, no low energy absorption bands: instead they have higher energy CT and π,π^* transitions (Figure 4.8). Therefore, the immediate colouration upon dissolution of ETPI-CC can be concluded to arise from fast dissociation to ETPI in solution before reformation of the ETPI-CN dimer upon standing in the dark. The dark green colouration of the ETPI-CC crystals can be attributed to photochromism on their surface, which occurs even under minimal exposure to ambient light. The slower rate of colour formation following dissolution and irradiation of ETPI-CN confirms its greater kinetic stability relative to ETPI-CC.

In conclusion, it has been identified that photocrystallisation can be used to produce the thermodynamically less stable 2C-2′C HABI isomer. This method has facilitated the production of diffraction-quality single crystals of this unusual dimer mode for a colour-tuned TPIR derivative, allowing the determination of its SC-XRD structure and revealing its relatively long C-C bond (1.60 Å). This technique should be widely applicable to other photochromic systems in which a less stable (and less soluble) form of a molecule is produced upon irradiation. We have also identified that the 2C-2′C dimer is only stable in the solid state, dissociating rapidly to the radical upon dissolution before reforming the thermodynamically more stable 2C-1′N form in the dark. The ability of these molecules to interconvert between sp^2 and sp^3 geometries at the 2-position of the imidazole-type ring is quite remarkable.

(**a**)

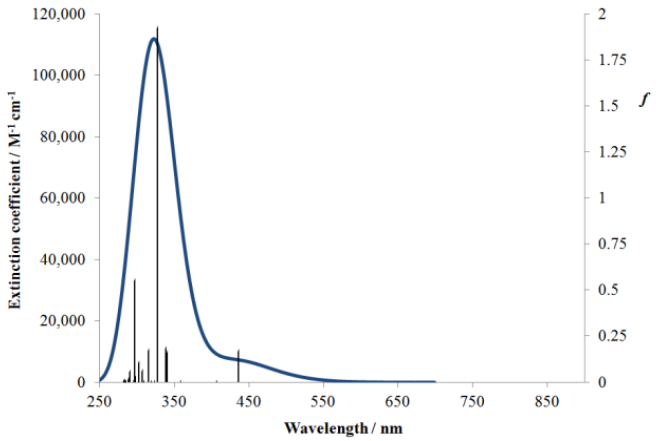

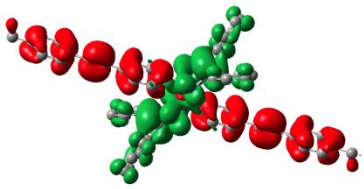

S$_1$ ← **S**$_0$; LUMO ← HOMO (98%)

f = 0.169; 436 nm (2.84 eV)

Assignment: ^{1}CT

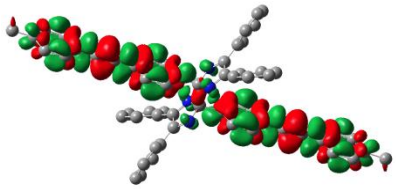

S$_6$ ← **S**$_0$; LUMO+2 ← HOMO (94%)

f = 1.924; 327 nm (3.79 eV)

Assignment: $^1\pi,\pi^*$

(**b**)

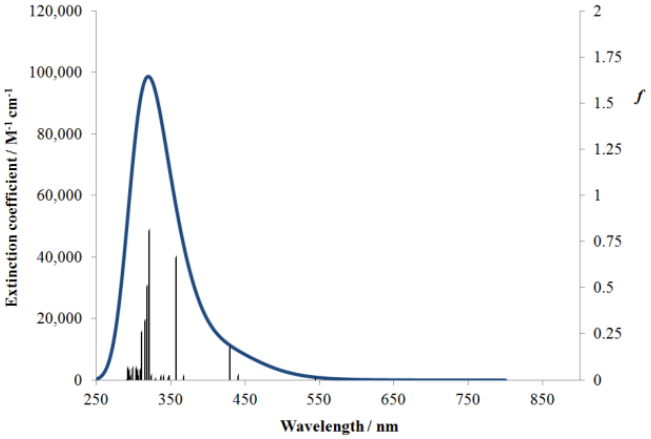

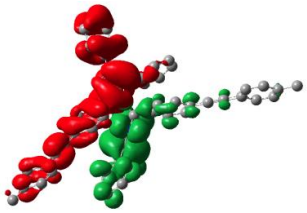

S$_1$ ← **S**$_0$; LUMO ← HOMO (98%)

f = 0.004; 544 nm (2.28 eV)

Assignment: ^{1}CT

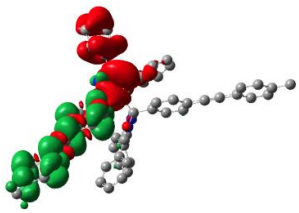

S$_5$ ← **S**$_0$; LUMO+2 ← HOMO (95%)

f = 0.663; 357 nm (3.48 eV)

Assignment: Mixed ^{1}CT / $^1\pi,\pi^*$

Figure 4.8. Calculated UV-visible absorption spectra, EDDMs, transition details and assignments for (**a**) ETPI-CC and (**b**) ETPI-CN. For further details see Figure 4.7, with the exception that calculations were not run unrestricted.

* * * *

Very recently, Abe and co-workers reported the structure of a non-photochromic biphenyl-tethered 2C-2′C dimer (Figure 4.9).[35] A similar structure was then also inferred for a related 1,1′-binaphthyl dimer by $^{13}C\{^{1}H\}$ NMR. This second compound was found to be a negative photochromic material. In this system, a colourless 2C-2′C dimer is formed upon irradiation of a coloured spiro derivative *via* a short-lived (9.4 μs) biradical, with the orange colour of the spiro compound bleaching upon irradiation. The 2C-2′C bond length (1.562(2) Å) of the biphenyl compound is not as long as that found here for ETPI-CC, which is attributable to the constrained nature of the tethered system. It was also possible for Abe to study the solution photochemistry of these species; this highlights the increased stability of the tethered 2C-2′C dimer relative to the standard system that was found to be unstable in solution.

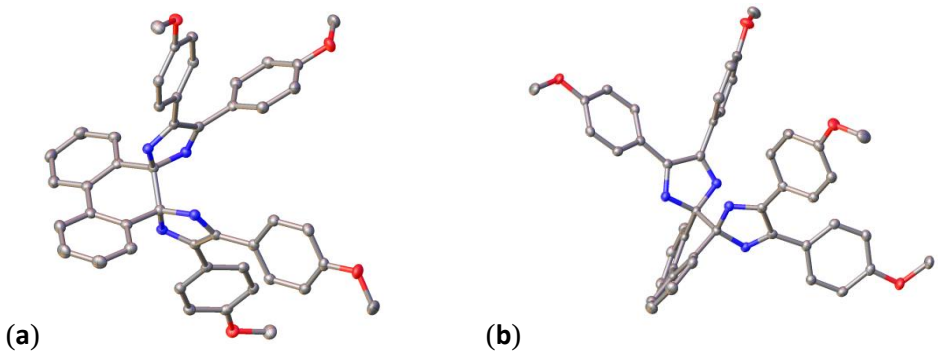

Figure 4.9. The recently reported biphenyl-tethered 2C-2′C dimer of a TPIR radical from Abe and co-workers.[35] Hydrogen atoms and an acetonitrile solvent molecule have been omitted for clarity. Element (colour): carbon (grey), nitrogen (blue), oxygen (red). Atomic displacement parameters are shown at 50% probability. (**a**) and (**b**) show two different orientations of the molecule. View (**a**) is close to that depicted in the original publication, while the second orientation (**b**) highlights the twisted nature of the dimer.

4.2. Formation of peroxides by TPIR systems

One often stated advantage of TPIR materials has been their relative stability towards both oxygen and water,[36] with which radicals are normally highly reactive. However, some early reports alluded to the formation of unidentified, non-chromic by-products following long term use in aerated media.[37, 38] It has also been reported previously that 2,5-[38, 39] and 4,5-epidioxides[40] of the unsubstituted TPIR analogue are produced in aerated solution by reaction with singlet oxygen, generated upon irradiation in the presence of a photosensitiser. In addition, hydroperoxides and 2,5-epidioxides have been produced from the parent closed-shell imidazoles by reaction with singlet oxygen.[41-43] Very recently it has been observed that a naphthalene tethered TPIR dimer can form an adduct with O_2 to give a bridged peroxide.[44] It was suggested in that report that this was a consequence of the two radicals being held in close proximity, and that bridged peroxide species would not be expected in conventional, non-tethered systems due to diffusion of the two radicals away from each other in solution.

In this section, the assumption that tethered TPIR systems are unique in their reactivity with oxygen to form endoperoxides is challenged by the isolation of the analogous peroxides of simple, non-tethered derivatives, indicating that this is a more general phenomenon for this class of material.

4.1.1. Results and discussion

Initially, a derivative that was hindered from dimerising through the 2-position of the imidazolyl ring was designed. It was believed that inducing a large torsional angle between the planes of the imidazolyl ring and the phenyl ring in the 2-position would inhibit dimerisation through this position. An *ortho tert*-butyl substituent on the 2-position phenyl ring was therefore selected as this group was expected to participate additionally in an unfavourable steric interaction with the heterocycle ring upon dimerisation in either of these modes.[i] The parent imidazole compound, 2-(2′-*tert*-butylphenyl)-4,5-diphenylimidazole, 2-tBu-TPI-H, was synthesised in a three step procedure consisting of modifications of known methods (Scheme 4.2). This briefly comprised the conversion of 2-*tert*-butylaniline to 2-*tert*-butyliodobenzene[45] *via* the

[i] It is noted that the induced twist would not be expected to hinder dimerisation through the 4-position; for instance, the 4C-4′C mode should still be accessible.

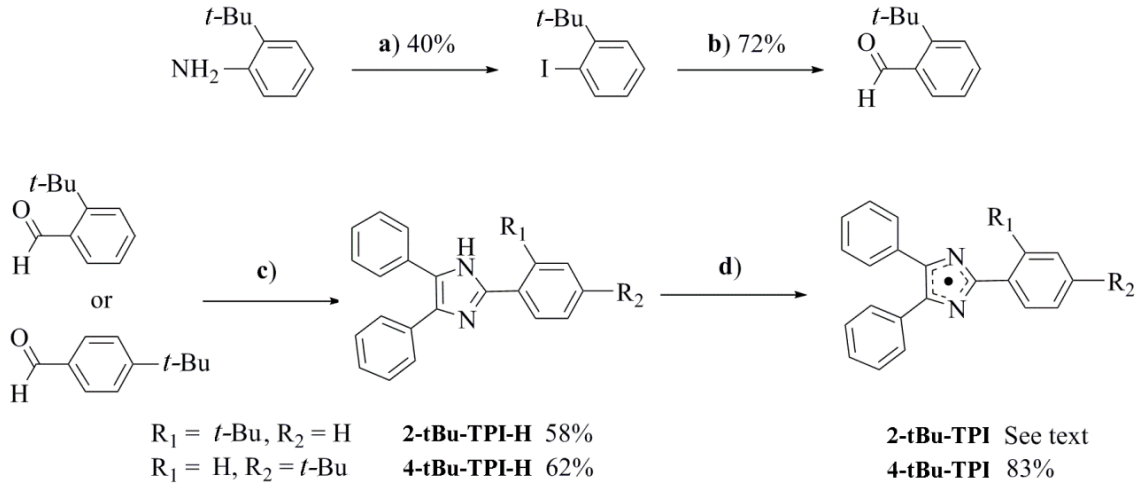

Scheme 4.2. Syntheses of the triphenylimidazoles 2-tBu-TPI-H and 4-tBu-TPI-H and their corresponding radical species 2-tBu-TPI and 4-tBu-TPI. Conditions: **a**) i) H_2SO_4, H_2O, $NaNO_2$, -40 °C, 10 min. ii) 3 eq. KI, H_2O, -15 °C → 0 °C, 1 h; **b**) i) 1.3 eq. *n*-BuLi, THF, -78 °C, 30 min. ii) 3 eq. DMF, -78 °C → r.t., 2 h; **c**) 1 eq. benzil, 2.5 eq. NH_4OAc, acetic acid, μw 180 °C, 5 min; **d**) 100 eq. KOH, 50 eq. $K_3[Fe(CN)_6]$, 1:1 CH_2Cl_2:H_2O, r.t., 2 h.

diazonium salt, lithium-halogen exchange with *n*-BuLi and quenching with *N*,*N*-dimethylformamide to produce 2-*tert*-butylbenzaldehyde.[46] This was followed by a condensation with benzil and ammonium acetate in acetic acid to form the imidazole ring under microwave irradiation.[47] The SC-XRD structure of 2-tBu-TPI-H was obtained and is shown in Figure 4.10. The structure contains the expected, highly stabilising and strong N-H···N hydrogen bonding motif, producing infinite chains through the structure. Macroscopically, this results in strongly anisotropic, unidirectional crystal growth, leading to very thin, pseudo-1D, needle habited crystals, which made the production of single crystals suitable for SC-XRD challenging for most of the imidazoles studied. Phenomenologically, the inclusion of solvent, such as ethanol in the structure of ETPI-H (*vide supra*), can lead to disruption of the expected hydrogen bonding motif and therefore ultimately to more desirable crystal habits.

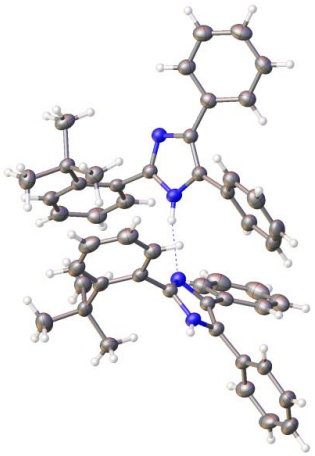

Figure 4.10. SC-XRD molecular structure of 2-tBu-TPI-H at 120 K. The asymmetric unit contains two independent molecules, *i.e.* $Z' = 2$, both of which are shown here. The N-H···N hydrogen bond is indicated by a dashed line. Element (colour): carbon (grey), nitrogen (blue), hydrogen (white). Atomic displacement parameters are shown at 50% probability.

The structure of this compound confirms that the *tert*-butyl group has the desired effect of forcing the phenyl ring out of co-planarity with respect to the imidazole ring (torsion angle of 74.3(3)° and 76.7(3)° for the two symmetry independent molecules) to a greater extent than that observed for the *o*-methyl derivative (torsion angle of 43.0°, CSD Refode: ADELEB[48]) or the unsubstituted analogue (torsion angle of 20.7°, NORDII[49]). Compound 2-tBu-TPI-H was readily oxidised to the imidazolyl radical, 2-tBu-TPI, using excess $K_3[Fe(CN)_6]$ in a biphasic system of CH_2Cl_2 and aqueous KOH solution. The oxidation could be monitored qualitatively by the increase in purple colouration, attributable to the radical.[50] Following work-up, the colour disappeared and a very low solubility, off-white solid was obtained. Mass spectrometry confirmed that a small portion of the sample was a dimer (m/z = 702.4), but also indicated that the sample contained a compound with m/z = 735.4 that was inconsistent with the expected product, as well as some of the parent imidazole (m/z = 352.5). The observed dimer is proposed to be bonded through the 4-positions of the imidazolyl rings, although its exact nature has not been elucidated. It is noted that a mass consistent with a dimer was observed in the ESI-MS of the majority of the parent imidazoles studied throughout this work, assumed to be due to dimerisation upon ionisation *in situ*; therefore, the dimer observed following oxidation of 2-tBu-TPI-H may be a result of this effect with the residual starting material. The presence of the imidazole is due to either incomplete

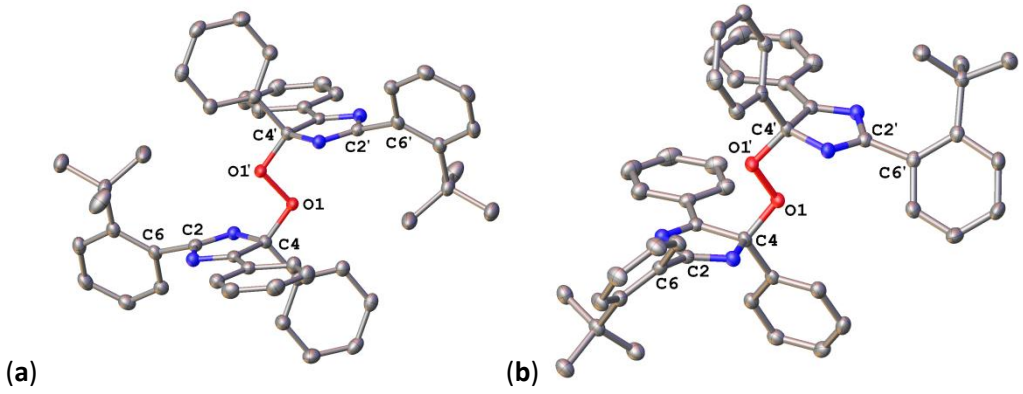

Figure 4.11. SC-XRD molecular structures of 2-tBu-TPI-O_2. (**a**) Isomer I (**b**) Isomer II. Note the restricted rotation about the bond C2-C6 and the chiral centre at C4. Hydrogen atoms are omitted for clarity. Element (colour): carbon (grey), nitrogen (blue), oxygen (red). Atomic displacement parameters are shown at 50% probability. Primed atoms are generated by the following symmetry operations: (**a**) (2-*x*, -*y*, 1-*z*) and (**b**) (-*x*, *y*, ½-*z*).

oxidation or proton abstraction by the radical from the solvent, as has been reported previously for other derivatives.[51, 52] Repeated attempts at the oxidation resulted in a similar product distribution. Single crystals suitable for SC-XRD were produced from a saturated 1,2-dichloroethane solution of the crude product mixture after a period of approximately one month at 5 °C. This experiment revealed the formation of a peroxide, 2-tBu-TPI-O_2, in which two TPIR-derived moieties are bridged through a C4-O1-O1′-C4′ linkage (Figure 4.11a), with a composition consistent with the accurate mass-spectrum of the major reaction product. The O1-O1′ bond length is 1.478(1) Å, while the C4-O1′ bond length is 1.412(1) Å, which are both similar to the related tethered system (bond lengths: O-O 1.475(1) Å, C-O 1.429(2) Å).[44] The C4-O1-O1′ angle is 104.5(1)°, considerably smaller than the tethered peroxide, for which the angle is 110.3(1)°. The peroxide contains two chiral carbon atoms (C4 and C4′) and two chiral axes (C2-C6 and C2′-C6′) between the nitrogen heterocycles and the 2-*tert*-butylphenyl rings arising from the hindered rotation. This results in multiple diastereomers and atropisomers of this peroxide, which has made further separation unfeasible. The SC-XRD structure of a second isomer (Isomer II) was obtained and is also shown in Figure 4.11b. The O1-O1′ bond length of this second isomer is marginally longer at 1.496(2) Å than the first isomer (I), while the C4-O1 bond length is 1.424(1) Å and the C4-O1-O1′ angle is 104.7(1)°.

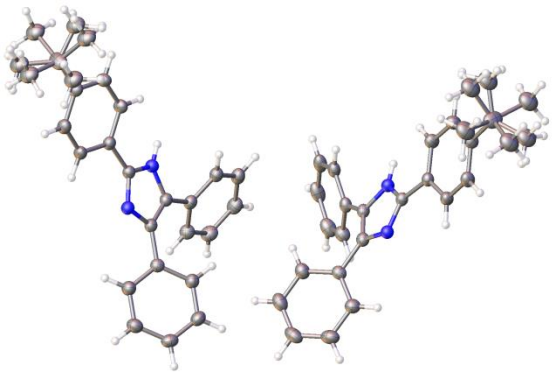

Figure 4.12. SC-XRD molecular structure of 2-(4'-tertbutylphenyl)-4,5-diphenylimidazole, 4-tBu-TPI-H, at 120 K. $Z' = 2$, both of which are shown here. The *tert*-butyl groups are disordered, modelled over two sites with 50% occupancy each. The atomic displacement parameters of the disordered *tert*-butyl groups have been constrained to be the same magnitude in both orientations. Element (colour): carbon (grey), nitrogen (blue), hydrogen (white). Atomic displacement parameters are shown at 50% probability.

To establish if the introduction of the *tert*-butyl group in the 2-position of the phenyl ring had influenced the formation of the peroxide by shifting the equilibrium to the radical form, the structural isomer of 2-tBu-TPI-H, 2-(4′-*tert*-butylphenyl)-4,5-diphenylimidazole, 4-tBu-TPI-H, was synthesised. In this isomer, rotation about the single bond between the imidazole ring and the phenyl ring in 2-position is unhindered and normal dimerisation modes (Scheme 3.1) are assumed to be accessible. This compound was made using commercially available 4-*tert*-butylbenzaldehyde under analogous conditions to those employed in the synthesis of 2-tBu-TPI-H (Scheme 4.2). The SC-XRD structure of 4-tBu-TPI-H, crystallised from nitromethane, is shown in Figure 4.12; this structure is also stabilised by N-H···N hydrogen bonding. The torsion angles between the imidazole and 2-position phenyl rings for this isomer are reduced to 17.9(3)° and 18.9(3)° for the two symmetry independent molecules, similar to the unsubstituted analogue, as expected.

Oxidation of this imidazole afforded compound 4-tBu-TPI (purple colouration observed). ^{1}H and ^{13}C{^{1}H} NMR indicated that an unsymmetric dimer had been isolated without obvious degradation to the peroxide, whilst the SC-XRD structure of a sample crystallised from hexanes confirmed it to be the common 2C-1′N dimer, 4-tBu-TPI-CN

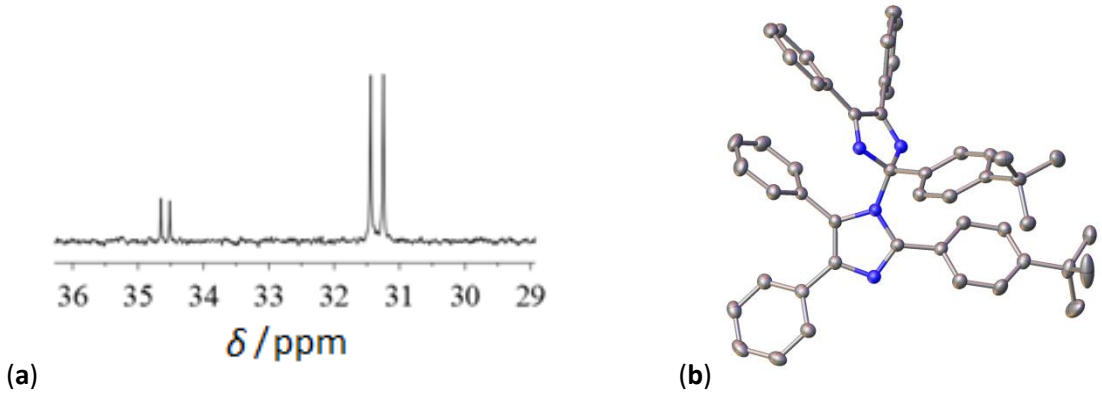

Figure 4.13. (**a**) The inequivalent *tert*-butyl signals in the 101 MHz $^{13}C\{^{1}H\}$ NMR ($CDCl_3$) spectrum of 4-tBu-TPI-CN. (**b**) SC-XRD molecular structure of 4-tBu-TPI-CN (Form I). Hydrogen atoms are omitted for clarity. Element (colour): carbon (grey), nitrogen (blue). Atomic displacement parameters are shown at 50% probability.

(Figure 4.13). In addition, 4-tBu-TPI-CN was crystallised from methanol and its SC-XRD structure determined (Form II) (not shown). Upon storage in ethyl acetate solution under the same conditions as those outlined for 2-tBu-TPI-O_2, further crystals were obtained and examined by SC-XRD. It was found that this was the analogous peroxide 4-tBu-TPI-O_2 (Figure 4.14a), bridged through a similar C4-O1-O1′-C4′ moiety as that observed for 2-tBu-TPI-O_2. Interestingly, this compound undergoes a reversible single crystal to single crystal polymorphic transition in the temperature range 145-150 K. It was possible to obtain the structure above (160 K) and below (100 K) the transition using the same crystal. The crystal was cycled through the transition three times before a structure was collected, thus confirming the reversibility of the process. It was found that the transition is associated with a doubling of the crystallographic *b*-axis and the lowering of symmetry from *I*2/*a* to $P2_1/c$ upon cooling. This is associated with partial ordering of the high temperature disordered *tert*-butyl groups upon cooling. The low-temperature form (Form II) is shown in Figure 4.14b.

The formation of the peroxide from the radical is perhaps surprising because the equilibrium between the dimer and radical forms for unhindered systems is believed to lie predominantly towards the dimer in the absence of light or heat.[53] Peroxide formation of this compound was observed by ESI^+ MS for samples stored in ethyl acetate, CH_2Cl_2 and chloroform, although in the latter case, a significant proportion of imidazole starting material was re-formed, ascribed to proton abstraction from the more acidic solvent.

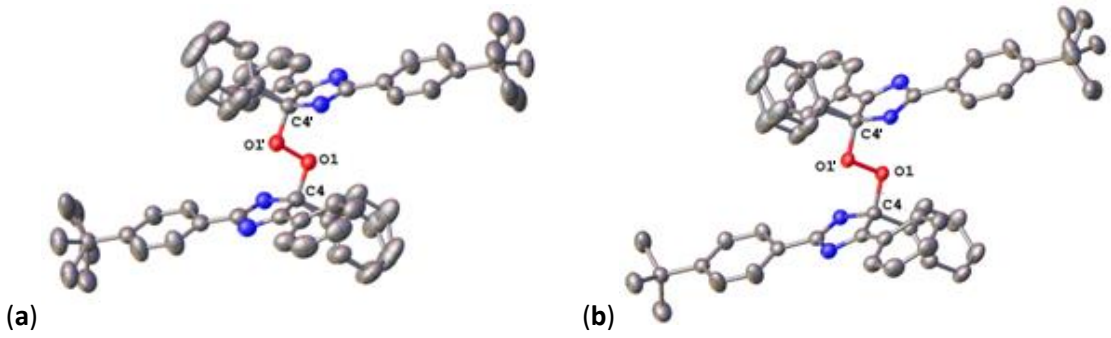

Figure 4.14. SC-XRD molecular structure of the peroxide of the 4-(4'-*tert*-butylphenyl)-4,5-diphenylimidazole radical, 4-tBu-TPI-O_2, at (**a**) 160 K (Form I) and (**b**) 100 K (Form II). The *tert*-butyl group and one phenyl group is disordered, modelled over two sites with 50% occupancy each. Hydrogen atoms and in (**b**) a second symmetry independent molecule have been omitted for clarity. Element (colour): carbon (grey), nitrogen (blue), oxygen (red). Atomic displacement parameters are shown at 50% probability. Primed atoms in (**a**) are generated by the symmetry operation (1-*x*, 1-*y*, 1-*z*).

It is therefore remarkable that this product is formed under the conditions of the crystallisation in which the sample was kept both dark and below 5 °C. An ethyl acetate solution of 4-tBu-TPI-CN stored for an extended period (*ca.* six months) under these conditions resulted in sufficient peroxide deposit to perform differential scanning calorimetry (DSC) and thermal gravimetric analysis (TGA) (Figure 4.15). These experiments revealed that the peroxide undergoes a strongly exothermic decomposition when heated above 163 °C, with concomitant and continued mass loss. No processes were observed before the decomposition event in the DSC of 4-tBu-TPI-O_2 and therefore it is believed the thermal stability of these non-tethered systems differs to that of the tethered peroxide that undergoes thermal rearrangement.[44] The build up of this moderately thermally unstable and non-photochromic peroxide is clearly undesirable.

A dilute acetonitrile solution of the 2C-1′N dimer of 4-tBu-TPI-CN was irradiated at 365 nm by a handheld lamp (*ca.* 100 mW) positioned 2 cm from the sample under an oxygen atmosphere for 30 minutes, to investigate the timescale of the formation of the peroxide upon irradiation. The sample was then analysed by accurate ESI^+ MS (Figure 4.16) and found to contain a significant proportion of peroxide material, even after this short period of time. The 2,5- and 4,5-endoperoxides of the monomeric imidazole, reported previously as triphenylimidazole chemiluminescence intermediates,[38-40] were not detected. A control solution of the dimer at the same

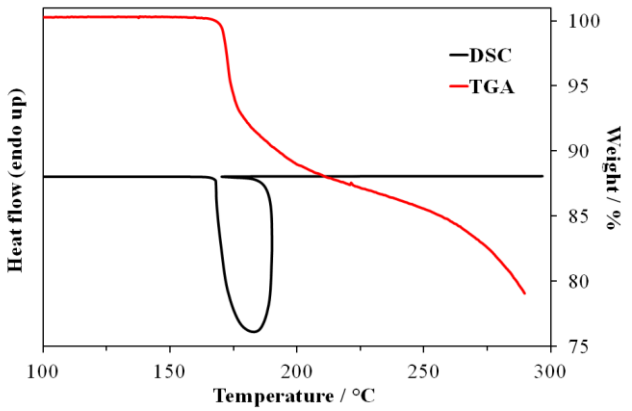

Figure 4.15. DSC (left *y*-axis) and TGA (right *y*-axis) thermograms of compound 4-tBu-TPI-O_2.

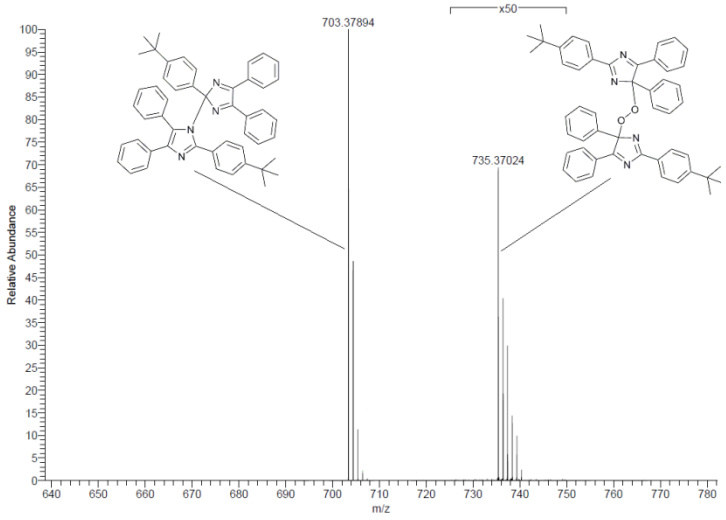

Figure 4.16. Accurate ESI^+ MS showing the generation of the peroxide 4-tBu-TPI-O_2 (*m*/*z* = 735.3702, calcd. for [4-tBu-TPI-O_2+H]$^+$ = 735.3699) following 30 min of 365 nm irradiation of an acetonitrile solution of 4-tBu-TPI-CN (*m*/*z* = 703.3789, calcd. for [4-tBu-TPI-CN+H]$^+$ = 703.3800) under an oxygen atmosphere.

concentration under an oxygen atmosphere kept in the dark did not show the formation of the peroxide on this timescale, indicating it is the monomeric radical formed upon irradiation that is susceptible to reaction with oxygen.

To explore further the generality of the observed degradation, five simple TPIR dimers, previously reported by Cescon and co-workers,[3] namely the parent unsubstituted radical dimer, the *o*-chloro substituted dimer that is used as a polymerisation initiator, the *p*-chloro isomer, the *o*-methyl derivative and the mesityl derivative, were investigated for peroxide formation. The chosen compounds span an

order of magnitude of dimerisation rates from the relatively rapid *o*-chloro, intermediate rate *o*-methyl, to the slower *p*-chloro.[3] Thus, using a similar method to that described for the 4-*tert*-butyl example above, a sample of each was irradiated (365nm) under an oxygen atmosphere and the formation of by-products was followed by ESI^+ MS. In each case peroxide formation was observed.

Although the reaction of oxygen with a radical may not be surprising in itself, the fact that these compounds have often been lauded as being 'air-stable' makes it an interesting observation. The formation of peroxides in these systems raises concerns for their use in device applications because they would be expected to degrade after long term use if oxygen is not excluded from the TPIR layer. The removal of oxygen during the synthesis of TPIRs is also recommended in order to minimise the quantity of the non-photochromic peroxide material produced. It has been suggested that suppression of radical diffusion by tethering should increase the propensity for peroxide adduct formation;[44] however, this is not consistent with the results presented here. Indeed, in the case of fast switching species, in which the radical form is fleeting, it may be expected that the rate of production of peroxide would be attenuated compared to the conventional systems shown here. However, for long term use of these materials, this attenuation may not be sufficient.

In summary, peroxide degradation products of two non-tethered TPIR systems have been isolated that raise concerns about the possible use of these materials in long lifespan electronic applications. These species have been isolated as single crystals and their structures determined by single crystal X-ray diffraction. It has additionally been shown that the peroxide can be formed in detectable quantities within 30 minutes when the dimer is irradiated under an oxygen atmosphere. Using mass spectrometry, the generality of the formation of the peroxide has been established in a series of known TPIR dimers. Therefore, it has been found that this is not just a phenomenon particular to bridged TPIR species, as has been suggested previously, but also occurs for much simpler non-tethered derivatives.

4.3. Dihydropyrene (DHP) photochromes

Dihydropyrenes (DHP) have been studied extensively for their photochromic behaviour.[54] These systems undergo a transformation from a coloured ring-closed form to a colourless ring-open structure upon irradiation with visible light while UV light induces the back reaction (Figure 3.1). This is unusual because for most photochromic systems irradiation at any absorbed wavelength results in the formation of a lower energy absorbing species through various mechanisms. These systems are, therefore, termed negative photochromes. Negative photochromes potentially lend themselves to experiments in which the structure of the photogenerated species is determined in the solid-state by SC-XRD because, as the material undergoes conversion to the colourless form, it permits transmission of irradiation deeper into the crystal, allowing further transformation. This is in contrast to standard photochromes that, although they have often been studied by SC-XRD with *in situ* irradiation, suffer from increased absorption of the excitation source as conversion proceeds, limiting the process predominantly to the surface, often with an overall conversion of less than 10%. While a crude structure often can be determined with such a low conversion, it is certainly not ideal and therefore only limited information about the photogenerated species can be garnered due to large estimated standard deviations in the structural parameters. Probably the most studied example of a DHP is that with *tert*-butyl groups in the 2- and 7-positions, 2,7-DHP-tBu due to its relative ease of synthesis and therefore was targeted for SC-XRD with *in situ* irradiation. The inclusion of *tert*-butyl groups has the added benefit that they can act as 'space-opening' entities[55] that permit large structural changes. The synthesis has been reported in detail previously by Mitchell,[54] but is outlined here, in particular, highlighting the adaption of some of the steps. The synthetic pathway is summarised in Scheme 4.3.

Conversion of 4-*tert*-butyltoluene to the bis-bromomethyl derivative was achieved by reflux with paraformaldehyde and HBr in acetic acid, with the steric bulk of the *tert*-butyl group directing the bromomethylation *ortho* to the methyl group exclusively (step **a**). This earlier bromomethylation procedure[56] was found to be more convenient, in terms of yield, purity and ease of isolation, than a $ZnBr_2$ catalysed reaction with 1,3,5-trioxane reported more recently by the same author.[54]

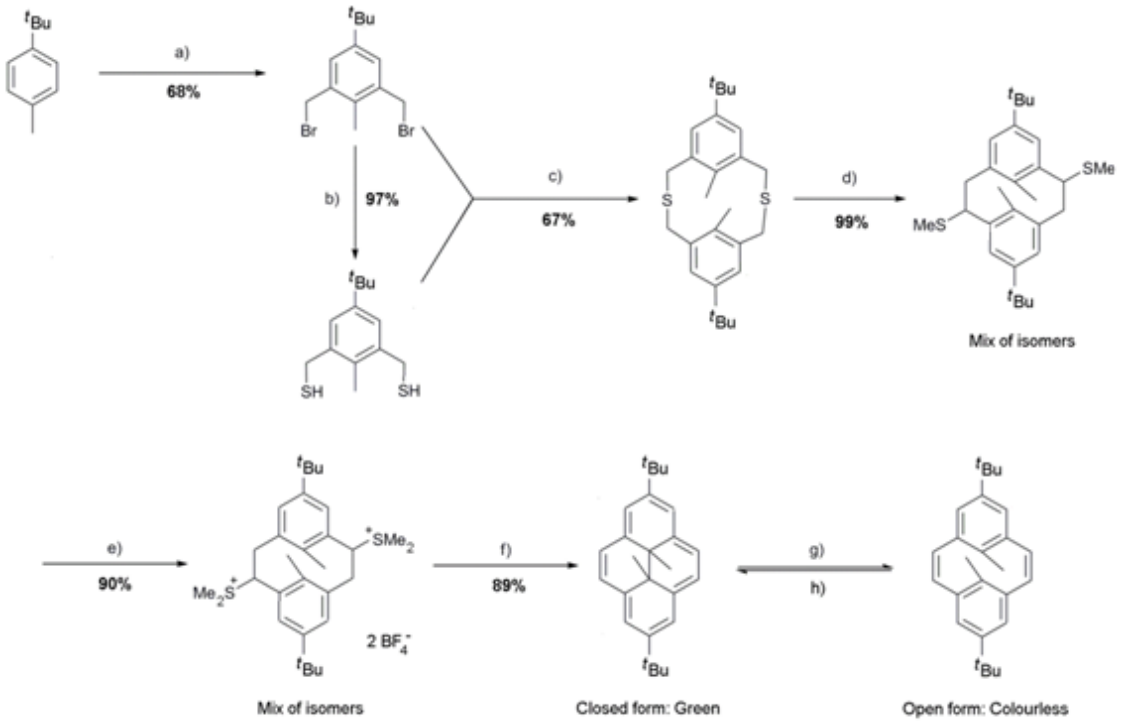

Scheme 4.3. A modified procedure for the synthesis of dihydropyrene 2,7-DHP-tBu. **a**) 3 eq. 33 wt% HBr in acetic acid, $(CHO)_n$, 120 °C, 96 h; **b**) (i) Thiourea, EtOH, 80 °C, 3 h (ii) NaOH, H_2O, 100 °C, 2 h; **c**) Slow addition (1 ml h^{-1}, 0.1 M in toluene) of bis-bromomethyl (from step **a**) and bis-mercaptomethyl (from step **b**) compounds to 5 eq. KOH, 2.5 eq. $NaBH_4$, 9:1 EtOH:H_2O (300 ml), N_2, r.t.; **d**) (i) *n*-BuLi, THF, 1 h, N_2, 0 °C (ii) MeI; **e**) Meerwein's reagent, CH_2Cl_2, N_2, 0 °C, 4 h; **f**) KO^{t}Bu, THF, 70 °C, 16 h; **g**) Visible light; **h**) UV light.

A portion of the bromomethylated product was then refluxed with thiourea in ethanol, followed by hydrolysis to give the bis-mercaptomethyl analogue (step **b**). It is important to completely remove all traces of ethanol to avoid formation of a mixture containing ethoxy ethers (observed by GC-MS and ^{1}H NMR) that complicate purification; this was previously omitted from the description of the experimental procedure wherein the base was added directly to the ethanol solution. The molecular structures from SC-XRD analysis of these intermediates are shown in Figure 4.17.

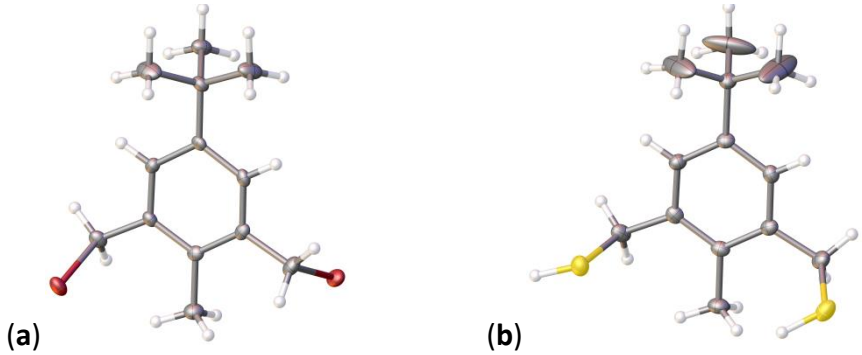

Figure 4.17. SC-XRD molecular structures of (**a**) 2,6-bis(bromomethyl)-4-*tert*-butyltoluene and (**b**) 2,6-bis(mercaptomethyl)-4-*tert*-butyltoluene. Element (colour): carbon (grey), bromine (red), sulfur (yellow) and hydrogen (white). Atomic displacement parameters are shown at 50% probability.

Coupling of the bromomethyl and thiol compounds under high dilution (syringe pump) and reducing ($NaBH_4$) conditions afforded the dithia[3.3]metacyclophane in good yield (67%). The high dilution conditions were essential to avoid the formation of oligomers and larger cyclic compounds that were observed by ESI^+ MS when a dropping funnel was employed. The product could be purified by recrystallisation from toluene to give large, block-habited crystals from which the SC-XRD structure was obtained, as shown in Figure 4.18.

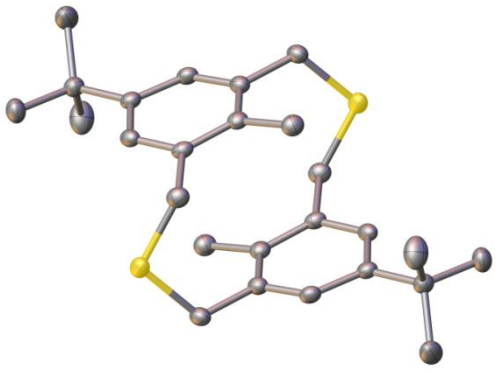

Figure 4.18. SC-XRD molecular structure of 6,15-di-*tert*-butyl-*anti*-9,18-dimethyl-2,11-dithia[3.3]metacyclophane. Element (colour): carbon (grey), sulfur (yellow) and hydrogen (white). Hydrogen atoms and a second symmetry independent molecule have been omitted for clarity. Atomic displacement parameters are shown at 50% probability.

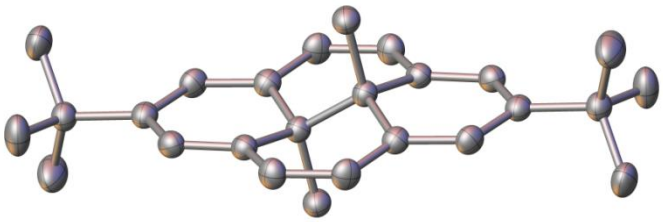

Figure 4.19. SC-XRD molecular structure of 2,7-di-*tert*-butyl-*trans*-10b,10c-dimethyl-10b,10c-dihydropyrene (2,7-DHP-tBu) from the structure of Form I. Element (colour): carbon (grey). Hydrogen atoms have been omitted for clarity. Atomic displacement parameters are shown at 50% probability.

A 1,2-Wittig rearrangement and subsequent reaction with methyl iodide gave a two isomer mixture of a ring contracted [2.2]metacyclophane intermediate with two exocyclic SMe groups in near quantitative yield. The SMe groups were then methylated in high yield (90%) using the commercially available, and stable, Meerwein's reagent (trimethoxonium tetrafluoroborate, Me_3OBF_4), rather than the related Borch reagent (dimethoxycarbonium tetrafluoroborate, $(MeO)_2CHBF_4$) that has been described elsewhere.[54] Hofmann elimination of SMe_2 using KO^{t}Bu as the base gave the desired 2,7-DHP-tBu product. These last three steps can be conducted without full purification of the intermediates, making this a relatively efficient and high yielding (79%) preparation. The ^{1}H NMR spectrum of 2,7-DHP-tBu has a strongly shielded, low frequency methyl resonance at -4.04 ppm due to the location of the methyl group above and internal to the diatropic ring current of the 14π-electron aromatic system.

Screening of crystallisation solvents (slow evaporation method) led to three different crystalline forms being isolated. Form I was produced from MeOH, acetone or hexanes and was confirmed to be the known (AGURUP[57]), monoclinic *C*2/c structure by SC-XRD. A second, monoclinic $P2_1/c$ polymorph was crystallised from acetonitrile and THF, and a monoclinic $P2_1/c$ monosolvate was formed from 1,2-dichloroethane. The crystal structures of all three forms were determined, and as expected, there are only minor differences between the 2,7-DHP-tBu molecular structures (see Figure 4.19) for a representative example from Form I); however; the packing does differ (Figure 4.20, Figure 4.21 and Figure 4.22). In Form II, the molecule is disordered over two sites, related by a C_2 rotation about the long axis of the DHP (assuming free rotation of the *tert*-butyl groups).

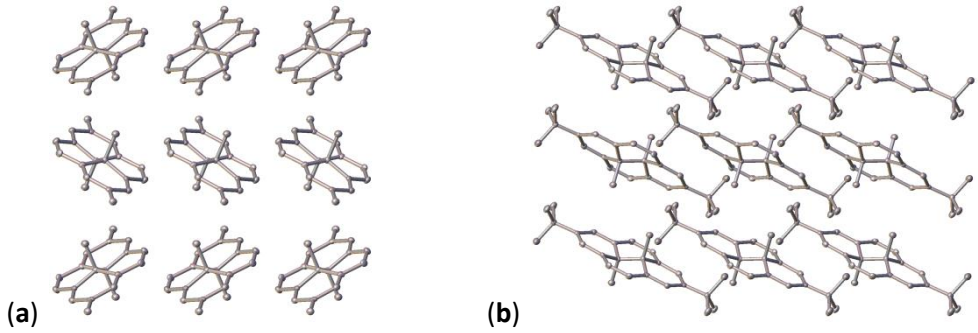

Figure 4.20. Crystal packing of 2,7-DHP-tBu Form I viewed down (**a**) (1 0 0) and (**b**) (0 1 0). Hydrogen atoms and the ^{t}Bu methyl groups in (**a**) have been omitted for clarity. Atomic displacement parameters are shown at 50% probability.

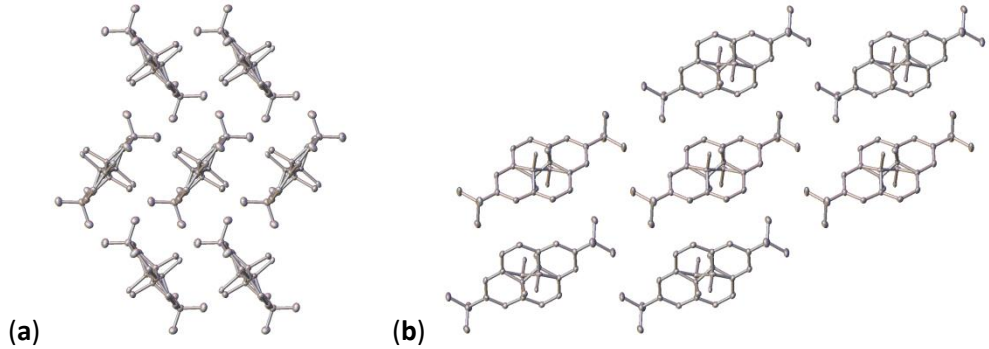

Figure 4.21. Crystal packing of 2,7-DHP-tBu Form II viewed down (**a**) (1 0 0) and (**b**) (0 1 0). Hydrogen atoms have been omitted for clarity. Atomic displacement parameters are shown at 50% probability. The molecules are disordered over two sites, modelled with 50% occupancy each.

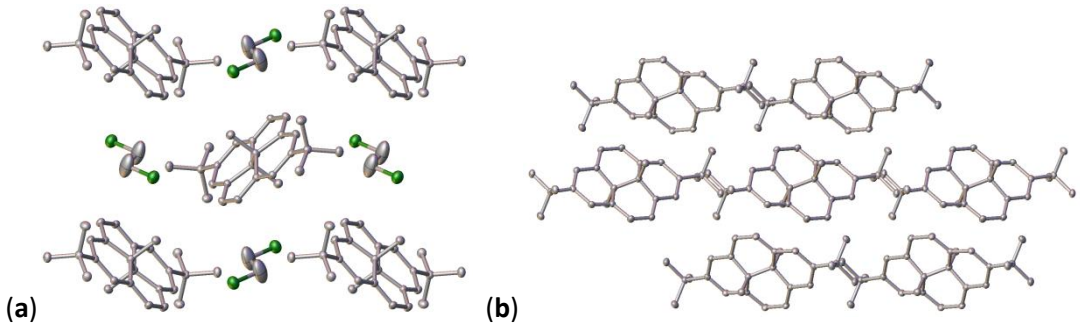

Figure 4.22. Crystal packing of 2,7-DHP-tBu 1,2-dichloroethane solvate viewed down (**a**) (1 0 0) and (**b**) (0 1 0). Hydrogen atoms and in (**b**) the solvate molecules have been omitted for clarity. Atomic displacement parameters are shown at 50% probability.

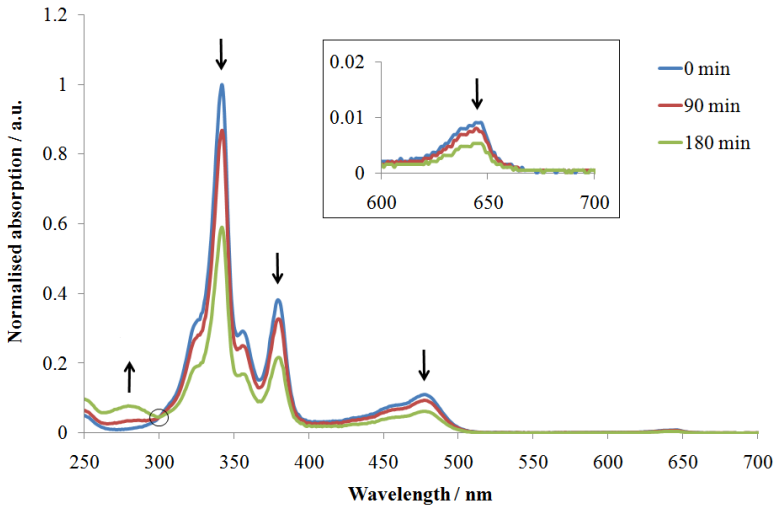

Figure 4.23. Normalised absorption spectra of a CH_2Cl_2 solution (*ca.* 2 x 10^{-5} M) 2,7-tBu-DHP recorded at intervals during continuous wave irradiation at 475 nm. An isosbestic point at 298 nm is highlighted. **Inset**: The low extinction coefficient (900 M^{-1} cm^{-1})[58] low energy absorption band.

The ring opening of the DHP is accompanied by a large structural change; therefore, it was expected that the crystal form may influence the ease with which the molecule can interconvert in the solid state. This is due to differences in the immediate vicinity of the molecules in terms of access to voids and overall ease with which transformation can propagate along particular directions within the structure. Therefore, each of the three forms was investigated by SC-XRD with *in situ* irradiation by a 405 nm diode laser. Unfortunately and very disappointingly, conversion significant enough to differentiate by SC-XRD could not be detected, either at 120 K or at room temperature. Visible photochromism was also not observed. The cause of this difficulty lies in the slow conversion between the closed and open forms. A dilute CH_2Cl_2 solution irradiated for three hours at 475 nm showed only a small decrease in the concentration of the initial closed form (Figure 4.23).

In addition, the conjugation length changes between the two forms, which is undoubtedly the origin of the difference in colour. The next proposal was to explore this property further by introducing extended π-conjugation to the 2- and 7-positions of the DHP. Initially, a DHP was targeted in which 2-bromomesitylene was used as the starting material. This material was chosen because it would introduce a bromine atom at both the 2- and 7-positions of the DHP allowing extension of the π-conjugation through various Pd-catalysed coupling reactions. Ultimately, a derivative containing an

electron donating group on one side and an electron withdrawing group on the other was desired to probe the change in charge transfer across the system upon ring-opening or ring-closing of the DHP. The advantage of using 2-bromomesitylene rather than 4-bromotoluene is the inherent regioselectivity of the bromomethylation step. The bis-bromomethylation step proceeded cleanly using a method previously developed for mesitylene,[56] and the conversion to the bis-mercaptomethyl derivative could also be readily achieved under the same condition as those used for 2,7-DHP-tBu. However, although coupling of these two components under high dilution conditions gave the required bis-thioether bridged cyclophane as a mixture with trimeric oligomers (by ESI^+ MS), the product is practically insoluble, which made further purification and reaction of this derivative unfeasible. The same procedure was attempted with 2-iodomesitylene, synthesised from 2-bromomesitylene. However, the conditions used successfully for the bromomethylation of 2-bromomesitylene lead to protodeiodination of 2-iodomesitylene and thus complex mixtures of mono-, di- and tri-bromomethylated mesitylene were obtained. Cross-reaction of 2,6-bis(mercaptomethyl)-4-*tert*-butyltoluene and 2,4-bis(bromomethyl)-6-bromomesitylene was attempted in the hope that a more soluble intermediate might be formed. However, although the product was slightly more soluble than the cyclophane derived from the two mesitylene derivatives, it was still not soluble enough for efficient purification. Attempts to react the crude product in a Sonogashira reaction were unsuccessful.

It has been reported that it is possible to remove the *tert*-butyl group from DHPs by a retro Friedel-Crafts reaction in which stoichiometric $AlCl_3$ is used with a *tert*-butyl group accepter, such as benzene or biphenyl.[59] It was anticipated that the product of this reaction could then be subjected to Ir(I)-catalysed direct C–H borylation that would be expected to be regioselective for the 2- and 7-positions, as used for pyrene in section 2.2.[60] The Bpin group could then be converted to the bromo or, using a very recently reported method,[61] iodo derivative for further coupling reactions. However, this literature procedure was not reproducible, with starting material 2,7-DHP-tBu and various chlorinated derivatives observable by GC-MS. Similar results were obtained in the presence of superstoichiometric quantities of nitromethane, which purportedly activates the $AlCl_3$ in this reaction.[59]

To conclude, while the common 2,7-DHP-tBu dihydropyrene is relatively simple to synthesise, the chemistry required for more highly functionalised derivatives is challenging, with several of the more obvious routes being so far unsuccessful. It is

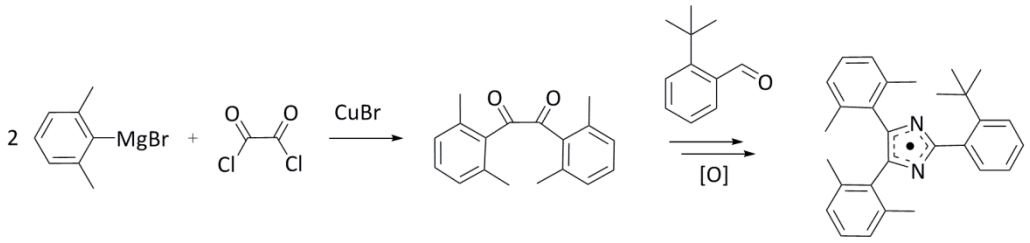

Scheme 4.4. Proposed reaction scheme for the synthesis of a more sterically hindered TPIR.

also clear that faster switching photochromic materials are required for *in situ* irradiation crystallography experiments.

4.4. Future work

The compound 2-tBu-TPI-H was initially synthesised in an attempt to produce a derivative that was hindered from dimerising in one of the standard modes involving the 2-position of the imidazolyl radical. While the use of the *ortho*-*tert*-butyl group appears to be sufficient to do this, the oxygen sensitivity of the compound is increased; in particular, the 4-position is susceptible to oxidation. It would be desirable therefore to synthesise a derivative in which the 4- and 5-positions were sterically hindered to diminish the oxygen sensitivity of the radical. The simplest way to do this would be to use 2,6-dimethylated benzil as a starting material. This diketone has been reported in 97% yield from the reaction of two equivalents of 2,6-dimethylphenylmagnesium bromide and CuBr (to produce the organocopper species *in* situ) with oxalyl chloride.[62] Similarly, it has been prepared by the reaction of the same Grignard reagent with 1,1′-oxalylimidazole, but without the need for the copper salt, in a reduced yield of 70%.[63] Thus, this would be a simple, but viable, extension of the work (Scheme 4.4).

A low-level (DFT/B3LYP/3-21G) optimisation of the structure of the proposed radical, indicates that the 2,6-dimethylphenyl rings would be expected to be twisted out of plane by *ca.* 50°, relative the imidazolyl ring. This steric bulk should be sufficient to kinetically inhibit reaction with oxygen and also to thermodynamically disfavour the formation of the peroxide through an induced interaction of a methyl group with the imidazolyl ring. Once such a stable radical has been produced, its properties, both in the solid state and solution, would be studied by a combination of crystallography, magnetic measurements and EPR.

While isolation of a stable radical of the kind outlined above may be seen as an interesting curiosity, the strategy employed has the disadvantage that delocalisation of the radical is necessarily limited to the imidazolyl ring due to disruption of the π-conjugation with the rest of the molecule upon twisting. It would also be desirable to investigate systems in which the electronic communication is not so limited, allowing the colour tuning of the TPIR system to be fully exploited. The obvious suggestion is to make derivatives with a longer π-conjugation length than ETPI. One caveat, however, is that strongly reduced solubility was experienced with some larger imidazole and bisimidazole compounds synthesised, but not herein reported; therefore, solubilising moieties (such as alkyl groups) would be required. Trivial examples being the introduction of thiophene or vinyl linkers that are known to be better at mediating (excited state) charge transfer than the alkynyl analogues used here.[64] Introduction of electron withdrawing groups to the terminus of a derivative of ETPI would be expected to induce a spectral shift by simple redistribution of electron density throughout the molecule.

The study of diradical (or higher) systems would be of interest[65] in the emerging area of molecular spintronics, which is the utilisation of the electron's spin rather than its charge in electronic devices.[66] The modulation of communication between two radicals upon introduction of electron-rich and electron-poor heterocycles into the conjugated linker and the role of steric interactions in disrupting interaction could be explored. Of particular importance is whether a ferromagnetic (triplet diradical, usually mediated through *meta*-linkages) or an anti-ferromagnetic (singlet diradical, usually with *ortho*- or *para*-bridges) coupling occurs between the spins. Systems wherein electronic communication between two or more radicals is switched upon application of external stimuli would be the next logical step. For instance, the known change from ferro- to antiferromagnetic coupling of two radicals with a 2,6-pyridyl linker upon protonation[67] or photoinduced structural changes could be exploited in this regard. Other stable radicals, such as the nitronyl nitroxide,[68] verdazyl[69] or trityl (Gomberg)[70] radicals, could be combined with the TPIR system to probe the magnetic coupling in hetero-systems. Finally, theoretical studies of diradicals with various bridges suggest that such materials should exhibit large TPA cross-sections; thus, bis-TPIRs could be investigated for these properties too.[71]

Although attempts to synthesise extended DHP derivatives were not met with great success here, this system is still of interest for colour- and conjugation-switching.

Some methods exist to produce simple 2- and 7-substitued derivatives,[72] but their lengthy synthesis is prohibitory when significant further functionalisation is desired. An alternative is to functionalise in the 4,9- or 4,10-positions of DHP, across the centre of the ring. These positions should be accessible by borylation, which has been reported recently to occur exclusively at these positions of pyrene when the 2- and 7-positions are blocked:[73, 74] this would allow direct access to a range of other functional groups.[75] Recently, a method to iodinate the 4-position of DHP has been reported,[76] and the resulting compounds used in Sonogashira coupling reactions to generate acetylide ligands for Pt(II). While other studies have looked at functionalising DHP in this position,[58, 77-79] few reports exist of substitution on both sides of the ring[80] and none are known in which charge transfer across the ring was investigated. Therefore, this may be a possible route to a material that can switch the extent of electronic communication between a donor and acceptor group across a DHP, albeit in an orthogonal direction to that initially intended.

4.5. References

1. A. Kikuchi, T. Iyoda and J. Abe, *Chem. Commun.*, 2002, 1484.
2. S. E. Wolkenberg, D. D. Wisnoski, W. H. Leister, Y. Wang, Z. Zhao and C. W. Lindsley, *Org. Lett.*, 2004, **6**, 1453.
3. G. R. Coraor, L. A. Cescon, R. Dessauer, E. F. Silversmith and E. J. Urban, *J. Org. Chem.*, 1971, **36**, 2262.
4. A. Kikuchi, F. Iwahori and J. Abe, *J. Am. Chem. Soc.*, 2004, **126**, 6526.
5. A. Kikuchi and J. Abe, *Chem. Lett.*, 2005, **34**, 1552.
6. P. Liao, M. E. Itkis, R. T. Oakley, F. S. Tham and R. C. Haddon, *J. Am. Chem. Soc.*, 2004, **126**, 14297.
7. M. Kawano, T. Sano, J. Abe and Y. Ohashi, *Chem. Lett.*, 2000, **29**, 1372.
8. X.-F. Huang, D.-W. Fu and R.-G. Xiong, *Cryst. Growth Des.*, 2008, **8**, 1795.
9. F. H. Allen, O. Kennard, D. G. Watson, L. Brammer, A. G. Orpen and R. Taylor, *J. Chem. Soc., Perkin Trans. 2*, 1987, S1.
10. C. Rüchardt and H. D. Beckhaus, *Angew. Chem. Int. Ed. Engl.*, 1980, **19**, 429.
11. R. Winiker, H. D. Beckhaus and C. Rüchardt, *Chem. Ber.*, 1980, **113**, 3456.
12. M. A. Flammtermeer, H. D. Beckhaus, K. Peters, H. G. Vonschering and C. Rüchardt, *Chem. Ber.*, 1985, **118**, 4665.
13. G. Kaupp and J. Boy, *Angew. Chem., Int. Ed. Engl.*, 1997, **36**, 48.
14. A. A. Leitch, C. E. McKenzie, R. T. Oakley, R. W. Reed, J. F. Richardson and L. D. Sawyer, *Chem. Commun.*, 2006, 1088.
15. P. R. Schreiner, L. V. Chernish, P. A. Gunchenko, E. Y. Tikhonchuk, H. Hausmann, M. Serafin, S. Schlecht, J. E. P. Dahl, R. M. K. Carlson and A. A. Fokin, *Nature*, 2011, **477**, 308.
16. A. A. Fokin, L. V. Chernish, P. A. Gunchenko, E. Y. Tikhonchuk, H. Hausmann, M. Serafin, J. E. P. Dahl, R. M. K. Carlson and P. R. Schreiner, *J. Am. Chem. Soc.*, 2012, **134**, 13641.
17. X. Chen, X. Wang, Z. Zhou, Y. Li, Y. Sui, J. Ma, X. Wang and P. P. Power, *Angew. Chem. Int. Ed.*, 2013, **52**, 589.
18. K. B. Wiberg, *Tetrahedron*, 1968, **24**, 1083.

19. E. Kiepek, Y. Zhou, S. Hoz, E. Rozental, P. M. Kazmaier and E. Buncel, *Can. J. Chem.*, 2005, **83**, 1448.
20. A. Tam, G. Moe and W. Happer, *Phys. Rev. Lett.*, 1975, **35**, 1630.
21. T. Okutsu, K. Nakamura, H. Haneda and H. Hiratsuka, *Cryst. Growth Des.*, 2003, **4**, 113.
22. H. Adachi, K. Takano, Y. Hosokawa, T. Inoue, Y. Mori, H. Matsumura, M. Yoshimura, Y. Tsunaka, M. Morikawa, S. Kanaya, H. Masuhara, Y. Kai and T. Sasaki, *Jpn. J. Appl. Phys.*, 2003, **42**, L798.
23. T. Okutsu, K. Furuta, M. Terao, H. Hiratsuka, A. Yamano, N. Ferté and S. Veesler, *Cryst. Growth Des.*, 2005, **5**, 1393.
24. A. P. O'Mullane, N. Fay, A. Nafady and A. M. Bond, *J. Am. Chem. Soc.*, 2007, **129**, 2066.
25. C. Zhao and A. M. Bond, *J. Am. Chem. Soc.*, 2009, **131**, 4279.
26. A. J. Alexander and P. J. Camp, *Cryst. Growth Des.*, 2008, **9**, 958.
27. O. V. Dolomanov, L. J. Bourhis, R. J. Gildea, J. A. K. Howard and H. Puschmann, *J. Appl. Crystallogr.*, 2009, **42**, 339.
28. C. Duffus, P. J. Camp and A. J. Alexander, *J. Am. Chem. Soc.*, 2009, **131**, 11676.
29. M. R. Ward and A. J. Alexander, *Cryst. Growth Des.*, 2012, **12**, 4554.
30. B. A. Garetz, J. E. Aber, N. L. Goddard, R. G. Young and A. S. Myerson, *Phys. Rev. Lett.*, 1996, **77**, 3475.
31. J. Zaccaro, J. Matic, A. S. Myerson and B. A. Garetz, *Cryst. Growth Des.*, 2000, **1**, 5.
32. X. Sun, B. A. Garetz and A. S. Myerson, *Cryst. Growth Des.*, 2006, **6**, 684.
33. X. Sun, B. A. Garetz and A. S. Myerson, *Cryst. Growth Des.*, 2008, **8**, 1720.
34. M. R. Ward, S. McHugh and A. J. Alexander, *Phys. Chem. Chem. Phys.*, 2012, **14**, 90.
35. S. Hatano, T. Horino, A. Tokita, T. Oshima and J. Abe, *J. Am. Chem. Soc.*, 2013, **135**, 3164.
36. K. Mutoh and J. Abe, *Chem. Commun.*, 2011, **47**, 8868.
37. T. Hayashi and K. Maeda, *Bull. Chem. Soc. Jpn.*, 1962, **35**, 2057.
38. J. Sonnenberg and D. M. White, *J. Am. Chem. Soc.*, 1964, **86**, 5685.
39. E. H. White and M. J. C. Harding, *J. Am. Chem. Soc.*, 1964, **86**, 5686.
40. G. Rio and B. Serkiz, *J. Chem. Soc., Chem. Commun.*, 1975, 849.

41. M. L. Graziano, M. R. Iesce and R. Scarpati, *J. Chem. Soc., Chem. Commun.*, 1979, 7.
42. H.-S. Ryang and C. S. Foote, *J. Am. Chem. Soc.*, 1979, **101**, 6683.
43. P. Kang and C. S. Foote, *J. Am. Chem. Soc.*, 2002, **124**, 9629.
44. S. Hatano and J. Abe, *Phys. Chem. Chem. Phys.*, 2012, **14**, 5855.
45. N. Fey, J. A. S. Howell, J. D. Lovatt, P. C. Yates, D. Cunningham, P. McArdle, H. E. Gottlieb and S. J. Coles, *Dalton Trans.*, 2006, 5464.
46. J. A. Varela, D. Peña, B. Goldfuss, D. Denisenko, J. Kulhanek, K. Polborn and P. Knochel, *Chem. Eur. J.*, 2004, **10**, 4252.
47. S. E. Wolkenberg, D. D. Wisnoski, W. H. Leister, Y. Wang, Z. J. Zhao and C. W. Lindsley, *Org. Lett.*, 2004, **6**, 1453.
48. T. Seethalakshmi, A. Puratchikody, D. E. Lynch, P. Kaliannan and S. Thamotharan, *Acta Crystallogr., Sect. E: Struct. Rep. Online*, 2006, **62**, o2803.
49. D. Yanover and M. Kaftory, *Acta Crystallogr., Sect. E: Struct. Rep. Online*, 2009, **65**, o711.
50. T. Hayashi and K. Maeda, *Bull. Chem. Soc. Jpn.*, 1960, **33**, 565.
51. G. R. Coraor, L. A. Cescon, R. Dessauer, A. S. Deutsch, H. L. Jackson, A. MacLachlan, K. Marcali, E. M. Potrafke and R. E. Read, *J. Org. Chem.*, 1971, **36**, 2267.
52. D. Lavabre, G. Levy, J. P. Laplante and J. C. Micheau, *J. Phys. Chem.*, 1988, **92**, 16.
53. R. Dessauer, *Photochemistry, History and Commercial Applications of Hexaarylbiimidazoles: All About HABIs, 1st edn.*, Elsevier, Amsterdam, 2006.
54. R. H. Mitchell, T. R. Ward, Y. Chen, Y. Wang, S. A. Weerawarna, P. W. Dibble, M. J. Marsella, A. Almutairi and Z.-Q. Wang, *J. Am. Chem. Soc.*, 2003, **125**, 2974.
55. K. Amimoto and T. Kawato, *J. Photochem. Photobiol., C*, 2005, **6**, 207.
56. A. W. van der Made and R. H. van der Made, *J. Org. Chem.*, 1993, **58**, 1262.
57. R. V. Williams, J. R. Armantrout, B. Twamley, R. H. Mitchell, T. R. Ward and S. Bandyopadhyay, *J. Am. Chem. Soc.*, 2002, **124**, 13495.

58. R. H. Mitchell, C. Bohne, S. G. Robinson and Y. Yang, *J. Org. Chem.*, 2007, **72**, 7939.
59. T. Yamato, J.-I. Matsumoto, K. Tokuhisa, K. Tsuji, K. Suehiro and M. Tashiro, *J. Chem. Soc., Perkin Trans. 1*, 1992, 2675.
60. D. N. Coventry, A. S. Batsanov, A. E. Goeta, J. A. K. Howard, T. B. Marder and R. N. Perutz, *Chem. Commun.*, 2005, 2172.
61. B. M. Partridge and J. F. Hartwig, *Org. Lett.*, 2013, **15**, 140.
62. F. Babudri, V. Fiandanese, G. Marchese and A. Punzi, *Tetrahedron Lett.*, 1995, **36**, 7305.
63. R. H. Mitchell and V. S. Iyer, *Tetrahedron Lett.*, 1993, **34**, 3683.
64. A. Bhaskar, G. Ramakrishna, Z. Lu, R. Twieg, J. M. Hales, D. J. Hagan, E. Van Stryland and T. Goodson, *J. Am. Chem. Soc.*, 2006, **128**, 11840.
65. A. Rajca, *Chem. Rev.*, 1994, **94**, 871.
66. S. Sanvito, *Chem. Soc. Rev.*, 2011, **40**, 3336.
67. A. P. West, S. K. Silverman and D. A. Dougherty, *J. Am. Chem. Soc.*, 1996, **118**, 1452.
68. V. Barone, I. Cacelli and A. Ferretti, *J. Chem. Phys.*, 2009, **130**, 094306.
69. B. D. Koivisto and R. G. Hicks, *Coord. Chem. Rev.*, 2005, **249**, 2612.
70. M. Gomberg, *J. Am. Chem. Soc.*, 1900, **22**, 757.
71. M. Nakano, K. Yoneda, R. Kishi, H. Takahashi, T. Kubo, K. Kamada, K. Ohta, E. Botek and B. Champagne, *J. Chem. Phys.*, 2009, **131**, 114316.
72. R. H. Mitchell, *Eur. J. Org. Chem.*, 1999, **1999**, 2695.
73. Z. Liu, Y. Wang, Y. Chen, J. Liu, Q. Fang, C. Kleeberg and T. B. Marder, *J. Org. Chem.*, 2012, **77**, 7124.
74. M. N. Eliseeva and L. T. Scott, *J. Am. Chem. Soc.*, 2012, **134**, 15169.
75. I. A. I. Mkhalid, J. H. Barnard, T. B. Marder, J. M. Murphy and J. F. Hartwig, *Chem. Rev.*, 2009, **110**, 890.
76. P. Zhang, D. J. Berg, R. H. Mitchell, A. Oliver and B. Patrick, *Organometallics*, 2012, **31**, 8121.
77. P. A. Liddell, G. Kodis, J. Andréasson, L. de la Garza, S. Bandyopadhyay, R. H. Mitchell, T. A. Moore, A. L. Moore and D. Gust, *J. Am. Chem. Soc.*, 2004, **126**, 4803.
78. R. H. Mitchell and S. Bandyopadhyay, *Org. Lett.*, 2004, **6**, 1729.

79. P. Zhang, Z. Brkic, D. J. Berg, R. H. Mitchell and A. G. Oliver, *Organometallics*, 2011, **30**, 5396.

80. N. Vilà, G. Royal, F. Loiseau and A. Deronzier, *Inorg. Chem.*, 2011, **50**, 10581.

Chapter 5

Experimental

5. Introduction

This chapter outlines the photophysical, electrochemical, computational, analytical and synthetic methods and protocols employed during the course of this work.

5.1. Photophysical measurements

5.1.1. General considerations

All photophysical measurements were made using GPR grade solvents. Care was taken to minimise the exposure of the Ir complexes to light while in chlorinated solvents during preparative, purification and analytical stages as it had been observed previously in both luminescence and NMR spectroscopy experiments that related complexes can be photolytically degraded in these solvents. Variable temperature photophysical measurements (77 K to 298 K) were made using an Oxford Instruments DN 1704 optical cryostat with liquid nitrogen cooling. The solvent mixture 5:5:2 (*v*/*v*) diethyl ether:2-methylbutane:EtOH (EPA), which forms an optically transparent glass upon cooling (T_g = ~138 K), was used as the solvent for low temperature measurements. An Oxford Instruments ITC 601 thermostatic controller was used for temperature regulation. All described techniques and instrumentation (*vide infra*) are adapted for use at low temperature.

5.1.2. UV-visible absorption spectroscopy

Absorption spectra of solutions in quartz cuvettes of path length $l = 1$ cm with an absorbance of $A < 0.5$ at wavelengths longer than 300 nm were measured on an ATI-Unicam UV2-100 spectrometer operated with the Unicam Vision (*ver*. 3.50) software. Baseline correction was achieved by reference to pure solvent. Extinction coefficients, ε, were determined in dilute solution from the Beer-Lambert law: $\log_{10}(I_0/I_t) = A = \varepsilon cl$, where c is the sample concentration. Three independently weighed samples, each followed by two dilutions with the appropriate solvent, gave a total of six measurements of the absorbance at different concentrations, from which the extinction coefficient was obtained by linear regression in Microsoft Excel.

5.1.3. One-photon photoluminescence spectroscopy

Excitation and emission photoluminescence spectra were recorded on a Horiba Jobin Yvon SPEX Fluorolog-3-22 Tau-3 spectrofluorometer. The emission detector used was either the supplied Hamamatsu R928P photomultiplier tube (PMT) (used for the majority of samples) or a Perkin Elmer SPCM-AQR Si avalanche photodiode when the sample had significant emission above 750 nm, where the standard PMT is less sensitive. DataMax (*ver.* 2.20) software was used throughout. Samples for fluorescence measurements were held in standard commercial quartz cuvettes, l = 1 cm x 1 cm. For phosphorescence and long lifetime fluorescence (> ~10 ns) measurements, samples were degassed by repeated freeze-pump-thaw cycles using a turbomolecular pump, until the pressure gauge showed no further movement upon a new pump phase, typically at 5 x 10^{-5} mbar after three to four cycles, and sealed by a Teflon J. Young tap. Solutions had A = 0.10-0.15 at and above the excitation wavelength to minimise inner filter (geometric) effects and reabsorption. The data were corrected for the spectral response of the excitation monochromator (excitation spectra) or the emission monochromator and PMT (emission spectra). All spectra were continuously corrected for fluctuations in the xenon lamp intensity.

PLQYs were measured using an absolute method,[1] employing a home-made integrating sphere with the Fluorolog 3-22 Tau-3 spectrofluorometer. The sample was held in a cylindrical quartz tube (inner diameter 8 mm) inside a 100 mm diameter integrating sphere constructed from Labsphere Spectralon (> 99% reflectivity over the spectral range studied). Data analysis was conducted using a programme written in National Instruments (NI) LabVIEW (*ver.* 8.6).

5.1.4. Time-resolved two-photon absorption (TR-TPA) spectroscopy

Two-photon cross-sections were measured using the femtosecond TPA induced fluorescence method. A mode-locked, APE Pulse Switch cavity dumped, Coherent MIRA 900 Ti:sapphire laser was pumped by the 2nd harmonic (532 nm) of a continuous wave Coherent Verdi V6 Nd:YAG laser at a power of 4.5 W to create a pulsed excitation source. The pulse characteristics were: a temporal FWHM of ~150 fs, average power 10 mW at a repetition rate of ~2.5 MHz and an energy of 4 nJ pulse^{-1}. An Edmund Optics variable neutral density filter mounted on a translation stage was used

to control the light intensity incident on the sample, with the power monitored by splitting the beam to a photodiode of known response, calibrated against a free standing power meter. Gold mirrors, highly reflective of NIR radiation, were used with a 20x Olympus LWD C A20 microscope objective to focus the source onto the sample. A sample of known concentration (*ca.* 50 μM) in a suitable solvent was prepared in a 1 cm path length quartz cuvette. Two-photon excited photoluminescence spectra were collected with a Semrock FF735 (735 nm) dichroic mirror and detected with a 100 μm core fibre optic cable coupled Avantes Avaspec 2048FT CCD spectrograph fitted with a 700 nm shortpass filter to remove extraneous laser light. The TPA cross section (σ_2) was measured relative to fluorescein as a reference, as per the standard methodology of Webb *et al.*,[2, 3] using the equation:

$$\sigma_2^S = \frac{\sigma_2^R . \Phi^R . c^R . n^S . F^S(\lambda)}{\Phi^S . c^S . n^R . F^R(\lambda)}$$

The superscripts R and S refer to the reference and sample respectively, Φ_P is the one photon photoluminescence quantum yield, c is the concentration, n is the solvent refractive index and $F(\lambda)$ is the integrated two-photon emission spectrum. The sample and reference were recorded under identical pulse conditions. The concentration of the reference fluorescein was measured by UV-visible spectroscopy using ε(492 nm) = 88,000 $dm^3\ mol^{-1}\ cm^{-1}$. Literature $\sigma_2(\lambda)$ and Φ (0.9) values[2, 3] in 0.1 M $NaOH_{(aq)}$ were used for fluorescein. The system was calibrated to correct for the dark noise of the detector and the photoluminescence spectrum was typically averaged over 100 measurements of 250 ms integration time. A correction file for the spectral response of the collection optics and detector was generated using a standard lamp and subsequently applied to all spectra. In-house software written in NI LabVIEW (*ver.* 8.6) was used for data collection and analysis. Estimated error ± 20%.

Time-gated, two-photon excited photoluminescence spectra were acquired with a lower repetition rate of 25 kHz. The pulse energy was 30 nJ $pulse^{-1}$. The emission was detected using a Hamamatsu H10682-01 PMT attached to a dual-grating scanning Princeton Instruments Acton SP2150 monochromator. The TTL signal from the detector was gated using an AND logic gate with the timing being achieved using a variable duration TTL pulse synchronised with the laser cavity dumper driver. Spectra were recorded typically at 1 nm intervals with a 1 s integration time and averaged over

16 scans. Spectra were corrected for spectral response of the collection optics and detector and dark background.

To confirm that a two-photon process had been observed, the integrated two-photon induced emission spectra were recorded as a function of laser intensity. To achieve this, an Edmund Optics variable neutral density filter, mounted on a translation stage, was used to control the light intensity incident on the sample, with the power monitored by a free-standing power meter whilst a series of spectra were recorded. The $log(F(\lambda))$ *vs.* $log(P)$ graphs were linear with a gradient, within experimental error, of two, as required for a two-photon process, over the power range used to measure σ_2.

5.1.5. Lifetime measurements

Phosphorescence lifetime measurements were made using either time-resolved emission spectroscopy or time-correlated multi-photon counting spectroscopy. Fluorescence lifetime measurements were made using the time-correlated single-photon counting method. The experimental set-up for each of these is detailed below.

5.1.5.1. Time-resolved emission spectroscopy

The fundamental of an N_2 laser (337 nm, 10 μJ, 10 Hz) was employed as an excitation source in a home-made fluorimeter. Emission was collected at 90° to the excitation by a Hamamatsu R928 PMT as a function of time, selecting an observed wavelength close to the peak emission with a Horiba Jobin Yvon Triax 320 monochromator set at a bandpass of between 0.1-2.0 nm. The signal was averaged over a minimum of 64 pulses and converted to a digital signal by a Tetronix TDS 340 digital storage oscilloscope. The decay data were fitted to exponential functions of the form $I(t) = I_0\exp(-t/\tau)$ using the Solver function in Microsoft Excel by varying the intensity at $t = 0$, $I_{0,}$ and the lifetime, τ, and minimising the χ^2 distribution.

5.1.5.2. Time-correlated multi-photon counting (TCMPC)

In a home-made set-up, the fundamental of an N_2 laser (337 nm, 10 μJ, 10 Hz) was used as an excitation source with emission detected in a 90° geometry by an ID-Quantique ID-100-50 single-photon counting avalanche diode at a wavelength selected by a monochromator with a 1 nm bandpass. The signal was digitised using an NI USB-5133

8 bit, 100 Ms s^{-1} digitiser and processed and recorded by in-house NI LabVIEW (*ver.* 8.6) software. Analysis was performed in Microsoft Excel as above.

5.1.5.3. Time-correlated single photon counting (TCSPC)

The fluorescence lifetimes were measured by time-correlated single photon counting (TCSPC) using the third-harmonic (300 nm) of the Coherent Ti:sapphire laser described for TR-TPA spectroscopy measurements, mode-locked at 900 nm and operating at a repetition rate of 4 MHz. The fluorescence emission was collected at right angles to the excitation source, with the emission wavelength selected using a Horiba Jobin Yvon Triax 190 monochromator and detected by a cooled IBH TBX-04 PMT. Timing was achieved using an Ortec 567 time-to-amplitude converter and an E. G. & G Trumpcard pulse height analyser (PHA), and data were recorded using Maestro (*ver.* 5.10) software. Fluorescence decays were recorded to a minimum of 10,000 counts in the peak channel of the PHA with a record length of 1000 channels. The instrument response function (IRF) was measured using a dilute LUDOX silica colloidal suspension as the scattering sample, setting the monochromator at the emission wavelength of the laser, giving an IRF of approximately 200 ps. The resulting intensity decay was a convolution of the fluorescence decay with the IRF, and iterative reconvolution of the IRF with one or two decay functions and non-linear least-squares analysis were used to analyse the data in Microsoft Excel using the solver function. The quality of the fit was judged by the calculated value of the reduced χ^2 and Durbin-Watson parameters and visual inspection of both the residual and the autocorrelated residuals.

5.2. Electrochemical methods

Cyclic voltammetry (CV) was performed using dry solvents under a nitrogen atmosphere in which the solution was maintained stationary. A scan rate of v = 100 mV s^{-1} was used with a 0.1 M $N(n\text{-}Bu)_4BF_4$, CH_2Cl_2 solution at a concentration of *ca.* 1 x 10^{-4} M analyte. A gastight, single-compartment, three-electrode cell equipped with a Pt disk working electrode, Pt wire counter electrode, and Pt wire pseudo-reference electrode was used and data collected on an Autolab PG-STAT 30 potentiostat. The working electrode was polished with alumina paste before each scan. Redox potentials have been adjusted such that they are reported relative to the

ferrocene/ferrocenium (Fc/Fc^+) couple at 0.0 V using an internal standard of the decamethylferrocene/decamethylferrocenium couple (Fc^*/Fc^{*+}) (Fc^*/Fc^{*+} = -0.59 V *vs.* Fc/Fc^+).[4]

5.3. Computational methods

All calculations were carried out using the Gaussian '09 (Revision A.1) package[5] or Q-Chem (ver. 4).[6] The initial geometry input for optimisation calculations was based on the crystallographic coordinates where possible, or from a chemically intuitive geometry, when experimental data were not available, to maximise the probability of locating the global minimum on the potential energy surface. Density functional theory (DFT) was used exclusively in this work for optimisations. Ground-state structures were typically calculated using the B3LYP hybrid exchange-correlation functional, composed of Becke's three parameter exchange[7] and Lee, Yang and Parr's correlation[8] functionals. The B3LYP functional is a relatively reliable (possibly only due to cancellation of errors) and much used functional, essentially the *de facto* choice in the literature for ground-state structures and energies of moderately large compounds at an acceptable computational cost, allowing rapid comparison with literature calculations. Alternative functionals were also used where appropriate: M06-2X,[9] where dispersion was potentially important, *cf.* the **ETPI** dimers or CAM-B3LYP[10] in the case of the pyrene derivatives, where it has been shown to predict the correct state ordering in other similar compounds.[11] Frequency calculations, performed on each optimised structure at the same level of theory, returned only positive (real) vibrational frequencies, indicating minima had been located. Stability calculations, using the keyword *stable*, were performed at the same level of theory for the six lowest excitations (default). These calculations identified the presence of internal instabilities (with respect to orbital ordering) and actual ($\omega_{STAB} < 0$ eV) or near ($\omega_{STAB} \rightarrow 0$ eV) external instablities in the Hartree-Fock wavefunction with respect to an unrestricted calculation.[12, 13] Solvent effects were generally not included, except where explicitly stated, as it is considered that the choice of solvent model generally has a larger effect than the genuine change expected due to solvent effects. Where solvent effects were included, the polarisable continuum model (PCM) was employed with the united atom Kohn-Sham (UAKS) topological model. The UAKS model is optimised for the PBE0 functional, which is of a similar level to B3LYP, and hence its use is appropriate. Acetonitrile (ε_r = 35.688)

was chosen as the solvent because it is the most polar solvent used experimentally and thus acts as the limiting case to compare with the gas-phase calculations. Spin-orbit coupling was also omitted as, like solvent effects, the method chosen for its inclusion has a large effect on the outcome and because it is not available in Gaussian '09, which was the programme used predominantly in this work.

Potential energy surfaces of the ligands 1- and 2-pypyrH as a function of the dihedral angle between the pyridine and pyrene rings were calculated starting from the DFT optimised ground state geometry by scanning in fixed steps of 5° this dihedral angle and optimising all other degrees of freedom. Optimisation calculations were also performed on the T_1 states of some of the complexes, using an analogous procedure as that described for the ground state; similarly, calculations to assign electrochemical data were performed on the approximately charged (generally, mono or dicationic) species at the same level of theory as the neutral species. Calculations were unrestricted for radicals, thus separate spin orbitals for the α and β electrons are considered. Wiberg Bond Indices[14] were calculated within the natural bond orbital formalism with B3LYP and M06-2X functionals and the 6-31G(d) basis set and are considered a measure of the bond order between a pair of atoms. Inclusion of diffuse orbitals has been shown to introduce errors in natural bond orbital analysis and therefore they were omitted.[15]

For calculations conducted on Ir complexes, either the 6-31+G or 6-31G(d) basis set[16] was used for light atoms (H, C, N, O) and the Los Alamos National Laboratories 2nd double zeta (LANL2DZ)[17] basis set was used for both the valence and effective core potential (ECP) functions of the Ir atoms. For purely organic systems, the slightly larger basis set 6-31+G(d) was used. Orbital surfaces and spin density plots, generated from the output of the DFT calculations, were viewed in the programme GaussView (*ver*. 4.1). The Pople split-valence double-zeta basis set 6-31G, consists of a linear combination of six Gaussian type functions for the core electrons and a combination of two functions consisting of three and one Gaussians for the valence electrons was chosen as a basis set with enough flexibility to produce acceptable results at a moderate cost. This was supplemented with either polarisable functions in the case of the 6-31+G basis set or diffuse d orbitals on all elements except hydrogen to give the 6-31G(d) basis set or both in the case of 6-31+G(d). These basis sets are, however, only defined for atoms with an atomic number up to that of zinc, and thus is inappropriate for iridium. The LANL2DZ was designed for heavy atoms in an attempt to describe the effects

associated with the core electrons moving at relativistic speeds and so its use is appropriate here. In addition, the use of an ECP reduces the computational cost by minimising the need to consider the core electrons that are of limited importance in determining properties such as geometry, conjugation and the energies of excited states: the properties of interest here.

Time-dependent (TD)-DFT calculations were performed on the optimised ground-state geometries over 10-15 states (1:1 singlets:triplets) for organometallic species or 20-25 states (singlets) for organic molecules using either the B3LYP or CAM-B3LYP functionals with the same basis set used for the optimisation. For TD-DFT calculations, especially when CT is involved, B3LYP often fails to accurately reproduce experimental results because of its incorrect description of long-range, two electron interactions,[18] which it describes by a $-0.2r_{12}^{-1}$ function as opposed to the true $-r_{12}^{-1}$ dependence.[19] This is more correctly described by the CAM-B3LYP functional, newly implemented in Gaussian 09, but with little additional computational cost, and thus it was selected for many of the TD-DFT calculations here. Tamm-Dancoff Approximation[20, 21] TD-DFT[22] (TDA) calculations were conducted using Q-Chem.[6] These calculations were necessary when a near triplet instability exists in the ground state wavefunction, as identified by a stability calculation. Electron density difference maps were constructed by mathematical manipulation of surfaces in GaussView (*ver.* 4.1).

5.4. Synthetic methods

5.4.1. General considerations

All reagents were purchased from Sigma-Aldrich (U.K.), Acros (U.K.), Alfa Aesar (U.K.), Fischer (U.K.), AllyChem (China) or Precious Metals Online (Australia) and were used as received without further purification, with the following exceptions: tetra-*n*-butylammonium fluoride 1 M THF solution was dried and stored over activated 4 Å molecular sieves; pyrene was purified by passage through a short (*ca.* 5 cm) column (SiO_2; hexanes); spectroscopic grade cyclohexane was purified by passage through a column (two layer Al_2O_3 and SiO_2) that had been activated by heating overnight at > 450 °C. The catalyst *cis*-dichlorobis(triphenylphosphine)palladium(II) ($[PdCl_2(PPh_3)_2]$) was kindly provided by Prof. T. B. Marder's research group, while

tetrakis(triphenylphosphine)palladium(0) ([$Pd(PPh_3)_4$]) was synthesised from $PdCl_2$, PPh_3 and hydrazine monohydrate (as reducing agent) using a known procedure.[23] Anhydrous and anaerobic conditions were maintained with standard Schlenk apparatus, operating under an inert atmosphere of dry nitrogen using dry solvents obtained from the departmental Innovative Technologies Inc. Solvent Purification System. All water used was de-ionised.

Column chromatography was performed on FluorChem LC60A 40-63 μm silica gel and monitored by thin layer chromatography (TLC), performed using 254 nm fluorescent Polygram Sil G/UV254 0.2 mm silica plates and visualised under UV light (254 and 365 nm) or by exposure to iodine vapour. All enantiomeric iridium complexes were isolated as racemic mixtures.

Microwave reactions were carried out in septum-containing, crimp-capped, sealed vials in a Personal Chemistry Emrys Optimizer automated microwave synthesis system. The wattage was automatically adjusted to maintain the desired temperature for the desired period of time. The temperature and pressure inside the vial were monitored throughout. An Innovative Technology Inc. glovebox was used to prepare the reaction mixture for the borylation of pyrene under an atmosphere of dry nitrogen.

5.4.2. Analytical techniques

5.4.2.1. Nuclear magnetic resonance (NMR) spectroscopy

NMR spectra were recorded on Varian Mercury-200, Varian Mercury-400, Varian Inova-500, Varian VNMRS-600 or Varian VNMRS-700 spectrometers at 25 °C, expect where stated otherwise. Chemical shifts, δ, are internally referenced to the residual protiated solvent (δ_H/ppm $CHCl_3$ 7.26 (s), $CHDCl_2$ 5.32 (t), DMSO-d_5H 2.50 (quintet), acetone-d_5H 2.05 (quintet), benzene-d_5H 7.16 (s)) or the solvent ^{13}C resonance (δ_C/ppm $CDCl_3$ 77.16 (t), DMSO-d_6 39.52 (m), benzene-d_6 128.06 (t)).[24, 25] The symbol $^{13}C\{^1H\}$ refers to a broadband ^1H decoupled ^{13}C spectrum. Assignment was aided, where necessary, by the following 2D-NMR experiments: ^1H–^1H correlation spectroscopy (COSY), nuclear Overhauser effect spectroscopy (NOESY), ^1H-^{13}C heteronuclear single quantum coherence (HSQC) spectroscopy and ^1H-^{13}C heteronuclear multiple bond correlation (HMBC) spectroscopy. Inequivalent carbon atoms are numbered sequentially, as indicated on their chemical structure; protons are signified by H_n, where

n is the number of the carbon atom to which they are bonded, except where bonded to a heteroatom, in which case they are numbered separately. (*N.B.* This is for NMR spectroscopy assignment purposes and may differ to the numbering scheme used for systematic compound names and crystal structures). The $^{13}C\{^{1}H\}$ spectra are reported to one decimal place; however, where more than one peak could be resolved within 0.1 ppm, the number of inequivalent ^{13}C environments is indicated parenthetically. Spectra were viewed and analysed using both Varian VNMRJ and Mestrelab Research MestReNova (*ver.* 7.0) software.

A solvent other than $CDCl_3$ was selected for NMR spectroscopy when solubility dictated, an overlap of the residual solvent resonance obscured key spectral features or where a different solvent was expected to separate peaks in a crowded region of the spectrum. The NMR spectra of imidazoles, for instance, are reported in DMSO-d_6. In this solvent the N–H proton is non-labile, allowing this proton to be observed in the ^{1}H spectrum. In addition, the phenyl rings in the 4- and 5-positions of the imidazole are chemically inequivalent on the ^{1}H NMR timescale in this solvent.

5.4.2.2. Mass spectrometry (MS)

Mass spectra were recorded using one of the following instruments, dependent on the nature of the sample and the analysis required: an Applied Biosystems Voyager DESTR matrix assisted laser desorption/ionisation time-of-flight (MALDI-TOF) MS (in positive mode); a Micromass LCT electrospray ionisation (ESI) MS (in positive mode) in a flow of MeOH or MeCN; a Waters Xevo QTOF, equipped with an atmospheric pressure solids analysis probe (ASAP); or by GC-MS using electron ionisation (EI) (in positive mode). GC-MS was performed using an Agilent Technologies 6890 N chromatograph equipped with a 5983 inert mass selective detector and a 10 m fused silica capillary column (5% cross-linked phenylmethylsilicone) using ultra high purity helium as the carrier gas with the following conditions: injector temperature 250 °C, detector temperature 300 °C, the oven temperature was ramped from 70 °C to 280 °C at 20 °C min^{-1}. MS data were processed using Waters MassLynx (*ver.* 4.1). Accurate mass spectrometry (Acc-MS) utilised a lock-mass correction to provide < 3 mDa precision and used Elemental Composition (ver. 4.0) embedded within Waters MassLynx (*ver.* 4.1) for analysis. The deviation between calculated and experimental mass in units of parts per million (ppm) is provided for each accurate mass presented.

5.4.2.3. Single crystal X-ray crystallography

X-ray crystallography was performed in collaboration with Drs. K. Fucke, M. R. Probert and C. M. Robertson. Single crystals suitable for single crystal X-ray diffraction structure determination were selected (based both upon appearance and the extinction of transmitted light through cross-polarisers), soaked in perfluoropolyether oil and mounted on a glass fibre or on a MiTeGen cryoloop sample holder. Diffraction data were collected on several diffractometers and the specific instrument used is indicated by the following letters with the crystal data for each structure: (**A**) Bruker Proteum/APEX II with a Bruker Microstar Cu rotating anode source equipped with multilayer focusing optics to select Cu Kα radiation (λ = 1.54188 Å); (**B**) Bruker SMART CCD 6000 using graphite monochromated Mo Kα radiation (λ = 0.71073 Å); (**C**) Oxford Diffraction Gemini S Ultra using graphite monochromated Mo Kα radiation (λ = 0.71073 Å); (**D**) Synchrotron beamline I19 at the Diamond Light Source located in Didcot, Oxfordshire, using X-ray radiation tuned to λ = 0.6689 Å. All were equipped with an open flow nitrogen Oxford Cryosystems Cobra Cryostream[26] device for low temperature measurements (typically 100-160 K). For data reduction, the Bruker APEX2 suite or the Bruker SAINT (*ver.* 7.68A) suite, in combination with Oxford Diffraction CrysAlis software (*ver.* 1.171.33.55), were employed and in all cases, all data were used for integration without constraints. The structures were subsequently solved and refined with OLEX2 (*ver.* 1.2).[27] All non-hydrogen atoms were treated anisotropically, except where highly disordered groups were problematic (typically *t*-Bu or TIPS groups); the hydrogen atoms were calculated using riding models and refined isotropically. All pictures of molecular structures have been generated in OLEX2 (*ver.* 1.2).

5.4.2.4. Vibrational spectroscopy

Raman spectra were measured with a Horiba Jobin Yvon LabRAM HR confocal Raman microscope using either a He:Ne (633 nm) laser or a laser diode (785 nm) where the particular laser selected was dependent on the fluorescence of the sample. Samples were mounted atop glass microscope slides. A grating with 600 grooves mm^{-1} was employed with a resolution of *ca.* 4 cm^{-1}.

Fourier transform infrared (FT-IR) spectra were recorded with a Perkin-Elmer Spectrum 100 attenuated total reflection (ATR) spectrometer with Perkin-Elmer Spectrum Express (*ver*. 1.01) software. Typically only the most intense peaks with energies greater than 1500 cm^{-1} (FT-IR) or 1000 cm^{-1} (Raman) are listed, except where they provide a characteristic peak outside of this range. IR data were processed in Bio-Rad Laboratories KnowItAll Academic Edition software. Bands are designated strong (s), weak (w), broad (br.) or as a shoulder (sh.) relative to other peaks; peaks that are extreme examples of these descriptors are prefixed by very (v).

5.4.2.5. Miscellaneous

A CE-400 Elemental Analyzer was used for elemental analysis (C, H, N). Melting points (m.p.) were recorded on a TA Instruments Q1000 differential scanning calorimeter and are taken as the onset of the melting event. The same instrument was used to study peroxide decomposition. A sample of *ca.* 1−3 mg was weighed on an ultra microbalance into an aluminium pan that was then sealed. The sample was heated from room temperature (25 °C) to 300 °C in a linear ramp at a rate of 10 °C min^{-1}. Dry nitrogen was used as the purge gas (50 ml min^{-1}). The instrument was calibrated with an indium standard (99.999% purity, melting m.p. 156.6 °C, heat of fusion 28.45 J g^{-1}). Thermogravimetric analysis was performed on a Perkin Elmer Pyris 1 purged with CP grade helium at a rate of 50 ml min^{-1}. The temperature programme used for DSC was also used for TGA. Analytical TLC (as above) was performed on all samples to indicate purity. Analytical high performance liquid chromatography (HPLC) analysis was performed through an XBridge 4.6 x 100 mm, 5 μm, C_{18} column with gradient elution (9:1 MeOH:water to 19:1 MeOH:water over 10 min) with a flow rate of 1 ml min^{-1}.

5.5. Chapter 1 synthetic protocols

5.5.1. 2-(Tri-*n*-butylstannyl)pyridine

An adaption of the method described by Bianchini et al.,[28] who synthesised the compound in 93% yield on the same scale using diethyl ether as the solvent.

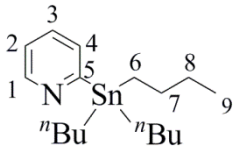

$C_{17}H_{31}NSn$
M_r = 368.1

In a nitrogen-filled two-neck round bottom flask, 2-bromopyridine (3.0 ml, 5.0 g, 32 mmol) was dissolved in tetrahydrofuran (THF) (15 ml) and cooled to -78 °C. To the cooled solution was added slowly *n*-butyllithium (1.6 M in hexanes, 20 ml, 32 mmol) and then the mixture was stirred for 1 h at -78 °C. The compound tri-*n*-butylstannyl chloride (8.6 ml, 10.3 g, 32 mmol) was added slowly and the solution was stirred for a further 30 min before being warmed to r.t., at which time the solution turned dark green. To quench the reaction, water (25 ml) was added cautiously and the mixture was stirred for 10 min under air until the solution turned bright orange. The organic layer was separated and the aqueous layer was extracted with diethyl ether (3 x 20 ml). The combined organics were dried over anhydrous K_2CO_3, filtered and reduced *in vacuo* to a brown oil. Flash chromatography (SiO_2; CH_2Cl_2) afforded the title compound as an orange-brown oil (10.2 g, 88%). The oil was used without further purification and was estimated to be of approximately 90% purity by ^{1}H NMR (impurities likely arise from partial protodestannylation).

^{1}H NMR (400 MHz; $CDCl_3$): δ_H/ppm 8.72 (1 H, m, H_1), 7.40 (1 H, m), 7.09 (2 H, m), 1.52 (6 H, m, H_6), 1.29 (6 H, m, H_7), 1.10 (6 H, m, H_8), 0.86 (9 H, t, J = 7.0 Hz, H_9). **^{13}C{^{1}H} NMR** (101 MHz; $CDCl_3$): δ_C/ppm 174.2 ($J_{C\text{-}Sn}$ not observed, C_5), 150.6 ($J_{C\text{-}Sn}$ = 59 Hz, C_1), 133.3 ($J_{C\text{-}Sn}$ = 31 Hz, C_3), 132.5 ($J_{C\text{-}Sn}$ = 76 Hz, C_4), 122.1 ($J_{C\text{-}Sn}$ = 11 Hz, C_2), 29.3 ($J_{C\text{-}Sn}$ = 10 Hz), 27.6 ($J_{C\text{-}Sn}$ = 7 Hz), 13.9 ($J_{C\text{-}Sn}$ = 5 Hz), 9.9 ($J_{C\text{-}119Sn}$ = 338 Hz, $J_{C\text{-}117Sn}$ = 322 Hz, C_6). **Acc-MS** (ESI$^+$): *m/z* 366.1538 (M^+), calcd. for $C_{17}H_{32}N^{116}Sn$ 366.1552 ($|\Delta m/z|$ = 3.8 ppm). Analyses match those previously reported.[28]

5.5.2. 4-(2′-Pyridyl)benzophenone: pybpH

Reported in a patent from Gracel Display Inc.,[29] *who synthesised the compound in 85% yield on a 54 mmol scale using a similar Stille coupling.*

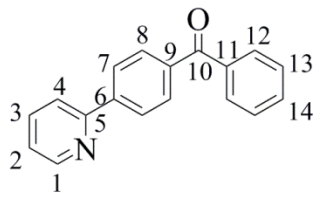

$C_{18}H_{13}NO$
M_r = 259.3

The compounds 4-bromobenzophenone (1.35 g, 5.15 mmol) and 2-(tri-*n*-butylstannyl)pyridine (1.75 ml, 5.47 mmol) were dissolved in toluene (5 ml) in which lithium chloride (0.21 g, 5.0 mmol) was suspended. The suspension was degassed by three freeze-pump-thaw cycles and back-filled with nitrogen. The catalyst [$Pd(PPh_3)_4$] (60 mg, 1 mol%) was added under a stream of nitrogen and the suspension was heated at 75 °C for 16 h. The reaction mixture was eluted through a short (*ca*. 5 cm) column (SiO_2; diethyl ether). The solution was reduced in volume to *ca.* 20 ml, to which aqueous HCl (5 M, 2 ml) and H_2O (10 ml) were added. The aqueous layer was separated, basified with K_2CO_3 and extracted with CH_2Cl_2 (3 x 20 ml). The combined organics were dried over anhydrous K_2CO_3, filtered and reduced in volume *in vacuo* to a yellow oil, which solidified upon standing to a yellow-brown solid. The solid was recrystallised from hexanes to afford the product as a white crystalline material (1.10 g, 83%). Single crystals suitable for X-ray diffraction were grown as colourless prisms by slow cooling of an EtOH solution.

FT-IR (solid): $\tilde{\nu}_{max}$/cm^{-1} 3055 (w), 1649 (s, C=O), 1597 (Ar), 1585 (Ar), 1574 (Ar). **^{1}H NMR** (400 MHz; $CDCl_3$): δ_H/ppm 8.74 (1 H, d, J = 4.4 Hz, H_1), 8.11 (2 H, d, J = 8.4 Hz), 7.91 (2 H, d, J = 8.4 Hz), 7.80 (4 H, m), 7.60 (1 H, t, J = 7.2 Hz), 7.50 (2 H, t, J = 7.2 Hz), 7.29 (1 H, dd, J = 8.8 and 4.4 Hz, H_2). **GC-MS** (EI^+; 1 peak): *m/z* 259 (M^+). **Acc-MS** ($ASAP^+$): *m/z* 259.0995 (M^+), calcd. for $C_{18}H_{13}NO$ 259.0997 ($|\Delta m/z|$ = 0.8 ppm). No analyses were provided in the first report of this compound.[29]

Crystal data (Instrument **B**): $C_{18}H_{13}NO$, (0.38 x 0.25 x 0.06) mm^3, ρ = 1.316 g cm^{-3}, triclinic, $P\bar{1}$, Z = 4, a = 9.457(1) Å, b = 11.393(2) Å, c = 13.088(2) Å, α = 111.003(4)°,

β = 95.796(4)°, γ = 90.187(4)°, V = 1308.6(3) Å^3, T = 120(2) K, μ(Mo Kα) = 0.082 mm^{-1}, 6542 reflections measured of which 3738 independent (R_{int} = 0.0300), 2608 reflections with $I > 2\sigma(I)$, final R indices: wR_2 = 0.1758 (all data), R_1 = 0.0587 ($I > 2\sigma(I)$).

5.5.3. Di-μ-chlorido-tetrakis(4-(2′-pyridyl)benzophenonido-κ^2*N*,*C*$^{3'}$) diiridium(III): [{Ir(pybp)$_2$(μ-Cl)}$_2$]

Reported in a patent from Gracel Display Inc.,[29] *who synthesised the compound in 68% yield (recalculated) on a 10.5 mmol scale using a similar method.*

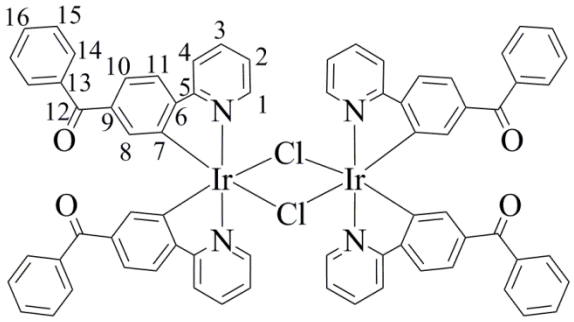

$C_{72}H_{48}Cl_2Ir_2N_4O_4$
M_r = 1488.5

The compounds 4-(2′-pyridyl)benzophenone (116 mg, 0.45 mmol) and $IrCl_3 \cdot 3H_2O$ (78 mg, 0.22 mmol) were suspended in a 2:1 (*v*/*v*) mixture of 2-ethoxyethanol and water (6 ml) and heated at 110 °C for 6 h. The solution was allowed to cool to r.t. before water (40 ml) was added, precipitating a bright orange solid that was filtered, washed with water (3 x 10 ml) and EtOH (2 x 5 ml), dissolved in CH_2Cl_2 (20 ml), dried over $MgSO_4$, filtered and reduced *in vacuo* to afford the title compound as an orange powder (120 mg, 73%). Single crystals of the acetone trisolvate suitable for X-ray diffraction were grown as red prisms by evaporation of an acetone solution.

FT-IR (solid): $\tilde{\nu}_{max}$/cm^{-1} 3065 (w, br.), 2962 (w, CH), 2926 (w, CH), 2855 (br.), 2044 (br.), 1978 (w), 1650 (s, C=O), 1607 (Ar), 1597 (Ar), 1581 (Ar), 561 (Ar), 542 (Ar), 1476 (s), 1269 (s), 1250 (s), 774 (s), 731 (s), 703 (s), 675 (s), 644 (s). **^{1}H NMR** (700 MHz; $CDCl_3$): δ_H/ppm 9.21 (4 H, d, J = 7.7 Hz, H_1), 7.89 (4 H, d, J = 7.7 Hz, H_4), 7.64 (4 H, td, J = 7.7 and 1.4 Hz, H_3), 7.58 (4 H, d, J = 7.7 Hz, H_{11}), 7.46 (8 H, d, J = 7.7 Hz, H_{14}), 7.44 (8 H, t, J = 7.7 Hz, H_{16}), 7.28 (8 H, t, J = 7.7 Hz, H_{15}), 7.26 (4 H,

d, J = 4.9 Hz, H_{10}), 6.71 (4 H, td, J = 7.7 and 1.4 Hz, H_2), 6.24 (4 H, d, J = 1.4 Hz, H_8). **$^{13}C\{^1H\}$ NMR** (176 MHz; $CDCl_3$): δ_C/ppm 196.8 (C_{12}), 167.4 (C_2), 151.9 (C_1), 148.4 (C_7), 148.2 (C_9), 144.0 (C_6),138.1 (C_{15}), 137.2 (C_{11}), 136.9 (C_3), 132.5 (C_8), 131.8 (C_{16}), 130.0 (C_{14}), 128.0 (C_{13})), 124.0 (C_{10}), 123.5 (C_5), 119.9 (C_4). **MS** (MALDI$^+$): *m/z* 743.9 ($[M/2]^+$). The molecular ion was not observed by MALDI$^+$, ASAP$^+$ or ESI$^+$ MS. No analyses were provided in the first report of this compound.[29]

Crystal data (Instrument **B**): $Ir_2C_{72}H_{48}N_4O_4Cl_2 \cdot 3(CH_3)_2CO$, (0.24 x 0.21 x 0.10) mm^3, ρ = 1.515 g cm^{-3}, triclinic, $P\bar{1}$, Z = 2, a = 12.7289(3) Å, b = 13.9838(3) Å, c = 19.7809(4) Å, α = 71.488(1)°, β = 84.709(1)°, γ = 86.168(1)°, V = 3321.9(1) Å^3, T = 120(2) K, μ = 4.091 mm^{-1}, 15892 reflections measured of which 9480 independent (R_{int} = 0.0185), 8336 reflections with $I > 2\sigma(I)$, final R indices: wR_2 = 0.0700 (all data), R_1 = 0.0232 ($I > 2\sigma(I)$).

5.5.4. Acetylacetonato-κ^2*O,O′*-bis(4-(2′-pyridyl)benzophenonide-κ^2*N,C*$^{3′}$) iridium(III): [Ir(pybp)$_2$(acac)]

Reported in a patent from Gracel Display Inc.,[29] *who synthesised the compound in 80% yield (recalculated) on a 14 mmol scale using a similar method.*

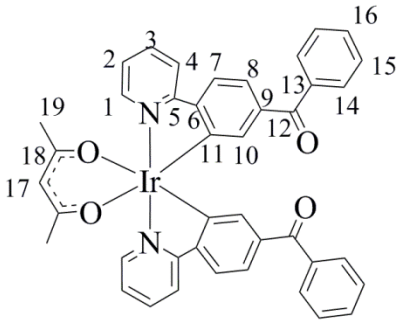

$C_{41}H_{31}IrN_2O_4$
M_r = 807.9

The compounds [{Ir(pybp)$_2$(μ-Cl)}$_2$] (50 mg, 0.033 mmol), acetylacetone (0.1 ml, 1 mmol) and K_2CO_3 (50 mg) were suspended in EtOH (10 ml) and heated at 70 °C for 4 h. The solution was allowed to cool to r.t. before water (30 ml) was added and the resultant suspension was filtered. The isolated solid was washed with water (3 x 10 ml) and hexanes (2 x 5 ml), dissolved in CH_2Cl_2, dried over $MgSO_4$, filtered and reduced *in vacuo* to afford the title compound as a red solid (47.6 mg, 93%). Single crystals of

the chloroform monosolvate suitable for X-ray diffraction were grown as orange prisms by slow evaporation of a $CDCl_3$ solution (NMR sample).

FT-IR (solid): $\tilde{\nu}_{max}$/cm^{-1} 3058 (w), 2923 (w), 1647 (s, C=O), 1606 (w, Ar), 1575 (s, Ar), 1562 (s, Ar), 1514 (s). **^{1}H NMR** (400 MHz; $CDCl_3$): δ_H/ppm 8.50 (2 H, ddd, J = 5.6, 1.6 and 0.8 Hz, H_1), 7.87 (2 H, d, J = 8.0 Hz), 7.67 (2 H, td, J = 8.0 and 1.5 Hz), 7.63 (2 H H, d, J = 8.0 Hz), 7.55 (4 H, dd, J = 8.0 and 1.5 Hz), 7.47 (2 H , tt, J = 7.6 and 1.2 Hz), 7.27-7.36 (6 , m), 7.14 (2 H, ddd, J = 7.2, 5.6 and 1.2 Hz, H_2), 6.59 (2 H, d, J = 1.6 Hz, H_{10}), 5.25 (1 H, s, H_{17}), 1.81 (6 H, s, H_{19}). **Acc-MS** (ASAP$^+$): *m/z* 806.1861 (M^+), calcd. for $^{191}IrC_{41}H_{31}N_2O_4$ 806.1890 ($|\Delta m/z|$ = 3.6 ppm). NMR analysis matches that reported previously.[29]

Crystal data (Instrument **B**): $IrC_{41}H_{31}N_2O_4 \cdot CDCl_3$, (0.48 x 0.22 x 0.08) mm^3, ρ = 1.705 g cm^{-3}, monoclinic, $P2_1/c$, Z = 4, a = 11.8914(3) Å, b = 23.5409(6) Å, c = 12.8978 (3) Å, β = 92.147(1)°, V = 3608.0(2) Å^3, T = 120(2) K, μ(Mo Kα) = 3.970 mm^{-1}, 31310 reflections measured of which 5179 independent (R_{int} = 0.0500), 4614 reflections with $I > 2\sigma(I)$, final R indices: wR_2 = 0.0757 (all data), R_1 = 0.0331 ($I > 2\sigma(I)$).

5.6. Chapter 2 synthetic protocols

5.6.1. 4-Phenylpyridine

Reported several times, including by Conejo-Garcia et al.,[30] who synthesised this compound in 93% yield on a 2 mmol scale by a similar Suzuki-Miyaura coupling.

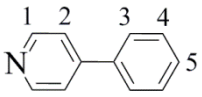

$C_{11}H_9N$
M_r = 155.2

The compounds 4-bromopyridine hydrochloride (1.95 g, 10 mmol) and benzeneboronic acid (1.36 g, 11 mmol) were dissolved in a mixture of THF (50 ml) and aqueous sodium hydroxide (20 ml, 2 M) and the solution was purged with nitrogen. The catalyst $[Pd(PPh_3)_4]$ (0.25 g, 2 mol%) was added under a stream of nitrogen and the solution was heated at 70 °C for 16 h. The resultant dark brown solution was cooled to r.t. and the

THF was removed *in vacuo*. The organic product was extracted into CH_2Cl_2 (3 x 15 ml), dried over $MgSO_4$, filtered and reduced *in vacuo* to a light brown solid. The crude solid was purified by flash chromatography (SiO_2; CH_2Cl_2) affording the title compound as a light brown solid (1.19 g, 77%).

^{1}H NMR (700 MHz; $CDCl_3$): δ_H/ppm 8.66 (2 H, dd, J = 4.6 and 1.4 Hz, H_1), 7.64 (2 H, d, J = 7.6 Hz, H_3), 7.52-7.47 (4 H, m, H_2 and H_4), 7.46-7.42 (1 H, m, H_5). **GC-MS** (EI^+; 1 peak) *m/z* 155 (M^+). Analyses match those reported previously.[30]

5.6.2. 2,4-Diphenylpyridine: dppyH

Reported several times, including by Sicre et al.,[31] who synthesised this compound in 85% yield on a 0.32 mmol scale by an alternative Suzuki-Miyaura coupling of 2,4-dibromopyridine and benzeneboronic acid. Here an adaption of the phenylation conditions described for the synthesis of 2-phenylpyridine was employed, using commercial phenyllithium solution.[32]

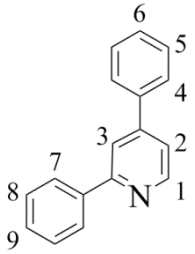

$C_{17}H_{13}N$
M_r = 231.3

The compound 4-phenylpyridine (1.05 g, 6.8 mmol) was dissolved in dry toluene (10 ml) and cooled to 0 °C. To this solution phenyllithium (4.0 ml, 1.8 M in dibutyl ether, 7.2 mmol) was added dropwise and stirred for 20 min. The mixture was then heated at 90 °C for 1 h. The mixture was allowed to cool to r.t. and was subsequently quenched cautiously with water (15 ml). The toluene layer was separated, and the aqueous layer was extracted with CH_2Cl_2 (3 x 10 ml). The combined organic layers were reduced *in vacuo* to leave a yellow-brown oil. This oil was dissolved in diethyl ether (15 ml) and extracted with aqueous HCl (3 ml, 3 M) and water (10 ml). The aqueous layer was separated, neutralised with K_2CO_3, extracted with diethyl ether (3 x 10 ml), dried over anhydrous K_2CO_3, filtered and reduced *in vacuo* to afford the title compound as a light brown solid (0.61 g, 39%).

^{1}H NMR (700 MHz; $CDCl_3$): δ_H/ppm 8.74 (1 H, dd, J = 5.11 and 0.6 Hz, H_1), 8.06 (2 H, dd, J = 8.1 and 1.2 Hz, H_7), 7.94 (1 H, dd, J = 1.6 and 0.6 Hz, H_3) 7.72-7.68 (2 H, m, H_4), 7.54-7.49 (4 H, m, H_5 and H_8), 7.48-7.43 (3 H, m, H_2, H_6 and H_9). **GC-MS** (EI^+; 1 peak) *m/z* 231 (M^+). Analyses match those reported previously.[31]

5.6.3. 2-(4′-(Phenylethynyl)phenyl)pyridine: 2-(pep)pyH

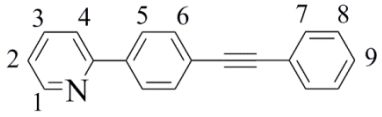

$C_{19}H_{13}N$
M_r = 255.3

The compounds 4-(phenylethynyl)benzeneboronic acid (1.0 g, 4.5 mmol), 2-bromopyridine (0.47 ml, 5.0 mmol) and K_2CO_3 (2.0 g) were dissolved in a mixture of dimethoxyethane (40 ml) and water (15 ml). The solution was purged with nitrogen for 30 min before the catalyst [$Pd(OAc)_2$] (50 mg, 5 mol%) and ligand PPh_3 (240 mg, 20 mol%) were added. The solution was heated at reflux (100 °C) for 15 h. The solution was allowed to cool to r.t. and was then extracted with CH_2Cl_2 (3 x 30 ml). The organic layer was separated, dried over $MgSO_4$, filtered and reduced *in vacuo* to give a cream-white solid. The crude material was purified by column chromatography (SiO_2; CH_2Cl_2) and recrystallised from EtOH to give the product as a cream-white solid (0.869 g, 76%).

^{1}H NMR (300 MHz; $CDCl_3$): δ_H/ppm 8.72 (1 H, d, J = 6.0 Hz, H_1), 8.02 (2 H, d, J = 8.5 Hz, H_5), 7.77 (2 H, m), 7.65 (2 H, d, J = 8.5 Hz, H_6), 7.56 (2 H, m), 7.37 (3 H, m), 7.26 (1 H, m). **^{13}C{^{1}H} NMR** (75 MHz; $CDCl_3$): δ_C/ppm 156.8, 150.0, 139.2, 137.0, 132.2, 131.9, 128.6, 127.0, 124.1, 123.4, 122.6, 120.8, 90.9, 89.5. **Acc.-MS** ($ASAP^+$): *m/z* 255.1074 (M^+), calcd. for $C_{19}H_{13}N$ 255.1048 ($|\Delta m/z|$ = 10 ppm).

Typical procedure for the synthesis of bis-heteroleptic complexes of the form [IrL_2(acac)]

An adaption of the methods of Nonoyama et al.[33] and Sprouse et al.[34] for the synthesis of [{$IrL_2(\mu$-Cl)}$_2$] species, followed by an adaption the method of Lamansky et al.[35] for the synthesis of [IrL_2(acac)] species.

$IrCl_3 \cdot 3H_2O$ (350 mg, 0.99 mmol) was dissolved in 2:1 2-ethoxyethanol:water (15 ml) with L (2.2 eq.) and then the and the resultant solution and the resultant solution was heated at 110 °C for 10 h. The reaction mixture was then allowed to cool to r.t. and water (25 ml) was added, affording a solid, which was filtered, washed with water (2 x 5 ml), dissolved in CH_2Cl_2 (30 ml), dried over $MgSO_4$, filtered and reduced *in vacuo* to leave a yellow-brown or orange solid. Flash column chromatography on silica gel (CH_2Cl_2 with 1 vol% EtOH) was used to remove fore-running fractions. The crude material was dissolved in 2-ethoxyethanol (15 ml) with acetylacetone (0.1 ml, excess) and K_2CO_3 (100 mg) and heated at 65 °C for 1 h. The solution was allowed to cool to r.t. and water (30 ml) was added, giving a yellow suspension that was filtered, washed with water (2 x 5 ml), dissolved in CH_2Cl_2, dried over $MgSO_4$, filtered and reduced *in vacuo* to leave an oily solid. This was triturated with hexanes (3 x 5 ml) and reduced *in vacuo* to leave a solid that was purified by column chromatography (see below).

5.6.4. Acetylacetonato-κ^2*O*,*O*′-bis(2-(4′-(phenylethynyl)phenyl)pyridine-κ^2*N*,*C*$^{2'}$) iridium(III): [Ir(2-(pep)ppy)$_2$(acac)]

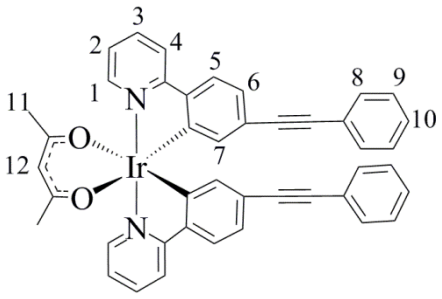

$C_{43}H_{31}IrN_2O_2$
M_r = 799.9

Column chromatography (SiO_2; CH_2Cl_2) afforded the title compound as a yellow solid (62 mg, 36%).

^{1}H NMR (700 MHz; CD_2Cl_2): δ_H/ppm 8.51 (2 H, d, J = 5.6 Hz, H_1), 7.93 (2 H, d, J = 8.1 Hz, H_4), 7.86-7.83 (2 H, m, H_3), 7.61 (2 H, d, J = 8.0 Hz, H_5), 7.42-7.40 (4 H, m, H_8), 7.31-7.29 (6 H, m, H_9 and H_{10}), 7.25 (2 H, ddd, J = 7.1, 5.6 and 1.4 Hz, H_2), 7.06 (2 H, dd, J = 8.0 and 1.6 Hz, H_6), 6.40 (2 H, d, J = 1.6 Hz, H_7), 5.30 (1 H, s, H_{12}), 1.81 (6 H, s, H_{11}). **Acc-MS** (ASAP$^+$): 799.2048 ([M+H]$^+$), calcd. for $^{191}IrN_2O_2C_{43}H_{32}$ 799.2070 ($|\Delta m/z|$ = 2.8 ppm).

5.6.5. Acetylacetonato-κ^2*O*,*O′*-bis(2,4-diphenylpyridine-κ^2*N*,*C*$^{2′}$) iridium(III): [Ir(dppy)$_2$(acac)]

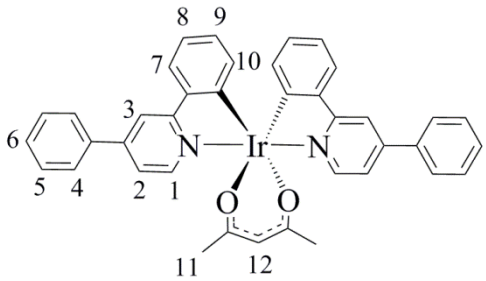

$C_{39}H_{31}IrN_2O_2$
M_r = 751.9

Column chromatography (SiO_2; 19:1 (*v*/*v*) CH_2Cl_2:hexanes) afforded the title compound as a yellow solid (118 mg, 53%).

^{1}H NMR (400 MHz; $CDCl_3$): δ_H/ppm 8.56 (2 H, d, J = 6.0 Hz, H_1), 8.06 (2 H, d, J = 1.9 Hz, H_3), 7.80 (4 H, d, J = 7.4 Hz, H_4), 7.65 (2 H, dd, J = 7.8 and 0.9 Hz, H_7), 7.60-7.54 (4 H, m, H_5), 7.52-7.47 (2 H, m, H_6), 7.37 (2 H, dd, J = 6.0 and 1.9 Hz, H_2), 6.86-6.81 (2 H, m, H_8), 6.74-6.70 (2 H, m, H_9), 6.37 (2 H, dd, J = 7.7 and 0.9 Hz, H_{10}), 5.25 (1 H, s, H_{12}), 1.82 (6 H, s, H_{11}). **Acc-MS** (ASAP$^+$): *m*/*z* 750.1978 (M$^+$), calcd. for $^{191}IrN_2O_2C_{39}H_{31}$ 750.1992 ($|\Delta m/z|$ = 1.9 ppm).

5.6.6. Acetylacetonato-κ²*O*,*O*′-bis(4-(2′-pyridyl)benzaldehyde-κ²*N*,*C*³′) iridium(III): [Ir(fppy)$_2$(acac)]

Reported previously by Chen et al.,[36] who synthesised this compound in 60% yield on a 1 mmol scale using a similar method.

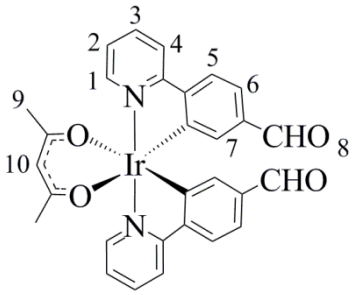

$C_{29}H_{23}IrN_2O_4$
M_r = 655.7

Column chromatography (SiO_2; CH_2Cl_2) afforded the title compound as a red solid (9 mg, 7%).

^{1}H NMR (300 MHz; $CDCl_3$): δ_H/ppm 9.64 (2 H, s, H_8), 8.58 (2 H, d, J = 5.1 Hz, H_1), 8.01 (2 H, d, J = 7.8 Hz, H_4), 7.89 (2 H, td, J = 7.4 Hz, H_3), 7.71 (2 H, d, J = 8.1 Hz), 7.32 (4 H, m), 6.71 (2 H, d, J = 1.5 Hz, H_7), 5.27 (1 H, s, H_{10}), 1.81 (6 H, s, H_9). **Acc-MS** (ASAP$^+$): *m/z* 654.1262 (M^+), calcd. for $^{191}IrC_{29}H_{23}N_2O_4$ 654.1264 ($\Delta m/z$| = 0.3 ppm). Analyses match those reported previously.[36]

Typical procedure for the synthesis of tris-heteroleptic complexes of the form [Ir(ppy)L′(acac)]

An adaption of the methods of Nonoyama et al.[33] and Sprouse et al.[34] for the synthesis of [{IrL$_2$(μ-Cl)}$_2$] species, followed by an adaption the method of Lamansky et al.[35] for the synthesis of [IrL$_2$(acac)] species.

$IrCl_3 \cdot 3H_2O$ (350 mg, 0.99 mmol) was dissolved in 2:1 2-ethoxyethanol:water (15 ml) with 2-phenylpyridine (0.23 ml, 1.5 mmol) and L′ (0.5 mmol) and the resultant solution was heated at 110 °C for 10 h. The reaction mixture was cooled to r.t. and water (25 ml) was added, affording a solid that was filtered, washed with water (2 x 5 ml), dissolved in CH_2Cl_2 (30 ml), dried over $MgSO_4$, filtered and reduced *in vacuo* to leave a yellow-brown or orange solid. Flash column chromatography (SiO_2; CH_2Cl_2/1 vol% EtOH) was

used to remove fore-running fractions from the mix of dimers. This crude mixture was dissolved in 2-ethoxyethanol (15 ml) with acetylacetone (0.1 ml, excess) and K_2CO_3 (100 mg) and heated at 65 °C for 1 h. Upon cooling to r.t., water (30 ml) was added giving a yellow suspension, which was filtered, washed with water (2 x 5 ml), dissolved in CH_2Cl_2, dried over $MgSO_4$, filtered and reduced in vacuo to leave an oily solid. This was triturated with hexanes (3 x 5 ml) to remove excess acacH and reduced in vacuo to leave a solid that was purified by column chromatography (see below). Yields are based on the functionalised 2-phenylpyridine ligand.

5.6.7. Acetylacetonato-κ^2*O,O′*-(2-(4′-(phenylethynyl)phenyl)pyridine-κ^2*N,C*$^{2′}$)-(2-phenylpyridine-κ^2*N,C*$^{2′}$) iridium(III): [Ir(2-(pep)py)(ppy)(acac)]

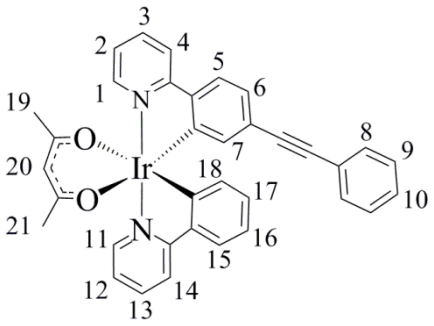

$C_{35}H_{27}IrN_2O_2$
M_r = 699.8

Column chromatography on silica gel (9:1 CH_2Cl_2:hexanes) afforded the title compound (24 mg, 7%) as a yellow solid.

^{1}H NMR (500 MHz; CD_2Cl_2): δ_H/ppm 8.51-8.48 (1 H, m, H_1 and H_{11}), 7.93-7.88 (2 H, m, H_4 and H_{14}), 7.83-7.78 (2 H, m, H_3 and H_{13}), 7.61 (1 H, d, J = 7.8 Hz, H_{15}), 7.57 (1 H, d, J = 8.0 Hz, H_5), 7.41-7.38 (2 H, m, H_8), 7.31-7.28 (3 H, m, H_9 and H_{10}), 7.25-7.20 (2 H, m, H_2 and H_{12}), 7.04 (1 H, dd, J = 8.0 and 1.5 Hz, H_6), 6.88-6.85 (1 H, m, H_{16}), 6.70 (1 H, ddd, J = 8.5, 7.6 and 1.2 Hz, H_{17}), 6.41 (1 H, d, J = 1.5 Hz, H_7), 6.21 (1 H, dd, J = 7.6 and 0.6 Hz, H_{18}), 5.29 (1 H, s, H_{20}), 1.97 (6 H, s, H_{19} and H_{21}). **Acc-MS** (ASAP$^+$): *m/z* 698.1678 (M^+), calcd. for $^{191}IrN_2O_2C_{35}H_{27}$ 698.1679 ($|\Delta m/z|$ = 0.1 ppm). **HPLC**: 100%.

5.6.8. Acetylacetonato-κ^2*O*,*O*′-(2,4-diphenylpyridine-κ^2*N*,*C*$^{2'}$)-(2-phenylpyridine-κ^2*N*,*C*$^{2'}$) iridium(III): [Ir(dppy)(ppy)(acac)]

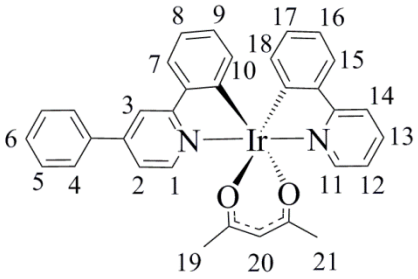

$C_{33}H_{27}IrN_2O_2$
M_r = 675.8

Column chromatography (SiO_2; CH_2Cl_2) afforded the title compound (25 mg, 7%) as a yellow solid.

^{1}H NMR (700 MHz; $CDCl_3$): δ_H/ppm 8.55-8.53 (2 H, m, H_1 and H_{11}), 8.05 (1 H, d, J = 2.0 Hz, H_3), 7.86 (1 H, d, J = 8.2 Hz, H_{14}), 7.80 (2 H, dd, J = 8.0 and 1.2 Hz, H_4), 7.74 (1 H, ddd, J = 8.2 and 7.5 Hz, H_{13}), 7.64 (1 H, d, J = 7.7 Hz, H_7), 7.58-7.54 (3 H, m, H_5 and H_{15}), 7.51-7.48 (1 H, m, H_6), 7.36 (1 H, dd, J = 5.9 and 2.0 Hz, H_2), 7.14 (1 H, ddd, J = 7.5, 5.7 and 1.4 Hz, H_{12}), 6.84-6.79 (2 H, m, H_8 and H_{16}), 6.72-6.68 (2 H, m, H_9 and H_{17}), 6.35 (1 H, dd, J = 7.7 and 0.9 Hz, H_{10}), 6.28 (1 H, d, J = 7.6 and 1.0 Hz, H_{18}), 5.23 (1 H, s, H_{20}), 1.80 (6 H, s, H_{19} and H_{21}). **Acc-MS** (ASAP$^+$): *m/z* 674.1695 (M^+), calcd. for $^{191}IrN_2O_2C_{33}H_{27}$ 674.1679 ($|\Delta m/z|$ = 2.4 ppm). **HPLC**: 98%.

5.6.9. Acetylacetonato-κ²*O*,*O*′-2-phenylpyridine-κ²*N*,*C*²′-(4-(2′-pyridyl)benzaldehyde-κ²*N*,*C*³′) iridium(III): [Ir(fppy)(ppy)(acac)]

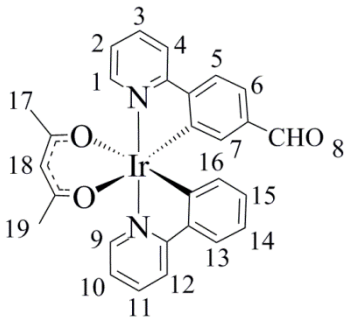

$C_{28}H_{23}IrN_2O_3$
M_r = 627.7

Column chromatography (SiO_2; CH_2Cl_2 / 2 vol% EtOH) afforded the title compound (33 mg, 11%) as a red solid. Red plate-habited crystals suitable for SC-XRD were grown by slow evaporation of a saturated MeCN solution.

^{1}H NMR (400 MHz; acetone-d_6): δ_H/ppm 9.65 (1 H, s, H_8), 8.65 (1 H, ddd, J = 5.7, 1.6 and 0.8 Hz, H_1), 8.58 (1 H, ddd, J = 5.7, 1.6 and 0.8 Hz, H_9), 8.28-8.25 (1 H, m, H_4), 8.14-8.10 (1 H, m, H_{12}), 8.03 (1 H, ddd, J = 8.2, 7.5 and 1.6 Hz, H_3), 7.97 (1 H, ddd, J = 8.2, 7.5 and 1.6 Hz, H_{11}), 7.88 (1 H, d, J = 8.0 Hz, H_5), 7.69-7.66 (1 H, m, H_{13}), 7.47 (1 H, ddd, J = 7.5, 5.7 and 1.4 Hz, H_2), 7.38 (1 H, ddd, J = 7.5, 5.7 and 1.4 Hz, H_{10}), 7.29 (1 H, dd, J = 8.0 and 1.5 Hz, H_6), 6.79 (1 H, d, J = 1.5 Hz, H_7), 6.77 (1 H, ddd, J = 7.7, 7.2 and 1.2 Hz, H_{14}), 6.62 (1 H, ddd, J = 7.6, 7.2 and 1.4 Hz, H_{15}), 6.18 (1 H, ddd, J = 7.6, 1.2 and 0.5 Hz, H_{16}), 5.30 (1 H, s, H_{18}), 1.72 (3 H, s, H_{17} or H_{19}), 1.71 (3 H, s, H_{17} or H_{19}). **Acc-MS** (ASAP$^+$): δ 626.1310 (M^+), calcd. for $^{191}IrN_2O_3C_{28}H_{23}$ 626.1315 ($|\Delta m/z|$ = 0.88 ppm). **HPLC**: 92%.

Crystal data (instrument **C**): $C_{28}H_{23}N_2O_3Ir$, (0.34 x 0.14 x 0.02) mm^3, ρ = 1.839 g cm^3, monoclinic, $P2_1/n$, Z = 4, a = 11.4809(3) Å, b = 9.6890(3) Å, c = 20.4035(6) Å, β = 92.427(1)°, V = 2267.6(1) Å^3, T = 120(2) K, μ(Mo K_α) = 5.922 mm^{-1}, 11138 reflections collected, 3271 independent (R_{int} = 0.0399), 2815 reflections with $I > 2\sigma(I)$, final R indices: wR_2 = 0.0729 (all data), R_1 = 0.0289 ($I > 2\sigma(I)$).

An alternative, one-pot method for the synthesis of [Ir(fppy)(ppy)(acac)] was also conducted. Thus, on the same scale, the diiridium μ-chloro-bridged dimer was produced by heating $IrCl_3 \cdot 3H_2O$ with a mixture of ppyH and fppyH ligands in aqueous

2-ethoxyethanol. After 4 h, acacH (10 eq.) and K_2CO_3 (10 eq.) were added to the mixture and heating was continued for a further 0.5 h. The mixture of products could be isolated by the same work-up as the two-step method. Column chromatography using the same solvent conditions as above gave material with identical analytical data. Although this method is quicker, it is easier to obtain material of higher purity using the two-step procedure.

5.6.10. 4-(Trimethylsilylethynyl)benzonitrile

Reported several times, including by Blackburn et al.,[37] who synthesised this compound in 96% yield by a similar method on a 340 mmol scale using [Pd(PPh$_3$)$_2$Cl$_2$] as catalyst.

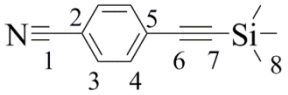

$C_{12}H_{13}NSi$
M_r = 199.3

The compound 4-bromobenzonitrile (5.14 g, 28 mmol) was dissolved in a mixture of NEt_3 (30 ml) and THF (20 ml). The solution was degassed by three freeze-pump-thaw cycles and back-filled with nitrogen. To this solution was added TMSA (4 ml, 29 mmol) and the solution was degassed one time further. The catalysts [Pd(PPh$_3$)$_4$] (280 mg, 1 mol%) and copper(I) iodide (50 mg, 1 mol%) were added under a stream of nitrogen and the solution was heated at 60 °C for 18 h, in which time the reaction mixture turned from yellow to black, with concomitant salt (NEt_3HBr) formation. The solvents were removed *in vacuo* and the residue was eluted through a short (*ca*. 5 cm) column (SiO_2; diethyl ether). The solvent was evaporated *in vacuo* to afford the title compound as a pale brown solid (5.67 g, 99%).

FT-IR (solid): $\tilde{\nu}_{max}$/cm^{-1} 2957 (w), 2235 (CN), 2158 (C≡C), 1603 (Ar), 1498 (Ar), 833 (s, Si-C). **Raman** (solid): $\tilde{\nu}_{max}$/cm^{-1} 2231 (CN), 2156 (C≡C), 1602 (w, Ar), 1176 (w). **^{1}H NMR** (400 MHz; $CDCl_3$): δ_H/ppm 7.58 (2 H, m, H_3), 7.52 (2 H, m, H_4), 0.26 (9 H, s, H_8). **GC-MS** (EI$^+$; 1 peak): *m*/*z* 199 (M^+), 20%), 184 ([M-Me]$^+$, 100). Analyses match those previously reported.[38]

5.6.11. 4-Ethynylbenzonitrile

Standard deprotection conditions as described by Wuts and Greene.[39]

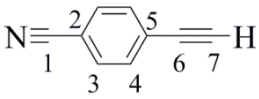

C_9H_5N
M_r = 127.1

The compound 4-(trimethylsilylethynyl)benzonitrile (1.11 g, 5.6 mmol) was dissolved in MeOH (50 ml), following which K_2CO_3 (300 mg) was added. The suspension was stirred for 4 h at r.t. The solvent was removed *in vacuo* and the residue was eluted through a short (*ca*. 5 cm) column (SiO_2; CH_2Cl_2). The fore-running fraction was collected and concentrated *in vacuo* to afford the title compound as a pale yellow solid (710 mg, 100%).

M.p. 139 °C (dec.) (from CH_2Cl_2), lit. 144-146 °C (from ethanol).[40] **FT-IR** (solid): $\tilde{\nu}_{max}$/cm^{-1} 3232 (s, alkyne CH), 3090 (w), 2229 (CN), 2105 (C≡C), 1927 (w), 1800 (w), 1677 (w), 1602, 1499. **Raman** (solid): $\tilde{\nu}_{max}$/cm^{-1} 2873 (w), 2228 (s, CN), 2199, 2104 (s, C≡C), 1601 (Ar), 1176. **^{1}H NMR** (400 MHz; $CDCl_3$): δ_H/ppm 7.62 (2 H, d, J = 8.2 Hz, H_3), 7.57 (2 H, d, J = 8.2 Hz, H_4), 3.30 (1 H, s, H_7). **^{13}C{^{1}H} NMR** (101 MHz; $CDCl_3$): δ_C/ppm 132.9 (C_3), 132.3 (C_4), 127.2 (C_5), 118.5 (C_1), 112.5 (C_2), 82.1 (C_6), 81.8 (C_7). **GC-MS** (EI$^+$; 1 peak): *m*/*z* 127 (M^+). Analyses match those previously reported.[38]

5.6.12. 2-Bromopyrene

Reported by Crawford et al.,[41] *who synthesised this compound in 54% yield (two steps) on the same scale by sequential regioselective borylation and bromination of pyrene.*

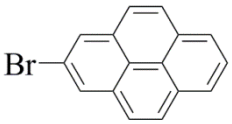

$C_{16}H_9Br$
M_r = 281.1

In a nitrogen filled glove box, pyrene (2.0 g, 9.9 mmol), B_2Pin_2 (2.5 g, 9.8 mmol), $([Ir(\mu\text{-OMe})(COD)]_2$ (60 mg, 1 mol%) and dtbpy (80 mg, 2 mol%) were dissolved in hexanes (15 ml) and 2-MeTHF (3 ml) and the solution was heated at 80 °C for 16 h.

The crude product was analysed by GC-MS, showing > 80% 2-(Bpin)pyrene with the remainder 2,7-bis(Bpin)pyrene and unreacted pyrene. The solvents were removed *in vacuo* and the crude mixture was dissolved in 1:1 (*v*/*v*) MeOH:water (100 ml) with $CuBr_2$ (6.50 g, 30 mmol, 3 eq.) and heated at 90 °C for 16 h. The solution was allowed to cool to r.t. before water (100 ml) was added to affect precipitation of a white solid that was collected by filtration. The crude product was recrystallised from hexanes to remove predominantly 2,7-dibromopyrene as a brown solid. The solution was reduced *in vacuo* and the solid was subjected to column chromatography (SiO_2; CH_2Cl_2) to give 2-bromopyrene as an off-white solid (1.26 g, 45%).

M.p. 125 °C (from CH_2Cl_2), lit. 125-126 °C (hexanes).[41] **FT-IR** (solid): ν_{max}/cm^{-1} 3049 (CH), 3035 (CH), 2968 (w), 1937, 117, 1876, 1800, 1749, 1665, 1628, 1600 (Ar), 1588 (s, Ar), 1428 (s), 1428 (s), 831 (s), 818 (s), 703 (s). **^{1}H NMR** (400 MHz; $CDCl_3$) 8.25 (s, 2 H), 8.18 (2 H, d, J = 8.0), 8.07 (2 H, d, J = 9.0 Hz), 8.02 (1 H, t, J = 8.0 Hz), 7.94 (2 H, d, J = 9.0 Hz). **^{13}C{^{1}H} NMR** (101 MHz; $CDCl_3$): δ_C/ppm 132.8, 130.9, 128.8, 127.2, 126.4 (2 C resolved), 126.0, 125.9, 125.1, 120.1. **GC-MS** (EI$^+$): *m/z* 280 (M^+, $C_{16}H_9{}^{79}Br$, 60%), 201.1 ([M-Br]$^+$, 70), 140 (15), 100.2 (100) with characteristic bromine isotope pattern. Analyses match those previously reported.[41]

5.6.13. 2-(2′-Pyridyl)pyrene: 2-pypyrH

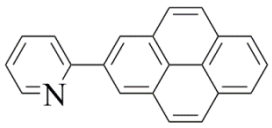

$C_{21}H_{13}N$
M_r = 279.3

The compounds 2-bromopyrene (383 mg, 1.36 mmol) and 2-(tri-*n*-butylstannyl)pyridine (90% purity, 0.50 ml, 570 mg, 1.54 mmol) were dissolved in toluene (10 ml) and degassed by three freeze-pump-thaw cycles. The catalyst [$Pd(PPh_3)_4$] (50 mg, 4 mol%) was added under a stream of nitrogen and the solution was heated at reflux (110 °C) for 20 h. The solution was allowed to cool to r.t., eluted through a short (*ca*. 5 cm) column (SiO_2; CH_2Cl_2) and the fore-running fraction reduced *in vacuo* to give a yellow oil. A diethyl ether solution (10 ml) of the crude product was purified by extraction with aqueous HCl (5 M, 3 ml) and water (20 ml). The aqueous layer was neutralised with K_2CO_3 and extracted with CH_2Cl_2 (30 ml). The organic layer was dried over anhydrous

K_2CO_3, filtered and concentrated *in vacuo* to give the title compound as a tan-brown solid (325 mg, 82%). Flash chromatography (SiO_2; CH_2Cl_2) could be used to remove a small quantity of a brown impurity, recovering the product as a cream white solid, which recolourised upon storage under air over a period of weeks. Single crystals suitable for X-ray diffraction were grown as colourless prisms by slow evaporation of a MeCN solution.

M.p. 138 °C (from CH_2Cl_2). **Elem. Anal.** Found C, 90.01; H, 4.70; N, 5.13. Calcd. for $C_{21}H_{13}N$: C, 90.29; H, 4.69; N, 5.01%. **FT-IR** (solid): $\tilde{\nu}_{max}$/cm^{-1} 3157 (w, br.), 3096 (w, CH), 3059 (CH), 3038 (CH), 3029 (CH), 3003 (CH), 2926 (br.), 1983, 1911, 1847, 1764, 1710, 1674, 1645, 1618 (Ar), 1585 (s, Ar), 1568 (s), 781 (s), 705 (s). **^{1}H NMR** (400 MHz; $CDCl_3$): δ_H/ppm 8.83 (1 H, d, J = 4.9 Hz), 8.80 (2 H, s), 8.14-8.20 (4 H, m), 8.09 (2 H, d, J = 8.8 Hz), 8.06 (1 H, d, J = 7.8 Hz), 8.0 (1 H, t, J = 7.8 Hz), 7.86 (1 H, td, J = 7.8 and 1.7 Hz), 7.29-7.34 (1 H, m). **^{13}C{^{1}H} NMR** (101 MHz; $CDCl_3$): δ_C/ppm 158.0, 150.1, 145.2, 137.3, 137.0, 131.8, 131.6, 128.0, 126.4, 125.4, 125.2, 124.8, 123.6, 122.6, 121.7. **Acc-MS** (ASAP$^+$): *m/z* 280.1126 ([M+H]$^+$), calcd. for $C_{21}H_{14}N$ 280.1126 ($|\Delta m/z|$ = 0.0 ppm).

Crystal data (Instrument **C**): $C_{21}H_{13}N$, (0.25 × 0.06 × 0.05) mm^3, ρ = 1.383 g cm^{-3}, monoclinic, $P2_1/c$, Z = 4, a = 4.5551(4) Å, b = 22.1192(19) Å, c = 13.390(2) Å, β = 96.148(12)°, V = 1341.3(3) Å^3, T = 120(2) K, μ(Mo Kα) = 0.080 mm^{-1}, 9403 reflections measured of which 2637 independent (R_{int} = 0.0383), 1628 reflections with $I > 2\sigma(I)$, final R indices: wR_2 = 0.0873 (all data), R_1 = 0.0444 ($I > 2\sigma(I)$).

5.6.14. Di-μ-chlorido-tetrakis(2-(2′-pyridyl)pyrenido-κ^2*N*,*C*$^{1'}$)diiridium(III): [{Ir(2-pypyr)$_2$(μ-Cl)}$_2$]

An adaption of the methods of Nonoyama et al.[33] *and Sprouse et al.*[34] *for the synthesis of [{IrL$_2$(μ-Cl)}$_2$] species.*

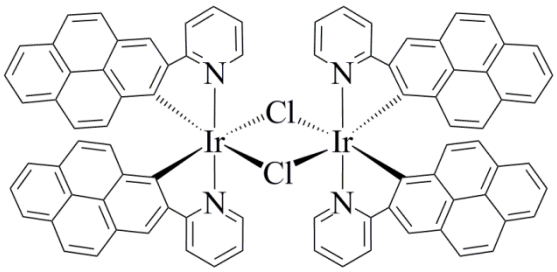

$C_{84}H_{48}Cl_2Ir_2N_4$
M_r = 1568.6

The compounds 2-pypyrH (217 mg, 0.78 mmol) and $IrCl_3 \cdot 3H_2O$ (138 mg, 0.39 mmol) were suspended in 2:1 (*v*/*v*) 2-ethoxyethanol:water (9 ml) and heated at reflux (110 °C) for 6 h, cooled to r.t. and stirred for a further 16 h, during which time the initially dark green solution turned orange. To the solution was added water (20 ml) and the resultant suspension was filtered. The obtained orange solid was washed with EtOH (3 x 10 ml) and dried under high vacuum to give a dark orange solid (199 mg, 65%). The compound is virtually insoluble, hindering purification and analysis.

5.6.15. Acetylacetonato-κ²*O*,*O′*-bis(2-(2′-pyridyl)pyrenido-κ²*N*,*C*¹′)iridium(III): [Ir(2-pypyr)$_2$(acac)]

An adaption the method of Lamansky et al.[35] *for the synthesis of [IrL$_2$(acac)] species*

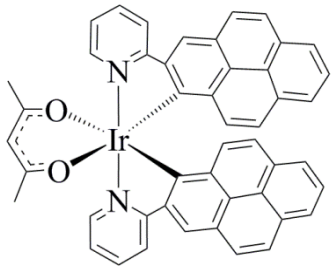

$C_{47}H_{31}IrN_2O_2$
M_r = 848.0

The compounds [{Ir(2-pypyr)$_2$(μ-Cl)}$_2$] (15 mg, 0.01 mmol), acetylacetone (0.05 ml, 0.5 mmol) and K_2CO_3 (50 mg) were suspended in a 1:1 (*v*/*v*) mixture of EtOH:acetone (10 ml) and heated at 60 °C for 4 h. The solution was allowed to cool to r.t. and reduced in volume *in vacuo* to an orange oil. The oil was triturated with hexanes (5 ml), affording a solid that was filtered, dissolved in CH_2Cl_2 and concentrated *in vacuo* to a dark orange-brown solid (14 mg, 83%). Single crystals suitable for X-ray diffraction were grown as orange needles by slow cooling of a CH_2Cl_2 solution.

Elem. Anal. Found C, 66.70; H, 3.67; N, 3.23. Calcd. for: $IrC_{47}H_{31}N_2O_2$: C, 66.57; H, 3.68; N, 3.30%. **^{1}H NMR** (400 MHz; $CDCl_3$): δ_H/ppm 8.64 (2 H, s), 8.44 (2 H, d, *J* = 8.0 Hz), 8.30 (2 H, d, *J* = 5.6 Hz), 8.01 (2 H, d, *J* = 9.0 Hz), 7.97 (2 H, td, *J* = 8.0 and 1.6 Hz), 7.83 (2 H, m), 7.79 (2 H, d, *J* = 9.0 Hz), 7.68 (2 H, s), 7.67 (2 H, d, *J* = 1.6 Hz), 7.14 (2 H, d, *J* = 9.0 Hz), 7.06 (2 H, td, *J* = 8.0 and 6.7 Hz), 6.74 (2 H, d, *J* = 9.0 Hz), 5.05 (1 H, s), 1.63 (6 H, s). **^{13}C{^{1}H} NMR** (176 MHz; $CDCl_3$): δ_C/ppm 185.0, 168.9, 150.6, 149.5, 144.9, 139.1, 137.6, 132.5, 132.3, 131.0, 128.2, 127.1, 125.8, 125.7, 125.3, 125.2, 125.0, 123.0 (2 C resolved by ^{1}H-^{13}C HSQC), 121.1, 120.5, 119.7, 100.0, 28.6. **Acc-MS** (ASAP$^+$): *m/z* 847.2073 ([M+H]$^+$), calcd. for $^{191}IrC_{47}H_{32}N_2O_2$ 847.2070 (|Δ*m/z* | = 0.3 ppm).

Crystal data (Instrument **B**): $IrC_{47}H_{31}N_2O_2$, (0.08 x 0.05 x 0.02) mm^3, ρ = 1.670 g cm^{-3}, monoclinic, *C*2/*c*, *Z* = 8, *a* = 42.7781(16) Å, *b* = 8.9946(3) Å, *c* = 18.0413(7) Å, β = 103.613(1)°, *V* = 6746.8(4) Å^3, *T* = 120(2) K, μ(Mo Kα) = 4.004 mm^{-1}, 13501

reflections measured of which 4214 independent (R_{int} = 0.1004), 2641 reflections with $I > 2\sigma(I)$, final R indices: wR_2 = 0.0539 (all data), R_1 = 0.0348 ($I > 2\sigma(I)$).

5.6.16. 1-Bromopyrene

Reported several times, including by Mitchell et al.,[42] *who synthesised this compound in 89% yield on a 1 mmol scale using a similar method.*

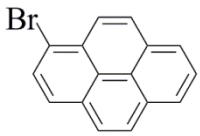

$C_{16}H_9Br$
M_r = 281.1

Under a nitrogen atmosphere, pyrene (2.03 g, 10 mmol) was dissolved in dry dimethylformamide (DMF) (13 ml) and the solution was transferred by cannula to a solution of *N*-bromosuccinimide (1.78 g, 10 mmol) in dry DMF (7 ml). The solution darkened immediately and was stirred at r.t. for 24 h. The solution was poured into water (100 ml) and the suspension was extracted with CH_2Cl_2 (3 x 30 ml). The combined organics were washed with water (3 x 30 ml), separated, dried over $MgSO_4$ and filtered. The solution was reduced *in vacuo* to a beige solid (2.23 g, 80%). ^{1}H NMR indicated exclusive monobromination, although traces of unsubstituted pyrene were still present (< 5% by GCMS), which were not separated further.

M.p. 97 °C (CH_2Cl_2), lit. 94 °C (unspecified).[42] **FT-IR** (solid): $\tilde{\nu}_{max}$/cm^{-1} 3035 (br., CH), 2970 (sh. CH), 1938, 1917, 1876, 1800 (w), 1748 (w), 1662 (w), 1638 (w), 1627 (w), 1600 (Ar), 1588 (Ar, 1544 (w), 832 (s), 818 (s), 752 (s), 704 (s). **^{1}H NMR** (400 MHz; $CDCl_3$): δ_H/ppm 8.40 (1 H, d, J = 5.3 Hz), 8.27 (1 H, d, J = 8.0 Hz), 8.19 (3 H, m), 8.10 (3 H, m), 8.05 (1 H, t, J = 8.0 Hz). **^{13}C{^{1}H} NMR** (101 MHz; $CDCl_3$): δ_C/ppm 159.7, 150.0, 136.6, 135.9, 131.6, 131.1, 128.8, 128.3, 128.1, 127.8, 127.7, 126.3, 126.0, 125.3, 125.0, 122.2. **GC-MS** (EI$^+$): *m/z* 280 (M^+, $C_{16}H_9{}^{79}Br$, 65%), 201.1 ([M-Br]$^+$), 60), 140 (15), 100.2 (100) with characteristic bromine isotope pattern. Analyses match those previously reported.[42]

5.6.17. 1-(2′-Pyridyl)pyrene: 1-pypyrH

Reported previously by Wu et al.,[43] who synthesised this compound in 47% yield on a 1.2 mmol scale by an alternative Suzuki-Miyaura coupling of 1-pyrenylboronic acid and 2-bromopyridine.

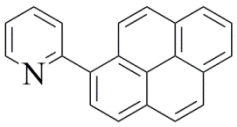

$C_{21}H_{13}N$
M_r = 279.3

The compounds 1-bromopyrene (283 mg, 1.0 mmol) and 2-(tri-*n*-butylstannyl)pyridine (90% purity, 0.40 ml, 450 mg, 1.2 mmol) were dissolved in toluene (7 ml). and degassed by three freeze-pump-thaw cycles. The catalyst $[Pd(PPh_3)_2Cl_2]$ (40 mg, 4 mol%) was added under a stream of nitrogen and the solution was heated at reflux (110 °C) for 20 h. After cooling to room temperature (r.t.), the solution was eluted through a short (*ca*. 5 cm) column (SiO_2; CH_2Cl_2) and reduced in volume *in vacuo* to a yellow oil. A diethyl ether solution (10 ml) of the crude product was purified by extraction with aqueous HCl (3 ml, 5 M) and water (20 ml). The aqueous layer was separated, neutralised with K_2CO_3 and subsequently re-extracted with CH_2Cl_2 (30 ml). The organic layer was dried over anhydrous K_2CO_3, filtered and concentrated *in vacuo* to give a cream white solid (196 mg, 70%). Single crystals suitable for X-ray diffraction were grown as colourless plates by slow evaporation of a CH_2Cl_2 solution. Upon storage under air for several weeks, the product turns dark yellow brown. Flash chromatography (SiO_2; CH_2Cl_2) can be used to remove the small quantity of brown impurity formed and recover the product as a cream white solid.

M.p. 87 °C (from CH_2Cl_2). **Elem. Anal.** Found: C, 90.11; H, 4.68; N, 5.09. Calcd. for $C_{21}H_{13}N$: C, 90.29; H, 4.69; N, 5.01%. **FT-IR** (solid): $\tilde{\nu}_{max}$/cm^{-1} 3073 (w, br., Ar) 3040 (Ar), 3023 (Ar), 2998 (br.), 2923 (br., C), 1901, 1853, 1811, 1762, 1692, 1584 (s, Ar), 1565 (s, Ar), 1537 (Ar), 1510 (Ar), 832 (s), 746 (s), 714 (s). **Raman** (solid): $\tilde{\nu}_{max}$/cm^{-1} 1629 (w, Ar), 1625 (s, Ar), 1597 (s, Ar), 1508 (Ar), 1414, 1387, 1277, 1264, 1238 (s). **^{1}H NMR** (400 MHz; $CDCl_3$): δ_H/ppm 8.89 (1 H, m), 8.40 (1 H, d, J = 5.3 Hz), 8.27 (1 H, d, J = 8.0 Hz), 8.19 (3 H, m), 8.10 (3 H, m), 8.05 (1 H, t, J = 8.0 Hz), 7.89 (1 H, m), 7.75 (1 H, m), 7.39 (1 H, m). **^{13}C{^{1}H} NMR** (101 MHz; $CDCl_3$): δ_C/ppm 159.7,

150.0, 136.6, 135.9, 131.6, 131.1, 128.8, 128.3, 128.1, 127.8, 127.7, 126.3, 126.0, 125.3, 125.0, 122.2. **GC-MS** (EI; 1 peak): *m/z* 279 (M^+). **Acc-MS** ($ASAP^+$): *m/z* 279.1038 (M^+), calcd. for $C_{21}H_{13}N$ 279.1048 ($|\Delta m/z|$ = 3.6 ppm). Analyses match those previously reported.[43]

Crystal data (Instrument **B**): $C_{21}H_{13}N$, (0.30 × 0.14 × 0.10) mm^3, ρ = 1.397 g cm^{-3}, monoclinic, $P2_1/c$, Z = 4, a = 3.8499(5) Å, b = 12.6863(15) Å, c = 27.185(3) Å, β = 90.715(5)°, V = 1327.6(3) $Å^3$, T = 120(2) K, μ(Mo Kα) = 0.081 mm^{-1}, 12745 reflections measured of which 3881 independent (R_{int} = 0.110), 1847 reflections with $I > 2\sigma(I)$, final R indices: wR_2 = 0.1398 (all data), R_1 = 0.0630 ($I > 2\sigma(I)$).

5.6.18. Di-μ-chlorido-tetrakis(1-(2′-pyridyl)pyrenido-$\kappa^2N,C^{2'}$)diiridium(III): [{Ir(1-pypyr)$_2$(μ-Cl)}$_2$]

An adaption of the methods of Nonoyama et al.[33] and Sprouse et al.[34] for the synthesis of [{IrL$_2$(μ-Cl)}$_2$] species.

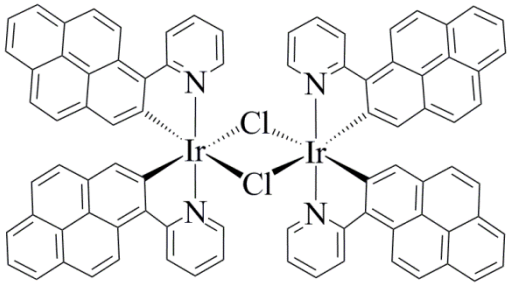

$C_{84}H_{48}Cl_2Ir_2N_4$
M_r = 1568.6

The compounds 1-pypyrH (57 mg, 0.20 mmol) and $IrCl_3 \cdot 3H_2O$ (35 mg, 0.10 mmol) were dissolved in trimethyl phosphate (4 ml) and heated at 90 °C for 36 h. The suspension was filtered and the orange solid was washed with EtOH and dried under high vacuum (58 mg, 75%). The compound is virtually insoluble, hindering purification and analysis.

5.6.19. Acetylacetonato-κ^2*O*,*O′*-bis(1-(2′-pyridyl)pyrenido-κ^2*N*,*C*$^{2′}$)iridium(III): [Ir(1-pypyr)$_2$(acac)]

An adaption of the method of Lamansky et al.[35] *for the synthesis of [IrL$_2$(acac)] species.*

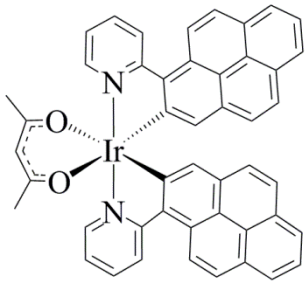

$C_{47}H_{31}IrN_2O_2$
M_r = 848.0

The compounds [{Ir(1-pypyr)$_2$(μ-Cl)}$_2$] (58 mg, 0.037 mmol), acetylacetone (0.05 ml, 0.5 mmol (excess)) and K_2CO_3 (50 mg) were suspended in a 1:1 (*v*/*v*) mixture of EtOH:acetone (10 ml) and heated at 60 °C for 4 h. The solution volume was reduced *in vacuo* to give an orange oil that was triturated with hexanes (5 ml), filtered, dissolved in CH_2Cl_2 and evaporated *in vacuo* to give a dark orange solid (27 mg, 87%). Single crystals of the CH_2Cl_2 monosolvate suitable for X-ray diffraction were grown as red plates by slow cooling of a CH_2Cl_2 solution.

^{1}H NMR (700 MHz; $CDCl_3$): δ_H/ppm 8.89 (2 H, d, *J* = 9.4 Hz), 8.76 (4 H, m), 8.08 (2 H, d, *J* = 9.4 Hz), 8.04 (2 H, d, *J* = 7.5 Hz), 7.97 (2 H, td, *J* = 7.9 and 1.3 Hz), 7.92 (2 H, d, *J* = 7.5 Hz), 7.79 (2 H, t, *J* = 7.5 Hz), 7.70 (2 H, d, *J* = 8.9 Hz), 7.41 (2 H, d, *J* = 8.9 Hz), 7.29 (2 H, m), 6.87 (2 H, s), 5.32 (1 H, s), 1.82 (6 H, s). **^{13}C{^{1}H} NMR** (151 MHz; $CDCl_3$): δ_C/ppm 185.1, 169.4, 149.3, 148.6, 139.3, 137.0, 131.4, 130.4, 130.2, 129.4, 128.8, 128.4, 128.0, 127.3, 125.8, 125.6, 125.1, 124.4, 123.7, 122.6, 122.4, 121.3, 100.8, 28.9. **Acc-MS** (ASAP$^+$): *m/z* 847.2026 ([M+H]$^+$), calcd. for $^{191}IrC_{47}H_{32}N_2O_2$ 847.2070 (|Δ*m/z*| = 5.2 ppm). Satisfactory elementary analysis data (low %C) for this isomer could not be obtained, attributable to non-stoichiometric loss of CH_2Cl_2 from the crystal lattice. This is supported by the traces of residual CH_2Cl_2 (*ca.* 0.4 eq. by integration) observable in the ^{1}H NMR spectrum of a vacuum dried sample and the single crystal X-ray structure, which is that of a CH_2Cl_2 monosolvate when freshly removed from the mother liquor. **Elem. Anal.** calcd for: $IrC_{47}H_{31}N_2O_2$:

C, 66.57; H, 3.68; N, 3.30 and for $IrC_{47}H_{31}N_2O_2 \cdot 0.4CH_2Cl_2$: C, 64.53; H, 3.64; N, 3.18. Found C, 64.79; H, 3.64; N, 3.15%

Crystal data (Instrument **B**): $IrC_{47}H_{31}N_2O_2 \cdot CH_2Cl_2$, (0.08 x 0.08 x 0.02) mm^3, ρ = 1.712 g cm^{-3}, orthorhombic, *Pbcn*, Z = 4, a = 7.8382(3) Å, b = 22.5797(8) Å, c = 20.4029(7) Å, V = 3611.0(2) $Å^3$, T = 120(2) K, μ(Mo Kα) = 3.892 mm^{-1}, 16957 reflections measured of which 2603 independent (R_{int} = 0.0865), 1702 reflections with $I > 2\sigma(I)$, final R indices: wR_2 = 0.1040 (all data), R_1 = 0.0386 ($I > 2\sigma(I)$).

5.6.20. 4-(Trimethylsilylethynyl)anisole

Reported several times, including by Van Overmeire et al.,[44] who synthesised this compound in quantitative yield by a similar method on a 21 mmol scale using [Pd(PPh$_3$)$_2$Cl$_2$] as catalyst.

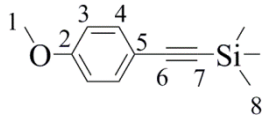

$C_{12}H_{16}OSi$
M_r = 204.3

The compound 4-iodoanisole (5.75 g, 24.6 mmol) was dissolved in a mixture of triethylamine (NEt_3) (30 ml) and THF (20 ml). The solution was then degassed by three freeze-pump-thaw cycles and back-filled with nitrogen. To this solution was added trimethylsilylacetylene (TMSA) (3.5 ml, 25 mmol) and the solution was degassed one time further. The catalysts [$Pd(PPh_3)_4$] (275 mg, 1 mol%) and CuI (50 mg, 1 mol%) were added to the solution under a stream of nitrogen and the solution was heated at 65 °C for 4.5 h, in which time the solution turned from yellow to green to black, with concomitant salt (NEt_3HI) formation. The solvents were removed *in vacuo* and the residue was eluted through a short (*ca*. 5 cm) column (SiO_2; 1:1 (*v*/*v*) hexanes:diethyl ether) and then reduced *in vacuo* to an orange oil. Trituration with hexanes produced a small amount of a solid impurity that was filtered off. The solution was reduced *in vacuo* to afford the title compound as a yellow-orange oil (5.0 g, 98%).

^{1}H NMR (400 MHz; $CDCl_3$): δ_H/ppm 7.40 (2 H, d, J = 8.6 Hz, H_4), 6.81 (2 H, d, J = 8.6 Hz, H_3), 3.79 (3 H, s, H_1), 0.24 (9 H, s, H_8). **^{13}C{^{1}H} NMR** (101 MHz; $CDCl_3$): δ_C/ppm 159.9 (C_2), 133.7 (C_4), 115.1 (C_5), 113.7 (C_3), 105.4 (C_6), 92.6 (C_7), 55.4 (C_1),

0.3 (C_8). **GC-MS** (EI^+; 1 peak): *m*/*z* 204 (M^+). Analyses match those previously reported.[45]

5.6.21. 4-(4′-Methoxyphenylethynyl)pyridine

Reported several times, including by Elangovan et al.,[37] who synthesised this compound in 86% yield (two steps) by deprotection of 4-(trimethylsilylethynyl)anisole using TBAF and Sonogashira coupling with 4-bromopyridine hydrochloride using [Pd(PPh$_3$)$_2$Cl$_2$] as catalyst under a H$_2$/N$_2$ atmosphere.

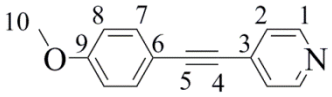

$C_{14}H_{11}NO$
M_r = 209.2

The compounds 4-(trimethylsilylethynyl)anisole (1.04 g, 5.1 mmol), 4-bromopyridine hydrochloride (923 mg, 4.7 mmol) and K_2CO_3 (400 mg) were dissolved in a 1:1:2 (*v*/*v*/*v*) mixture of MeOH, NEt_3 and MeCN (40 ml). The solution was degassed by three freeze-pump-thaw cycles and back-filled with nitrogen. The catalysts [Pd(PPh_3)$_4$] (55 mg, 1 mol%) and copper(I) iodide (10 mg, 1 mol%) were added to the solution under a stream of nitrogen and the solution was heated at 60 °C for 20 h, in which time the solution turned from yellow to brown with concomitant salt (NEt_3HBR) formation. The solvents were removed *in vacuo* and the residue was eluted through a short (*ca*. 5 cm) column (SiO_2; diethyl ether). The solution was then reduced *in vacuo* to afford a yellow solid. A diethyl ether solution (15 ml) of the crude product was extracted with aqueous HCl (5 M, 5 ml) and water (15 ml). The separated aqueous layer was neutralised with K_2CO_3, and re-extracted with CH_2Cl_2 (3 x 10 ml). The solution was dried over anhydrous K_2CO_3, filtered and reduced *in vacuo* to afford the title compound as a yellow solid (800 mg, 75%).

^{1}H NMR (400 MHz; $CDCl_3$): δ_H/ppm 8.57 (2 H, d, J = 6.4 Hz, H_1), 7.48 (2 H, d, J = 9.6 Hz, H_7), 7.35 (2 H, d, J = 6.4 Hz, H_2), 6.89 (2 H, d, J = 9.6 Hz, H_8), 3.83 (3 H, s, H_{10}). **^{13}C{^{1}H} NMR** (101 MHz; $CDCl_3$): δ_C/ppm 160.4 (C_9), 150.0 (C_1), 133.7 (C_7), 132.0 (C_6), 125.6 (C_2), 114.4 (C_8 and C_6), 96.2 (C_5), 86.8 (C_4), 55.6 (C_{10}). Analyses match those previously reported.[45]

5.6.22. 2-Phenyl-4-(4′-methoxyphenylethynyl)pyridine

Adaption of the phenylation conditions described for the synthesis of 2-phenylpyridine, using commercial phenyllithium solution.[32]

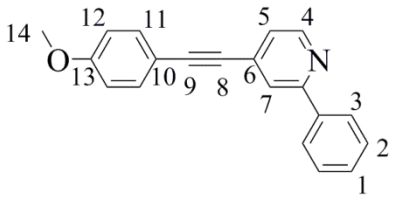

$C_{20}H_{15}NO$
M_r = 285.3

In a nitrogen-filled two-neck flask, the compound 4-(4′-methoxyphenylethynyl)pyridine (390 mg, 1.9 mmol) was dissolved in dry toluene (10 ml). The solution was cooled to 0 °C and phenyllithium (1.8 M in dibutyl ether, 1.1 ml, 2 mmol) was added slowly. The solution was stirred at this temperature for 1 h before being warmed to r.t. To quench the reaction, water (10 ml) was cautiously added and the resultant solution was stirred for 10 min. The organic layer was separated and the aqueous layer was extracted with CH_2Cl_2 (3 x 10 ml). The combined organics were concentrated *in vacuo* to a brown solid. Column chromatography (SiO_2; CH_2Cl_2 to 9:1 (*v*/*v*) CH_2Cl_2:EtOH) yielded a yellow oil that solidified upon standing to a yellow solid. Recrystallisation from hexanes afforded the title compound as yellow-brown spherulites of needle-habited crystals (98 mg, 18%). Single crystals suitable for X-ray diffraction were grown as colourless prisms by slow evaporation of a CH_2Cl_2 solution.

Raman (solid): $\tilde{\nu}_{max}$/cm^{-1} 3067 (w, CH), 2222 (sh.), 2197 (s, C≡C), 1600 (Ar), 1584 (Ar), 1291, 1274, 1251, 1212, 1183 (w), 1167 (w), 1134 (s), 1023, 999 (s), 982 (s), 745 (s). **^{1}H NMR** (400 MHz; $CDCl_3$): δ_H/ppm 8.67 (1 H, m, C_4), 8.01 (2 H, dd, J = 8.8 and 1.2 Hz, H_3), 7.83 (1 H, t, J = 0.8 Hz, H_7), 7.60 (1 H, m, H_1), 7.50 (4 H, m, H_2 and H_{11}), 7.30 (1 H, m, H_5), 6.91 (2 H, d, J = 8.8 Hz, H_{12}), 3.26 (3 H, s, H_{14}). **Acc-MS** (ASAP$^+$): *m/z* 285.1140 (M^+), calcd. for $C_{20}H_{15}NO$ 285.1154 ($|\Delta m/z|$ = 4.9 ppm).

Crystal data (Instrument **B**): $C_{20}H_{15}NO$, (0.38 x 0.32 x 0.02) mm^3, ρ = 1.270 g cm^{-3}, monoclinic, $P2_1$, Z = 2, a = 6.0534(6) Å, b = 7.7058(8) Å, c = 16.123(2) Å, β = 97.249(3)°, V = 746.1(1) Å^3, T = 120(2) K, μ(Mo Kα) = 0.078 mm^{-1}, 3765

reflections measured of which 2113 independent (R_{int} = 0.0209), 1837 reflections with $I > 2\sigma(I)$, final R indices: wR_2 = 0.0891 (all data), R_1 = 0.0326 ($I > 2\sigma(I)$).

5.6.23. 4-(4′-*tert*-Butylphenylethynyl)phenylacetylene

Standard deprotection conditions as described by Wuts and Greene.[39]

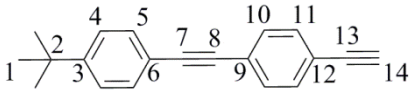

$C_{20}H_{18}$
M_r = 258.4

The compound (4-(4′-*tert*-butylphenylethynyl)phenylethynyl)trimethylsilane (810 mg, 2.5 mmol) was dissolved in MeOH (30 ml) with K_2CO_3 (0.5 g) and stirred at r.t. for 16 h. The solvent was removed *in vacuo* to afford the crude product as a dark brown solid. The crude material was purified by column chromatography (SiO_2: 2:1 (*v*/*v*) hexanes:CH_2Cl_2) to afford the title compound from the fore-running fraction as a white solid (300 mg, 47%).

^{1}H NMR (700 MHz; $CDCl_3$): δ_H/ppm 7.39 (6 H, m, H_5, H_{10} and H_{11}), 7.30 (2 H, d, J = 8.5 Hz, H_4), 3.09 (1 H, s, H_{14}), 1.26 (9 H, s, H_1). **^{13}C{^{1}H} NMR** (176 MHz; $CDCl_3$): δ_C/ppm 151.8 (C_3), 132.0, 131.4, 131.3, 125.4, 124.0, 121.6, 119.9, 91.6 (C≡C), 88.2 (C≡C), 83.3 (C≡C), 78.7 (C_{14}), 34.8 (C_2), 31.1 (C_1).

5.6.24. 4-(4′-(4′′-*tert*-Butylphenylethynyl)phenylethynyl)pyridine: tBu-pepepy

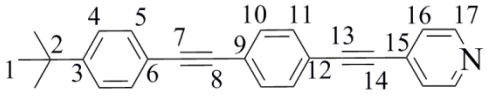

$C_{25}H_{21}N$
M_r = 335.4

The compounds 4-(4′-*tert*-butylphenylethynyl)phenylacetylene (258 mg, 1.0 mmol) and 4-bromopyridine hydrochloride (190 mg, 0.97 mmol) were suspended in 2:1 (*v*/*v*) MeCN:NEt_3 (45 ml) and degassed by three evacuation and nitrogen purge cycles with rapid stirring. The catalysts [$Pd(PPh_3)_4$] (20 mg, 1.7 mol%) and CuI (6 mg, 3 mol%) were added under a stream of nitrogen and the solution was heated at 65 °C for 5 h, allowed to cool to r.t. and stirred for a further 16 h. The solvents were removed *in vacuo*

and the crude solid eluted through a short (*ca*. 5 cm) column (SiO_2; diethyl ether). The eluate was reduced to *ca*. 20 ml and HCl (12 M, 0.3 ml) was added, causing the precipitation of a hygroscopic salt. The diethyl ether layer was separated and the salt was washed with further portions of diethyl ether (2 x 5 ml). To the salt was added CH_2Cl_2 (20 ml) and solid K_2CO_3 was used to produce the free-base pyridine. The solvent was removed *in vacuo* affording the title compound as a pale yellow solid (280 mg, 86%).

FT-IR (solid): $\tilde{\nu}_{max}/cm^{-1}$ 2954 (CH), 2869 (CH, 2212 (C≡C), 1895 (br.), 1827 (br.), 1707 (br.), 1588 (Ar), 1516 Ar), 830 (s), 809 (s), 669 (s). **Raman** (solid): $\tilde{\nu}_{max}/cm^{-1}$ 2210 (s, C≡C), 2173, 1591 (s, Ar), 1500 (w, Ar), 1177 (w), 1130, 1102, 976. **^{1}H NMR** (400 MHz; $CDCl_3$): δ_H/ppm 8.62 (2 H, d br., J = 4.5 Hz, H_{17}), 7.53 (4 H, s, H_{10} and H_{11}), 7.47 (2 H, dt, J = 8.3 and 1.9 Hz), 7.42 (2 H, dd, J = 4.5 and 1.5 Hz, H_{16}), 7.38 (2 H, dt, J = 8.3 and 1.9 Hz), 1.33 (9 H, s, H_1). **^{13}C{^{1}H} NMR** (176 MHz; $CDCl_3$): δ_C/ppm 152.2 (C_3), 149.6 (C_{17}), 132.0, 131.8 (2 C resolved), 131.6, 125.8, 125.6, 124.7, 121.6, 120.0, 94.2 (C_{13}), 92.3 (C_8), 88.4 (C_7), 88.3 (C_{14}), 35.0 (C_2), 31.3 (C_1). **Acc-MS** (ESI^+): *m*/*z* 336.1748 (M^+), calcd. for $C_{25}H_{22}N$ 336.1752 ($|\Delta m/z|$ = 1.2 ppm).

5.6.25. 4-(Triisopropylsilylethynyl)pyridine: 4-TIPSepy

An adaption of the method of Zeidan et al.[46] for the synthesis of 4-(trimethylsilylethynyl)pyridine.

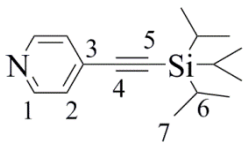

$C_{16}H_{25}NSi$
M_r = 259.5

The salt 4-bromopyridine hydrochloride (1.95 g, 10 mmol) was suspended in THF (20 ml) and NEt_3 (10 ml) and degassed by three evacuation and nitrogen purge cycles with rapid stirring. To the solution was added (triisopropylsilyl)acetylene (2.4 ml, 2.0 g, 11 mmol) and the mixture was degassed a further time. The catalysts [$Pd(PPh_3)_4$] (115 mg, 1 mol%) and CuI (40 mg, 2 mol%) were added under a stream of nitrogen to the solution and the reaction was stirred for 22 h at r.t, during which time the solution darkened, with concomitant salt (NEt_3HBr) formation. The solvents were removed *in*

vacuo. To the residue was added diethyl ether (20 ml) and the resultant suspension filtered. The filtrate was reduced *in vacuo* and the crude material was purified by column chromatography (SiO_2; CH_2Cl_2 to 3:1 (*v*/*v*) CH_2Cl_2:EtOH) to yield the title compound as a yellow oil (1.92 g, 75%) from the fore-running fraction.

^{1}H NMR (400 MHz; $CDCl_3$): δ_H/ppm 8.55 (2 H, dd, J = 4.3 and 1.6 Hz, H_1), 7.31 (2 H, dd, J = 4.3 and 1.6 Hz, H_2), 1.13 (21 H, m, H_6 and H_7). **^{13}C{^{1}H} NMR** (101 MHz; $CDCl_3$): δ_C/ppm 150.9 (C_1), 133.1 (C_3), 127.5 (C_2), 95.0 (C_5), 86.5 (C_4), 18.7 (C_7), 11.2 (C_6). **Acc-MS** (ESI^+): *m/z* 260.1823 ($[M+H]^+$), calcd. for $C_{16}H_{26}NSi$ 260.1835 ($|\Delta m/z|$ = 4.6 ppm).

5.6.26. Di-μ-iodido-tetrakis(4-((triisopropylsilyl)ethynyl)pyridine-κ*N*)-dicopper(I): [{Cu(TIPSepy)$_2$(μ-I)}$_2$]

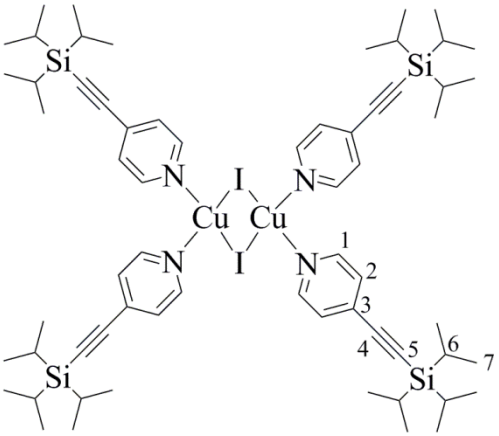

$C_{64}H_{100}Cu_2I_2N_4Si_4$
M_r = 1418.8

Also isolated from the above reaction, as the second fraction from the column, was the title copper(I) complex as a bright yellow solid (58 mg, 41% based on CuI). Single crystals suitable for X-ray diffraction were grown as yellow prisms by slow evaporation of a CH_2Cl_2 solution.

M.p. 131 °C (from CH_2Cl_2). **FT-IR** (solid): $\tilde{\nu}_{max}$/cm^{-1} 3075 (s, Ar), 3028 (vw, CH), 2942 (s, CH), 2894 (s, CH), 2163 (w, C≡C), 2067 (vw), 1945 (vw), 1691 (v), 1598 (s, Ar), 1207 (s), 827 (s), 664 (s). **Raman** (solid, 633 nm): $\tilde{\nu}_{max}$/cm^{-1} 2861 (w, CH), 2160 (s, C≡C), 1595 (s, Ar), 1207 (s), 1009 (s). **^{1}H NMR** was too broad and variable to give reliable data. **MS** gave only ligand fragments by MALDI, ASAP and ESI.

Crystal data (Instrument **C**): $C_{64}H_{100}Cu_2I_2N_4Si_4$, (0.44 x 0.08 x 0.05) mm^3 ρ = 1.310 g cm^{-3}, monoclinic, $P2_1/c$, Z = 2, a = 16.045(1) Å, b = 7.6568(6) Å, c = 29.281(2) Å, β = 91.777(6)°, V = 3595.5(4) $Å^3$, T = 120(2) K, μ(Mo Kα) = 1.554 mm^{-1}, 35244 reflections measured, 12031 independent (R_{int} = 0.1279), 6106 reflections with $I > 2\sigma(I)$, final R indices: wR_2 = 0.2537 (all data), R_1 = 0.0861 ($I > 2\sigma(I)$).

5.6.27. 2-Phenyl-4-((triisopropylsilyl)ethynyl)pyridine: 2-P-4-TIPSepyH

Adaption of the phenylation conditions described for the synthesis of 2-phenylpyridine, using commercial phenyllithium solution.[32]

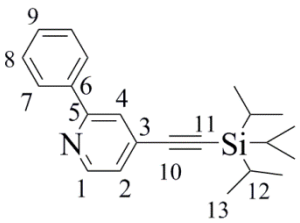

$C_{22}H_{29}NSi$
M_r = 335.6

The compound 4-TIPSepy (800 mg, 3.1 mmol) was dissolved in dry toluene (30 ml) under nitrogen. To the solution was added phenyllithium (5.5 ml, 1.8 M solution in dibutyl ether, 9.9 mmol). The solution was stirred for 5 h at r.t., in which time it turned from yellow to brown to black. To quench the reaction, water (20 ml) was cautiously added and stirred vigorously for 5 min, at which point the solution turned pale yellow-brown. The organic layer was separated and washed with water (2 x 20 ml). The organic layer was dried over K_2CO_3, filtered and reduced *in vacuo* to a brown oil. The crude material was purified by column chromatography (SiO_2; CH_2Cl_2) to obtain the title compound as an orange-brown oil (550 mg, 53%).

^{1}H NMR (400 MHz; $CDCl_3$): δ_H/ppm 8.64 (1 H, dd, J = 5.1 and 0.9 Hz, H_1), 7.98 (2 H, m, H_7), 7.75 (1 H, dd, J = 1.5 and 0.9 Hz, H_4), 7.51-7.41 (3 H, m, H_8 and H_9), 7.26 (1 H, dd, J = 5.1 and 1.5 Hz, H_2), 1.13-1.17 (21 H, m, H_{12} and H_{13}). **^{13}C{^{1}H} NMR** (101 MHz; $CDCl_3$): δ_C/ppm 157.8 (C_5), 149.8 (C_1), 139.0 (C_6), 132.4, 129.5 (C_9), 129.0 (C_8), 127.2 (C_7), 124.5 (C_2), 123.1 (C_4), 104.6, 96.6, 18.9 (C_{13}),11.4 (C_{12}). **Acc-MS** (ESI^+): *m/z* 336.2149 ($[M+H]^+$), calcd. for $C_{22}H_{30}NSi$ 336.2148 ($|\Delta m/z|$ = 0.3 ppm).

5.6.28. Di-μ-chlorido-tetrakis(2-phenyl-4-((triisopropylsilyl)ethynyl)pyridine-$\kappa^2C^{2'},N$)diiridium(III): [{Ir(2-p-4-TIPSepy)$_2$(μ-Cl)}$_2$]

An adaption of the methods of Nonoyama et al.[33] *and Sprouse et al.*[34] *for the synthesis of [{IrL$_2$(μ-Cl)}$_2$] species.*

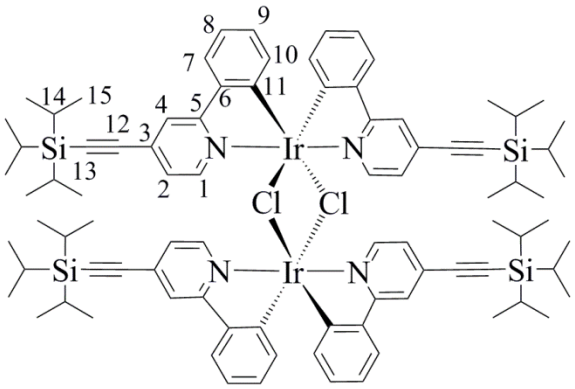

$C_{88}H_{112}Cl_2Ir_2N_4Si_4$
M_r = 1793.5

The compounds 2-p-4-TIPSepyH (550 mg, 1.64 mmol) and $IrCl_3 \cdot 3H_2O$ (277 mg, 0.78 mmol) were suspended in a 2:1 (*v*/*v*) mixture of 2-ethoxyethanol and water (9 ml) and heated at 110 °C for 6 h. During this time, the solution turned from pale yellow to dark orange. The solution was allowed to cool to r.t. and water (20 ml) was added to precipitate a bright orange solid that was filtered, washed with water (2 x 10 ml), dissolved in CH_2Cl_2 (20 ml), dried over $MgSO_4$, filtered and reduced *in vacuo* to an orange oily solid. The crude material was triturated with hexanes (5 ml) and then cold EtOH (5 ml) to remove excess ligand and dried *in vacuo*, affording the title compound as a bright orange solid (579 mg, 83%).

^{1}H NMR (500 MHz; $CDCl_3$): δ_H/ppm 9.14 (4 H, d, J = 5.9 Hz, H_1), 7.88 (4 H, d, J = 1.3 Hz, H_4), 7.48 (4 H, dd, J = 7.8 and 0.8 Hz, H_7), 6.85 (4 H, dd, J = 5.9 and 1.7 Hz, H_2), 6.75 (4 H, td, J = 7.5 and 0.8 Hz, H_8), 6.60 (4 H, td, J = 7.5 and 1.2 Hz, H_9), 5.90 (4 H, d, J = 8.0 Hz, H_{10}), 1.23 (84 H, m, H_{14} and H_{15}). **^{13}C{^{1}H} NMR** (126 MHz; $CDCl_3$): δ_C/ppm 168.5 (C_3), 151.9 (C_1), 145.5, 143.1, 132.1, 130.7, 129.7 (C_9), 124.1 (C_7), 123.7, 121.9, 121.7, 104.0 (C_{12}), 99.5 (C_{13}), 19.0 (C_{15}), 11.6 (C_{14}). **Acc-MS** (ASAP$^+$): *m/z* 894.3276 ([M/2]$^+$), calcd. for $C_{44}H_{56}N_2Si_2Cl^{191}Ir$ 894.3277 ($|\Delta m/z|$ = 0.1 ppm).

5.6.29. Acetylacetonato-κ^2*O*,*O′*-bis(2-phenyl-4-((triisopropylsilyl)ethynyl)-pyridine-κ^2*C*$^{2′}$,*N*)iridium(III): [Ir(2-p-4-TIPSepy)$_2$(acac)]

An adaption of the method of Lamansky et al.[35] *for the synthesis of [IrL$_2$(acac)] species.*

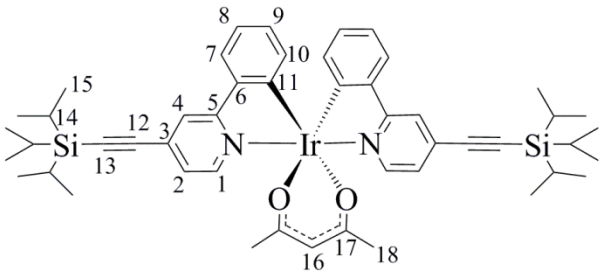

$C_{49}H_{63}IrN_2O_2Si_2$
M_r = 960.4

The compound [{Ir(2-p-4-TIPSepy)$_2$(μ-Cl)}$_2$] (100 mg, 56 μmol) was dissolved in a 1:1 (*v*/*v*) mixture of acetone and EtOH (15 ml). Acetylacetone (0.5 ml, excess) and K_2CO_3 (250 mg) were added and the suspension was heated at 65 °C for 30 min. The solvents were removed *in vacuo* and the residue was triturated with hexanes (5 ml) to remove excess acetylacetone. The resultant solid was purified by column chromatography (SiO_2: 2:1 (*v*/*v*) hexanes:CH_2Cl_2) to give the title compound from the second fraction as a bright orange solid (88 mg, 82%). Single crystals of the MeCN 0.25-solvate suitable for X-ray diffraction were grown as red prisms by slow evaporation of a MeCN solution.

FT-IR (solid): $\tilde{\nu}_{max}$/cm^{-1} 3060 (w, CH), 2941 (CH), 2864 (CH), 2164 (w, C≡C), 1606 (w, Ar), 1577 (Ar), 1521 (s, Ar), 1401 (s), 880 (s), 670 (s). **^{1}H NMR** (600 MHz; $CDCl_3$): δ_H/ppm 8.42 (2 H, d, *J* = 6.0 Hz, H_1), 7.85 (2 H, d, *J* = 1.7 Hz, H_4), 7.55 (2 H, dd, *J* = 7.7 and 1.1 Hz, H_7), 7.14 (2 H, dd, *J* = 6.0 and 1.7 Hz, H_2), 6.82 (2 H, td, *J* = 7.7 and 1.1 Hz, H_8), 6.71 (2 H, td, *J* = 7.7 and 1.1 Hz, H_9), 6.28 (2 H, dd, *J* = 7.7 and 1.1 Hz, H_{10}), 5.18 (1 H, s, H_{16}), 1.77 (6 H, s, H_{18}), 1.18 (42 H, m, H_{14} and H_{15}). **^{13}C{^{1}H} NMR** (151 MHz; $CDCl_3$): δ_C/ppm 184.9 (C_{17}), 168.5 (C_3), 147.8 (C_1), 144.1, 133.3 (C_{10}), 132.3, 129.5 (C_9), 124.2, 124.0, 121.1 (C_8), 120.8 (C_4), 104.0 (C_{16}), 101.0 (C_{12}), 98.9 (C_{13}), 28.9 (C_{18}), 18.8 (C_{14}), 11.4 (C_{15}). **Acc-MS** (ASAP$^+$): *m/z* 958.4045 ([M+H]$^+$), calcd. for $C_{49}H_{63}N_2O_2Si_2{}^{191}Ir$ 958.4034 (|Δ*m*/*z*| = 1.1 ppm).

Crystal data (Instrument **C**): $C_{49}H_{63}IrN_2O_2Si_2$·0.25(C_2H_3N), (0.57 x 0.23 x 0.15) mm^3, ρ = 1.320 g cm^{-3}, monoclinic, $P2_1/c$, *Z* = 8, *a* = 13.6621(4) Å, *b* = 23.3864(7) Å,

c = 30.7984(8) Å, β = 97.340(3)°, V = 9759.6(5) Å^3, T = 120(2) K, μ(Mo Kα) = 2.823 mm^{-1}, 56023 reflections measured, 21014 independent (R_{int} = 0.1116), 11271 reflections with $I > 2\sigma(I)$, final R indices: wR_2 = 0.1924 (all data) and R_1 = 0.0754 ($I > 2\sigma(I)$).

5.6.30. Acetylacetonato-κ^2*O*,*O′*-bis(2-phenyl-4-ethynylpyridine-κ^2*C*$^{2′}$,*N*)-iridium(III): [Ir(2-p-4-epy)$_2$(acac)]

Standard deprotection conditions as described by Wuts and Greene.[39]

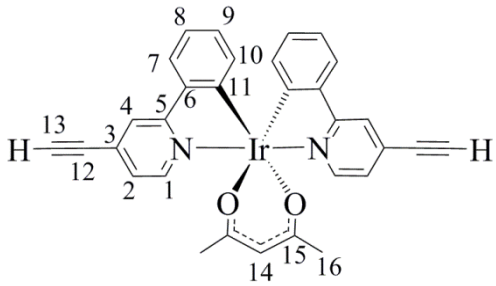

$C_{31}H_{23}IrN_2O_2$
M_r = 647.7

The compound [Ir(2-p-4-TIPSepy)$_2$(acac)] (20 mg, 0.03 mmol) was dissolved in dry THF (5 ml) with activated molecular sieves (4 Å) under an atmosphere of nitrogen. To the solution was cautiously added tetra-*n*-butylammonium fluoride (TBAF) (0.1 ml, 1 M solution in THF, 0.1 mmol), causing the solution to darken immediately. The solution was stirred at r.t. for 16 h, followed by removal of the solvent *in vacuo* and purification by column chromatography (SiO_2; CH_2Cl_2) to give the title compound as an orange solid (17 mg, 87%). **CAUTION:** The solution should not be heated above r.t. to remove the solvent as this causes extensive decomposition once dry. The deprotection can be monitored by TLC ([(SiO_2; 2:1 (*v*/*v*) CH_2Cl_2:hexanes): R_f (starting material) = 0.26 (orange emission, λ_{em} = 365 nm), R_f (product) = 0.19 (yellow emission, λ_{em} = 365 nm)]. This allows sequential one-pot deprotection / Sonogashira coupling reactions to be performed, eliminating the need to isolate the terminal acetylene if desired.

^{1}H NMR (400 MHz; $CDCl_3$): δ_H/ppm 8.46 (2 H, d, J = 6.0 Hz, H_1), 7.90 (2 H, s, H_4), 7.53 (2 H, d, J = 7.7 Hz, H_7), 7.16 (2 H, dd, J = 6.0 and 1.6 Hz, H_2), 6.82 (2 H, td, J = 7.5 and 1.0 Hz, H_8), 6.72 (2 H, td, J = 7.5 and 1.0 Hz, H_9), 6.26 (2 H, d, J = 7.5 Hz,

H_{10}), 5.21 (1 H, s, H_{14}), 3.41 (2 H, s, H_{13}), 1.79 (6 H, s, H_{16}). **Acc-MS** (ESI^+): *m/z* 646.1365 (M^+), calcd. for $C_{31}H_{23}N_2O_2{}^{191}Ir$ 646.1366 ($|\Delta m/z$ = 0.2 ppm).

5.6.31. Acetylacetonato-κ^2*O*,*O′*-2-phenylpyridine-κ^2*C*$^{2′}$,*N*-2-phenyl-4-((triisopropylsilyl)ethynyl)pyridine-κ^2*C*$^{2′}$,*N*-iridium(III): [Ir(2-p-4-TIPSepy)(ppy)(acac)]

An adaption of the methods of Nonoyama et al.[33] and Sprouse et al.[34] for the synthesis of [{IrL$_2$(μ-Cl)}$_2$] species, followed by an adaption the method of Lamansky et al.[35] for the synthesis of [IrL$_2$(acac)] species.

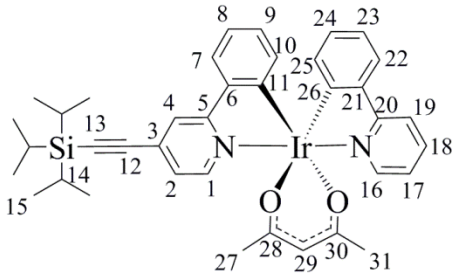

$C_{38}H_{43}IrN_2O_2Si$
M_r = 780.1

The compounds 2-p-4-TIPSepyH (678 mg, 0.79 mmol), 2-phenylpyridine (0.28 ml, 305 mg, 2.0 mmol) and $IrCl_3{\cdot}3H_2O$ (715 mg, 2.0 mmol) were suspended in a 3:1 (*v*/*v*) mixture of 2-ethoxyethanol and water (8 ml) and heated at 110 °C for 16 h. During this time, the solution turned from pale yellow to dark orange. The solution was allowed to cool to r.t and water (30 ml) was added, precipitating a bright orange solid, which was filtered, washed with water (2 x 10 ml) and dissolved in CH_2Cl_2 (4 x 20 ml).The CH_2Cl_2 solution was washed with water (10 ml), separated, dried over $MgSO_4$, filtered and reduced *in vacuo* to an orange oily solid. The crude material was triturated with hexanes (5 ml) affording the mixture of *μ*-dichloro-bridged diiridium dimers as an orange solid. The crude mixture was dissolved in a 1:1 (*v*/*v*) mixture of acetone:EtOH (30 ml) with acetylacetone (0.5 ml, excess) and in which K_2CO_3 (250 mg) was suspended. The mixture was heated at 60 °C for 4 h. The solvents were removed *in vacuo* and the residual orange solid was purified by column chromatography (SiO_2; 2:1 (*v*/*v*) CH_2Cl_2:hexanes to CH_2Cl_2), affording the compound [Ir(2-p-4-TIPSepy)$_2$(acac)] as the fore-running fraction (152 mg, 40%) as a bright orange solid and the title compound as the second fraction, also as a bright orange solid (136 mg, 22%).

FT-IR (solid): $\tilde{\nu}_{max}$/cm^{-1} 3056 (w, CH), 2941 (w, CH), 2864 (w, CH), 2162 (w, C≡C), 1606 (w, Ar), 1578 (w, Ar), 1516 (Ar), 754 (s), 729 (s), 670 (s). **^{1}H NMR** (700 MHz; $CDCl_3$): δ_H/ppm 8.49 (1 H, d, J = 5.4 Hz, H_1), 8.46 (1 H, d, J = 5.9 Hz, H_{16}), 7.85 (2 H, m), 7.72 (1 H, t, J = 7.6 Hz), 7.55 (2 H, m), 7.11-7.16 (2 H, m), 6.81 (2 H, m), 6.70 (2 H, m), 6.30 (1 H, d, J = 7.6 Hz), 6.26 (1 H, d, J = 7.6 Hz), 5.20 (1 H, s, H_{29}), 1.78 (6 H, s, H_{27} and H_{31}), 1.19 (21 H, m, H_{14} and H_{15}). **^{13}C{^{1}H} NMR** (176 MHz; $CDCl_3$): δ_H/ppm 184.8 (2 C resolved), 168.7, 168.6, 148.2, 148.1, 147.8, 147.6, 144.8, 144.2, 137.0, 133.2, 132.1, 129.5, 129.3, 124.1, 124.0 (2 C resolved), 121.6, 121.0, 120.9, 120.8, 118.5, 104.1, 100.5, 98.8, 29.6, 28.9 (2 C resolved), 18.8, 17.9, 12.4, 11.4. **Acc-MS** (ASAP$^+$): *m/z* 778.2726 (M^+), calcd. for $C_{38}H_{43}N_2O_2Si^{191}Ir$ 778.2700 ($|\Delta m/z|$ = 3.3 ppm).

5.6.32. Acetylacetonato-κ^2*O,O′*-2-phenylpyridine-κ^2*C$^{2′}$,N*-2-phenyl-4-ethynylpyridine-κ^2*C$^{2′}$,N*-iridium(III): [Ir(4-e-2-ppy)(ppy)(acac)]

Standard deprotection conditions as described by Wuts and Greene.[39]

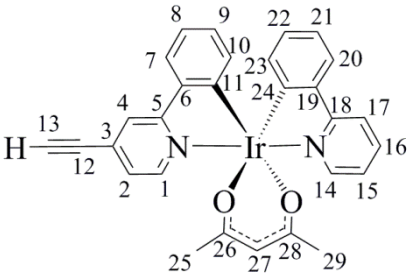

$C_{29}H_{23}IrN_2O_2$
M_r = 623.7

The compound [Ir(2-p-4-TIPSepy)(ppy)(acac)] (112 mg, 0.14 mmol) was dissolved in dry THF (10 ml) with activated molecular sieves (4 Å) under an atmosphere of nitrogen. To this solution was cautiously added TBAF (0.3 ml, 1 M solution in THF, 0.3 mmol), causing the solution to darken immediately. The solution was stirred at r.t. for 20 h, followed by removal of the solvent *in vacuo* and purification by column chromatography (SiO_2; 2:1 (*v*/*v*) CH_2Cl_2:hexanes) to give the title compound as a bright orange solid (81 mg, 90%). **CAUTION:** The solution should not be heated above r.t. to remove the solvent as this causes extensive decomposition once dry.

The deprotection can be monitored by TLC {(SiO_2; CH_2Cl_2): R_f (starting material) = 0.61 (orange emission, λ_{ex} = 365 nm), R_f (product) = 0.52 (yellow emission, λ_{ex} = 365 nm)}. This allows sequential one-pot deprotection / Sonogashira coupling reactions to be performed, eliminating the need to isolate the terminal acetylene if desired.

^{1}H NMR (400 MHz; $CDCl_3$): δ_H/ppm 8.46-8.52 (2 H, m, H_1 and H_{14}), 7.82-7.92 (2 H, m), 7.73 (1 H, t, J = 7.3 Hz), 7.50-7.56 (2 H, m), 7.11-7.17 (2 H, m), 6.78-6.84 (2 H, m), 6.66-6.72 (2 H, m), 6.56 (1 H, s), 6.22-6.29 (2 H, m), 5.21 (1 H, s, H_{27}), 3.40 (1 H, s, H_{13}), 1.78 (6 H, s, H_{25} and H_{29}). **Acc-MS** (ASAP$^+$): *m/z* 622.1365 (M^+), calcd. for $C_{29}H_{23}N_2O_2{}^{191}Ir$ 622.1366 ($|\Delta m/z|$ = 0.2 ppm).

5.6.33. Acetylacetonato-κ^2*O,O′*-2-phenylpyridato-κ^2*C^2′,N*-2-phenyl-4-(4′-(phenylethynyl)phenyl)ethynylpyridine-κ^2*C^2′,N*-iridium(III): [Ir(2-p-4-pepepy)$_2$(acac)]

Standard Sonogashira conditions as reviewed by Chinchilla and Nájera.[47, 48]

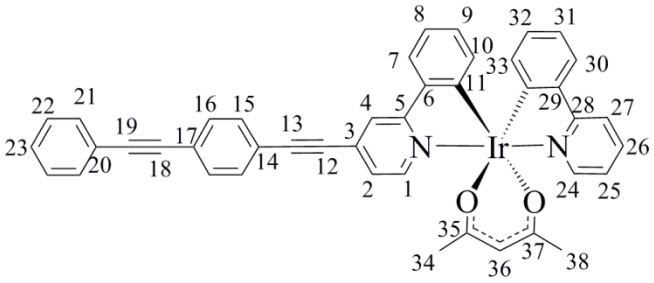

$C_{43}H_{31}IrN_2O_2$
M_r = 799.9

In a nitrogen-filled Schlenk tube were added [Ir(4-e-2-ppy)(ppy)(acac)] (65 mg, 0.10 mmol), 4-iodophenylethynylbenzene (60 mg, 0.2 mmol), THF (3 ml) and NEt_3 (3 ml). The solution was degassed by three evacuation and nitrogen back filling cycles. The catalysts [$Pd(PPh_3)_4$] (3 mg, 5 mol%) and CuI (1 mg, 5 mol%) were added under a stream of nitrogen and the solution was stirred at 60 °C for 6 h. The solvent was removed *in vacuo* and the crude product was purified by column chromatography (SiO_2; 2:1 (*v*/*v*) CH_2Cl_2:hexanes) to give the title compound as a dark orange solid (59 mg, 74%).

^{1}H NMR (700 MHz; $CDCl_3$): δ_H/ppm 8.49-8.51 (2 H, m, H_1 and H_{24}), 7.94 (1 H, d, J = 1.4 Hz), 7.86 (1 H, d, J = 8.5 Hz), 7.74 (1 H, td, J = 7.8 and 1.4 Hz), 7.54-7.61 (8 H, m), 7.36-7.40 (3 H, m), 7.19 (1 H, dd, J = 5.9 and 1.8 Hz, H_2), 7.15 (1 H, ddd, J = 7.3, 5.7 and 1.4 Hz, H_{25}), 6.80-6.84 (2 H, m), 6.69-6.72 (2 H, m), 6.27-6.31 (2 H, m), 5.22 (1 H, s, H_{36}), 1.80 (2 x 3 H, s). **^{13}C{^{1}H} NMR** (176 MHz; $CDCl_3$): δ_C/ppm 184.9 (2 C resolved), 168.8, 168.6, 148.3, 148.1, 148.0, 147.5, 144.8, 144.2, 137.0, 133.3, 133.2, 132.1, 131.9, 131.8 (2 C resolved), 129.5, 129.3, 128.8, 128.6, 124.6, 124.2, 124.0, 123.4, 123.0, 121.8, 121.6, 121.0 (2 C resolved), 120.4, 118.6, 100.6, 95.4, 92.1, 89.0, 88.5, 28.7 (2 C resolved), 14.1. **MS** (ASAP$^+$): m/z 826.2 ($[M+H]^+$), 726.2 ($[M-(acac)]^+$).

5.6.34. (Acetylacetonato-κ*O*,*O*)-(2-phenyl-4-(4′-(4′′-(cyanophenylethynyl)-phenyl) ethynylpyridine-*κ*N,C$^{2′}$) iridium(III): [Ir(2-p-4-CNpepepy)$_2$(acac)]

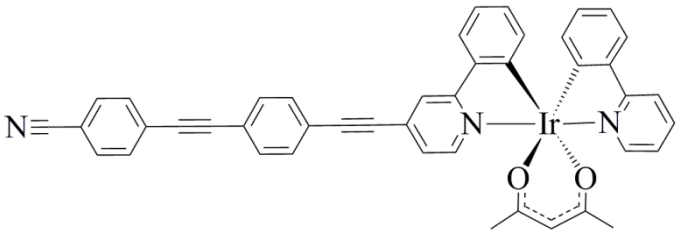

$C_{44}H_{30}IrN_3O_2$
M_r = 825.2

The compound [Ir(2-p-4-TIPSepy)(ppy)(acac)] (30 mg, 0.038 mmol) was dissolved in dry, degassed THF (3 ml) under nitrogen. To this solution was cautiously added TBAF (0.1 ml, 1 M solution in THF, 0.1 mmol), causing the solution to darken immediately. The reaction was monitored by TLC (*vide supra*) and after 2 h was complete. To the solution was added 4′-(4-iodophenylethynyl)benzonitrile (60 mg, 0.2 mmol) and NEt_3 (3 ml). The solution was degassed by three evacuation and nitrogen back filling cycles. The catalysts [$Pd(PPh_3)_4$] (3 mg, 15 mol%) and CuI (1 mg, 15 mol%) were added under a stream of nitrogen and the solution was stirred at 60 °C for 6 h. The solvent was removed *in vacuo* and the crude product was purified by column chromatography (SiO_2; 2:1 (*v*/*v*) CH_2Cl_2:hexanes) to give the title compound as a dark red solid (22 mg, 70%).

^{1}H NMR (200 MHz; $CDCl_3$): δ_H/ppm 8.47-8.55 (2 H, m), 7.93 (1 H, d, J = 1.5 Hz), 7.86 (1 H, d, J = 8.0 Hz), 7.76 (1 H, dd, J = 7.1 and 1.5 Hz), 7.49-7.72 (10 H, m), 7.11-7.22 (2 H, m), 6.82 (2 H, tt, J = 7.3 and 1.5 Hz), 6.71 (2 H, td, J = 7.5 and 1.2 Hz),

6.28 (2 H, dt, J = 7.3 and 1.5 Hz), 5.22 (1 H, s), 1.80 (6 H, two overlapping singlets separated by *ca.* 0.5 Hz). **Acc-MS** (ASAP$^+$): *m/z* 823.1951 (M^+), calcd. for $^{191}IrC_{44}H_{30}N_3O_2$ 823.1944 ($|\Delta m/z|$ = 0.9 ppm).

5.7. Chapter 4 synthetic protocols

5.7.1. 4-Ethynylbenzaldehyde

Reported several times, including by Li et al.,[49] who synthesised this compound in 78% yield over two steps on a 0.9 mmol scale by a similar deprotection and Sonogashira coupling sequence.

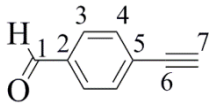

C_9H_6O
M_r = 130.1

The compound 4-bromobenzaldehyde (9.25 g, 50 mmol) was dissolved in a mixture of THF (30 ml) and NEt_3 (20 ml) and degassed by three freeze-pump-thaw cycles. Under a nitrogen atmosphere, trimethylsilylacetylene (7.1 ml, 4.93 g, 50 mmol) was added, the solution was degassed one further time and back-filed with nitrogen. The catalysts $[Pd(PPh_3)_2Cl_2]$ (350 mg, 1 mol%) and CuI (100 mg, 1 mol%) were added and the solution was heated at 65 °C for 20 h. The solution turned from yellow through orange to black. The solvents were removed *in vacuo* and the solid was eluted through a short (*ca*. 5 cm) column (SiO_2; diethyl ether). The solvent was reduced *in vacuo* to give a brown solid. The solid was dissolved in MeOH (40 ml), suspended with K_2CO_3 (0.5 g) and stirred at r.t. for 2 h. The solvent was removed *in vacuo*. To the residue was added CH_2Cl_2, (50 ml) and the suspension was sonicated for 5 min before filtering. The solution was reduced *in vacuo* to *ca.* 20 ml, eluted through a short (*ca*. 5 cm) column (SiO_2; CH_2Cl_2) and concentrated *in vacuo* to afford the title compound as an orange-yellow coloured solid (4.93 g, 76%).

M.p. 83 °C (from hexanes), lit. 84-86 °C (unspecified). **FT-IR** (solid): $\tilde{\nu}_{max}$/cm^{-1} 3215 (s, alkyne CH), 2961, 2840 (w) and 2742 (w, aldehyde CH), 2101 (w, C≡C), 1702 (C=O), 1664 (s), 1605 (s, Ar), 1562 (Ar). **Raman** (solid, 633 nm): $\tilde{\nu}_{max}$/cm^{-1} 2210 (vw), 2095 (s, C≡C), 1682 (w, br., CO), 1602 (s, Ar), 1209, 1193, 1169 (s). **^{1}H NMR**

(400 MHz; $CDCl_3$): δ_H/ppm 10.02 (1 H, s, H_1), 7.84 (2 H, d, J = 8.2 Hz, H_3), 7.64 (2 H, d, J = 8.2 Hz, H_4) and 3.29 (1 H, s, H_7). **$^{13}C\{^1H\}$ NMR** (400 MHz; $CDCl_3$): δ_C/ppm 191.5 (C_1), 136.1 (C_2), 132.8 (C_3), 129.6 (C_4), 128.4 (C_5), 82.8 (C_6), 81.2 (C_7). **GC-MS** (EI^+; 1 peak): m/z 130 (M^+). Analyses match those previously reported.[49]

5.7.2. 4-(4′-*tert*-Butylphenylethynyl)benzaldehyde

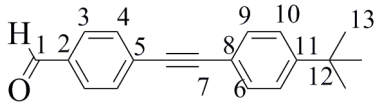

$C_{19}H_{18}O$
M_r = 262.3

The compound 4-ethynylbenzaldehyde (2.0 g, 15.3 mmol) was suspended in a 1:1 (*v*/*v*) mixture of THF and NEt_3 (20 ml) and degassed by two freeze-pump-thaw cycles. Under a nitrogen atmosphere, 1-bromo-4-*tert*-butylbenzene (2.7 ml, 3.32 g, 15.6 mmol) was added and the solution was degassed one further time. The catalysts $[Pd(PPh_3)_2Cl_2]$ (110 mg, 1 mol%) and CuI (30 mg, 1 mol%) were added under a stream of nitrogen and the solution was heated at 70 °C for 60 h. The solvents were removed *in vacuo* and the crude product was eluted through a short (*ca.* 5 cm) column (SiO_2; 1:1 (*v*/*v*) hexanes:diethyl ether) and reduced to a brown, oily solid. Recrystallisation from hot hexanes afforded the title compound as a light brown crystalline product (3.61 g, 90%).

M.p. 128 °C (from hexanes). **FT-IR** (solid): $\tilde{\nu}_{max}$/cm^{-1} 2969 (CH), 2874 (w, CH), 2831 (w, CH), 2817 (w, CH), 2731 (w, aldehyde CH), 2223 (C≡C), 1699 (s, C=O), 1600 (s, Ar), 1562 (s, Ar), 1517 (Ar), 1204, 830 (s), 724 (s). **Raman** (solid, 633 nm): $\tilde{\nu}_{max}$/cm^{-1} 3059 (w, CH), 2965 (w, CH), 2901 (w, CH), 2217 (s, C≡C), 2181 (w), 2161 (w), 1694 (w, C=O), 1595 (s, Ar), 1555 (w, Ar), 1492 (w), 1201 (w), 1164 (w), 1139 (w), 1099. **^{1}H NMR** (700 MHz; $CDCl_3$): δ_H/ppm 9.99 (1 H, s, H_1), 7.84 (2 H, d, J = 8.4 Hz, H_3), 7.65 (2 H, d, J = 8.4 Hz, H_4), 7.48 (2 H, d, J = 8.4 Hz, H_9), 7.39 (2 H, d, J = 8.4 Hz, H_{10}), 1.32 (9 H, s, H_{13}). **$^{13}C\{^1H\}$ NMR** (176 MHz; $CDCl_3$): δ_C/ppm 191.4 (C_1), 152.4 (C_{11}), 135.3 (C_2), 132.0 (C_4), 131.5 (C_9), 129.9 (C_5), 129.5 (C_3), 125.5 (C_{10}), 119.4 (C_8), 93.8 (C_7), 88.0 (C_6), 34.9 (C_{12}), 31.1 (C_{13}). **GC-MS** (EI^+; 1 peak): m/z 262 (M^+). **Acc-MS** ($ASAP^+$): m/z 263.1443 ($[M+H]^+$), calcd. for $C_{19}H_{19}O$ 263.1436 ($|\Delta m/z|$ = 2.7 ppm).

5.7.3. 2-(4′-(4′′-*tert*-Butylphenylethynyl)phenyl)-4,5-diphenylimidazole: ETPI-H

An adaption of the method of Wolkenberg et al.[50] *for the synthesis of 2,4,5-triphenylimidazoles.*

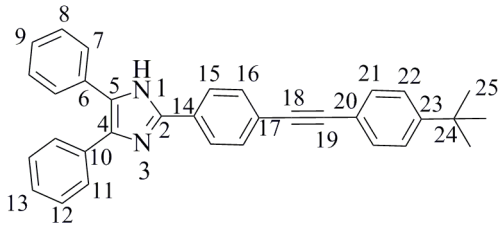

$C_{33}H_{28}N_2$
M_r = 452.6

The compounds 4-(4′-*tert*-butylphenylethynyl)benzaldehyde (200 mg, 0.76 mmol), benzil (0.160 mg, 0.76 mmol) and ammonium acetate (590 mg, 7.6 mmol, 10 eq.) were suspended in acetic acid (4 ml) and sealed in a microwave vial. The solution was heated at 180 °C under microwave irradiation for 5 min. The solution was allowed to cool to r.t before being poured into water (100 ml) and extracted with ethyl acetate (3 x 25 ml). The ethyl acetate layer were separated, combined, washed with brine (2 x 50 ml), dried over $MgSO_4$, filtered and reduced to a yellow solid *in vacuo*. The crude solid was recrystallised from hot MeCN to afford the title compound as yellow needles (220 mg, 64%). Single crystals of the EtOH disolvate suitable for X-ray diffraction were grown as yellow needles by slow cooling of an EtOH solution. A second form was grown from diethyl ether, but the crystals were of insufficient quality for structure determination.

M.p. 273 °C (from MeCN). **Elem. Anal.** Found: C, 87.14; H, 6.16; N, 6.09. Calcd. for $C_{33}H_{28}N_2$: C, 87.57; H, 6.24; N, 6.19%. **FT-IR** (solid): $\tilde{\nu}_{max}$/cm^{-1} 3050 (w, br.), 2961 (w), 2901 (w), 2870 (w), 1601 (Ar), 1586 (Ar), 1543 (Ar, w), 1507 (Ar, w), 841 (s), 830 (s), 766 (s), 694 (s). **Raman** (solid, 785 nm): $\tilde{\nu}_{max}$/cm^{-1} 2214 (s, C≡C), 1606 (s, Ar), 1538 (Ar), 1469 (Ar), 1408, 1253, 1184, 1147. **^{1}H NMR** (500 MHz; DMSO-d_6; 50 °C): δ_H/ppm 12.70 (1 H, s, H_1), 8.13 (2 H, d, J = 7.5 Hz, H_{15}), 7.63 (2 H, d, J = 7.5 Hz, H_{16}), 7.57 (2 H, d, J = 7.5 Hz), 7.47-7.53 (4 H, m), 7.41-7.46 (4 H, m), 7.37 (1 H, t, J = 7.2 Hz), 7.30 (2 H, t, J = 7.5 Hz), 7.22 (1 H, t, J = 7.2 Hz), 1.29 (9 H, s, H_{25}). **^{13}C{^{1}H} NMR** (126 MHz; DMSO-d_6, 50 °C): δ_C/ppm 152.3 (C_{23}), 145.5 (C_2), 138.4, 135.8, 132.3, 131.8, 131.7, 130.9, 129.4, 129.3, 129.1, 128.8, 128.5, 127.8, 127.3,

126.2, 126.0, 122.7 (C_{17}), 120.1 (C_{20}), 91.3 (C_{18}), 89.5 (C_{19}), 35.3 (C_{24}), 31.6 (C_{25}). **Acc-MS** (ESI^+): *m/z* 453.2330 ($[M+H]^+$), calcd. for $C_{33}H_{29}N_2$ 453.2331 ($|\Delta m/z|$ = 0.2 ppm).

Crystal data (Instrument **B**): $C_{33}H_{28}N_2 \cdot 2(C_2H_6O)$, (0.21 x 0.13 x 0.12) mm^3, ρ = 1.156 g cm^{-3}, monoclinic, $P2_1/c$, Z = 4, a = 11.089(1) Å, b = 29.010(3) Å, c = 9.965(1) Å, β = 102.424(3)°, V = 3130.4(6) $Å^3$, T = 120(2) K, μ(Mo K_α) = 0.071 mm^{-1}, 20707 reflections measured, 6420 independent (R_{int} = 0.0348), 4754 reflections with $I > 2\sigma(I)$, final R indices: wR_2 = 0.1339 (all data), R_1 = 0.0523 ($I > 2\sigma(I)$).

5.7.4. 2C-1′N and 2C-2′C Dimers of ETPI: ETPI-CN and ETPI-CC

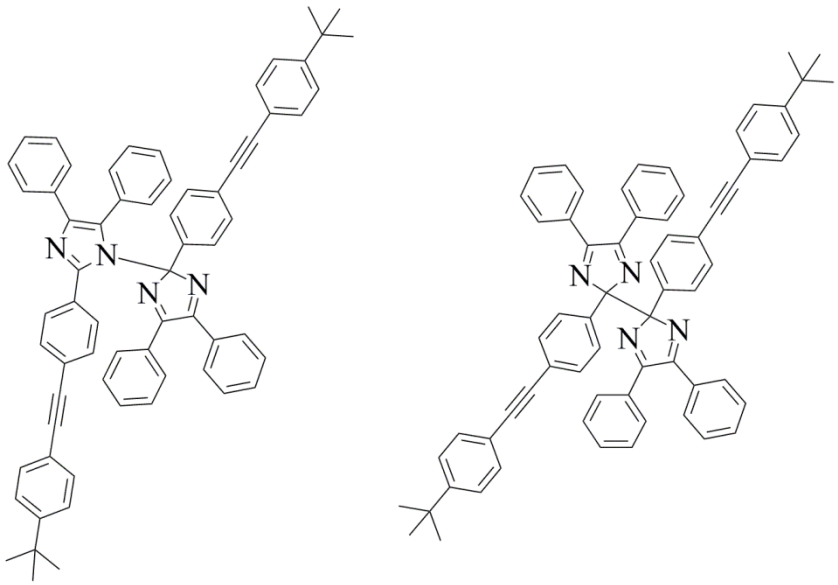

2C-1′N Dimer 2C-2′C Dimer

$C_{66}H_{54}N_4$
M_r = 903.2

The compound ETPI-H (53 mg, 0.12 mmol) was dissolved in CH_2Cl_2 (10 ml). To this was added KOH (188 mg, 3.4 mmol) dissolved in water (10 ml) and the biphasic mixture was purged with nitrogen for 10 min. Solid $K_3[Fe(CN)_6]$ (395 mg, 1.2 mmol) was added, and the solution was stirred at r.t. for 4 h with the exclusion of light. The aqueous layer was separated and the organic layer was washed with water (3 x 20 ml) until the washings were colourless. The CH_2Cl_2 layer was dried over $MgSO_4$, filtered and eluted through a short (*ca*. 5 cm) column (SiO_2; CH_2Cl_2). The CH_2Cl_2 solution was

concentrated *in vacuo* to a pale green solid (33 mg, 61%). Single crystals of the 2C-1′N dimer (ETPI-CN) suitable for synchrotron X-ray diffraction were grown as minute prisms by slow diffusion of hexanes anti-solvent into an acetone solution. Note the crystal structure is of sufficient quality to confirm connectivity only.

Raman (solid, 785 nm): $\tilde{\nu}_{max}$/cm^{-1} 2214 (C≡C, s), 1605 (Ar, s), 1538 (Ar, w), 1472 (Ar, w), 1115 (s). **^{1}H NMR** (400 MHz; C_6D_6): δ_H/ppm. 7.96 (2 H, d, J = 8.4 and 1.5 Hz), 7.69 (2 H, d, J = 8.4 and 1.5 Hz), 7.49 (2 H, dd, J = 8.4 and 1.8 Hz), 7.44 (2 H, dd, J = 8.4 and 1.8 Hz), 7.34-7.41 (4 H, m), 7.29 (2 H, dd, J = 8.4 and 1.8 Hz), 7.16-7.22 (6 H, m), 6.84-7.10 (16 H, m). **^{13}C{^{1}H} NMR** (101 MHz; C_6D_6): δ_C/ppm 167.2, 151.7, 151.6, 148.8, 139.2, 138.7, 135.6, 135.4, 133.6, 132.7, 131.9 (2 C resolved) 131.8, 131.7, 131.3, 131.2 (2 C resolved), 131.1, 131.0, 129.7, 126.8, 125.8, 125.7, 124.4, 123.7, 121.1, 120.7, 112.8, 91.3, 91.0, 89.7, 89.2, 34.7 (2 C resolved), 31.2, 31.1. **Acc-MS** (ASAP$^+$): *m/z* 903.4456 ([M+H]$^+$), calcd. for $C_{66}H_{55}N_4$ 903.4427 ($|\Delta m/z|$ = 3.2 ppm).

Crystal data (**ETPI-CN**) (Instrument **D**): $C_{66}H_{54}N_4$, (0.07 x 0.06 x 0.03) mm^{-1}, ρ = 1.054 g cm^{-3}, triclinic, $P\bar{1}$, Z = 2, a = 10.503(4) Å, b = 14.511(6) Å, c = 19.926(8) Å, α = 86.646(6)°, β = 82.585(6)°, γ = 70.912(5)°, V = 2846(2) Å^3, T = 100(2) K, μ(Synchrotron, λ = 0.6689 Å) *N.A.*,[i] 4788 reflections measured, 4782 independent (R_{int} *N.A.*), 2221 reflections with $I > 2\sigma(I)$, final R indices: wR_2 = 0.2521 (all data), R_1 = 0.0905 ($I > 2\sigma(I)$).

Single crystals suitable for synchrotron X-ray diffraction of the **ETPI-CC** dimer were grown as green needles by irradiating a chloroform solution of the **ETPI-CN** dimer (*ca.* 10 mM) with a 365 nm LED (*ca.* 100 mW) from approximately 2 cm.

Raman (solid, 785 nm): $\tilde{\nu}_{max}$/cm^{-1} 2217 (C≡C, s), 1602 (Ar, s), 1115 (s), 910 (w).

Crystal data (**ETPI-CC)** (Instrument **D**): $C_{66}H_{54}N_4$, (0.06 x 0.02 x 0.02) mm^3, ρ = 1.233 g cm^{-3}, triclinic, $P\bar{1}$, Z = 1, a = 10.017(3) Å, b = 11.112(3) Å, c = 11.721(3) Å, α = 69.889(3)°, β = 87.557(3)°, γ = 83.195(3)°, V = 1216.5(6) Å^3, T = 150(2) K, μ(Synchrotron, λ = 0.6689 Å) *N.A.*,[i] 10462 reflections measured, 4666

[i] Insufficient data for an absorption correction

independent (R_{int} = 0.0231), 3641 reflections with $I > 2\sigma(I)$, final R indices: wR_2 = 0.1725 (all data), R_1 = 0.0576 ($I > 2\sigma(I)$).

5.7.5. 2-*tert*-Butyliodobenzene

Reported several times, including by Fey et al.,[51] *who synthesised this compound in 60% yield on a 147 mmol scale by a similar Sandmeyer reaction.*

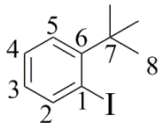

$C_{10}H_{13}I$
M_r = 260.1

The compound 2-*tert*-butylaniline (5 ml, 4.79 g, 32.1 mmol) was added to a solution of concentrated H_2SO_4 (6 ml) diluted with water (24 ml), forming a pale pink suspension, and cooled to -40 °C. Sodium nitrite (2.29 g, 33.1 mmol) dissolved in water (20 ml) was added and the solution stirred for 10 min. The temperature was adjusted to -15 °C and a pre-cooled solution of KI (17.1 g, 103 mmol) in water (40 ml) was added, at which point the solution turned red. The solution was stirred for a further 1 h whilst warming to 0 °C. The solution was cautiously neutralised with dilute aqueous NaOH solution (1 M, 100 ml) before being extracted with hexanes (3 x 30 ml). The hexanes layers were combined and dried over $MgSO_4$, filtered and the solvent removed *in vacuo*. The crude material was eluted through a short (*ca*. 5 cm) column (SiO_2; hexanes) to give the title compound as a red oil (3.37 g, 40%).

^{1}H NMR (400 MHz; $CDCl_3$): δ_H/ppm 8.00 (1 H, dd, J = 7.9 and 1.4 Hz), 7.44 (1 H, dd, J = 7.9 and 1.7 Hz), 7.28 (1 H, td, J = 7.3 and 1.4 Hz), 6.83 (1 H, td, J = 7.3 and 1.7 Hz), 1.53 (9 H, s). **^{13}C{^{1}H} NMR** (101 MHz; $CDCl_3$): δ_C/ppm 150.27 (C_6), 143.70, 128.04, 127.67, 127.64, 95.27, 36.85 (C_7), 30.01 (C_8). **GC-MS** (EI^+; 1 peak): *m/z* 260 (M^+), 245 ($[M\text{-}CH_3]^+$). Analyses matched those previously reported.[51]

5.7.6. 2-*tert*-Butylbenzaldehyde

Reported several times, including by Varela et al.,[52] who synthesised this compound in 89% yield on a 17 mmol scale using tert-butyllithium as the lithiating reagent.

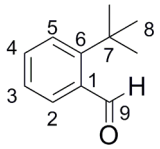

$C_{11}H_{14}O$
$M_r = 162.2$

To a nitrogen filled flask was added a solution of 2-*tert*-butyliodobenzene (1.02 g, 3.9 mmol) in dry THF (10 ml). The solution was cooled to -78 °C before *n*-butyllithium (1.6 M in hexanes, 3.2 ml, 5.1 mmol) was added causing the solution to turn orange. The solution was stirred for 30 min at -78 °C. Dry dimethylformamide (1 ml, 0.94 g, 12.3 mmol) was added dropwise and stirred for a further 2 h. Water (15 ml) was added cautiously and the flask opened to air causing the now red solution to turn green. The organic layer was separated and the aqueous layer extracted with diethyl ether (2 x 10 ml). The combined organic layers were dried over $MgSO_4$, filtered and eluted through a short (*ca*. 5 cm) column (SiO_2; diethyl ether) to remove a yellow impurity and excess DMF. The crude material was purified by Kugelrohr distillation (0.2 mbar) giving the product as the lowest boiling point fraction (454 mg, 72%). **CAUTION:** It was observed that the product degraded (yellow colouration developed) within the course of a couple of days if exposed to light or kept at r.t. and therefore should be prepared and used immediately.

^{1}H NMR (400 MHz; $CDCl_3$): δ_H/ppm 10.85 (1 H, s, H_9), 7.93 (1 H, d, J = 7.8 Hz), 7.44-7.54 (2 H, m), 7.28-7.36 (1 H, m), 1.52 (9 H, s, H_8). Analysis matched that previously reported.[52]

5.7.7. 2-(2′-*tert*-Butylphenyl)-4,5-diphenylimidazole: 2-tBu-TPI-H

An adaption of the method of Wolkenberg et al.[50] *for the synthesis of 2,4,5-triphenylimidazoles.*

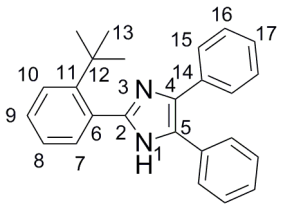

$C_{25}H_{24}N_2$
M_r = 352.5

The compounds 2-*tert*-butylbenzaldehyde (356 mg, 2.2 mmol), benzil (463 mg, 2.2 mmol) and ammonium acetate (385 mg, 5.0 mmol) were suspended in acetic acid (4 ml), sealed in a microwave vial and heated at 180 °C under microwave irradiation for 5 min. The solution was allowed to cool to r.t before being poured into ice-water (30 ml), neutralised with K_2CO_3 and extracted with CH_2Cl_2 (3 x 20 ml). The CH_2Cl_2 layers were separated, combined, dried over $MgSO_4$, filtered and reduced to a beige solid *in vacuo*. The crude solid was recrystallised from hot MeCN as white needles (445 mg, 58%). Single crystals suitable for X-ray diffraction were produced by recrystallisation from nitromethane as colourless plates.

M.p. 266 °C (from MeCN). **Elem. Anal.** Found: C, 84.99; H, 6.80; N 7.80. Calcd. for $C_{25}H_{24}N_2$: C, 85.19; H, 6.86; N 7.95%. **FT-IR** (solid): $\tilde{\nu}_{max}$/cm^{-1} 3072 (CH), 3033 (CH), 2972 (CH), 2912 (CH), 1604 (Ar), 1546 (Ar), 1505 (w, Ar), 1483(s), 1445 (s), 758 (s), 739 (s), 694 (s). **^{1}H NMR** (500 MHz; DMSO-d_6): δ_H/ppm 12.40 (1 H, s, H_1), 7.52-7.59 (3 H, m), 7.45-7.49 (2 H, m), 7.42 (1 H, td, J = 7.6 and 1.7 Hz), 7.38 (2 h, t, J = 8.1 Hz), 7.4 (1 H, dd, J = 7.6 and 1.7 Hz), 7.26-7.33 (4 H, m), 7.19 (1 H, tt, J = 7.4 and 1.3 Hz), 1.29 (9 H, s). **^{13}C{^{1}H} NMR** (126 MHz; DMSO-d_6): δ_C/ppm 149.78, 147.70, 135.54, 135.38, 132.35, 131.20, 131.19, 128.93, 128.62, 128.15, 127.85, 127.35, 127.02, 126.51, 126.45, 126.31, 125.16, 36.04, 31.52. **Acc-MS** (ESI$^+$): *m/z* 353.2022 ([M+H]$^+$), calcd. for $C_{25}H_{25}N_2$ 353.2018 ($|\Delta m/z|$ = 1.1 ppm).

Crystal data (Instrument **D**): $C_{25}H_{24}N_2$, (0.03 x 0.01 x 0.01) mm^3, ρ = 1.159 g cm^{-3}, monoclinic, $P2_1/c$, Z = 8, a = 9.692(2) Å, b = 19.705(5) Å, c = 21.494(5) Å, β = 100.178(3)°, V = 4040.3(16) Å^3, T = 120(2) K, μ(Synchrotron,

λ = 0.6689 Å) = 0.068 mm^{-1}, 31649 reflections measured, 6990 independent (R_{int} = 0.0859), 4663 reflections with $I > 2\sigma(I)$, final R indices: wR_2 = 0.1471 (all data), R_1 = 0.0559 ($I > 2\sigma(I)$).

5.7.8. 2-(4′-*tert*-Butylphenyl)-4, 5-diphenylimidazole: 4-tBu-TPI-H

An adaption of the method of Wolkenberg et al.[50] *for the synthesis of 2,4,5-triphenylimidazoles.*

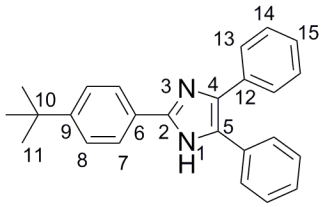

$C_{25}H_{24}N_2$
M_r = 352.5

The compounds 4-*tert*-butylbenzaldehyde (0.2 ml, 194 mg, 1.2 mmol), benzil (253 mg, 1.2 mmol) and ammonium acetate (360 mg, 4.7 mmol) were suspended in acetic acid (4 ml) and sealed in a microwave vial. The solution was heated at 180 °C under microwave irradiation for 5 min. The solution was allowed to cool to r.t before being poured into ice-water (30 ml), neutralised with K_2CO_3 and extracted with CH_2Cl_2 (3 x 20 ml). The CH_2Cl_2 layers were separated, combined, dried over $MgSO_4$, filtered and reduced to a pale yellow solid *in vacuo*. The crude solid was recrystallised from hot MeCN as white needles (261 mg, 62%). Alternatively, the crude material could be recrystallised from hot ethyl acetate, followed by cooling (-10 °C). Single crystals suitable for X-ray diffraction were produced by recrystallisation from MeCN as colourless laths.

M.p. 286 °C (from MeCN). **Elem. Anal.** Found: C, 84.84; H, 6.84; N, 7.84. Calcd. for $C_{25}H_{24}N_2$: C, 85.19; H, 6.86; N, 7.95%. **FT-IR** (solid): $\tilde{\nu}_{max}$/cm^{-1} 3064 (CH), 3026 (CH)), 2969 (CH), 2910, 2873, 1605 (Ar), 1585 (Ar), 1491 (s)), 1451 (s), 837 (s), 764 (s), 694 (s). **^{1}H NMR** (600 MHz; DMSO-d_6): δ_H/ppm 12.61 (1 H, s, H_1), 8.02 (2 H, dt, J = 8.7 and 2.0 Hz), 7.56 (2 H, dd, J = 7.0 and 1.3 Hz), 7.50 (4 H, tt, J = 7.3 and 2.0 Hz), 7.44 (2 H, t, J = 7.9 Hz), 7.37 (1 H, tt, J = 7.3 and 1.3 Hz), 7.30 (2 H, t, J = 7.9 Hz), 7.22 (1 H, tt, J = 7.3 and 1.3 Hz), 1.32 (9 H, s). **^{13}C{^{1}H} NMR** (151 MHz; DMSO-d_6): δ_C/ppm 150.75, 145.61, 136.95, 135.25, 131.16, 128.60, 128.41, 128.12,

127.93, 127.67, 127.65, 127.05, 126.41, 125.39, 125.00, 34.41, 31.05. **Acc-MS** (ESI^+): *m/z* 353.20145 ($[M+H]^+$), calcd. for $C_{25}H_{25}N_2$ 353.20176 ($|\Delta m/z|$ = 0.2 ppm).

Crystal data (Instrument **D**): $C_{25}H_{24}N_2$, M_r = 352.46, (0.30 x 0.08 x 0.01) mm^3, ρ = 1.174 g cm^{-3}, monoclinic, $P2_1/c$, Z = 8, a = 36.809(6) Å, b = 12.205(2) Å, c = 8.9185(15) Å, β = 95.551(2)°, V = 3987.9(11) $Å^3$, T = 120(2) K, μ(Synchrotron, λ = 0.6689 Å) = 0.069 mm^{-1}, 39090 reflections measured, 9628 independent (R_{int} = 0.0576), 8181 reflections with $I > 2\sigma(I)$, final R indices: wR_2 = 0.2205 (all data), R_1 = 0.0834 ($I > 2\sigma(I)$).

5.7.9. 2C-1′N Dimer of 2-(4′-*tert*-butylphenyl)-4,5-diphenylimidazolyl radical: 4-tBu-TPI-CN

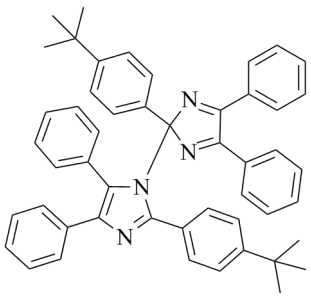

$C_{50}H_{46}N_4$
M_r = 702.9

The compound 4-tBu-TPI-H (76 mg, 0.22 mmol) was dissolved in CH_2Cl_2 (25 ml). A solution of KOH (1.35 g, 24 mmol) and $K_3[Fe(CN)_6]$ (3.7 g, 11 mmol) dissolved in water (25 ml) was added and the biphasic system was rapidly stirred for 2 h. The CH_2Cl_2 layer was separated and washed with water (3 x 20 ml) until the aqueous layer was colourless. The CH_2Cl_2 layer was dried over $MgSO_4$, filtered and reduced *in vacuo* to a light and temperature sensitive yellow solid. Flash chromatography (SiO_2; 3:1 (*v*/*v*) hexanes:CH_2Cl_2) afforded the title compound as a yellow-green solid (64 mg, 83%). Single crystals suitable for X-ray diffraction were produced by recrystallisation from hexanes as pale yellow plates (Form I) or from MeOH as pale yellow plates (Form II).

M.p. 177 °C (from CH_2Cl_2). **^{1}H NMR** (400 MHz; $CDCl_3$): δ_H/ppm 7.38-7.49 (6 H, m), 7.24-7.32 (12 H, m), 7.11-7.16 (4 H, m), 7.06-7.11 (4 H, m), 6.93 (2 H, dt, J = 8.6 and 1.8 Hz), 1.27 (9 H, s), 1.20 (9 H, s). **^{13}C{^{1}H} NMR** (101 MHz; $CDCl_3$): δ_C/ppm 166.39, 151.18, 150.91, 149.23, 137.91, 135.35, 134.69, 132.99, 132.21, 131.80, 131.55,

131.02, 130.53, 129.90, 129.40, 128.14, 127.81, 127.68, 127.46, 127.18, 126.15, 124.62, 124.44, 112.49, 34.65, 34.51, 31.44, 31.25. **Acc-MS** (ESI^+): *m/z* 703.37958 ($[M+H]^+$, 100%), calcd. for $C_{50}H_{47}N_4$ 703.37952 ($|\Delta m/z|$ = 0.1 ppm); 351.18631 ($[M/2]^+$, 5), calcd. for $C_{25}H_{23}N_2$ 351.18558 ($|\Delta m/z|$ = 0.7 ppm).

Crystal data (Form I) (Instrument **A**): $C_{50}H_{46}N_4$, (0.26 x 0.20 x 0.11) mm^3, ρ = 1.161 g cm^{-3}, monoclinic, $P2_1/n$, Z = 4, a = 12.6166(2) Å, b = 12.1515(2) Å, c = 26.5190(4) Å, β = 98.3060(4)°, V = 4023.0(1) $Å^3$, T = 100(2) K, μ(Cu Kα) = 0.519 mm^{-1}, 43177 reflections measured, 7083 independent (R_{int} = 0.0291), 6530 reflections with $I > 2\sigma(I)$, final R indices: wR_2 = 0.0903 (all data), R_1 = 0.0353 ($I > 2\sigma(I)$).

Crystal data (Form II) (Instrument **A**): $C_{50}H_{46}N_4$, (0.18 x 0.11 x 0.09) mm^3, ρ = 1.036 g cm^{-3}, triclinic, $P\bar{1}$, Z = 2, a = 12.1735(2) Å, b = 12.2821(3) Å, c = 15.1686(3) Å, α = 111.6050(4)°, β = 101.1490(4)°, γ = 98.8910(5)°, V = 2004.46(7) $Å^3$, T = 120(2) K, μ(Cu Kα) = 0.521 mm^{-1}, 25172 reflections measured, 6673 independent (R_{int} = 0.0243), 6470 reflections with $I > 2\sigma(I)$, final R indices: wR_2 = 0.0943 (all data), R_1 = 0.0373 ($I > 2\sigma(I)$).

5.7.10. Attempted oxidation of 2-tBu-TPI-H to the 2-(2′-*tert*-butylphenyl)-4,5-diphenylimidazolyl radical dimer: 2-tBu-TPI-CN. Formation of the peroxide of 2-(2′-*tert*-butylphenyl)-4,5-diphenylimidazolyl radical: 2-tBu-TPI-O_2

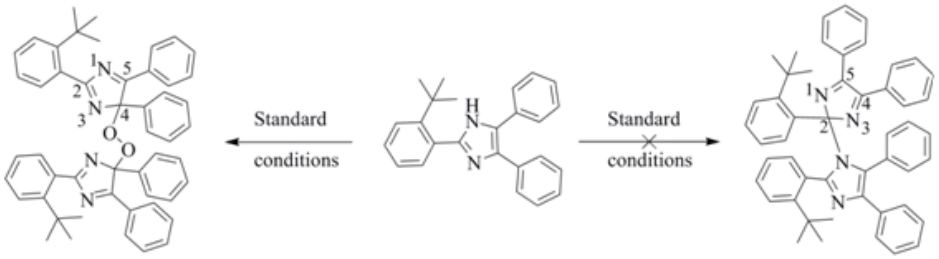

$C_{50}H_{46}N_4O_2$
M_r = 734.9

2-tBu-TPI-O_2

Mixture of isomers

$C_{50}H_{46}N_4$
M_r = 702.9

2-tBu-TPI-CN

The compound 2-(2′-*tert*-butylphenyl)-4,5-diphenylimidazole (75 mg, 0.22 mmol) was dissolved in CH_2Cl_2 (25 ml). A solution of KOH (1.35 g, 24 mmol) and $K_3[Fe(CN)_6]$ (3.7 g, 11 mmol) dissolved in water (25 ml) was added and the biphasic system was rapidly stirred for 2 h. The CH_2Cl_2 layer was separated and washed with water (3 x 20 ml) until the aqueous layer was colourless. The CH_2Cl_2 layer was dried over $MgSO_4$, filtered and reduced *in vacuo* to an off-white solid. NMR showed a complicated mixture of products that could not be separated. The mixture is believed to contain various peroxides of 2-(2′-*tert*-butylphenyl)-4,5-diphenylimidazolyl radical as evidenced by accurate mass spectrometry and X-ray crystallography. The mixture is also believed to contain traces of a dimer species, based on accurate mass spectrometry, although the nature of its dimerisation has not been established (see discussion, Chapter 4, Section 4.2).

Acc-MS ($ASAP^+$): *m/z* 702.3739 (M^+), calcd. for $C_{50}H_{46}N_4$ 702.3722 ($|\Delta m/z|$ = 2.4 ppm); 351.1852 ($[M/2]^+$), calcd. for $C_{25}H_{23}N_2$ 351.1861 ($|\Delta m/z|$ = 2.6 ppm).

Single crystals of two types suitable for X-ray diffraction were produced as colourless blocks from ethyl acetate (Isomer I) and colourless blocks (Isomer II) by recrystallisation from 1,2-dichloroethane.

Acc-MS (ASAP$^+$): *m/z* 735.3677 ([M+H]$^+$), calcd. for $C_{50}H_{47}N_4O_2$, 735.3699 ($|\Delta m/z|$ = 4.1 ppm).

Crystal data (Isomer I) (Instrument **A**): $C_{50}H_{46}N_4O_2$, (0.22 × 0.16 × 0.08) mm^3, ρ = 1.226 g cm^{-3}, monoclinic, $P2_1/n$, Z = 2, a = 8.88770(10) Å, b = 23.4338(4) Å, c = 10.4997(2) Å, β = 114.4170(3)°, V = 1991.21(6) Å^3, T = 100(2) K, μ(Cu Kα) = 0.585 mm^{-1}, 15174 reflections measured, 3528 independent (R_{int} = 0.0248), 3365 reflections with $I > 2\sigma(I)$, final R indices: wR_2 = 0.0907 (all data), R_1 = 0.0350 ($I > 2\sigma(I)$).

Crystal data (Isomer II) (Instrument **A**): $C_{50}H_{46}N_4O_2$, (0.24 x 0.18 x 0.09) mm^3, ρ = 1.226 g cm^{-3}, monoclinic, $C2/c$, Z = 4, a =18.7885(5) Å, b = 10.0808(3) Å, c = 21.5264(5) Å, β = 102.418(1)°, V = 3981.8(2) Å^3, T = 100(2) K, μ(Cu Kα) = 0.585 mm^{-1}, 16975 reflections measured, 3282 independent (R_{int} = 0.0408), 3105 reflections with $I > 2\sigma(I)$, final R indices: wR_2 = 0.0976 (all data), R_1 = 0.0367 ($I > 2\sigma(I)$).

5.7.11. Peroxide of 2-(4′-*tert*-butylphenyl)-4,5-diphenylimidazolyl radical: 4-tBu-TPI-O_2

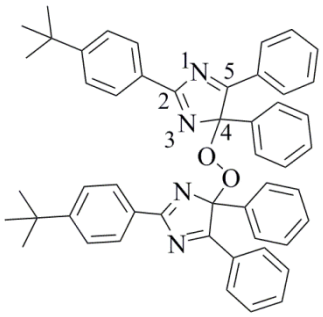

$C_{50}H_{46}N_4O_2$
M_r = 734.9
Mixture of diastereomers

Single crystals of Form I suitable for X-ray diffraction were produced by recrystallisation from ethyl acetate as colourless blocks. The sample undergoes a phase transition from Form I to Form II in the temperature range 145-150 K. The structure of

both forms was measured from the same crystal. To ensure that the crystal didn't crack, the sample was cooled slowly from 290 K (2 K min^{-1}) to just above the phase transition (160 K) and diffraction data were collected for Form I. The crystal was then cooled to 100 K, below the phase transition, and diffraction data were collected for Form II. The crystal was then cycled through the transition three times, measuring a unit cell matrix each time, confirming the reversibility of the single crystal to single crystal transformation.

M.p. 169 °C (dec.) (1,2-dichloroethane). **Acc-MS** (ESI^+): *m/z* 735.3702 ($[M+H]^+$), calcd. for $C_{50}H_{47}N_4O_2$, 735.3699 ($|\Delta m/z|$ = 0.4 ppm).

Crystal data (Form I) (Instrument **A**): $C_{50}H_{46}N_4O_2$, (0.28 x 0.12 x 0.10) mm^3, ρ = 1.180 g cm^{-3}, monoclinic, *I*2/*a*, *a* = 16.1305(10) Å, *b* = 15.4759(6) Å, *c* = 16.6219(6) Å, β = 94.2670(10)°, *V* = 4137.9(3) $Å^3$, *T* = 160(2) K, *Z* = 4, μ(Cu Kα) = 0.563 mm^{-1}, 15378 reflections measured, 3209 independent (R_{int} = 0.0405), 3005 reflections with $I > 2\sigma(I)$, final *R* indices: wR_2 = 0.1379 (all data), R_1 = 0.0498 ($I > 2\sigma(I)$).

Crystal data (Form II) (Instrument **A**): $C_{50}H_{46}N_4O_2$, (0.28 x 0.12 x 0.10) mm^3, ρ = 1.193 g cm^{-3}, monoclinic, $P2_1/c$, *a* = 16.0313(4) Å, *b* = 30.9627(9) Å, *c* = 16.5171(5) Å, β = 93.7920(10) Å, *V* = 8180.7(4) $Å^3$, *T* = 100(2) K, *Z* = 8, μ(Cu Kα) = 0.570 mm^{-1}, 62341 reflections measured, 12830 independent (R_{int} = 0.0480), 11361 reflections with $I > 2\sigma(I)$, final *R* indices: wR_2 = 0.1659 (all data), R_1 = 0.0577 ($I > 2\sigma(I)$).

5.7.12. 2-(2′-Methylphenyl)-4,5-diphenylimidazole: 2-Me-TPI-H

An adaption of the method of Wolkenberg et al.[50] *for the synthesis of 2,4,5-triphenylimidazoles.*

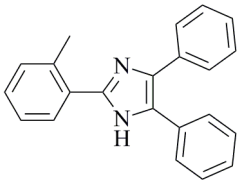

$C_{22}H_{18}N_2$
M_r = 310.4

The compounds *o*-tolualdehyde (0.24 ml, 250 mg, 2.1 mmol), benzil (420 mg, 2.0 mmol) and ammonium acetate (1.54 g, 20 mmol) were suspended in acetic acid (4 ml) and sealed in a microwave vial. The solution was heated at 180 °C under microwave irradiation for 10 min. The solution was allowed to cool to r.t before being poured into water (50 ml) and extracted with CH_2Cl_2 (3 x 20 ml). The CH_2Cl_2 layers were separated, combined, washed with water (2 x 20 ml), dried over $MgSO_4$, filtered and reduced *in vacuo* to a yellow, oily solid. The crude material was recrystallised from hot MeCN to afford the title compound as white needles (332 mg, 53%).

M.p. 253 °C (from MeCN), lit. 255 °C (from EtOH).[53] **Elem. Anal.** Found: C, 84.77; H, 5.82; N, 8.97. Calcd. for $C_{22}H_{18}N_2$: C, 85.12; H, 5.85; N, 9.03%. **FT-IR** (solid): $\tilde{\nu}_{max}$/cm^{-1} (w, br., NH), 3060 (CH), 2960 (CH), 2922, 2851 (w), 1604 (w, Ar), 1585 (w, Ar), 1537 (w, Ar), 1504 (w, Ar), 764 (s), 729 (s), 670 (s). **^{1}H NMR** (700 MHz; DMSO-d_6): δ_H/ppm 12.64 (1 H, br. s, NH), 7.68-7.70 (1 H, m), 7.49-7.52 (4 H, m), 7.24-7.36 (9 H, m), 2.61 (3 H, s). **^{13}C{^{1}H} NMR** (176 MHz; DMSO-d_6): δ_C/ppm 146.4, 145.9, 136.8, 131.5, 130.1, 129.3, 129.1, 128.8, 128.1, 127.6, 126.2, 125.7, 118.4, 21.5, 1.6. **Acc-MS** (ESI$^+$): *m/z* 311.1535 ([M+H]$^+$), calcd. for $C_{22}H_{19}N_2$ 311.1548 (|Δ*m/z*| = 4.2 ppm).

5.7.13. 2-(2′,4′,6′-Trimethylphenyl)-4,5-diphenylimidazole: Mes-DPI-H

An adaption of the method of Wolkenberg et al.[50] *for the synthesis of 2,4,5-triphenylimidazoles.*

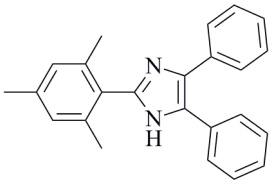

$C_{24}H_{22}N_2$
M_r = 338.4

The compounds mesitaldehyde (0.30 ml, 310 mg, 2.1 mmol), benzil (420 mg, 2.0 mmol) and ammonium acetate (1.54 g, 20 mmol) were suspended in acetic acid (4 ml) and sealed in a microwave vial. The solution was heated at 180 °C under microwave irradiation for 10 min. The solution was allowed to cool to r.t before being poured into water (50 ml) and extracted with CH_2Cl_2 (3 x 20 ml). The CH_2Cl_2 layers were separated, combined, washed with water (2 x 20 ml), dried over $MgSO_4$, filtered and reduced *in vacuo* to a light yellow, oily solid. The crude material was recrystallised from hot MeCN to afford the title compound as white needles (319 mg, 47%).

M.p. 231 °C (from MeCN). **^{1}H NMR** (700 MHz; $CDCl_3$): δ_H/ppm 12.43 (1 H, br. s, NH), 7.49 (4 H, m), 7.32 (4 H, m), 7.24 (2 H,), 6.95 (2 H, s), 2.27 (3 H, s), 2.15 (6 H, s). **^{13}C{^{1}H} NMR** (176 MHz; DMSO-d_6): δ_C/ppm 145.3, 138.5, 138.1, 130.7, 128.9, 128.4, 127.9, 127.4, 21.2, 20.4. **Acc-MS** (ESI^+): *m/z* 339.1860 ($[M+H]^+$), calcd. for $C_{24}H_{23}N_2$ 339.1861 ($|\Delta m/z|$ = 0.3 ppm).

5.7.14. 2-(1′-Naphthyl)-4,5-diphenylimidazole: Naph-DPI-H

An adaption of the method of Wolkenberg et al.[50] *for the synthesis of 2,4,5-triphenylimidazoles.*

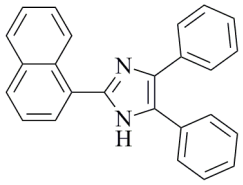

$C_{25}H_{18}N_2$
M_r = 346.4

The compounds 1-napthaldehyde (0.28 ml, 320 mg, 2.1 mmol), benzil (420 mg, 2.0 mmol) and ammonium acetate (1.54 g, 20 mmol) were suspended in acetic acid (4 ml) and sealed in a microwave vial. The solution was heated at 180 °C under microwave irradiation for 20 min. The solution was allowed to cool to r.t before being poured into water (50 ml) and extracted with CH_2Cl_2 (3 x 20 ml). The CH_2Cl_2 layers were separated, combined, washed with water (2 x 20 ml), dried over $MgSO_4$, filtered and reduced *in vacuo* to a yellow, oily solid. The crude material was recrystallised from hot MeCN twice to afford the title compound as off-white needles (508 mg, 74%).

M.p. 290 °C (from MeCN), lit. 290 °C (from EtOH).[53] **FT-IR** (solid): $\tilde{\nu}_{max}$/cm^{-1} 3385 (w, br., NH), 3059 (w, CH), 3036 (w, CH), 2960 (w, CH), 2845 (w, CH), 1951 (w), 1603 (Ar), 1585 (w, Ar), 1536 (w, Ar), 1503, 763 (s), 729 (s), 694 (s). **^{1}H NMR** (700 MHz; DMSO-d_6): δ_H/ppm 12.76 (1 H, s, NH), 9.16 (1 H, d, J = 8.8 Hz), 7.98 (2 H, d, J = 8.0 Hz), 7.94 (1 H, dd, J = 7.2 and 1.1 Hz), 7.58-7.62 (4 H, m), 7.52-7.57 (3 H, m), 7.42 (2 H, t, J = 7.7 Hz), 7.35 (1 H, t, J = 7.5 Hz), 7.31 (2 H, t, J = 7.7 Hz), 7.22 (1 H, t, J = 7.6 Hz). **^{13}C{^{1}H} NMR** (176 MHz; DMSO-d_6): δ_C/ppm 146.0, 137.6, 135.8, 134.1, 131.5, 130.8, 129.4, 129.1, 128.8, 128.7, 128.7, 128.4, 128.1, 127.9, 127.6, 127.2, 127.12, 127.0, 127.0, 126.5, 125.7. **Acc-MS** (ESI$^+$): *m/z* 347.1550 ([M+H]$^+$), calcd. for $C_{25}H_{19}N_2$ 347.1548 ($|\Delta m/z|$ = 0.6 ppm).

5.7.15. 2-(2′-Chlorophenyl)-4,5-diphenylimidazole: 2-Cl-TPI-H

An adaption of the method of Wolkenberg et al.[50] *for the synthesis of 2,4,5-triphenylimidazoles.*

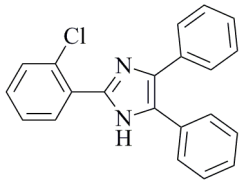

$C_{21}H_{15}ClN_2$
M_r = 330.8

The compounds 2-chlorobenzaldehyde (0.90 ml, 1.12 g, 8.0 mmol), benzil (1.68 g, 8.0 mmol) and ammonium acetate (6.20 g, 80 mmol) were suspended in acetic acid (15 ml) and sealed in a microwave vial. The solution was heated at 180 °C under microwave irradiation for 10 min. The solution was allowed to cool to r.t before being poured into water (50 ml) and extracted with CH_2Cl_2 (3 x 20 ml). The CH_2Cl_2 layers were separated, combined, washed with water (2 x 20 ml), dried over $MgSO_4$, filtered and reduced *in vacuo* to a cream coloured solid. The crude material was recrystallised from hot MeCN twice to afford the title compound as a white powder (1.98 g, 75%).

M.p. 198 °C (from MeCN), lit. 197-198 °C (from EtOH).[53] **FT-IR** (solid): $\tilde{\nu}_{max}$/cm^{-1} 3060 (CH), 3032 (CH), 2905 (CH), 2830, 2769, 2249 (w), 1601 (w, Ar), 1584 (w, Ar), 1503 (Ar), 765 (s), 736 (s), 700 (s), 695 (s). **^{1}H NMR** (600 MHz; DMSO-d_6): δ_H/ppm 12.63 (1 H, s, NH), 7.61 (1 H, s), 7.55 (2 H, d, J = 7.2 Hz), 7.45-7.52 (4 H, m), 7.43 (2 H, m), 7.36 (1 H, m), 7.31 (2 H, m), 7.23 (1 H, m). **^{13}C{^{1}H} NMR** (151 MHz; DMSO-d_6): δ_C/ppm 143.4, 136.9, 135.1, 131.6, 131.5, 130.9, 130.2, 130.2, 130.0, 128.7, 128.2 (2 C resolved), 128.0, 127.7, 127.2 (2 C resolved). **Acc-MS** (ESI$^+$): *m/z* 331.1003 ([M+H]$^+$), calcd. for $C_{21}H_{16}N_2{}^{35}Cl$ 331.1002 (|Δ*m/z*| = 0.3 ppm).

5.7.16. 2-(4′-Chlorophenyl)-4,5-diphenylimidazole: 4-Cl-TPI-H

An adaption of the method of Wolkenberg et al.[50] *for the synthesis of 2,4,5-triphenylimidazoles.*

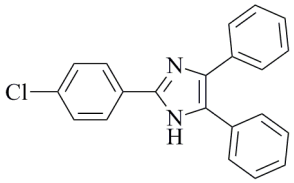

$C_{21}H_{15}ClN_2$
M_r = 330.8

The compounds 4-chlorobenzaldehyde (704 mg, 5.0 mmol), benzil (1.05 g, 5.0 mmol) and ammonium acetate (3.86 g, 50 mmol) were suspended in acetic acid (12 ml) and sealed in a microwave vial. The solution was heated at 180 °C under microwave irradiation for 10 min. The solution was allowed to cool to r.t before being poured into water (50 ml) and extracted with CH_2Cl_2 (3 x 20 ml). The CH_2Cl_2 layers were separated, combined, washed with water (2 x 20 ml), dried over $MgSO_4$, filtered and reduced *in vacuo* to a white solid. The crude material was recrystallised from hot MeCN twice to afford the title compound as a white powder (1.27 g, 77%).

M.p. 266 °C (from MeCN), lit. 264 °C (from EtOH).[53] **Elem. Anal.** Found: C, 75.97; H, 4.60; N, 8.63. Calcd. for $C_{21}H_{15}ClN_2$: C, 76.24; H, 4.57; N, 8.47%. **FT-IR** (solid): $\tilde{\nu}_{max}$/cm^{-1} 3675 (w), 2989 (CH), 2902 (CH), 1602 (w, Ar), 1505 (Ar), 834 (s), 733 (s), 697 (s). **^{1}H NMR** (400 MHz; DMSO-d_6): δ_H/ppm 12.82 (1 H, s br., NH), 8.12 (2 H, d, J = 7.8 Hz), 7.54 (6 H, s), 7.25-7.40 (6 H, m). **^{13}C{^{1}H} NMR** (151 MHz; DMSO-d_6): δ_C/ppm 145.2, 133.5, 129.9, 129.5, 129.1 (br.), 128.5 (br.), 127.9, 127.5. Acc-MS (ESI$^+$): *m/z* 331.1012 ([M+H]$^+$), calcd. for $C_{21}H_{16}N_2{}^{35}Cl$ 331.1002 ($|\Delta m/z|$ = 3.0 ppm).

5.7.17. 2,6-Bis(bromomethyl)-4-*tert*-butyltoluene

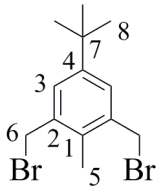

$C_{13}H_{18}Br_2$
M_r = 334.1

The compound 4-*tert*-butyltoluene (12.0 ml, 10.3 g, 69.5 mmol) was dissolved in acetic acid (30 ml). To the solution was added paraformaldehyde (6.85 g, 230 mmol, 3.3 eq.), forming a suspension, to which HBr (33 wt% in acetic acid, 45 ml, 250 mmol, 3.6 eq.) was slowly added. The solution was heated at 120 °C for 64 h. Analysis of a sample by ^{1}H NMR indicated a mixture of mono- and bis-bromomethyl products; therefore, additional paraformaldehyde (6.6 g, 220 mmol) and HBr (33 wt%, 40 ml, 220 mmol) were added to the solution and heating was continued for a further 22 h. The solution was allowed to cool to r.t., poured into ice-water (400 ml), extracted with CH_2Cl_2 (2 x 200 ml), dried over $MgSO_4$ and filtered. The volume of the organic layer was reduced to *ca*. 30 ml and purified by eluting through a short (*ca*. 5 cm) column (SiO_2; CH_2Cl_2). The fore-running fraction was reduced *in vacuo* to give an off-white solid. The crude material was recrystallised from hot hexanes to afford the title compound as a white solid (15.9 g, 68%). Single crystals suitable for X-ray diffraction were grown as needles by slow evaporation of a hexanes solution. **CAUTION:** Lachrymatory.

M.p. 83°C (dec.) (from CH_2Cl_2), lit. 92-93 °C (from hexanes).[54] **FT-IR** (solid): $\tilde{\nu}_{max}$/cm^{-1} 2970 (CH), 2955 (CH), 2863 (CH), 1605 (Ar), 1483 (s), 1463, 1444. **^{1}H NMR** (400 MHz; $CDCl_3$): δ_H/ppm 7.30 (2 H, s, H_3), 4.54 (4 H, s, H_6), 2.41 (3 H, s, H_5), 1.31 (9 H, s, H_8). **^{13}C{^{1}H} NMR** (101 MHz; $CDCl_3$): δ_C/ppm 149.6, 136.7, 134.0, 128.2, 34.6, 33.3, 31.4, 14.1. **GC-MS** (EI$^+$; 1 peak): *m*/*z* 332 (M^+, $C_{13}H_{18}{}^{79}Br_2$) with characteristic bromine isotope pattern. **MS** (ASAP$^+$; 100 °C): *m/z* 253.0 ([M-Br]$^+$), 197.0 ([M-(Br + *t*-Bu)]$^+$), 161.1 ([M-(2 Br)]$^+$). MS by ESI$^+$ or ASAP$^+$ at other temperatures did not lead to the molecular ion being observed and it is assumed that the compound easily fragments to the observed ions using these techniques. Analyses match those previously reported.

Crystal data (Instrument **C**): $C_{13}H_{18}Br_2$, (0.59 × 0.07 × 0.04) mm^3, ρ = 1.665 g cm^{-3}, monoclinic, $P2_1/c$, Z = 4, a = 9.5061(3) Å, b = 17.3230(3) Å, c = 8.8057(3) Å, β = 113.163(4)°, V = 1333.17(7) Å^3, T = 120(2) K, μ = 6.049 mm^3, 30316 reflections measured, 3398 independent (R_{int} = 0.0687), 2748 reflections with $I > 2\sigma(I)$, final R indices: wR_2 = 0.0694 (all data), R_1 = 0.0347 ($I > 2\sigma(I)$).

5.7.18. 2,6-Bis(thiomethyl)-4-*tert*-butyltoluene

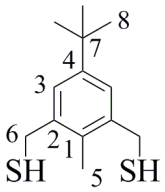

$C_{13}H_{20}S_2$
M_r = 240.4

The compounds 2,6-bis(bromomethyl)-4-*tert*-butyltoluene (5.00 g, 14.8 mmol) and thiourea (2.52 g, 32.8 mmol) were dissolved in EtOH (50 ml) and heated at reflux (80 °C) for 3 h. The solvent was removed *in vacuo* to give a yellow oil. The oil was purged with nitrogen for 15 min before NaOH (4 g, 100 mmol), dissolved in water (50 ml), was added. Complete removal of the EtOH was essential to avoid the formation of an ethoxy ether product under the basic conditions. The suspension was heated at reflux (100 °C) for 2 h, at which point all material had been converted to the product (by TLC) and had dissolved to form a colourless solution. Careful neutralisation with conc. H_2SO_4 afforded a white suspension, which was extracted with CH_2Cl_2 (50 ml), washed with water (50 ml), separated, dried over $MgSO_4$, filtered and reduced *in vacuo* to afford the title compound as a white solid (3.47 g, 97%). Single crystals suitable for X-ray diffraction were grown as prisms by slow cooling of a toluene solution. **CAUTION:** Malodorous.

M.p. 88 °C (from CH_2Cl_2), lit. 96-97 °C (from hexanes).[55] **FT-IR** (solid): $\tilde{\nu}_{max}$/cm^{-1} 2953 (s, C-H), 2899 (sh.), 2864, 2531 (SH), 1607 (w), 1573 (w), 1482 (s). **^{1}H NMR** (400 MHz; $CDCl_3$): δ_H/ppm 7.17 (2 H, s, H_3), 3.77 (4 H, d, J = 6.8 Hz, H_6), 2.39 (3 H, s, H_5), 1.68 (2 H, t, J = 6.8 Hz, SH), 1.31 (9 H, s, H_9). **^{13}C{^{1}H} NMR** (101 MHz; $CDCl_3$): δ_C/ppm 149.5, 139.8, 131.1, 125.5, 34.6, 31.5, 28.06, 14.3. **MS** (ASAP$^+$; 100 °C): m/z 207.1 ([M-SH]$^+$), 173.1 ([M-(2 x SH)]$^+$). MS by GC-MS (EI$^+$), ESI$^+$ or ASAP$^+$ at

other temperatures did not lead to the molecular ion being observed and it is assumed that the compound easily fragments to the observed ions using these techniques. Analyses match those previously reported.[54, 55]

Crystal data (Instrument **C**): $C_{13}H_{20}S_2$, (0.46 × 0.31 × 0.18) mm^3, ρ = 1.217 g cm^{-3}, monoclinic, $P2_1/c$, Z = 4, a = 10.8277(6) Å, b = 12.7500(7) Å, c = 9.6443(5) Å, β = 99.862(5)°, V = 1311.8(1) Å^3, T = 120(2) K, μ = 0.374 mm^{-1}, 9581 reflections measured, 3128 independent (R_{int} = 0.0515), 2416 reflections with $I > 2\sigma(I)$, final R indices: wR_2 = 0.1828 (all data), R_1 = 0.0601 ($I > 2\sigma(I)$).

5.7.19. 6,15-Di-*tert*-butyl-*anti*-9,18-dimethyl-2,11-dithia[3.3]metacyclophane

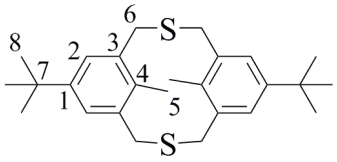

$C_{26}H_{36}S_2$
M_r = 412.7

The compounds KOH (1.5 g, 27 mmol) and $NaBH_4$ (0.5 g, 13 mmol) were dissolved in a mixture of EtOH (270 ml) and water (30 ml) and purged with nitrogen bubbling for 15 min. To this was added at r.t. a nitrogen purged toluene solution (50 ml) of 2,6-bis(bromomethyl)-4-*tert*-butyltoluene (1.67 g, 5 mmol) and 2,6-bis(thiomethyl)-4-*tert*-butyltoluene (1.20 g, 5 mmol) at a rate of 1 ml h^{-1} from a syringe pump. The solution was stirred for an additional 3 h at r.t. before being reduced to a white solid *in vacuo*. The solid was dissolved in CH_2Cl_2 (50 ml) and washed with water (3 x 10 ml). The organic layer was dried over $MgSO_4$, filtered and reduced *in vacuo*, and recrystallised from toluene to give a white solid (1.39 g, 67%). Single crystals suitable for X-ray diffraction were grown as colourless prisms by slow evaporation of a toluene solution.

M.p. 255 °C (dec.) (from toluene), lit. 255-256 °C (from benzene).[56] **FT-IR** (solid): $\tilde{\nu}_{max}$/cm^{-1} 2953 (s, CH), 2905 (sh., CH), 2866 (CH), 1767 (w), 1701 (w), 1605 (Ar), 1572 (w, Ar), 1480 (s), 882 (s), 752 (s), 643 (s). **^{1}H NMR** (400 MHz; $CDCl_3$): δ_H/ppm 7.29 (4 H, s, H_2), 3.67 (8 H, s, H_6), 1.33 (18 H, s, H_8), 1.24 (6 H, s, H_5). **MS** (ESI$^+$) 413.2 (M$^+$, 50%), 236.1 (100), 185.1 (60). Analyses match those previously reported.[54]

Crystal data (Instrument **C**): $C_{26}H_{36}S_2$, (0.36 x 0.19 x 0.16) mm^3, ρ = 1.179 g cm^{-3}, triclinic, $P\bar{1}$, Z = 2, a = 9.5783(8) Å, b = 10.8093(8) Å, c = 12.439(1) Å, α = 65.476(3)°, β = 85.729(4)°, γ = 82.881(3)°, V = 1162.23(16) $Å^3$, T = 120(2) K, μ(Mo Kα) = 0.238 mm^{-1}, 9575 reflections measured of which 6447 independent (R_{int} = 0.0681), 3483 reflections with $I > 2\sigma(I)$, final R indices: wR_2 = 0.1103 (all data), R_1 = 0.0523 ($I > 2\sigma(I)$).

5.7.20. 2,7-Di-*tert*-butyl-*trans*-10b,10c-dimethyl-10b,10c-dihydropyrene

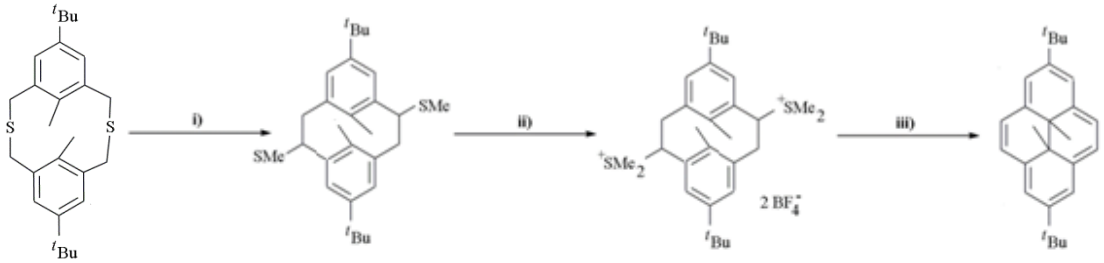

Mix of isomers Mix of isomers $C_{22}H_{18}N_2$
M_r = 310.4

i) The compound 6,15-di-*tert*-butyl-*anti*-9,18-dimethyl-2,11-dithia[3.3]metacyclophane (331 mg, 0.8 mmol) was dissolved in dry THF (15 ml) under an atmosphere of nitrogen and cooled in an ice-water bath to 0 °C. To this was cautiously added *n*-BuLi (2 ml, 1.6 M in hexanes, 3.2 mmol, 4 eq.) and the solution was stirred for 1 h, during which time it turned yellow-brown. The reaction was quenched by the addition of iodomethane (0.25 ml, 570 mg, 4.0 mmol), causing the solution to immediately turn white. The solution was stirred for a further 15 min before being exposed to air. Water (5 ml) was added cautiously and the THF was removed *in vacuo* before the aqueous layer was extracted with CH_2Cl_2 (3 x 10 ml). The organic layer was separated, dried over $MgSO_4$, filtered and reduced *in vacuo* to afford the product of the 1,2-Wittig Rearrangement as a white solid (353 mg, 99%) and as a mix of two isomers.

ii) The product from step (**i**) (353 mg, 0.8 mmol) was dissolved in dry CH_2Cl_2 (10 ml) under an atmosphere of nitrogen and cooled to 0 °C in an ice-water bath. To this was added solid Meerwein's reagent (trimethyloxonium tetrafluoroborate) (345 mg, 2.33 mmol, 2.9 eq.) and the suspension was stirred for 30 min at this temperature before being warmed to r.t. and stirred for a further 4 h. To the solution was added ethyl acetate, which caused a white precipitate to form. The solid was filtered and washed

with ethyl acetate (5 x 10 ml) until the washings were colourless. The solid was dried under high vacuum for 2 h to give the intermediate salt as a white solid (460 mg, 90%).

iii) The salt (251 mg, 0.39 mmol) was dissolved in dry THF (10 ml) under an atmosphere of nitrogen. The base KO^{t}Bu (150 mg, 1.34 mmol) was added and the solution was heated at reflux (70 °C) for 16 h, during which time the initially yellow solution turned green. The solution was cooled to r.t. and reduced *in vacuo* to a crude green solid. Water (20 ml) and CH_2Cl_2 (20 ml) were added and the solution shaken until all solids were dissolved. The CH_2Cl_2 layer was separated and further washed with water (2 x 20 ml), dried over $MgSO_4$, filtered and reduced *in vacuo* to a green solid. Column chromatography (SiO_2; hexanes) yielded as the fore-running fraction the title compound (120 mg, 89%) as a dark green solid. Single crystals could be grown as green plates (Form I) by slow evaporation from MeOH (alternatively from acetone or hexanes), as green needles (Form II) by slow evaporation from MeCN (alternatively from THF), or as a green blocks (1,2-dichloroethane solvate) from 1,2-dichloroethane with a prismatic habit.

M.p 205 °C (from hexanes, Form I), 208°C (from MeCN, Form II), lit. 203-204 °C (from hexanes).[54] **FT-IR** (solid): $\tilde{\nu}_{max}$/cm^{-1} 3041 (w, CH), 2947 (w, CH), 2864 (CH), 1598 (w, Ar), 881 (s), 670 (s). **Raman** (solid): $\tilde{\nu}_{max}$/cm^{-1} 2949 (v br., CH), 1894 (w), 1857 (w), 1749, 1704, 1610 (Ar), 1547 (Ar), 1368, 1341, 1114, 1089, 797 (s). **^{1}H NMR** (400 MHz; $CDCl_3$): δ_H/ppm 8.53 (4 H, s), 8.45 (4 H, s), 1.69 (18 H, s, *tert*-Bu), -4.04 (6 H, s, Me). **Acc-MS** (ASAP$^+$): *m/z* 345.2587 ([M+H]$^+$), calcd. for $C_{26}H_{33}$ 345.2582 ($|\Delta m/z|$ = 1.4 ppm). Analyses match those previously reported.[54]

Crystal data (Form I) (Instrument **C**): $C_{26}H_{32}$, (0.29 x 0.22 x 0.08) mm^3, ρ = 1.130 g cm^{-3}, monoclinic, $P2_1/c$, Z = 2, a = 11.6639(6) Å, b = 6.1681(3) Å, c = 14.1550(7) Å, β = 95.982(5)°, V = 1012.82(9) Å^3, T = 120(2) K, μ(Mo Kα) = 0.063 mm^{-1}, 11344 reflections measured, 2493 independent (R_{int} = 0.0763), 1695 reflections with $I > 2\sigma(I)$, final R indices: wR_2 = 0.1521 (all data), R_1 = 0.0719 ($I > 2\sigma(I)$).

Crystal data (Form II) (Instrument **C**): $C_{26}H_{32}$, (0.26 x 0.10 x 0.06) mm^3, ρ = 1.155 g cm^{-3}, monoclinic, $C2/c$, Z = 4, a = 14.379(1) Å, b = 11.7604(9) Å, c = 11.7230(9) Å, β = 91.02(2)°, V = 1982.1(3) Å^3, T = 120(2) K,

μ(Mo Kα) = 0.064 mm^{-1}, 7290 reflections measured, 3942 independent (R_{int} = 0.0326), 2141 reflections with $I > 2\sigma(I)$, final R indices: wR_2 = 0.1124 (all data), R_1 = 0.0419 ($I > 2\sigma(I)$).

Crystal data (1,2-dichloroethane solvate) (Instrument **C**): $C_{26}H_{32}.C_2H_4Cl_2$, (0.52 × 0.34 × 0.10) mm^3, ρ = 1.220 g cm^{-3}, monoclinic, $P2_1/c$, Z = 4, a = 10.1177(6) Å, b = 11.6616(7) Å, c = 11.2050(7) Å, β = 115.246(3)°, V = 1195.8(1) Å^3, T = 120(2) K, μ(Mo Kα) = 0.284 mm^{-1}, 11134 reflections measured, 2466 independent (R_{int} = 0.0497), 2065 reflections with $I > 2\sigma(I)$, final R indices: wR_2 = 0.1571 (all data), R_1 = 0.0544 ($I > 2\sigma(I)$).

5.7.21. 2,4-Bis(bromomethyl)-6-bromomesitylene

An adaption of the method of Mitchell et al. for the synthesis of 2,6-bis(bromomethyl)-4-tert-butyltoluene.

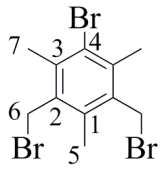

$C_{11}H_{13}Br_3$
M_r = 384.9

The compound bromomesitylene (10 ml, 13 g, 65 mmol) was dissolved in acetic acid (30 ml) to which paraformaldehyde (6.5 g, 220 mmol, 3.4 eq.) was added, forming a suspension, followed by the slow addition of HBr (33 wt% in acetic acid, 40 ml, 220 mmol, 3.4 eq.). The solution was heated at 120 °C for 96 h. The solution was cooled to r.t. and water (100 ml) was added to precipitate a white solid that was isolated by filtration washed with water (2 x 50 ml) and then ethyl acetate (2 x 10 ml) to remove a small amount of the higher solubility mono-bromomethyl product. The solid was dried under high vacuum to yield the title product (16.7 g, 67%) as a white solid. **CAUTION:** Lachrymatory.

M.p. 140 °C (from acetic acid/water). **FT-IR** (solid): $\tilde{\nu}_{max}$/cm^{-1} 2924 (w, CH), 1568 (w, Ar), 615 (s, CBr). **^{1}H NMR** (400 MHz; $CDCl_3$): δ_H/ppm 4.59 (4 H, s, H_6), 2.56 (6 H, s, H_7), 2.43 (3 H, s, H_5). **^{13}C{^{1}H} NMR** (101 MHz; $CDCl_3$): δ_C/ppm 138.5, 136.2, 134.1,

128.0, 30.6, 21.1, 15.4. **Acc-MS** (ASAP$^+$ 50 °C): *m/z* 381.8564 (M^+), calcd. for $C_{11}H_{13}{}^{79}Br_3$ 381.8567 ($|\Delta m/z| = 0.3$ ppm) with characteristic bromine isotope pattern.

5.7.22. 2,4-Bis(thiomethyl)-6-bromomesitylene

An adaption of the method of Mitchell et al.[54] *for the synthesis of 2,6-bis(thiomethyl)-4-tert-butyltoluene.*

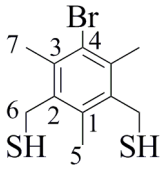

$C_{11}H_{15}BrS_2$
$M_r = 291.3$

The compounds 3,5-bis-bromomethyl-2,4,6-trimethylbromobenzene (3.84 g, 10 mmol) and thiourea (1.71 g, 22 mmol) were dissolved in EtOH (20 ml) and heated at reflux (80 °C) for 3.5 h. The solvent was removed *in vacuo* to give a white solid that was purged with nitrogen for 15 min before NaOH (2.7 g, 68 mmol) dissolved in water (40 ml) was added. Complete removal of the EtOH was essential to avoid the formation of an ethoxy ether product under the basic conditions. The suspension was heated at reflux (100 °C) for 2 h, at which point all material had been converted to the product (by TLC) and had dissolved to form a colourless solution. Careful neutralisation with conc. H_2SO_4 afforded a white suspension, which was extracted with CH_2Cl_2 (30 ml), washed with water (30 ml), separated, dried over $MgSO_4$, filtered and reduced *in vacuo* to afford the title compound as a white solid (2.65 g, 92%). **CAUTION:** Malodorous.

M.p. 96 °C (from CH_2Cl_2). **FT-IR** (solid): $\tilde{\nu}_{max}$/cm^{-1} 2924 (w, CH), 2528 (SH), 1548 (w, Ar), 1440 (s) and 1379 (s, Ar). **^{1}H NMR** (400 MHz; $CDCl_3$): δ_H/ppm 3.81 (4 H, d, J = 6.4 Hz, H_6), 2.53 (6 H, s, H_7), 2.41 (3 H, s, H_5), 1.60 (2 H, t, J = 6.4 Hz, SH). **^{13}C{^{1}H} NMR** (101 MHz; $CDCl_3$): δ_C/ppm 137.3, 135.3, 128.1, 107.4, 25.1, 21.1, 15.7. **GC-MS** (EI$^+$; 1 peak): *m/z* 290 (M^+, $C_{11}H_{15}S_2{}^{79}Br$) with characteristic bromine isotope pattern. **Acc-MS** (ASAP$^+$, 50 °C): *m/z* 289.9781 (M^+), calcd. for $C_{11}H_{15}S_2{}^{79}Br$ 289.9799 ($|\Delta m/z| = 6.2$ ppm).

5.8. References

1. L. Porrès, A. Holland, L.-O. Pålsson, A. P. Monkman, C. Kemp and A. Beeby, *J. Fluoresc.*, 2006, **16**, 267.
2. M. A. Albota, C. Xu and W. W. Webb, *Appl. Opt.*, 1998, **37**, 7352.
3. C. Xu and W. W. Webb, *J. Opt. Soc. Am. B*, 1996, **13**, 481.
4. N. G. Connelly and W. E. Geiger, *Chem. Rev.*, 1996, **96**, 877.
5. *Gaussian 09, Revision A.1*, M. J. Frisch, G. W. Trucks, H. B. Schlegel, G. E. Scuseria, M. A. Robb, J. R. Cheeseman, G. Scalmani, V. Barone, B. Mennucci, G. A. Petersson, H. Nakatsuji, M. Caricato, X. Li, H. P. Hratchian, A. F. Izmaylov, J. Bloino, G. Zheng, J. L. Sonnenberg, M. Hada, M. Ehara, K. Toyota, R. Fukuda, J. Hasegawa, M. Ishida, T. Nakajima, Y. Honda, O. Kitao, H. Nakai, T. Vreven, J. A. Montgomery, J. E. Peralta, F. Ogliaro, M. Bearpark, J. J. Heyd, E. Brothers, K. N. Kudin, V. N. Staroverov, R. Kobayashi, J. Normand, K. Raghavachari, A. Rendell, J. C. Burant, S. S. Iyengar, J. Tomasi, M. Cossi, N. Rega, J. M. Millam, M. Klene, J. E. Knox, J. B. Cross, V. Bakken, C. Adamo, J. Jaramillo, R. Gomperts, R. E. Stratmann, O. Yazyev, A. J. Austin, R. Cammi, C. Pomelli, J. W. Ochterski, R. L. Martin, K. Morokuma, V. G. Zakrzewski, G. A. Voth, P. Salvador, J. J. Dannenberg, S. Dapprich, A. D. Daniels, Farkas, J. B. Foresman, J. V. Ortiz, J. Cioslowski and D. J. Fox, Wallingford CT, 2009.
6. Y. Shao, L. F. Molnar, Y. Jung, J. Kussmann, C. Ochsenfeld, S. T. Brown, A. T. B. Gilbert, L. V. Slipchenko, S. V. Levchenko, D. P. O'Neill, R. A. Di Stasio Jr, R. C. Lochan, T. Wang, G. J. O. Beran, N. A. Besley, J. M. Herbert, C. Y. Lin, T. van Voorhis, S. Hung Chien, A. Sodt, R. P. Steele, V. A. Rassolov, P. E. Maslen, P. P. Korambath, R. D. Adamson, B. Austin, J. Baker, E. F. C. Byrd, H. Dachsel, R. J. Doerksen, A. Dreuw, B. D. Dunietz, A. D. Dutoi, T. R. Furlani, S. R. Gwaltney, A. Heyden, S. Hirata, C.-P. Hsu, G. Kedziora, R. Z. Khalliulin, P. Klunzinger, A. M. Lee, M. S. Lee, W. Z. Liang, I. Lotan, N. Nair, B. Peters, E. I. Proynov, P. A. Pieniazek, Y. M. Rhee, J. Ritchie, E. Rosta, C. David Sherrill, A. C. Simmonett, J. E. Subotnik, H. L. Woodcock III, W. Zhang, A. T. Bell, A. K. Chakraborty, D. M. Chipman, F. J. Keil, A. Warshel, W. J. Hehre, H. F. Schaefer III, J.

Kong, A. I. Krylov, P. M. W. Gill and M. Head-Gordon, *Phys. Chem. Chem. Phys.*, 2006, **8**, 3172.

7. A. D. Becke, *J. Chem. Phys.*, 1993, **98**, 5648.
8. C. Lee, W. Yang and R. G. Parr, *Phys. Rev. B*, 1988, **37**, 785.
9. Y. Zhao and D. Truhlar, *Theor. Chem. Acc.*, 2008, **120**, 215.
10. T. Yanai, D. P. Tew and N. C. Handy, *Chem. Phys. Lett.*, 2004, **393**, 51.
11. A. G. Crawford, A. D. Dwyer, Z. Liu, A. Steffen, A. Beeby, L.-O. Pålsson, D. J. Tozer and T. B. Marder, *J. Am. Chem. Soc.*, 2011, **133**, 13349.
12. M. J. G. Peach, M. J. Williamson and D. J. Tozer, *J. Chem. Theory Comput.*, 2011, **7**, 3578.
13. M. J. G. Peach and D. J. Tozer, *J. Phys. Chem A*, 2012, **116**, 9783.
14. K. B. Wiberg, *Tetrahedron*, 1968, **24**, 1083.
15. L. Goodman and R. R. Sauers, *J. Comput. Chem.*, 2007, **28**, 269.
16. W. J. Hehre, R. Ditchfield and J. A. Pople, *J. Chem. Phys.*, 1972, **56**, 2257.
17. P. J. Hay and W. R. Wadt, *J. Chem. Phys.*, 1985, **82**, 299.
18. M. J. G. Peach, T. Helgaker, P. Salek, T. W. Keal, O. B. Lutnaes, D. J. Tozer and N. C. Handy, *Phys. Chem. Chem. Phys.*, 2006, **8**, 558.
19. T. Yanai, *Chem. Phys. Lett.*, 2004, **393**, 51.
20. I. Tamm, *J. Phys. (USSR)*, 1945, **9**, 449.
21. S. M. Dancoff, *Phys. Rev.*, 1950, **78**, 382.
22. S. Hirata and M. Head-Gordon, *Chem. Phys. Lett.*, 1999, **314**, 291.
23. J. R. Malpass, D. A. Hemmings, A. L. Wallis, S. R. Fletcher and S. Patel, *J. Chem. Soc., Perkin Trans. 1*, 2001, 1044.
24. H. E. Gottlieb, V. Kotlyar and A. Nudelman, *J. Org. Chem.*, 1997, **62**, 7512.
25. G. R. Fulmer, A. J. M. Miller, N. H. Sherden, H. E. Gottlieb, A. Nudelman, B. M. Stoltz, J. E. Bercaw and K. I. Goldberg, *Organometallics*, 2010, **29**, 2176.
26. J. Cosier and A. M. Glazer, *J. Appl. Crystallogr.*, 1986, **19**, 105.
27. O. V. Dolomanov, L. J. Bourhis, R. J. Gildea, J. A. K. Howard and H. Puschmann, *J. Appl. Crystallogr.*, 2009, **42**, 339.
28. C. Bianchini, D. Gatteschi, G. Giambastiani, I. Guerrero Rios, A. Ienco, F. Laschi, C. Mealli, A. Meli, L. Sorace, A. Toti and F. Vizza, *Organometallics*, 2007, **26**, 726.

29. Gracel Display Inc., *Eur. Pat. 2 019 108 A2*, 2008.
30. A. Conejo-García, L. Pisani, M. del Carmen Núñez, M. Catto, O. Nicolotti, F. Leonetti, J. M. Campos, M. A. Gallo, A. Espinosa and A. Carotti, *J. Med. Chem.*, 2011, **54**, 2627.
31. C. Sicre, J. L. Alonso-Gómez and M. M. Cid, *Tetrahedron*, 2006, **62**, 11063.
32. B. S. Furniss, A. J. Hannaford, P. W. G. Smith and A. R. Tatchell, *Vogel's Textbook of Practical Organic Chemistry*, Longman Scientific & Tecnical, London, 5th edn., 1996, ch. 8, p. 1170.
33. M. Nonoyama, *Bull. Chem. Soc. Jpn.*, 1974, **47**, 767.
34. S. Sprouse, K. A. King, P. J. Spellane and R. J. Watts, *J. Am. Chem. Soc.*, 1984, **106**, 6647.
35. S. Lamansky, P. Djurovich, D. Murphy, F. Abdel-Razzaq, R. Kwong, I. Tsyba, M. Bortz, B. Mui, R. Bau and M. E. Thompson, *Inorg. Chem.*, 2001, **40**, 1704.
36. H. Chen, Q. Zhao, Y. Wu, F. Li, H. Yang, T. Yi and C. Huang, *Inorg. Chem.*, 2007, **46**, 11075.
37. B. K. Blackburn, A. Lee, M. Baier, B. Kohl, A. G. Olivero, R. Matamoros, K. D. Robarge and R. S. McDowell, *J. Med. Chem.*, 1997, **40**, 717.
38. J. M. Tour, A. M. Rawlett, M. Kozaki, Y. Yao, R. C. Jagessar, S. M. Dirk, D. W. Price, M. A. Reed, C.-W. Zhou, J. Chen, W. Wang and I. Campbell, *Chem. Eur. J.*, 2001, **7**, 5118.
39. P. G. M. Wuts and T. W. Greene, *Greene's Protective Groups in Organic Synthesis*, John Wiley & Sons Inc., Hoboken, New Jersey, 4th edn., 2007, ch. 8, pp. 927-933.
40. D. P. Kelly, S. A. Bateman, R. F. Martin, M. E. Reum, M. Rose and A. R. D. Whittaker, *Aust. J. Chem.*, 1994, **47**, 247
41. A. G. Crawford, A. Steffen, J. C. Collings, A. S. Batsanov, J. A. K. Howard, T. B. Marder, Z. Liu, I. A. I. Mkhalid, M.-H. Thibault, N. Schwarz and G. Alcaraz, *Chem. Eur. J.*, 2012, **18**, 5022
42. R. H. Mitchell, Y.-H. Lai and R. V. Williams, *J. Org. Chem.*, 1979, **44**, 4733.
43. W. Wu, W. Wu, S. Ji, H. Guo and J. Zhao, *Eur. J. Inorg. Chem.*, 2010, **2010**, 4470.

44. I. Van Overmeire, S. A. Boldin, K. Venkataraman, R. Zisling, S. De Jonghe, S. Van Calenbergh, D. De Keukeleire, A. H. Futerman and P. Herdewijn, *J. Med. Chem.*, 2000, **43**, 4189.
45. A. Elangovan, Y.-H. Wang and T.-I. Ho, *Org. Lett.*, 2003, **5**, 1841.
46. T. A. Zeidan, S. V. Kovalenko, M. Manoharan, R. J. Clark, I. Ghiviriga and I. V. Alabugin, *J. Am. Chem. Soc.*, 2005, **127**, 4270.
47. R. Chinchilla and C. Nájera, *Chem. Rev.*, 2007, **107**, 874.
48. R. Chinchilla and C. Nájera, *Chem. Soc. Rev.*, 2011, **40**, 5084.
49. Z. Li, F. W. Fowler and J. W. Lauher, *J. Am. Chem. Soc.*, 2008, **131**, 634.
50. S. E. Wolkenberg, D. D. Wisnoski, W. H. Leister, Y. Wang, Z. Zhao and C. W. Lindsley, *Org. Lett.*, 2004, **6**, 1453.
51. N. Fey, J. A. S. Howell, J. D. Lovatt, P. C. Yates, D. Cunningham, P. McArdle, H. E. Gottlieb and S. J. Coles, *Dalton Trans.*, 2006, 5464.
52. J. A. Varela, D. Peña, B. Goldfuss, D. Denisenko, J. Kulhanek, K. Polborn and P. Knochel, *Chem. Eur. J.*, 2004, **10**, 4252.
53. N. Azizi, N. Dado and A. K. Amiri, *Can. J. Chem.*, 2011, **90**, 195.
54. R. H. Mitchell, T. R. Ward, Y. Chen, Y. Wang, S. A. Weerawarna, P. W. Dibble, M. J. Marsella, A. Almutairi and Z.-Q. Wang, *J. Am. Chem. Soc.*, 2003, **125**, 2974.
55. K. Chifuku, T. Sawada, Y. Kuwahara and H. Shosenji, *Mol. Cryst. Liq. Cryst.*, 2007, **470**, 369.
56. M. Tashiro and T. Yamato, *J. Org. Chem.*, 1981, **46**, 1543.